Defining the role of P2X4 receptor in prostate cancer

A thesis submitted in fulfilment of the requirements
for the degree of Doctor of Philosophy
by

Jiepei He

Supervised by Dr. Ning Wang

Department of Oncology and Metabolism

The University of Sheffield

List of contents

List of figures

Chapter 1

Chapter 2

Chapter 3

Chapter 4

Chapter 5

Chapter 6

APPENDIX

List of Table

Chapter 1

Chapter 2

Chapter 4

Chapter 5

Chapter 6

APPENDIX

List of abbreviations

ADT	Androgen deprivation therapy
AI	Androgen-independent
ATCC	American Type Culture Collection
ATP	Adenosine triphosphate
BAM	A data format
BMP	Bone morphogenetic protein
BV	Bone volume
BV/TV	Bone volume fraction
C4-2B4	An human prostate cancer cell lines
cDNA	Complementary DNA
CHO	Chinese hamster ovary
COX-2	Cyclooxygenase-2
CRISPR/Cas9	Clustered regularly interspaced short palindromic repeats
CRPC	Castration-resistant prostate cancer
Ct	Cycle threshold
CXCL	Chemokine ligand
CXCL5	C-X-C motif chemokine 5
CXCR	Chemokine receptor
DA	Anisotropy
DMEM	Dulbecco’s modified Eagle’s medium
DMSO	Dimethyl sulfoxide

DU145	DU-145, human prostate cancer cell line
ECM	Extracellular matrix
EDTA	Ethylenediaminetetraacetic acid
EMT	Epithelial to mesenchymal transition
ERG	ETS-related gene
EtBr	Ethidium Bromide
FAK	Focal adhesion kinase
FCS	Foetal calf serum
FDA	Food and drug administration
FGF	Fibroblast growth factor
FVB/NJ mice	FVB is an albino, inbred laboratory mouse
GAPDH	A reference house-keeping gene, Glyceraldehyde 3-phosphate dehydrogenase
GBM	Glioblastoma multiforme
GFP	Green fluorescent protein
GO	Gene ontology
gRNAs	Guide RNAs
HPV/HPVs	Human papillomaviruses
IARC	International agency for research on cancer
IGF	Insulin-like growth factor
IGF-1	Insulin like growth factor-1
KEGG	Kyoto Encyclopedia of Genes and Genomes
KO	Knock-out
MAPK	Mitogen-activated protein kinase

M-CSF	Macrophage colony-stimulating factor
MET	Mesenchymal to epithelial transition
Micro-CT	Micro-computed tomography
MMP2	Matrix metallopeptidase 2
MMP9	Matrix metallopeptidase 9
mRNA	Messenger RNA
Myc-CaP	mouse prostate cancer cells
NFκB	Nuclear factor-κB
NGS	Next-generation sequencing
NOD/SCID mice	Nonobese diabetic/severe combined immunodeficiency mouse
P1R	P1 receptor
P2X1R	P2X1 receptor
P2X2R	P2X2 receptor
P2X4R	P2X4 receptor
P2X5R	P2X5 receptor
P2X6R	P2X6 receptor
P2X7R	P2X7 receptor
P2XR	P2X receptor
P2XP4	P2X purinoceptor 4
P2YR	P2Y receptor
p53	Tumour protein p53
pAKT	Phosphorylated protein kinase
PBS	Phosphate-buffered saline

PCa	Prostate cancer
PCR	Polymerase chain reaction
PDGF	Platelet-derived growth factor
PGE2	Prostaglandin E2
PHLPP	Leucine rich repeat protein phosphatases
PSA	Urokinase-type plasminogen activator
PTEN	Phosphatase and tensin homolog
PTH	Parathyroid hormone
RANKL	The RANK/receptor activator of NF-kappa B ligand
REDOX	Incorporates an oxidation-reduction
ROI	A region of interest
SMI	Structure model index
SREs	Skeletal-related events
Tb.N	Trabecular number
Tb.Sp	Trabecular separation
Tb.Th	Trabecular thickness
TE	Tris-EDTA
TGF-β	Transforming growth factor-β
TMs	Transmembrane domains
TM	Melting temperature
TNP-ATP	P2X4R agonist
TRAP	Tartrate-resistant acid phosphatase
TV	Total volume
VEGF	Vascular endothelial growth factor

WT	Wild type

Acknowledgements

I would like to express my sincere gratitude to the following people for their invaluable contributions and support throughout my PhD:

First and foremost, I would like to thank my supervisor, Dr. Ning Wang, for his exceptional guidance, support, and patience. He has been an incredible supervisor, always available to discuss my project, provide helpful feedback, and guide me towards the right direction. I have learned so much from him about being a good researcher, and he has been instrumental in helping me navigate the challenges of the PhD journey. Without his support, I would not have been able to achieve my goals.

I am grateful to my second supervisor, Professor Alison Gartland, for her invaluable expertise and feedback. I would like to thank Dr. Karan M Shah for his assistance in solving problems in my experiments and providing valuable advice. I am also grateful to my group member, Dr. Hector Manuel Arredondo Carrera, for his kind assistance.

I would like to express my gratitude to Dr. Ning Wang for his assistance with intracardiac mouse injections, blood withrow and mouse dissection. I am also grateful to Dr. Hector for his drug daily administration in mouse. Susan Clark's assisted in cell sorting and Orla Gallagher's contribution to bone sample preparation. I would like to extend my heartfelt gratitude to Dr. Ning Wang, Professor Alison Gartland, Professor Timothy M Skerry, Professor Niklas Rye Jørgensen, Maryam Yazdanparast and Alex Sprules for their invaluable feedback on my PhD thesis. I would like to thank Yuhan Zhou for P2X4R related preliminary work.

I would also like to extend my thanks to my friends in the oncology and metabolism department, from all different nationalities. Norain and Vicky, in particular, have been incredibly supportive and caring throughout my PhD journey. I would like to express my gratitude to my partner, Yuan, for his unwavering support and encouragement during the writing process.

Last but not least, I would like to express my deepest gratitude to my parents, in particular, for their unwavering love and support. To my mom Mao and dad He, I am forever grateful for their constant encouragement and belief in me. I love them both and wish them all the best.

Publications

Articles:

Jiepei He, Yuhan Zhou, Hector M. Arredondo Carrera, Alexandria Sprules , Ramona Neagu , Sayyed Amin Zarkesh , Colby Eaton , Jian Luo , Alison Gartland and Ning Wang. Inhibiting the P2X4 receptor suppresses prostate cancer growth *in vitro* and *in vivo*, suggesting a potential clinical target[J]. Cells, 2020, 9(11): 2511.

Song H, Arredondo Carrera H M, Sprules A, Ying Ji, Tongsong Zhang, **Jiepei He**, Eleanor Lawrence, Alison Gartland, Jian Luo, Ning Wang. C-terminal variants of the P2X7 receptor are associated with prostate cancer progression and bone metastasis–evidence from clinical and pre-clinical data[J]. Cancer Communications, 2022.

Abstract:

He J, Zhou Y, Arredondo Carrera H M, Ning Wang, Alison Gartland. Defining the role of P2X4 receptor in the prostate cancer bone metastasis. ECTS 2022, Helsinki, Finland. Bone Reports, 16:101209, May 2022

He J, Zhou Y, Arredondo Carrera H M, Alison Gartland, Ning Wang. Defining the role of P2X4 receptor in prostate cancer. The Mellanby Centre for Bone Research, Department of Oncology & Metabolism, Sheffield, United Kingdom. Journal of Bone Oncology, Volume 18, March 2022

Abstract

Prostate cancer (PCa) is the most frequently diagnosed cancer in men, causing considerable morbidity and mortality. The P2X4 receptor (P2X4R) is a receptor for ATP that is highly expressed in many cancer types and is positively associated with tumourigenesis. However, the role of P2X4R in PCa progression is not well understood. I hypothesized that P2X4R plays a critical role of pro-tumourigenesis in PCa.

Firstly in the project, the effect of pharmacologically inhibiting P2X4R, with the selective P2XR4 antagonists 5-BDBD and PSB-12062, on PCa (PC3 and C4-2B4 cells) migration, invasion, and apoptosis were examined in insert assay and Caspase 3/7 assays *in vitro*. The results demonstrated that inhibiting P2X4R impaired the growth and mobility of PCa cells but not apoptosis. In BALB/c immunocompromised nude mice inoculated with human PC3 cells subcutaneously (10^6 cells/injection), 5-BDBD showed anti-tumourigenic effects. These studies suggest that P2X4R enhances PCa tumour formation and is a clinically targetable candidate for which inhibitors are already available and can potentially suppress disease progression.

Secondly, to further understand the role of P2X4R in PCa biology, particularly in PCa bone metastasis, gene P2RX4 was knocked out in human PC3 cells using the CRISPR/Cas9 system (Santa Cruz:sc-401779). Successful P2X4R knock-out (KO) clones were confirmed and verified using RT-PCR, Sanger sequencing, and functional calcium assay (Fluo-4 Direct™). Cell proliferation, viability, migration, invasion and apoptosis were examined using CyQUANT®, AlamarBlue, Cell MeterTM Caspase 3/7 assays, scratch assay and insert transwell respectively. To test metastatic bone potential *in vivo*, PC3 wildtype (WT) and KO cells (10^5 cells/injection) were intracardiacally injected into 6-week-old male BALB/c immunocompromised mice (10 mice/group). Mice were euthanized 25 days post-inoculation and bone micro-architectural changes in tibias were analysed using micro-CT *ex vivo*, with tumour burden quantified in the metaphysis region of tibias using H&E stained sections and osteoMeasure. Results showed that depleting P2X4R significantly reduced cell proliferation, invasion and increased apoptosis compared to WT controls *in vitro*. Micro-CT analysis suggested KO cells caused less bone destruction than WT cells,

including higher trabecular bone volume fraction, trabecular thickness, trabecular number, and cortical bone volume. There was almost no presence of tumours in KO cell injected mouse tibias, while over 50% of bone marrow areas were occupied by WT PCa cells. The body weight of mice injected with KO cells was significantly heavier than mice injected with WT cells at the endpoint. These studies demonstrated that targeting P2X4R suppresses the process of tumour bone metastasis and indicates a potential pharmacological target.

Thirdly, RNA-seq was performed to understand further the mechanism for P2X4R deficiency correlated reduction in PCa tumourigenicity. Total RNA was isolated from PC3 WT and KO cells by RNA Miniprep System, then the RNA samples were sent out to Source BioScience (Nottingham, UK) for RNA sequencing. Bioinformatics tools, including Galaxy European, David, and Gorilla performed bioinformatics analysis of the RNA-seq. The results demonstrated that P2X4R deficiency in PCa cells caused dramatically up-regulate the anti-tumour genes, and it also significantly increased cell adhesion function and characteristic of the epithelia gene, which may delay the process of PCa. Regulation of the WNT and PEG2 signals might also reduce cell proliferation, enhance apoptosis, and affect angiogenesis. These findings provide important insights into the underlying biology of P2X4R and PCa progression.

These results highlight the P2X4R as a potential therapeutic target for the treatment of aggressive PCa, especially for PCa bone metastasis.

CHAPTER 1:

INTRODUCTION

1.1 Epidemiology

PCa is the foremost cancer type diagnosed and the second foremost cause of cancer-related mortality in males in the United Kingdom. From 2014 to 2016, approximately 47,700 and 130 novel cases of PCa were reported annually and daily, respectively, in the United Kingdom. Additionally, in 2016, PCa constituted 26% of all new cancer cases in males in the United Kingdom. Notably, in the past decade, the incidence of PCa has been highest in males aged 75 to 79 years. According to Cancer Research UK, an estimated 84% of patients with clinically localised PCa who receive effective treatments can survive. Regarding the global prevalence of PCa, the International Agency for Research on Cancer (IARC) has reported that in 2020, there were 1.4 million new cases of PCa leading to 375,000 deaths worldwide, making it the fifth leading cause of cancer death in men globally (IARC; Cancer Research UK; PCa: Statistics, ACS). In the United States, PCa is the most commonly diagnosed cancer in men, with an estimated 248,530 new cases and 34,130 deaths expected in 2021. PCa has a higher incidence rate in some developed countries such as North America, Europe, and Australia. However, there has been an increasing incidence of PCa in many countries, including those in Asia and Africa.

1.1.1 Incidence of PCa

The prostate gland is located below the bladder and surrounds the urethra, typically the size of a chestnut, with the urethra passing through the middle. It secretes a fluid that is a component of semen (Docherty, 2015). Age is the primary risk factor for PCa, with the risk of developing the disease increasing as men age. Men over 55 years of age are at the highest risk of developing PCa (Zheng et al., 2020). In the United States, between 2001 and 2007, only less than 3% of PCa cases were in patients under 50 years old, while those over 50 accounted for the majority of cases (Rawla, 2019). Obesity is another risk factor for PCa, with obese men at a higher risk of dying from the disease (Bandini et al., 2017). Unhealthy lifestyle habits such as high stress and a lack of exercise can also increase the risk of PCa, just as many diseases. Smoking and drinking have also been suggested as risk factors for PCa. Race and genetics

may also play a role in the incidence of this disease, with research suggesting a higher risk in men of African descent (Taitt, 2018). Additionally, evidence has shown that men with a family history of PCa are at a three times higher risk of developing the disease than those without a family history (Grönberg, 2003).

1.1.2 TNM Classification system of PCa

In 1994, researchers in the United States established the TNM classification system for PCa, which divides cancer into stages based on the primary tumour (T), lymph nodes (N), and distant metastasis (M) (Makoto, 1993, Eichelberger and Cheng, 2004). According to the TNM system, stages of PCa can be classified as stages T, stages N and stages M (Table 1). There are six T stages of PCa: TX to T0 indicates no present tumour to be detected; afterwards, T1 to T4 can be further divided into three subcategories in each stage. At the T1 stage, no detectable tumour is clinically present, and the tumour can only be identified by incidental histologic findings of less than 5% (T1a$\leqslant$5%, T1b>5%, T1c: tumour detected by needle biopsy). In the T2 stage, the tumour is confined within the prostate gland (T2a: tumour involves half or less of a lobe; T2b: tumour involves more than half of a lobe but not both lobes; T2c: tumour involves both lobes). At the T3 stage, the tumour extends beyond the prostate capsule (T3a: unilateral extracapsular extension; T3b: bilateral extracapsular extension; T3c: tumour invades seminal vesicle). At the T4 stage, the tumour is fixed or invades adjacent structures other than the seminal vesicles (T4a: tumour invades the bladder neck, external sphincter, or rectum; T4b: tumour invades the levator muscles or is fixed to the pelvic wall) (Figure 1.1).

Node (N) stage present whether the cancer has spread to the lymph nodes, lymph nodes metastasis include stage NX, N0 and N1. NX means no regional lymph nodes have been assessed. N0 describes no cancer cells in the nearby lymph nodes, and N1 represents cancer cells that have metastasized in the lymph nodes near prostate.

Metastasis (M) describes whether cancer has spread to different body parts, including M0 and M1. M0 means cancer has not spread to other areas or organs in the body.

M1 signifies that cancer has metastasized or spread to distant sites beyond the prostate gland and nearby lymph nodes. There are three subcategories in M1: M1a indicates cancer cells in distant lymph nodes outside the pelvis; M1b indicates cancer cells in bones; M1c indicates cancer cells in other organs such as lungs, liver, or brain (Rosen and Sapra, 2022) (Cancer Research UK). The UICC TNM Classification is an anatomical system that records the primary and regional nodal extent of the tumour and the absence or presence of metastases.

Table 1.1: TNM classification system

Stage	Definition of criteria for inclusion
TX	Primary tumours cannot be assessed
T0	No evidence of tumour to be detected
T1	No clinically apparent tumour was detected, not palpable nor visible by imaging T1a: Tumour an incidental histologic finding; 5% of tissue resected T1b: Tumour an unexpected histologic finding; >5% of tissue resected T1c: Tumour identified by needle biopsy (e.g., because of imaging elevated serum PSA)
T2	Confined within the prostate T2a: Tumour involves half of a lobe or less T2b: Tumour involves more than half of a lobe but not both lobes T2c: Tumour involves both lobes
T3	Tumour extends through the prostate capsule T3a: Unilateral extracapsular extension T3b: Bilateral extracapsular extension T3c: Tumour invades seminal vesicles
T4	The tumour is fixed or invades adjacent structures other than seminal vesicles T4a: Tumour invades bladder neck or external sphincter or rectum T4b: Tumour invades levator muscles or is fixed to the pelvic wall
NX	No regional lymph nodes are to be assessed
N0	No evidence of regional lymph node metastasis
N1	Regional lymph node metastasis
M0	No distant metastasis
M1	Cancer has metastasized to distant sites M1a: Cancer cells in nearby lymph nodes outside the pelvis M1b: Cancer cells in the bones M1c: Cancer cells in other organs of the body

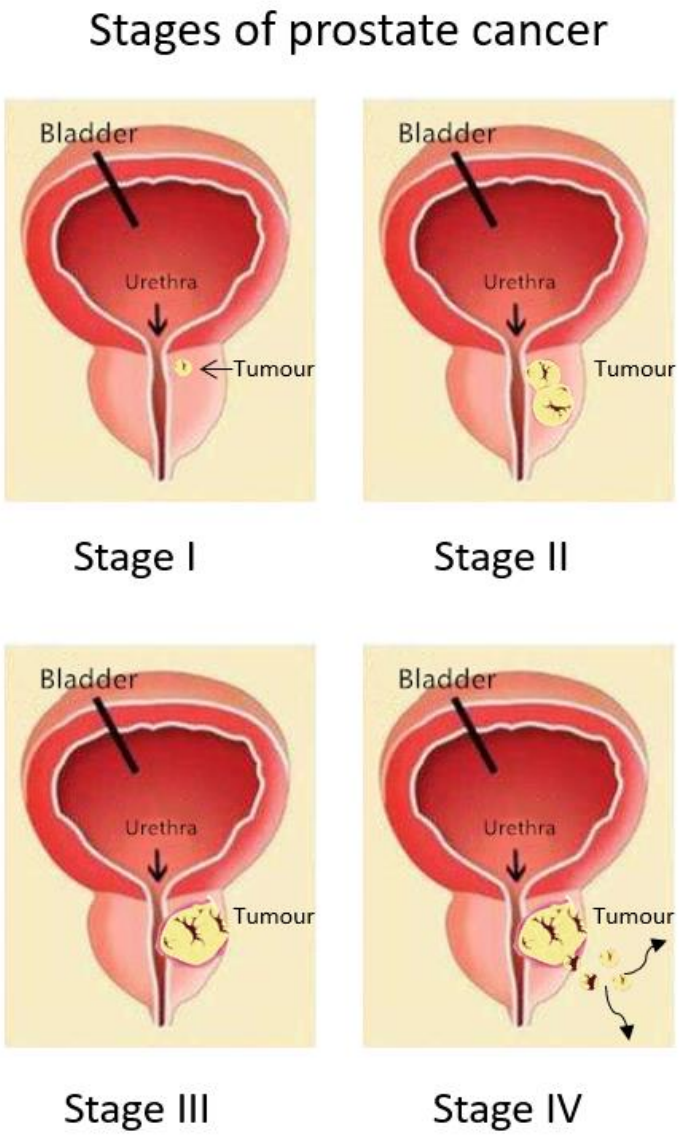

Figure 1.1: Stages of PCa. Stage I means the cancer is too small to be seen on a scan or felt during the prostate examination. Stage II means the cancer is entirely inside the prostate gland. Stage III means cancer has broken through the capsule (covering) of the prostate gland. Stage IV means cancer has spread into other body organs nearby, such as the rectum, bladder, or pelvic wall. The elements were downloaded from the internet and modified to explain the classification of different stages in PCa (SchrlSder et al., 1992).

1.2 PCa metastasis

PCa is considered a complex disease, and metastasis in advanced PCa is a common phenomenon. PCa can metastasise to distant organs such as the liver, lungs, and brain but preferentially to bone. More than 70% of patients with advanced PCa are estimated to develop skeletal metastasis (Florencio-Silva et al., 2015). Therefore, PCa is recognized as bone-affiliated cancer, which causes significant mortality and morbidity. Among 1,589 routine autopsies performed on PCa patients aged > 40 years, heterogeneous metastases were presented in 35% of patients with involvement in bone (90%), lung (46%), liver (25%), pleura (21%), and adrenals (13%) (Bubendorf et al., 2000).

1.2.1 Skeleton metastases

The skeletal metastases of PCa significantly impact the quality of life of affected patients. This condition leads to various symptoms such as bone pain, pathological fracture, spinal cord compression, and anaemia. The metastatic process typically starts in the prostate and progresses to the lower spine, pelvis, and, eventually, long bones such as the femur. Once established in the bone, the pain experienced by patients tends to intensify, leading to potential complications and other medical conditions such as fractures(Logothetis and Lin, 2005). A study in 2000 showed that approximately 80% of men died from PCa-derived bone metastases (Bubendorf et al., 2000a). The data also indicated that bone metastasis is the leading cause of patients' mortality with advanced PCa.

Bone metastasis is commonly categorized as either osteolytic (bone destructive) or osteoblastic (bone forming, sclerotic). In the case of PCa, bone metastases are frequently classified as osteoblastic, while breast cancer and myeloma are typically associated with osteolytic metastasis (Honore et al., 2000, Mundy, 2002).

1.2.2 Process of PCa bone metastasis

The process of tumour evolution in prostate metastases to bone is a complex phenomenon. The primary PCa cells stimulate the formation of small blood vessels in their vicinity, allowing cancer cells to enter the circulation. It is a prerequisite for the occurrence of metastasis that the cancer cells that survive the journey through the circulation can enter the wide-channelled sinusoids of the bone marrow cavity and are suitably positioned to form bone metastases. Once the cancer cells reach the bone, they interact with the local stromal and immune cells present in the bone microenvironment. The specialized bone cells, including osteoclasts, osteoblasts, and osteocytes, the mineralized bone matrix, and other cell types within the bone, create a unique milieu that provides a fertile ground for promoting cancer growth (Mundy, 2002) (Figure 1.2).

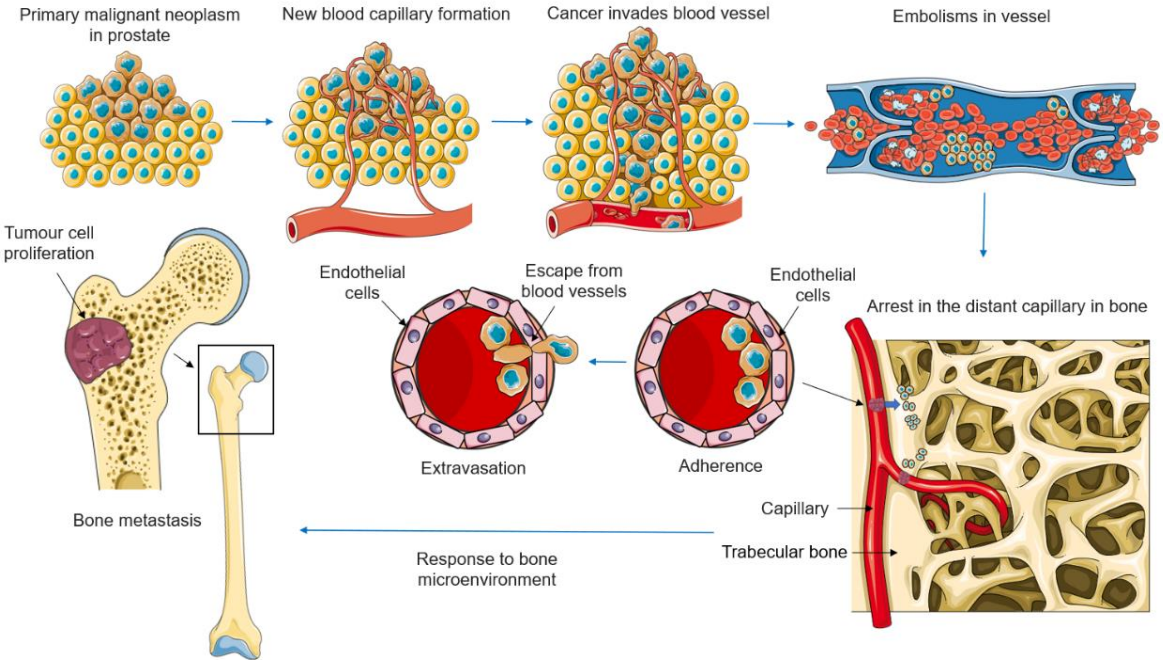

Figure 1.2: Process of PCa bone metastasis. The primary malignant neoplasm originates in the prostate, leading to the promotion of new blood vessel formation. PCa cells invade these blood vessels and transport the cancer cells to capillary beds in the bone. Over time, clusters of tumour cells and other blood cells combine to form embolisms that eventually lodge in distant capillaries within the bone. Cancer cells can enhance their adherence to vascular endothelial cells to facilitate their escape from blood vessels and spread throughout the bone. Once the cancer cells have established themselves in the bone, they are exposed to the various factors present in the bone microenvironment that promote tumour growth and ultimately result in bone metastasis (Mundy, 2002). All elements in the figure were generated from Smart, an online Servier medical art with copyright free (https://smart.Servier.com/).

1.3 Seed and soil hypothesis

In 1889, the English surgeon Stephen Paget proposed the famous hypothesis called “seed and soil” for the first time (Paget, 1889). The seed and soil hypothesis suggests that when a plant goes to seed, its seeds can be dispersed in various directions, but they can only germinate and thrive in suitable soil. This hypothesis has been applied to cancer research, and studies have revealed that the characteristics of cancer cells, or "seeds," play a crucial role in tumour progression and outgrowth. Additionally, the elements of the "soil," such as the microenvironment of distant organs, including bone, are also believed to play a vital role in promoting colonization and facilitating the outgrowth of metastases. Therefore, both the characteristics of cancer cells and the microenvironment of the distant organ play significant roles in the development and progression of cancer (Liu et al., 2017). However, the pathophysiology of bone metastasis is complex, and the process involves a significant number of different cell populations and several regulatory proteins (Langley and Fidler, 2011).

1.4 Mechanisms of bone metastasis

As mentioned above, PCa bone metastasis can occur as either osteolytic or osteoblastic, depending on the characteristics of the cancer cells. The formation of osteoblastic lesions in the bone typically characterizes PCa bone metastases. This happens when tumour cells spread from the prostate and migrate to the bone, where they can establish new metastases (Mundy, 2002). Several mechanisms have been proposed to explain the occurrence of PCa. (1) Direct invasion: cancer cells directly invade bone tissue through physical aggression or by secreting enzymes that break down the bone (Gato et al., 2022). (2) Hematogenous spread: cancer cells spread to bones through the bloodstream (Suva et al., 2011b). (3) Recruitment of bone-residing cells: bone-residing cells such as osteoclasts or osteoblasts are recruited by cancer cells helping them to establish within the bone. (4) Bone microenvironment: based on the "seed and soil" hypothesis, the characteristics of the "seed" (cancer cells) and the "soil" (microenvironment) play critical roles in the establishment and progression of

cancer in bone (Yoneda and Hiraga, 2005). (5) Immunological factors: cancer cells evade the host's immune system and survive in the bone marrow niche (Capietto and Faccio, 2014). (6) Metabolic rewiring: cancer cells adapt to the metabolic conditions in the bone microenvironment in order to survive and grow (Flombaum, 2000). It is widely accepted that all these mechanisms may coincide and contribute to bone metastasis (Suva et al., 2011a, Coleman et al., 2020).

1.4.1 Bone cells

Figure 1.3 identifies four distinct cell types within bones. These bone cells collaborate to maintain the structure and mineral composition of both the compact and spongy bone layers (Florencio-Silva et al., 2015).

First, osteoblasts are cuboidal cells arranged in a densely packed layer along the bone surface. They account for 4-6% of all bone cells, and their primary function is to form new bone tissue. These cells secrete various substances, including collagen, proteins, and calcium salts. When combined, these materials create the bone matrix, a complex framework that provides support to the bones' structure. Second, osteocytes which constitute most (90-95%) of the cells in bone tissue. Osteocytes are, in fact, mature osteoblasts that have been encased and immobilized by the materials that they have generated and excreted. These mature bone cells have a long lifespan of up to 25 years. Third, osteoclasts whose primary function is to dissolve and reabsorb bone tissue. They are found on the surface of bone tissue and originate from white blood cells (monocytes and macrophages) rather than other bone cells. Osteoclasts are constantly engaged in breaking down and reabsorbing old bone tissue, while osteoblasts are involved in the formation of new bone tissue. The combined actions of these two types of cells are responsible for regulating the gradual reshaping of the bones. Forth, bone lining cells that cover inactive (non-remodelling) bone surfaces. They are thinly extended over bone surfaces possessing flat or slightly ovoid nuclei. Bone lining cells are responsible for preparing the surface of the bone by removing

non mineralised collagen fibrils through matrix metalloproteinases (Florencio-Silva et al., 2015, Del Fattore et al., 2012).

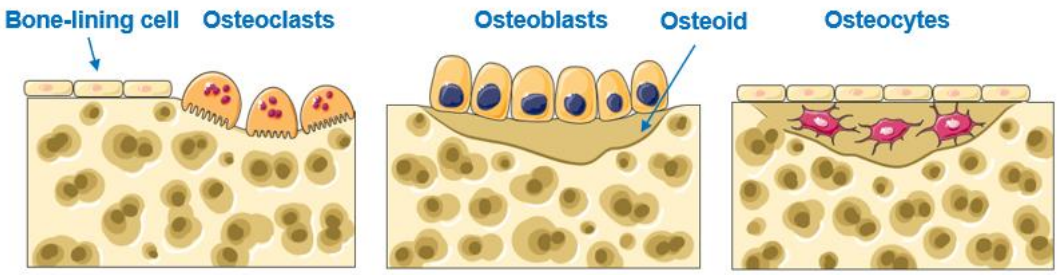

Figure 1.3: Distribution of bone cells. There are four different types of bone cells from left to right in the figure: bone-lining cells, osteoclasts, osteoblasts and osteocytes (Florencio-Silva et al., 2015). All elements in the figure were generated from Smart, an online Servier medical art with copyright-free (https://smart.Servier.com/).

1.4.2 Bone remodelling

The maintenance of bone health relies on the highly complex process of remodeling, which replaces old bone with new bone. This process is divided into three phases: resorption, transition, and formation. The process begins with bone resorption by osteoclasts, which recruit hematopoietic stem cells to specific areas of the bone surface, leading to the differentiation of these cells into pre-osteoclasts and ultimately mature osteoclasts that can resorb bone. This is followed by the transition (or reversal) phase, when resorption switches to new bone formation which is the final phase and is regulated by osteoblasts. This process is orchestrated through the coordinated actions of osteoclasts, osteoblasts, osteocytes, and bone lining cells (Florencio-Silva et al., 2015) (Figure 1.4).

Both systemic and local factors play crucial roles in the regulation of bone remodeling. Systemically, major regulators such as parathyroid hormone (PTH), calcitriol, and

various hormones including growth hormone, glucocorticoids, thyroid hormones, and sex hormones affect bone remodeling. Additionally, factors like insulin-like growth factors (IGFs), prostaglandins, tumour growth factor-beta (TGF-β), bone morphogenetic proteins (BMP), and cytokines contribute to this process. On the local level, a multitude of cytokines and growth factors have been recently discovered to impact bone cell functions. Moreover, the RANK/receptor activator of NF-kappa B ligand (RANKL)/osteoprotegerin (OPG) system tightly couples bone resorption and formation, allowing for a synchronized wave of bone formation to follow each cycle of bone resorption, thereby maintaining skeletal integrity (Hadjidakis and Androulakis, 2006).

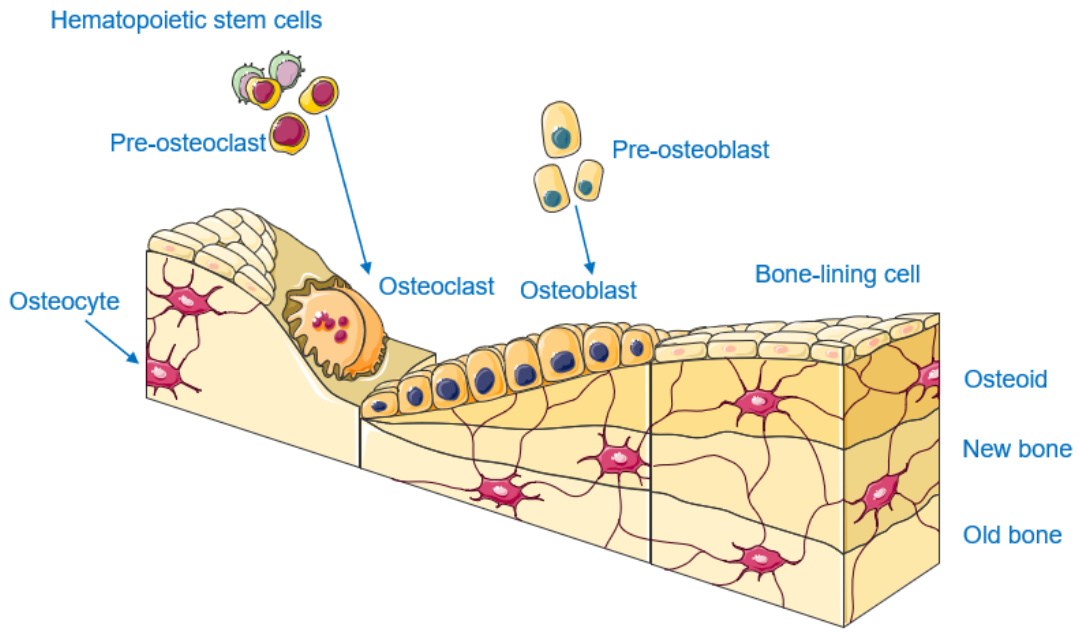

Figure 1.4: Bone remodelling model. The initial step in bone remodelling involves the activation of osteoclasts to initiate bone resorption. This is followed by a transitional period where the resorbed old bone is replaced with new forming bone. Ultimately, the creation of new bone is achieved through the action of osteoblasts (Florencio-Silva et al., 2015). All elements in the figure were generated from Smart, an online Servier medical art with copyright-free (https://smart.Servier.com/).

1.4.3 Hormones in bone remodeling

Regulatory hormones play a crucial role in bone remodeling. Key hormones involved in influencing mineral supply, monitoring blood levels, and maintaining bone homeostasis include PTH, calcitriol, calcitonin, sex hormones, growth hormones, thyroid hormones, cortisol, insulin and leptin (Tommy, 2004). The calciotropic hormone PTH is an endocrine remodeling signal generated to maintain calcium homeostasis (Raggatt and Partridge, 2010). In the bone microenvironment, PTH activates a seven-transmembrane G-protein-coupled receptor, the PTH receptor, on the surface of osteoblastic cells (Jüppner et al., 1991). This calcium-regulating hormone controls the level of calcium in the blood and stimulates both resorption and formation of bone (Tommy, 2004). Calcitonin prevents excessive blood calcium levels by inhibiting bone turnover and reabsorption. Vitamin D acts through the immature osteoblast to stimulate osteoclastogenesis (Baldock et al., 2006). Direct estrogen effects on osteocytes, osteoclasts, and osteoblasts lead to inhibition of bone remodeling, decreased bone resorption, and maintenance of bone formation, respectively (Khosla et al., 2012). Calcitriol is required for calcium absorption and involved in calcium regulation (Tommy, 2004). Thyroid hormones are required for skeletal maturation and adult bone maintenance. Excessive levels of cortisol can inhibit bone growth and contribute to glucocorticoid-induced osteoporosis (Tommy, 2004). Insulin plays a role in bone growth and regulates both bone formation and resorption. Leptin is a hormone that has direct and indirect effects on bone metabolism (Tommy, 2004) (Carter and Schipani, 2006). These hormones interact in complex ways to maintain bone health and balance.

1.4.4 Osteoblasts in bone metastasis

In PCa, bone metastases are frequently osteoblastic (Mundy, 2002). Prostate carcinomas have a tendency to develop in the skeletal system as a result of communication between the bone microenvironment and tumour cells. The bone offers various chemotactic factors, adhesion factors, and growth factors that enable prostate carcinoma cells to specifically target and multiply within the skeleton. In turn,

the prostate carcinoma cells produce osteoblastic and osteolytic factors that influence the process of bone remodelling. The resultant osteolysis caused by prostate carcinomas promotes the release of numerous growth factors present in the extracellular matrix of the bone, thereby intensifying the advancement of metastases.(Keller et al., 2001). Therefore, understanding these processes' mechanisms will explain the predilection of PCa for bone. Furthermore, it will provide new approaches to develop preventive agents or more effective therapies for PCa.

In 2005, Logothetis and Lin published an article in Nature, which provided insight into the role of osteoblasts in the formation of a tumourigenic microenvironment. Their findings suggested that interactions between PCa cells and osteoblasts played a crucial role in developing bone metastases in PCa, inducing the osteoblastic phenotype. Osteoblast-derived factors were found to contribute to PCa cells growth. Additionally, factors produced by PCa cells could alter the normal functional balance between osteoblastic and osteoclastic activities in the bone microenvironment, leading to the development of osteoblastic metastases. Moreover, osteoblasts could secrete factors that positively contribute to PCa cells metastasis in bone (Logothetis and Lin, 2005, Vakar‐Lopez et al., 2004, Zhang et al., 2002).

PCa can secrete paracrine factors that influence bone homeostasis that regulates osteoblast proliferation or differentiation (Logothetis and Lin, 2005). Transforming growth factor-β (TGF-β) is a family of pleiotropic growth factors highly associated with cancer progression. Bone morphogenetic protein (BMP) and TGF-β belong to the TGF-β superfamily. BMPs serve various functions in bone, including apoptosis, differentiation, proliferation, and morphogenesis (Vela et al., 2007). BMP-2 and BMP-6, in particular, enhance the invasive ability of PCa cells *in vitro*, potentially impacting the bone microenvironment (Dai et al., 2005). While, there is no direct effect on PCa cell proliferation of BMP-2, BMP-4, BMP-6, and BMP-7 (Dai et al., 2005). Dysregulated TGF-β signaling triggers a series of events that contribute to oncogenesis, such as increased proliferation, decreased apoptosis, epithelial-to-mesenchymal transition (EMT), and evasion of immune surveillance (Cao and Kyprianou, 2015). There are three well-known mammalian isoforms of TGF-β (TGF-β1, -β2, and -β3) that share

significant homology and similar functions (Lee et al., 2014). Insulin-like growth factor (IGF) regulates proliferation, differentiation, apoptosis inhibition, and cell cycle progression. IGF-I stimulates the expression of cyclin D1, enhancing cell cycle progression. Additionally, IGF-I also functions in inhibiting the apoptotic pathway. IGFs also play a role in tumour angiogenesis and cell migration (Gennigens et al., 2006). Fibroblast growth factor (FGF), FGF-8 is frequently overexpressed in prostate cancer and is associated with bone metastasis. FGF-8 affects both osteoblast and osteoclast differentiation (Valta et al., 2008). Platelet-derived growth factor (PDGF) and vascular endothelial growth factor (VEGF) effect on increase PCa cell proliferation (Logothetis and Lin, 2005, Li and Cozzi, 2007). The factors produced by PCa cells affect bone formation mainly through aiming osteoblasts (Wong et al., 2019).

1.4.5 Osteoclasts in bone metastasis

Similar to other cancers' metastasis to bone, in PCa, cancer cells stimulate osteoclasts to release factors and cytokines to resorb bone. The most essential factor is RANKL, which belongs to the TNF cytokine superfamily (Ono et al., 2020). The function of RANKL is to regulate osteoclast formation, activation, and survival in both normal bone modelling/remodelling and various pathological conditions, including tumour progression, which leads to increased bone turnover via RANKL signalling. Conversely, osteoprotegerin (OPG) protects bone from excessive resorption by binding to RANKL and preventing it from binding to receptor activator for nuclear factor kappa-B (RANK) (Boyce and Xing, 2008). This released factor stimulates bone resorption, which creates a favourable microenvironment for tumour growth and promotes the development of osteolytic lesions. As such, the activation of osteoclasts is believed to play a significant role in the development and progression of bone metastasis in PCa (Jin et al., 2011, Wong et al., 2019).

1.4.6 Main factors in the remodelling process in bone

The remodelling process in bone involves the coordinated activity of two types of bone cells: osteoblasts and osteoclasts. Osteoblasts are responsible for the formation of new bone, while osteoclasts are responsible for the resorption of old bone tissue. Factors that affect the process of bone remodelling are shown in Figure 1.5. A variety of signals and growth factors, including WNT signalling, BMP, TGF-β, IGF, PDGF, FGF and VEGF regulate this process. In the bone remodelling process, growth factors stimulate the differentiation of osteoblasts, which lay down new bone surfaces. WNT signalling can promote osteoblast differentiation (Logothetis and Lin, 2005). Osteoblasts also play a role in stimulating osteoclast differentiation and maturation. This occurs through the release of RANKL, which binds to the receptor activator of RANK on the surface of pre-osteoclasts. Osteoblasts also release macrophage colony-stimulating factor (M-CSF), which promotes osteoclast proliferation (Sims and Gooi, 2008). Osteoprotegrin is a decoy receptor for RANKL, which can inhibit

osteoclastogenesis by binding to RANKL and preventing it from binding to RANK on the surface of pre-osteoclasts. This helps regulate the balance between osteoblast and osteoclast activity in bone remodelling (Sims and Gooi, 2008).

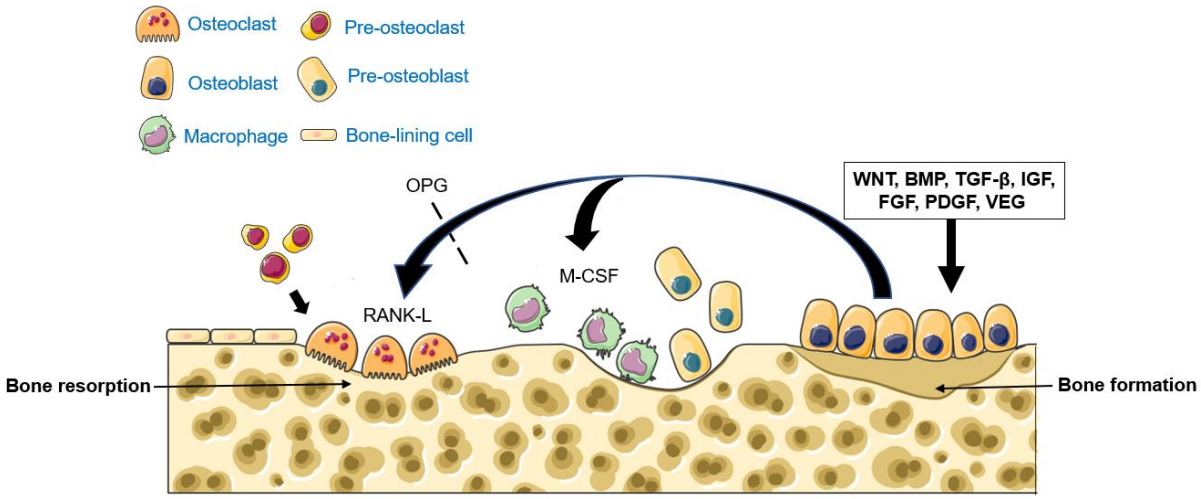

Figure 1.5: A simplified diagram of factors affecting the remodelling process in bone. Varies factors and WNT signalling stimulate osteoblast differentiation, leading to the formation of new bone. Osteoblasts also stimulate osteoclast differentiation and maturation through the release of RANKL. The proliferation of osteoclasts is also promoted by the release of macrophage colony-stimulating factor (M-CSF) (Logothetis and Lin, 2005). All elements in the figure were generated from Smart, an online Servier medical art with copyright-free (https://smart.Servier.com/).

1.5 Therapy of PCa bone metastasis

The USA Food and Drug Administration (FDA) has approved two classes of anti-resorptive agents to prevent skeletal-related events (SREs) in patients with established bone metastases. These include amino bisphosphonates (zoledronic acid and ibandronate), and denosumab, a fully human anti-RANKL monoclonal antibody (Fizazi et al., 2011, Hofbauer et al., 2021). Bone-targeted radioisotopes radium-223 treatment has also been approved by FDA, which is commonly used in men with

castration-resistant PCa (CRPC) and symptomatic bone metastases (Table 1.3) (Hofbauer et al., 2021). The summary information of each therapy for PCa bone metastases is shown in Table 1.3.

Bisphosphonates have been utilized to alleviate bone complications in patients with multiple myeloma. These drugs have also been investigated in clinical trials and have demonstrated efficacy in reducing skeletal complications and improving survival rates in both animal models and human patients (Farrell et al., 2018). Bisphosphonates have been shown to possess anti-tumour effects through three primary mechanisms. Firstly, they inhibit bone resorption, which can indirectly affect the growth and development of tumours in the bone. Secondly, they can directly affect tumour cells by impeding the growth of bone metastases in breast cancer patients. Lastly, they are believed to modulate the immune system and impact macrophages (Melani et al., 2007, Diel et al., 1998, Oades et al., 2002).

Denosumab exhibits strong anti-resorptive properties by neutralizing the receptor activator of nuclear factor RANKL, which inhibits osteoclast function at various stages, such as their differentiation, activation, and survival (Boyle et al., 2003). Clinical trials have reported that the efficacy of denosumab in treating bone metastasis in patients was induced by either PCa (Fizazi et al., 2011) or breast cancer (Stopeck et al., 2010). Denosumab has also been reported to be used in clinical trials. A study published in The Lancet analyzed the effects of denosumab on bone-metastasis-free survival in men with PCa. The study randomly assigned 1432 patients into two groups, with 716 receiving denosumab treatment and the other 716 receiving placebo. The results indicated that denosumab significantly delayed the time to the first bone metastasis and increased bone-metastasis-free survival time. However, the treatment did not affect the final survival rate of the patients (Fizazi et al., 2011). In a randomized, double-blind study, denosumab demonstrated superiority over zoledronic acid in delaying or preventing skeletal related events (SREs) in patients with breast cancer metastatic to bone. In addition, denosumab was generally well tolerated and offered the convenience of subcutaneous injection without requiring renal monitoring. As such,

denosumab presents a promising treatment option for patients with bone metastases (Stopeck et al., 2010).

Various radiation therapies are available for managing cancer and associated bone pain, such as radium-223. Although these treatments do not eradicate all cancer cells or provide a cure, they effectively alleviate bone pain and decelerate cancer growth (Parker et al., 2013). These radioisotopes are administered into the bloodstream, where they travel and accumulate in the bone tissue. Once the isotopes reach the bone metastases, they emit radiation, which selectively targets and damages the cancer cells while minimizing damage to healthy tissues. This is because bone tissue is particularly receptive to radiation therapy, allowing the radiation to be absorbed preferentially by the bone tissue, with less radiation being absorbed by surrounding healthy tissue. This approach can help to effectively treat bone metastases while minimizing the side effects that may occur from radiation therapy. In a clinical trial, 921 men with symptomatic CRPC and bone pain but limited nodal and no visceral metastases were given radioisotope therapy. Compared to placebo, radioisotope therapy alleviated bone pain and reduced the risk of skeletal-related events (such as fractures) in patients with PCa that has spread to the bones (Parker et al., 2013, He et al., 2022, Uccelli et al., 2022).

Table 1.2: Therapies for PCa bone metastases

Agents	Molecular target	Mechanism
Bisphosphonates	Farnesyl diphosphate Synthase	Inhibit osteoclast activity and tumour cell homing to the bone.
Denosumab	RANKL	Inhibits osteoclast differentiation and activation.
Radium-223	/	Cytotoxicity against PCa cells adjacent to areas of increased bone turnover and osteoblastic activity in osteosclerotic lesions.

1.6 Purinergic signalling

Purinergic signalling is a type of extracellular signalling that is mediated by purine nucleotides and nucleosides. These signals are transmitted through purinergic receptors, which are membrane receptors that mediate various physiological functions in response to the release of ATP or adenosine. There are three known distinct classes of purinergic receptors, which are called P1, P2X, and P2Y receptors (Praetorius and Leipziger, 2010, Eltzschig et al., 2012).

1.6.1 Purinergic receptors

Purinergic receptors can be classified into two groups, P1 and P2 receptors (also known as P1R and P2R). The P1R, also referred to as adenosine receptors, is a group of purinergic G protein-coupled receptors activated by adenosine as the endogenous ligand. In humans, there are four different types of adenosine receptors, which are A_1, A_{2A}, A_{2B} and A_3 receptors (Fredholm et al., 2001). P2R can be divided into two subclasses, namely P2X and P2Y receptors. P2X receptors are ionotropic receptors that function as ligand-gated ion channels. On the other hand, P2Y receptors are metabotropic receptors that are G-protein coupled. P2X receptors are non-selective membrane cation channels that are activated by extracellular ATP (Surprenant and North, 2009). These channels allow Na^+, K^+, and Ca^{2+} ions through the cytomembrane (Gallagher, 2004).

P2R is expressed in various immune and non-immune cells throughout the body. The P2 family consists of fifteen different receptors. The International Union of Pharmacology Committee on Receptor Nomenclature and Drug Classification recognises eight distinct P2YR subtypes, which are P2Y1, P2Y2, P2Y4, P2Y6, P2Y11, P2Y12, P2Y13, and P2Y14 receptors (Abbracchio et al., 2006) and seven P2X subtypes (P2X1 to 7 receptors) that are mainly ATP receptors. Being a vital component in providing energy for everyday life, ATP is also considered to have significant biological functions. It is suggested that ATP play its functional roles through

binding to ATP-binding receptors such as P2R. These receptors are widely distributed in tumour cells and the tumour microenvironment, as well as the central and peripheral nervous systems (Vickers, 2017).

1.7 Introduction of P2X4R

1.7.1 Definition and structure of P2X4R

The P2X4R is composed of three subunits, and each subunit has two transmembrane domains (TMs) linked by a large loop and intracellularly located N- and C-termini (Pelegrin et al., 2008) (Figure 1.6). When the P2X receptor is activated by ATP, it promotes subunit rearrangement, leading to the opening and closing of the ion channel. This allows for the influx of calcium (Ca^{2+}) and sodium (Na^{+}) ions, while also allowing for the efflux of potassium (K^{+}) ions. (Kawate et al., 2009b).

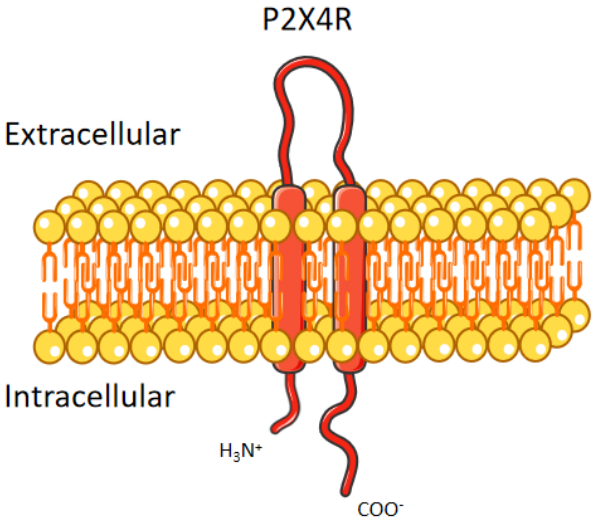

Figure 1.6: Structure of P2X4R. P2X4R are ATP-gated cation channels with only two TMs, called the N-and C-termini. This channel allows Ca^{2+}/Na^{+} influx and K^{+} efflux (Pelegrin et al., 2008). All elements in the figure were generated from Smart, an online Servier medical art with copyright-free (https://smart.Servier.com/)

1.7.2 Downstream signalling pathway of P2X4R

The activation of P2X4R channels in the plasma membrane by ATP leads to the influx of cations (Na+ and Ca2+), causing membrane depolarisation and activating downstream signalling pathways such as the regulation of neurotransmitter release in neurons (Neher and Sakaba, 2008) and microglial functions (Farber and Kettenmann, 2006). Activation of P2X4R has also been linked to the release of a crucial microglia-neuron signalling molecule called BDNF from microglia via the activation of p38 mitogen-activated protein kinase (MAPK) (Ulmann et al., 2010, Ulmann et al., 2008). In some cell types, peripheral macrophages can also express P2X4R which may contribute to pain pathways by releasing prostaglandin E2 (PGE2). PGE2 is a key molecule that plays a vital role in the activation, development, movement, and release of various immune cells, particularly those involved in innate immunity, such as macrophages. The PGE2 release is suggested to cause hypersensitivity in peripheral nociceptive pathways during inflammatory pain (Basbaum et al., 2009). It has also been proved that the P2X4R protein is primarily expressed in the epithelial and immune cells of the prostate (Maynard et al., 2022). P2X4R also plays a role in cancer's phosphatase and tensin homolog (PTEN) and leucine rich repeat protein phosphatases (PHLPP) crosstalk. In a study, P2X4R was downregulated by siRNA transfection in human embryonic kidney 293 cells (HEK293), which blocked the effect of PHLPP overexpression on the level of PTEN. This suggests that P2X4R may be involved in the regulation of PTEN by PHLPP (Ghalali et al., 2020). The researchers also found that TGFβ-1 enhanced the PHLPP levels, consistent with the observations of other researchers and that P2X4R played a crucial role in invasiveness induced by TGFβ-1 and in EMT. (Ghalali et al., 2020). Furthermore, a study conducted by Maynard in 2022 showed that cancer tissues in patients' samples lacking PTEN protein expression had significantly higher levels of P2X4R than those with normal levels of PTEN (Maynard et al., 2022).

1.7.3 P2X4R function in cancer cells

P2X4R are a subtype of ionotropic adenosine triphosphate receptors, which play an essential role in tumourigenesis. Evidence suggests P2X4R are involved in developing many cancer types including PCa (He et al., 2020), breast cancer (Chadet et al., 2022), glioma (Huo and Chen, 2019), colon tumour (Schmitt et al., 2022), and brain tumour (Guo et al., 2004). Recently, a study demonstrated that P2X4R is overexpressed in breast cancer biopsies from patients. The P2X4R promotes mammary cancer progression by sustaining autophagy and associated mesenchymal transition (Chadet et al., 2022). In addition, P2X4R has been shown to be highly expressed in all glioma cell lines (Huo and Chen, 2019). P2X4R has involved in glioma cell growth and apoptosis, making it a potential target for therapy (Huo and Chen, 2019). An animal study using rats as an experimental model system called C6 glioma for glioblastoma multiforme (GBM) demonstrated that the P2X4R was highly expressed in all areas of the tumour model (Guo et al., 2004). Activation of P2X4R has been shown to prevent apoptosis in colon cancer cells. (Schmitt et al., 2022). Moreover, a clinical study showed that P2X4R expression was significantly upregulated in lymphocytic leukaemia, and its expression level decreased effectively after treatment (Burnstock and Di Virgilio, 2013). Regarding P2X4R's functional role in the process of tumour development, most studies suggest that P2X4R may play a role in the development and progression of cancer, making it a potential target for therapy.

In addition, P2X4R is found to be widely expressed in diverse physiological processes, such as synaptic transmission (Kawate et al., 2009a), inflammation (Paalme et al., 2019), central nervous system (CNS) disorders (Stokes et al., 2017)**,** and gustation and nociception (Zhang et al., 2019). There was limited evidence of the relationship between inflammation in P2X4R and cancer progression. Research has shown a proinflammatory role of P2X4 purinergic receptors in hepatobiliary carcinoma that affects tumour formation (Asif et al., 2019).

1.7.4 P2X4R and PCa

Maynard et al. (2022) conducted a study that explored the relationship between P2X4R and PCa. They found that P2X4R is overexpressed in PCa tissues, particularly in epithelial and immune cells such as macrophages (mainly CD68+ macrophages) and neutrophils (mainly CD66+ neutrophils). The analysis of 491 PCa patients' cases showed elevated P2X4R expression in cancer compared to benign tissue, in prostatic intraepithelial neoplasia, and PCa cases with ERG positivity or PTEN loss. The study also showed that inhibiting P2X4R by antagonist 5-BDBD significantly decreased viability, migration, and invasion in PCa cell lines. Knocking down P2X4R attenuated PCa cells growth, migration, and invasion *in vitro*. In addition, knocking down P2X4R in Myc-CaP cells (using mouse PCa cells *in vivo*) resulted in significantly attenuated subcutaneous allograft growth in FVB/NJ mice ($p < 0.0001$). In conclusion, their data proved that P2X4R plays a vital role in PCa aggressiveness (Maynard et al., 2022).

1.8 The xenograft model *in vivo*

To understand the function of P2X4R in PCa metastasis progression, the translational xenograft model is vital in improving the understanding of the advanced PCa in this research. The first immunodeficient nude mouse model was reported in 1966. These mice lack body hair and a thymus gland, which means they cannot generate mature T lymphocytes and cannot elicit an adaptive immune response (SP'Nude, 1966). In 1983, severe combined immunodeficiency (SCID) mice were generated in the USA, and these mice have impaired differentiation of both T and B lymphocytes (Namekawa et al., 2019, Bosma et al., 1983). BALB/c nude mice were first generated in New York in 1920 and are now widely used in cancer research with animals. These mice have a strong inhibition of the immune system and a significantly reduced number of T-cells, making them useful for xenograft models in human cancer research (Flanagan, 1966).

The most widely utilized tool in PCa research is the use of human PCa cell lines transplanted into mice, referred to as xenograft or xenotransplantation. Recently, three

modes of xenograft have been employed, including subcutaneous, orthotopic, and subrenal capsule models. In subcutaneous injection, PCa cells are injected under the murine skin, while orthotopic injection directly delivers cancer cells to the prostate gland. The subrenal capsule is a new model that allows tumours to be implanted under the kidney capsule of immunocompetent murine animals (van Weerden and Romijn, 2000). Panels of human tumour xenografts implanted subcutaneously in nude mice are commonly used to screen anti-cancer drugs (Cunningham and You, 2015). Subcutaneous, intravenous, intraperitoneal injections of prostate tumour cells in the nude mouse have rarely resulted in metastases (van Weerden and Romijn, 2000) while intracardiac and orthotopic injections have led to developing PCa metastasis in the animals (Saar et al., 2015). The orthotopic model focuses on the primary tumour and local invasion and is suitable for studying distant metastasis, but it is rare for bone metastasis to occur in this model. On the other hand, the subrenal capsule model is a predominantly primary and local invasion xenograft mouse model that may be useful for studying distant metastasis (Lin et al., 2014). However, there are some limitations to these models. For example, the local microenvironment in these models may not be similar to the prostate microenvironment, which makes them unsuitable for studying metastasis (Lin et al., 2014). Another model involves injecting cells into the tail vein to encourage the development of bone metastases, but this method is challenging due to the fragility of the mouse tail vein (Geldof and Rao, 1990).

Intracardiac injection is the most commonly used method for studying PCa metastases to bone. The effectiveness of this approach is thought to be due to the tumour cells by passing the lung capillaries and being directly injected into the left ventricle of the heart (Berish et al., 2018). This method results in bone metastases that are pathologically more similar to human bone metastases, as the most frequently affected bones are the axial skeleton and spinal column, which are rich in red bone marrow content (Berish et al., 2018, Kuchimaru et al., 2018).

1.9 Preliminary data

Previous research conducted by Dr. Ning Wang and Yuhan Zhou have indicated that P2X4R is the most highly expressed P2R in three different PCa cell lines (PC3, C4-2B4, and LNCaP) as determined by quantitative real-time polymerase chain reaction (qRT-PCR) analysis (Figure 1.7). These findings suggest that P2X4R plays a critical role in the cellular function of these cell lines. Furthermore, inhibiting P2X4R has been shown to reduce both the growth and mobility of PCa cells. To provide evidence of this effect, PC3 and C4-2B4 PCa cell lines were subjected to 5-BDBD and PSB-12062, specific antagonists of P2X4R, and the proliferation and viability levels, and migration were measured, resulting in a significant reduction (Figure 1.8 & 1.9). These data suggest that P2X4R may promote tumour growth in PCa cells, result has been published in 2020 (He et al., 2020).

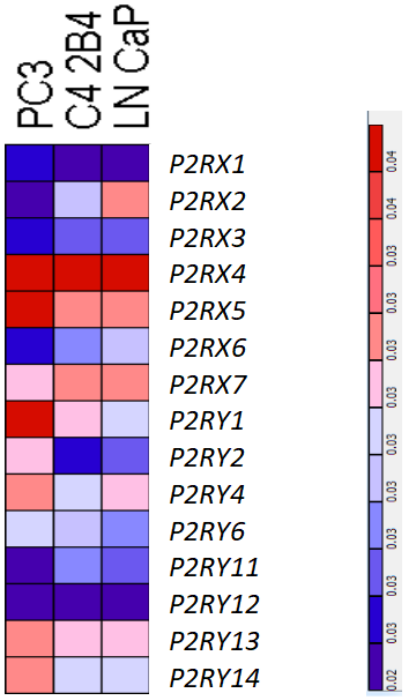

Figure 1.7: The heat map of P2X4R expression level in PCa cells. A gene expression heatmap generated based on qRT-PCR data showed that, when compared to other P2XRs and P2YRs, P2X4R expression is far higher than the other P2 receptors (He et al., 2020).

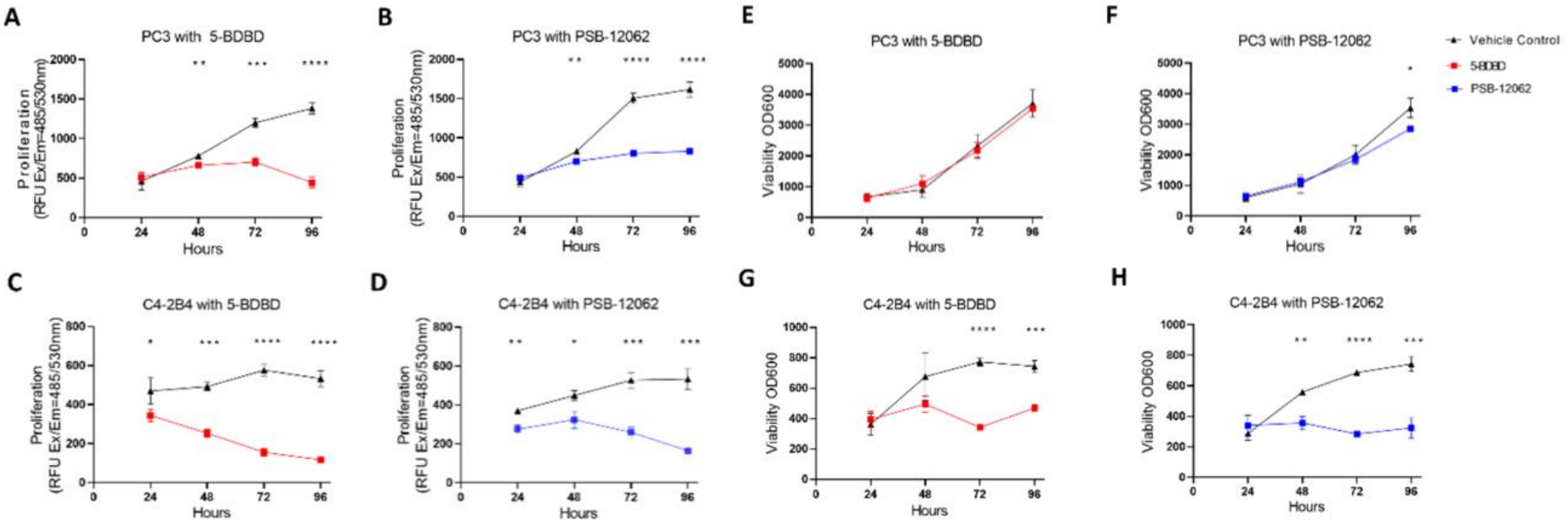

Figure 1.8: Inhibition of P2X4R significantly reduces proliferation and viability in PCa cells. Figure A-D represented the cell proliferation of PC3 and C4-2B4 with antagonists 5-BDBD and PSB-12062. Treatment of PC3 cells with 5-BDBD or PSB-12062 caused a significant reduction of over 60% and around 50%, respectively (Figure A&B). In C4-2B4 cells, treatment with both antagonists resulted in a reduction of approximately 70% in cell proliferation (Figure C&D). Figure E-H represented the cell viability of PC3 and C4-2B4 with antagonists 5-BDBD and PSB-12062. Inhibition of P2X4R resulted in significantly reduced cell viability in C4-2B4 by approximately 50% with two antagonists (Figure E&F); however, it did not affect PC3 (Figure G&H) (He et al., 2020).

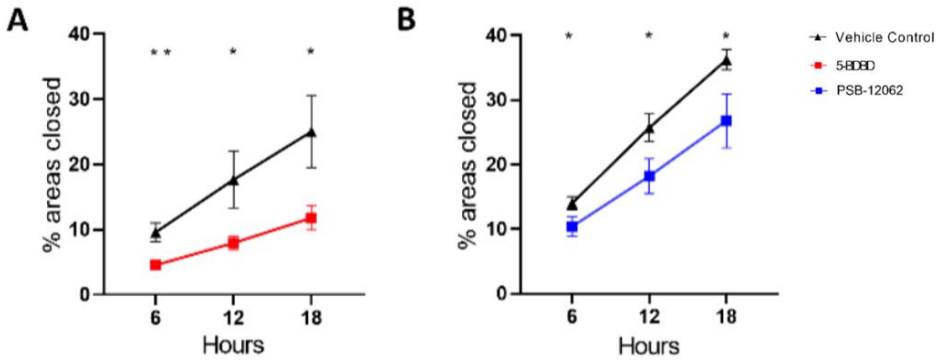

Figure 1.9: Inhibition of P2X4R reduce migration in PC3. Treatment of PC3 cells with 5-BDBD resulted in a reduction of approximately 50% in cell migration and around 30% reduction with PSB-12062 (He et al., 2020).

1.10 Hypothesis and objectives

As a major cause of male cancer deaths, with high morbidity due to its tendency to spread to the lymph nodes and bone, bone metastatic PCa with a low 5-year survival rate remains in urgent need for effective therapies. The high level of P2X4R expression in bone metastatic PCa indicates further research on its mechanisms of contribution to the progression of PCa in bone metastasis, offering the potential to be targeted in therapeutic intervention.

Previous findings indicating P2X4R as the most highly expressed P2 receptor in PCa cells and its significant involvement in cell proliferation, viability, and migration, resulted in the development of **the hypothesis that P2X4R has a pro-tumourigenic role in PCa cells**. Accordingly, six specific objectives were defined to test that hypothesis.

Objective 1 aims to determine the cellular changes of inhibiting P2X4R in PCa using agonist or antagonist, including calcium influx, migration, invasion, and apoptosis. (Chapter 3)

Objective 2 is to examine the consequence of P2X4R inhibition in PCa cells *in vivo* using a subcutaneous xenograft model. (Chapter 3)

Objective 3 involves genetically knocking out P2X4R in PCa cells using the CRISPR/Cas9 technology. (Chapter 4)

Objective 4 aims to determine the cellular changes induced by P2X4R knockout in PCa cells, including cell proliferation, migration, invasion, and apoptosis. (Chapter 5)

Objective 5 will determine whether genetic depletion of P2X4R affects PCa cells metastasis to the bone *in vivo*, using an intracardiac xenograft mouse model. (Chapter 5)

Objective 6 aims to examine the transcriptional alterations in P2X4R-deficient PCa cells using RNA-Seq bioinformatics analysis. (Chapter 6)

This project was conducted in four main steps: (1) P2X4R was inhibited in PCa cell lines PC3 and C4-2B4 by two P2X4R specific antagonists 5-BDBD and PSB-12062, followed by a series of *in vitro* and *in vivo* assays to understand the P2X4R function in PCa. (2) Genetically modified gene P2XP4 knockout PC3 cells were produced by CRISPR/Cas9 technology. (3) To understand the function of P2X4R in PCa bone metastasis, a series of *in vitro* assays were conducted using both the PC3 WT and P2X4R KO cells. In addition, an intracardiac xenograft mouse model was used to investigate the effects of P2X4R deficiency on PCa bone metastasis. (4) Finally, RNA-seq was performed to understand the transcriptional alterations resulting from P2X4R deficiency in PCa cells.

To depict the workflow of this project, a process diagram was created (Figure 1.10).

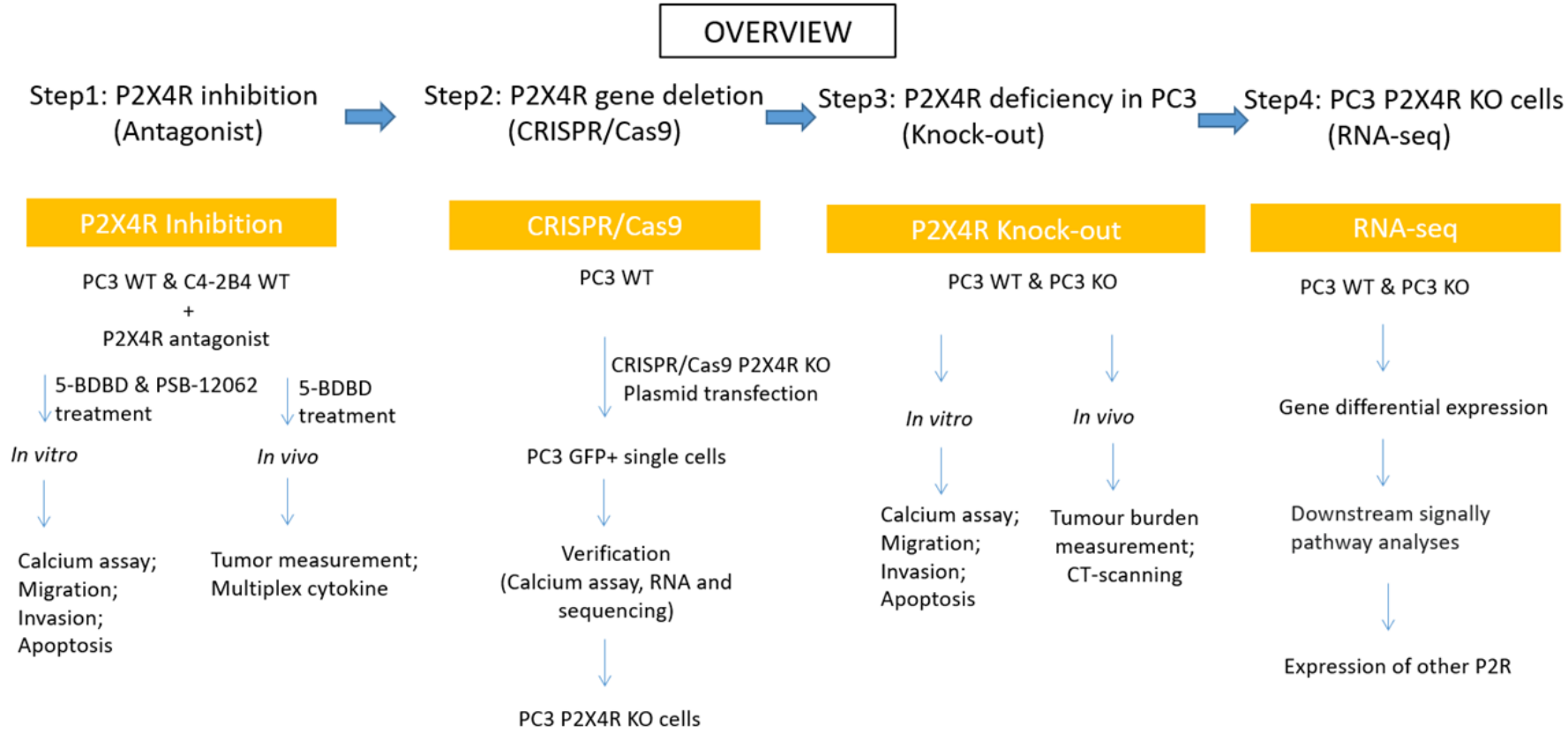

Figure 1.10: General project workflow. The project involves four main steps. In Step 1, P2X4R was inhibited by specific antagonists 5-BDBD and PSB-12062 in PC3 and C4-2B4 cells. *In vitro* assays included calcium influx, migration, invasion, and apoptosis, while *in vivo* assays included tumour measurement and multiplex cytokine assay. In Step 2, P2RX4 was genetically knocked out using the CRISPR/Cas9 system. The knock-out cells were verified using calcium influx, RT-PCR, and DNA sequencing. In Step 3, a series of *in vitro* and *in vivo* assays were performed using the P2X4R KO PC3 cells to investigate the role of P2X4R in PCa bone metastasis. *In vitro* assays included calcium influx, proliferation, viability, migration, invasion, and apoptosis measurement, while *in vivo* assays included tumour burden measurement and bone marrow CT-scan. In Step 4, RNA-seq analysis was performed to investigate the gene expression changes resulting from P2X4R depletion. The study included gene ontology and comparisons of other P2R expression levels.

CHAPTER 2:

MATERIALS & METHODS

2.1 Tissue culture

2.1.1 Cell lines

The PCa cellular models used in this project and their characteristics are summarized in Table 2.1.

Table 2.1: Cell lines used in this project

Cell lines	Description	Androgen-sensitivity	Bone metastasis type	Source	References
PC3	The PC3 cell line was first separated in 1979 from bone metastasis of PCa in a 62-year-old Caucasian male. PC3 cells have high metastatic potential compared to other PCa cells, such as DU145 cells (with moderate metastatic potential) and to LNCaP cells (with low metastatic potential).	Androgen-insensitive	Osteolytic	ATCC Corporation (Manassas, Virginia, USA)	(Pulukuri et al., 2005, Kaighn et al., 1979)
C4-2B4	This cell line was derived from the LNCaP cell line. Its androgen-independence and metastatic osteosclerotic lesions mimics the late stage of PCa. This cell line was transfected with luciferase gene which could able to identify them by bioluminescent techniques.	Androgen-insensitive	Osteoblastic	ATCC Corporation (Manassas, Virginia, USA)	(Thalmann et al., 1994)

2.1.2 Tissue culture maintenance

The cell lines were thawed from a -80°C freezer and then incubated in a 37°C water bath for 30 seconds to recover. They were cultured in T75 flasks using Dulbecco's modified Eagle's medium (DMEM) supplemented with 10% fetal calf serum (FCS) and 1% penicillin-streptomycin (pen-strep) at 37°C and 5% CO2. Cell monolayer confluence was estimated using an Olympus CK2 microscope at 10x magnification (Olympus, Tokyo, Japan). When the cell confluence reached over 80%, they were subcultured at a 1:10 dilution into a new T75 flask.

2.1.3 Cell passaging and counting

To maintain healthy cell cultures and to harvest cells, cell passage was performed when the confluence was greater than 80%. First, the medium from the flask was removed, and the cells were washed twice with 10 mL of phosphate-buffered saline (PBS) buffer. Then, 1 mL of trypsin-ethylenediaminetetraacetic acid (EDTA) was added to the cells and incubated at 37°C for 5 minutes. The cells were then suspended in 9 mL of pre-warmed DMEM and transferred to a centrifuge tube, where they were centrifuged at 1,000 rpm for 5 minutes. Cells were then seeded at a density of 1×10^6 - 2×10^6 cells in each T75 flask, with 10 mL of pre-warmed DMEM added. When a specific cell number was required, cells were counted using a haemocytometer (Thermo Fisher Scientific, Waltham, Massachusetts), as prepared in Figure 2.1. For cell counting, 10 µL of the 10 mL cell suspension was mixed with 10 µL of trypan blue, and the resulting mixture was placed on the haemocytometer. The live, unstained cells in four separated squares were then counted, and the average was multiplied by 10,000 (10^4), as shown in Figure 2.2.

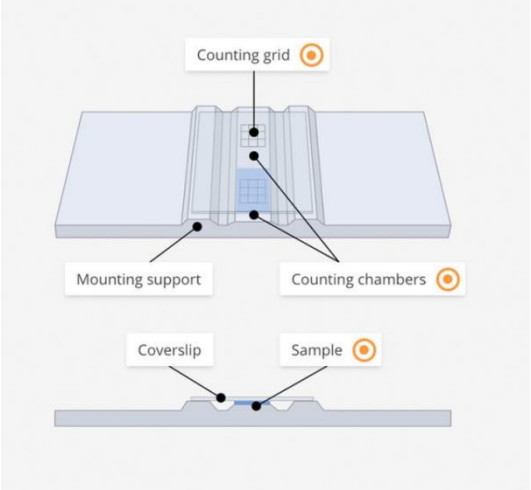

Figure 2.1: Hemocytometer structure. Hemocytometer contains three parts including a counting grid, mounting support and counting chambers. By counting the number of cells that are filled in counting chambers is possible to calculate the number of cells per millilitre volume.

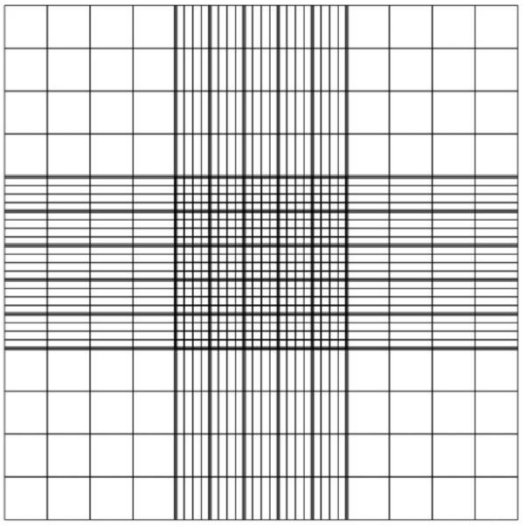

Figure 2.2: Hemocytometer gridlines. Hemocytometer diagram indicating one of the sets of 16 squares that should be used for counting. Count the four corners of the gridlines, average the number, the number of cell each millilitre volume is the average results multiply by 10000.

2.2 Inhibit P2X4R by antagonists *in vitro*

2.2.1 P2X4R antagonists

A range of P2X receptors (P2XR), including P2X4R, have been evaluated for their expression and therapeutic potential, with some studies focusing on the use of P2X4R antagonists (Ase et al., 2015). The most potent P2X4R agonist is TNP-ATP (2'-(or-3')-O-(Trinitrophenyl) Adenosine 5'-Triphosphate, Trisodium Salt), but it can also stimulate other P2XR, such as P2X7R. Therefore, the concentration of TNT-ATP used is critical. Additionally, TNP-ATP has a relatively weak antagonistic effect on P2X4R (Balázs et al., 2013). It is recommended that TNP-ATP be used in low concentrations to selectively stimulate P2X4R while having a weaker effect on other P2XRs.

Among the available P2X4R antagonists, 5-(3-bromophenyl)-1,3-dihydro-2H-benzofuro[3,2-e]-1,4-diazepine-2-one (5-BDBD) has been shown to be effective in calcium assays. Meanwhile, 10-[(4-Methylphenyl)sulfonyl]-10H-phenoxazine (PSB-12062) can inhibit calcium influx mediated by TNT-ATP (Layhadi et al., 2018), and 5-BDBD inhibits P2X4R currents (Wang et al., 2017). TNP-ATP has a half-maximal inhibitory concentration of 1.5 μM, while 5-BDBD has a half-maximal inhibitory concentration of 1.2 μM (Balázs et al., 2013). Two selective antagonists of P2X4R, 5-BDBD and PSB-12062, were utilized as inhibitors in P2X4R restriction assays (Table 2.2).

Table 2.2: Agonist and antagonists' detail

Compound	Description	Source
TNP-ATP	P2X receptor antagonist.	(Chen, 2013)
5-BDBD	Inhibits P2X4R mediated currents in Chinese hamster ovary (CHO) cells.	(Wang et al., 2017)
PSB-12062	Inhibit the calcium influx induced by TNT-ATP mediated by P2X4R	(Layhadi et al., 2018)

2.2.2 5-BDBD compound for *in vitro* and *in vivo*

To prepare the 5-BDBD solution, 5-BDBD was weighed and dissolved in dimethyl sulfoxide (DMSO) or distilled water to make a stock solution with a concentration of 10 mM. The stock solution was then diluted with culture medium or DMSO to the desired final concentration of 1 μM for *in vitro* studies and 10 mg/ml for *in vivo* studies (Figure 2.3).

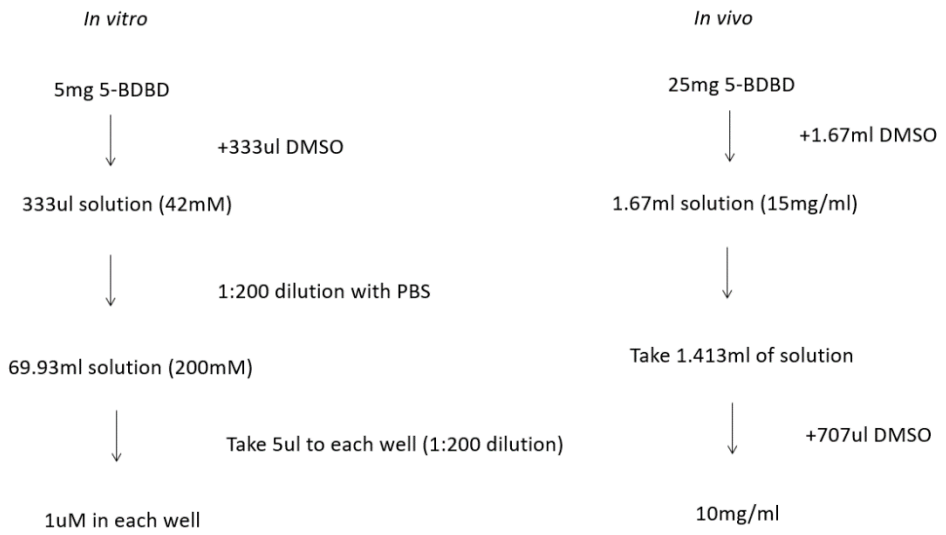

Figure 2.3：The process of preparing P2X4R antagonist 5-BDBD in vitro and in vivo. 5 mg of 5-BDBD powder was diluted with DMSO first. Then, the solution was diluted with PBS. The 5-BDBD were prepared into a stock concentration of 200 uM via serial dilution, 1:200 dilution each before assay to make the final concentration of 5-BDBD in each well was 1 uM *in vitro.* For *in vivo* assay, the final concentration of 5-BDBD is 10mg/ml diluted in DMSO.

2.3 Calcium assay

The fluorescent calcium assay is a crucial technique for analyzing cellular ion levels, particularly calcium ions, which serve as important second messengers involved in various physiological and signal transduction processes within cells. The principle of this technique involves labelling the calcium ions in samples with a fluorescent probe, allowing for the estimation of ion concentrations based on the intensity of the resulting fluorescence. The concentration of calcium ions in samples can be analysed by measuring the fluorescence intensity using a reader (Bondre et al., 2011).

The Fluo-4 Direct™ Calcium Assay Kit was utilized to assess the functionality of P2X4R and determine the optimal dosages of TNT-ATP in PCa cells. This homogeneous fluorescent calcium assay involves labelling calcium ions with fluorescent probes and estimating their concentration based on the intensity of fluorescence. The assay was performed on 10,000 cells per well in a 96-well plate, following the manufacturer's protocol for reagents' preparation (stored at -20°C). After washing the cells with PBS, 80 µl of fluoro-4 (x1) reagent was added to each well with different treatments and incubated for 45 minutes. Subsequently, 20 µl of TNT-ATP solution and 20 µl of ionomycin solution were added, and the well plate was placed in the FlexStation 3 Multi-Mode Microplate Reader. Data analysis was performed using Microsoft Excel and GraphPad Prism 8.

2.3.1 Optimizing TNT-ATP concentration

PC3 cells were treated with four specific concentrations of TNT-ATP agonists (30μM, 50μM, 100μM and 150μM) to find the optimal TNT-ATP concentration for activating P2X4R (Figure 2.4).

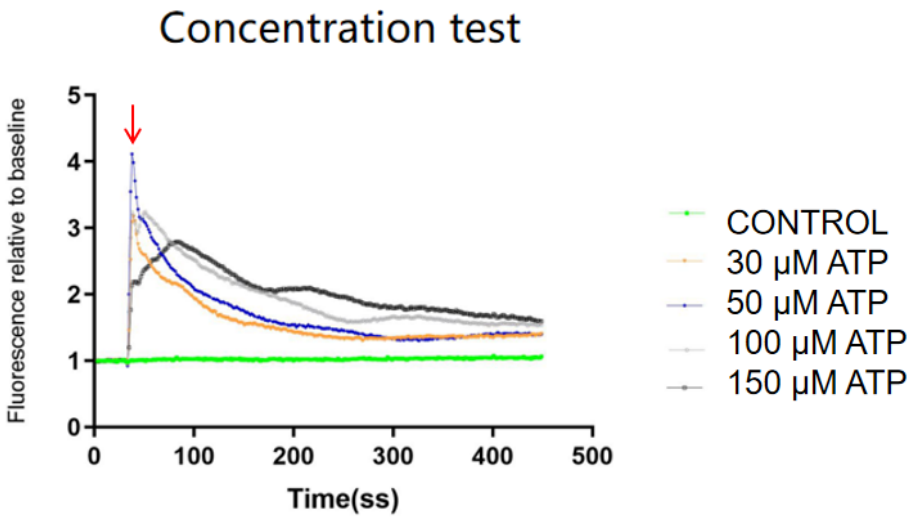

Figure 2.4: TNT-ATP concentration test. The highest peak is at 50 μM of TNT-ATP concentration, which suggests that P2X4R can be activated best at 50 μM of TNT-ATP compared to other concentrations, including 30 μM, 100 μM and 150 μM.

The calcium assay results indicated that the most effective concentration of TNT-ATP to activate P2X4R is 50 μM, with a mean peak value of 4.1 compared to 3.1 for 30 μM, 3.2 for 100 μM, and 2.8 for 150 μM. While TNT-ATP can also activate P2X7R, this requires a higher TNT-ATP concentration of over 100 μM (Staurengo-Ferrari et al., 2014). Hence, 50 μM TNT-ATP is the optimal concentration that exclusively activates P2X4R.

2.4 P2X4R knock out in PCa cells by CRISPR/Cas9 technology

Clustered Regularly Interspaced Short Palindromic Repeats (CRISPR/Cas9) is a powerful genomic editing system that can be programmed to target specific stretches of genetic code and edit DNA at precise locations. This technology allows for the modification of genes and the depletion of specific genes in living cells or organisms. The CRISPR/Cas9 system is an adaptive immune response system found in prokaryotes that uses non-coding RNAs to guide the Cas9 nuclease to induce site-specific DNA cleavage. This DNA damage is repaired by cellular DNA repair mechanisms through either the non-homologous end joining DNA repair pathway or the homology-directed repair pathway. The CRISPR/Cas9 system has been harnessed to create a simple, RNA-programmable method for genome editing in cancer cells, including prostate cancer, and can be used to generate gene knockout. A single guide RNA (sgRNA) is generated to direct the Cas9 nuclease to a specific genomic location, inducing double-strand breaks that are repaired via the NHEJ DNA repair pathway. This repair can introduce insertions and deletions that may disrupt gene function. A simple principle of CRISPR/Cas9 workflow is shown in Figure 2.5. The technique was first demonstrated in Zhang Feng's lab in 2012 and has since been widely used in genetic research (Ran et al., 2013b, Kawamura et al., 2015).

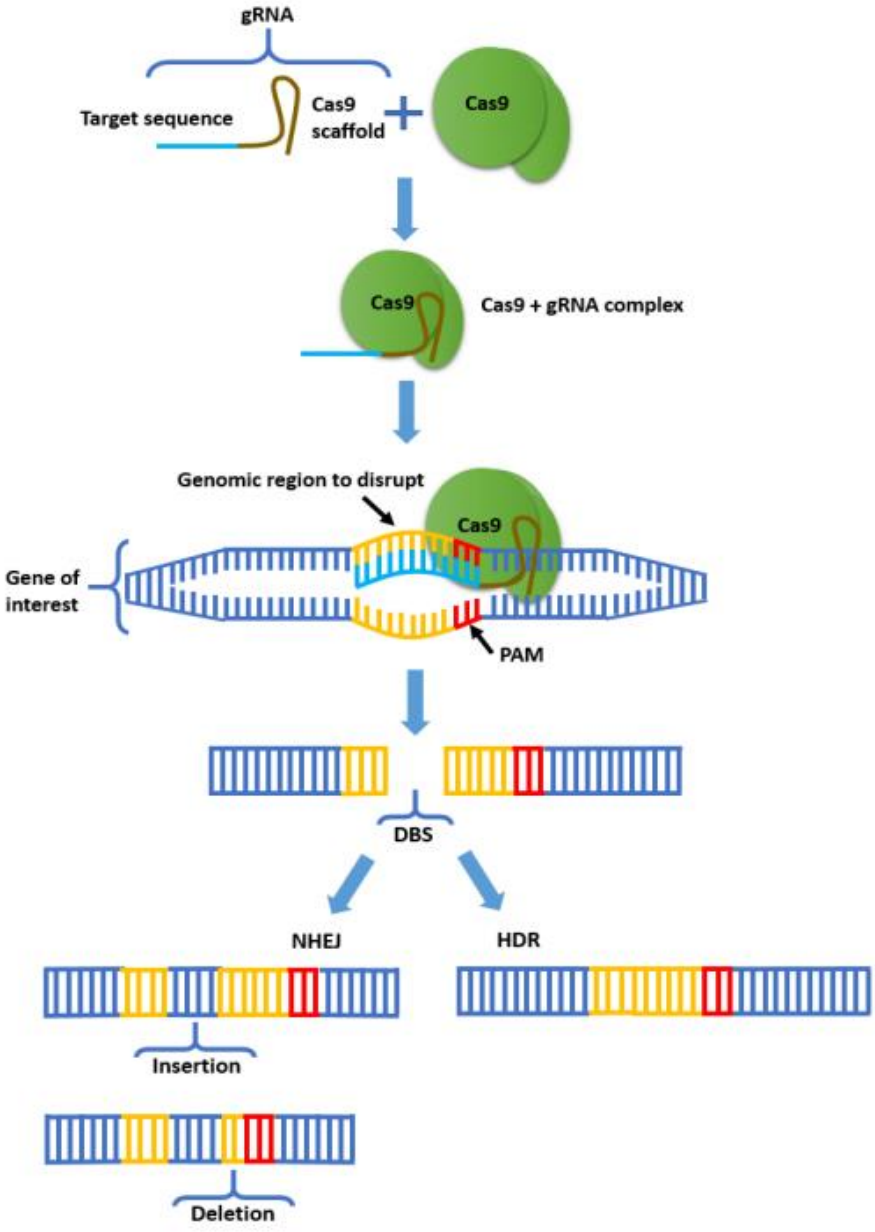

Figure 2.5: Principle of CRISPR/Cas9. SgRNA directly targets to the genomics DNA with Cas9 protein binding to the gRNA scaffold. Once binding has been done, Cas9 creates a double-strand break which can make to be repaired by a non-homologous end joining non-homologous end joining DNA repair pathway associated with deletions and insertions (indels) in the DNA or by a homology directed repair. The elements in this figure were downloaded from the internet, and comments were added manually (Hsu et al., 2014, Gridina, 2019).

2.4.1 Information of the P2X4R KO CRISPR/Cas9 plasmid

The P2RX4 KO CRISPR/Cas9 plasmid was purchased from Santa Cruz (sc-401779-KO-2) (Figure 2.6). It consists of three essential parts: a 20bp guide RNA, Cas9 protein sequence, and GFP selective markers. Three different sgRNAs have been designed in the plasmid to bind the target DNA. The gRNA sequence used for knockout P2RX4 was derived from the GeCKO(v2) library. According to information on the NCBI website, the sgRNAs were designed to target the functional region of the gene, making it lose the gene function upon genome DNA breakage. All products are provided as transfection-ready, purified plasmid DNA. P2RX4 CRISPR/Cas9 KO Plasmid (h2:sc-401779-KO-2) is a pool of 3 different gRNA plasmids. Detailed product information is provided in Table 2.3.

Table 2.3: SgRNA sequence of the P2X4R KO CRISPR/Cas9 plasmid

gRNA sequence	Sense:	Target Location
sc-401779-KO-2 A	CTCCGTTACGACCAAGGTCA	Exon3
sc-401779-KO-2 B	TCACGTTGGTCATGACGAAG	Exon4
sc-401779-KO-2 C	GTGCTTGTAGGAGTCTCAAC	Exon6 & intron

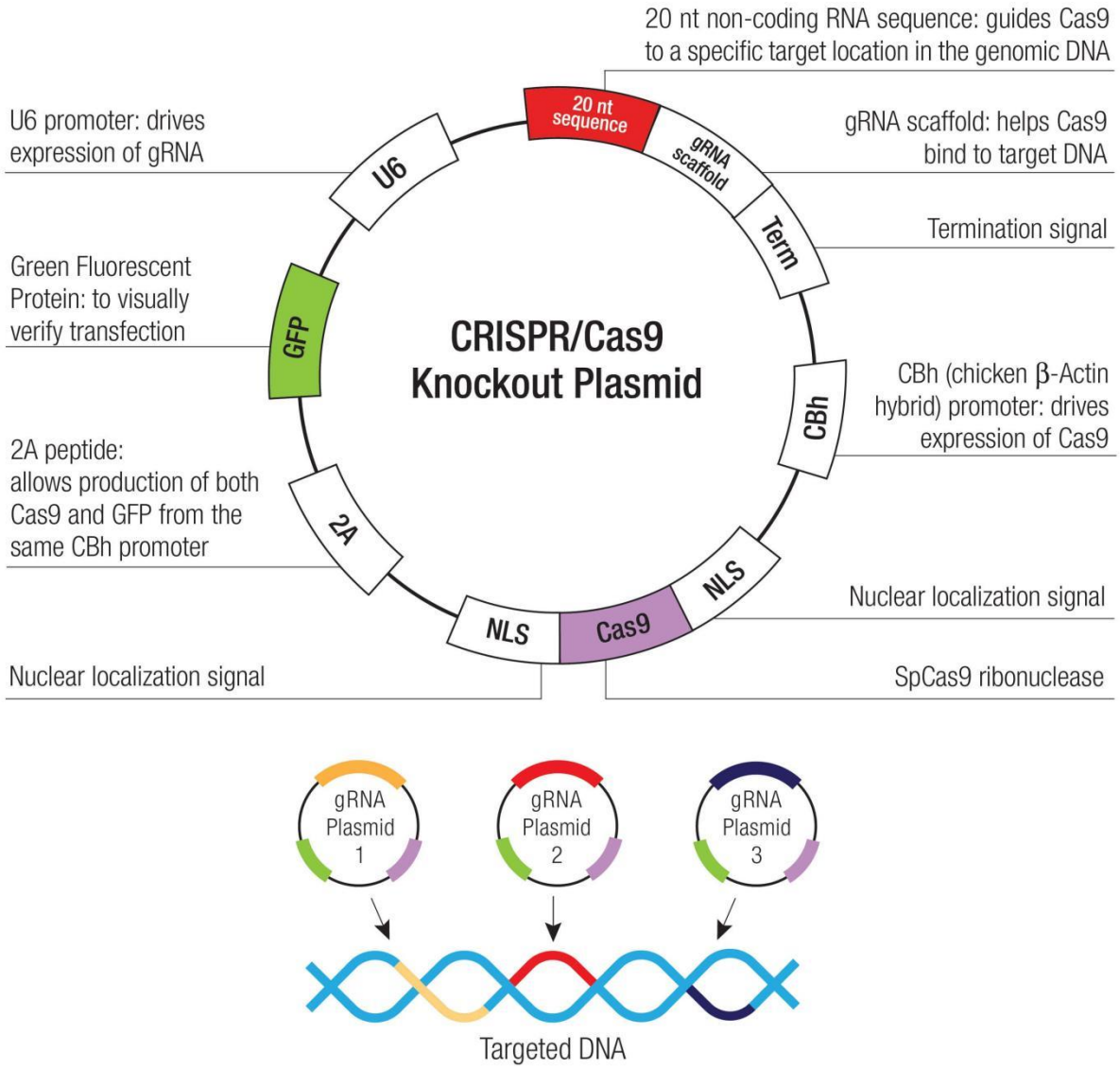

Figure 2.6: CRISPR/Cas9-directed Double Strand Break (DSB). The plasmid contained a promoter to drive the expression of gRNA; 20nt RNA sequence to target the specific location in genomics DNA; a gRNA scaffold to help bind to target DNA; termination signal to end the reaction. Cas9 sequence for transcribing a Cas9 protein; Cas9 sequence is between two nuclear localization signals. Three different gRNAs target to different sites in specific genomics DNA areas.

2.4.2 PC3 cells P2X4R KO transfection

PCa cell line PC3 was transfected with the P2X4R CRISPR/Cas9 KO plasmid using LipofectamineTM 3000. Single clones were selected by a cell sorting machine with a GFP signal and were seeded in a 96-well plate (Figure 2.7). The cells were first seeded at a density of 200,000 cells per well in a 6-well plate overnight. Prior to transfection, the cells were washed twice with PBS and changed to penicillin-streptomycin (pen-strep)-free 10% FCS DMEM medium, as antibiotics might affect transfection efficiency. Then 125ul of OptiMEM and 7.5ul of Lipofectamine 3000 (red top) were prepared per well in TUBE A, and 125ul of OptiMEM, 3.75ul P3000 (yellow top), and 20ul of DNA plasmid was prepared in TUBE B (10ul/1ug P2X4R plasmid in stock, using 2ug plasmid each time). For the negative control, everything was prepared the same, except that 20ul of PBS was added instead of DNA plasmid. The negative control was used to blank the GFP signals of PC3 WT cells before the actual cell sorting. 132.5ul of TUBE A and 148.75ul of TUBE B were mixed in another 2ml tube and incubated at room temperature for 10 minutes to allow the lysosomes to surround the DNA in TUBE C. Then, 281.25ul of TUBE C was added to each well drop by drop randomly. The volume for each component represents in Table 2.4. The medium was changed to a normal medium after 24 hours of transfection and incubated for another 24 hours. The cells were checked under the EVOS microscope (Olympus) to confirm the presence of GFP+ (GFP positive) cells. GFP+ cells were then sorted using the BD FACSMelody cell sorter, with the sorting completed by Susan Clark (The University of Sheffield). Finally, the cells were individually selected and seeded in a 96-well plate.

Table 2.4: Volume for each component applied in the LipofectamineTM 3000 transfection

Component	Volume
OptiMEM media	125µl
Lipofectamine 3000 reagent	7.5µl
Plasmid DNA	20µl (2ug)
P3000 reagent	5µl

Figure 2.7: Procedure for CRISPR/Cas9 transfection and selection.
Lipofectamine 3000 was used to transfect the P2X4R KO plasmid into cells. After 48h transfection, the cells were trypsinzed as individual cells and collected in the tube for the cell sorting, then a single clone was seeded individually in 96-well plate.

2.4.3 P2X4R KO positive clone tissue culture

The selected cells were cultured and expanded into a group of cells. After three weeks of cell sorting, the cells were treated with trypsin, split, and put in a new 96-well plate. After three days, the cells were transferred to a 24-well plate and cultured until confluence. Then, they were transferred to a 6-well plate for a week and subsequently to T25 flasks. When the cells reached confluency in T25 flasks, they were transferred to T75 flasks and maintained via normal tissue culture. The earliest passage number cells were frozen down when they reached confluency in the T75 flask.

2.5 P2X4R KO clone verification

The successful P2X4R KO individual clone was verified in the genomic, transcriptional and functional levels. Verification involved genomic DNA level including PCR and sequencing; transcriptional RNA level including RT-PCR and q-PCR. Measuring the functional effect of blocking P2X4R was verified by Flo-4 calcium assay.

2.5.1 P2X4R gene information

The P2RX4 gene information was downloaded from the Ensembl website (https://www.ensembl.org/Homo_sapiens/Transcript/Summary?db=core;g=ENSG00000135124;r=12:121209861-121234106;t=ENST00000359949). The P2RX4 gene contains 25,446 bp, including 13 coding exons and 12 introns. Target sgRNA1 is located in Exon 3, sgRNA2 is located in Exon 4, and sgRNA3 is located partially in Exon 6 and partially in the intron (Figure 2.8).

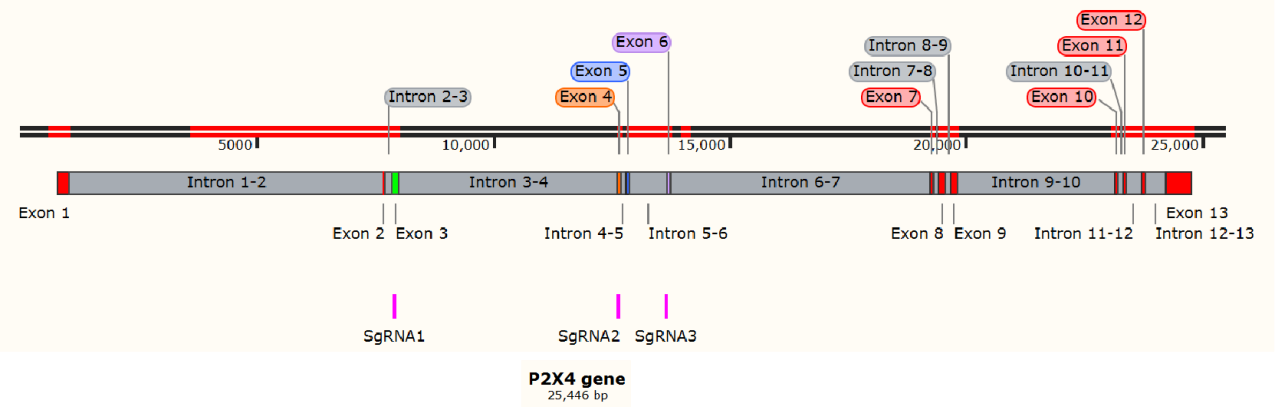

Figure 2.8: P2X4R genomic DNA sequence. Exons are shown in colour areas, while grey areas represent introns. SgRNAs are located between exon3 and exon6, which are in the function area of the P2X4R genomics gene.

2.5.2 Functional verification

The calcium assay is to verify the functional gene knock out in PCa cells. The principle and protocol used were the same as described in section 2.3, with the exception of the addition of antagonists.

2.5.3 P2X4R KO cells verification in DNA sequence

To verify the P2RX4 gene has been genetically knocked-out PCa cells, polymerase chain reaction (PCR) was used. PCR is a molecular technique that uses DNA primers to amplify a specific segment of genomic DNA through multiple rounds of DNA synthesis in a PCR machine. This technique relies on using a thermostable DNA polymerase, such as Taq polymerase, and requires DNA primers designed specifically for the DNA region of interest. The PCR system and program used in the thermocycler for PCR amplification are critical for the optimal amplification of the target DNA.

2.5.3.1 DNA extraction

DNA extraction was performed using the Wizard® Genomic DNA Purification kit instruction manual (Promega) according to the manufacturer protocol. The DNA samples were stored at -20°C.

2.5.3.2 Primer design

Primers were designed to amplify the sequence of the sgRNA target locations. There are several rules for designing primers, including the following properties: the length should be between 18-24 bases; the content of cytosine or guanine (C/G) should be between 40% to 60%; the primer should start and end with 1 or 2 C/G pairs; the melting temperature (Tm) should be around 50°C; and each pair of primers should not have complementary regions. To ensure better sequencing results, the designed product length should be between 500bp-1000bp. Based on these rules, the primer sequence information and locations are as follows: the PCR product designed for sgRNA1 is 994bp, for sgRNA2 is 511bp, and for sgRNA3 is 1427bp (Table 2.5) (Figure 2.9).

Table 2.5: Primer sequences and PCR product

Primer	Sequences	TM(℃)	GC%	PCR product
SgRNA1-F	5' ACATCGTACTTCCAGCCACT 3'	54.4	50.0	994bp
SgRNA1-R	5' CTCGGTCCCTTAGCACAT 3'	52.7	55.6	
SgRNA2-F	5' CGGTCAGTGTTTGAGTTG 3'	48.7	50.0	511bp
SgRNA2-R	5' CAGCAGTGAATGTAGAGGG 3'	50.5	52.6	
SgRNA3-F	5' TAACTGTCTTCCTCCGATTC 3'	51.6	45.0	1427bp
SgRNA3-R	5' GTCACCTGCACCCTTCTC 3'	52.2	61.1	

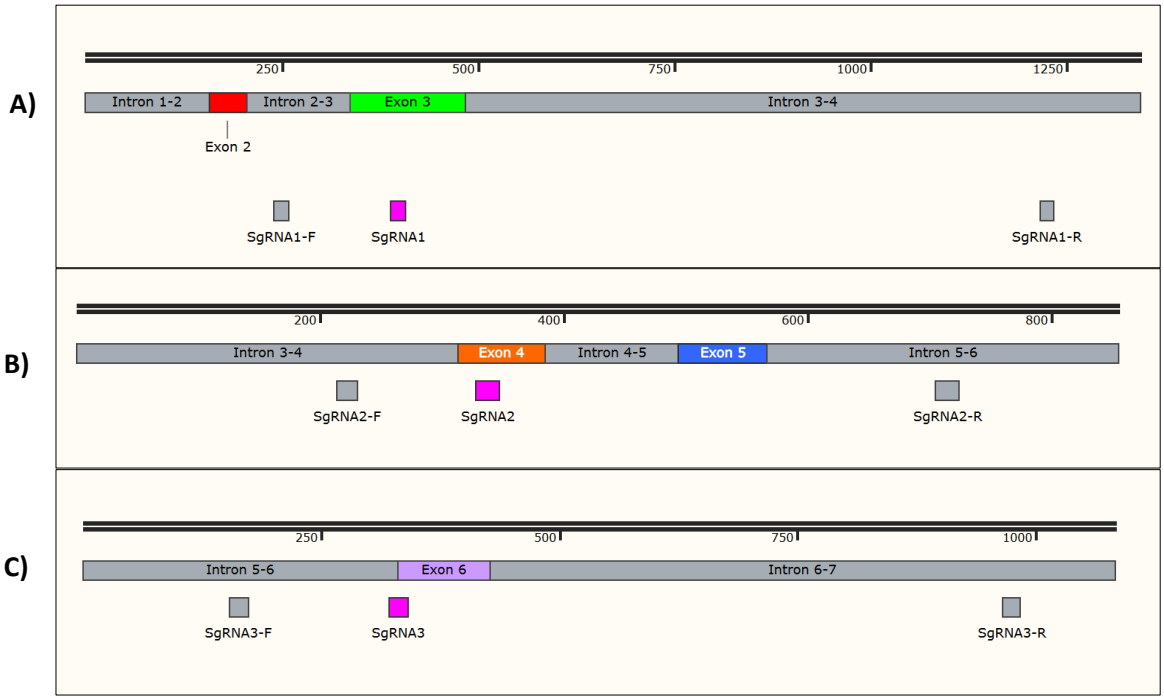

Figure 2.9: SgRNAs and corresponding primers location in P2X4R genomics gene. SgRNAs and corresponding primers location in P2RX4 genomics gene. A) SgRNA1 and primer location. B) SgRNA2 and primer location. C) SgRNA3 and primer location.

2.5.3.3 PCR assay

The PCR reactions used here and the thermocycler program are summarized in Table 2.6 and Table 2.7, respectively.

Table 2.6: PCR system

PCR mix	Compounds	Volume (ul)
PCR positive	PCR mix reagents	12.5
	Forward Primer	1
	Reverse Primer	1
	DNA/cDNA	2
	ddWater	8.5
	Total volume	25
PCR positive (PCR product purification)	PCR mix reagents	50
	Forward Primer	4
	Reverse Primer	4
	DNA/cDNA	8
	ddWater	34
	Total volume	100
PCR negative	PCR mix reagents	10
	Forward Primer	1
	Reverse Primer	1
	Nuclease-free water	2
	ddWater	8.5
	Total volume	25

Table 2.7: Thermocycler 35x programme used to amplify the PCR sample

Thermocycler programme	Temperature	Time
Heated lid	95°C	2 minutes
Start cycle	95°C	30 seconds
Denaturation	55-58°C	30 seconds
Annealing	72°C	30 seconds
Elongation	72°C	5 minutes
Cycle end	4°C	Hold

2.5.3.4 Electrophoresis

Gel electrophoresis is a technique used to separate DNA based on its nucleotide size and electrical charge. An electric current is used to move the molecules through an agarose gel. Electrophoresis is a general term that describes the migration and separation of charged particles (ions) under the influence of an electric field. The system consists of two electrodes of opposite charge (anode, cathode), connected by a conducting medium called an electrolyte (Kirkpatrick, 1990, Lee et al., 2012).

To prepare the gel, 25 mL of TAE buffer was measured using a graduated cylinder and poured into a 100 mL Erlenmeyer flask. 0.25 g of agarose was measured and added to the flask to produce a ~1.0% agarose gel. The flask was heated in a microwave for 30-60 seconds to melt the agarose and checked for complete dissolution. The agarose was then swirled and mixed before being allowed to cool for 10 minutes at room temperature. 2.5 µl of ethidium bromide (EtBr) was added and swirled to make it ~0.1%. The mixture was then poured onto an assembled gel tray with barriers in place, and any air bubbles were moved to the side or the bottom of the tray using a pipette tip. The gel comb was inserted into the tank. After about 10 minutes, the agarose solidified and turned translucent and glossy.

For electrophoresis, around 5-8 µl of each PCR sample fixed with loading buffer was added to the sample sink of the agarose gel. Electrophoresis was run for 30 minutes using a voltage of 50 V. Finally, the complete agarose gel was imaged using Bio-Rad gel imaging systems (Bio-Rad, USA).

2.5.3.5 DNA purification

PCR products >100 bp were purified using the QIAquick PCR Purification Kit. During this procedure, a silica membrane binds the DNA in a high-salt buffer, and elution is performed with a low-salt buffer or water, removing other impurities such as primers, nucleotides, enzymes, mineral oil, salts, agarose, ethidium bromide and other impurities. The PCR product volume used for purification was 100 µl, so 500 µl of Buffer PB was added to the PCR product, mixed well and transferred to a 1.5 ml PE tube. The mixture's colour should be yellow; if it appears orange or violet, 10 µl of 3 M sodium acetate, pH 5.0, was added and mixed, which changed the mixture's colour to yellow. The QIAquick spin column was assembled in a QIAquick collection tube, and the mixture (transferring the reagent several times if the volume was over 500 µl) was added to the QIAquick column and centrifuged at 13,000 rpm for 60 s. The DNA binds to the spin column, and the flow-through is discarded. Then, 750 µl of wash Buffer PE was added to the QIAquick column and centrifuged for 60 s, the flow-through was discarded, and the column was centrifuged for an additional 1 min to ensure the complete removal of the wash buffer. The QIAquick column was placed in a clean 1.5 ml microcentrifuge tube without a top, and 20 µl of nuclease-free water was added to dissolve the DNA in the column for 2 min at room temperature. The column was then centrifuged at 13,000 rpm to collect the DNA, and the pH value was adjusted to within 7.0-8.5. The PCR purification product was stored at -20°C because DNA may degrade in the absence of a buffering agent.

2.5.3.6 Sequencing

Samples and their corresponding primers were sent to the company GENEWIZ (www.genewiz.com) for sequencing. Before sending the samples, the DNA concentration and quality were measured using a NanoDrop. The concentration of DNA was required to be no less than 5 μg/μL with a 260/280 ratio of approximately 1.8 and a 260/230 ratio of approximately 2.0 to ensure successful sequencing.

2.6 P2X4R KO cells verification in transcriptional level

2.6.1 RNA extraction

The RNA extraction protocol was conducted using the ReliaPrep™ RNA Cell Miniprep System following the instructions provided in the manufacturer's instruction manual (Promega). The extracted RNA samples were stored at a temperature of -80°C in a freezer for future use.

2.6.2 Nano-drop RNA analysis

RNA/DNA quantity and quality after extraction were assessed using the NanoDrop 2000 by measuring the purity of RNA/DNA with a wavelength of 260 nm of absorbing ultraviolet light. In order to blank the initial reading, 1 μL of nuclease-free water was pipetted onto the pedestal before the RNA sample to ensure that the machinery was working properly and confirm no RNA/DNA contamination in the nuclease-free water was used for eluting. The concentration of RNA was measured in μg/μL. Two ratios, 260/280 (~2.0) and 260/230 (2.0-2.2), were recorded as indicators of RNA quality. A low 260/280 ratio may indicate contamination by residual phenol, guanidine, or other reagents used in the extraction protocol. The 260/230 ratio is considered a secondary measure of RNA sample purity and a low ratio may indicate contamination by

carbohydrate carryover or residual phenol. High-quality RNA is essential for downstream signal analysis.

2.6.3 cDNA synthesis

To confirm the modification of the P2RX4 gene at the RNA transcription level, complementary DNA (cDNA) was synthesized from RNA using the reverse transcription. Briefly, RNA samples were isolated from cells using the ReliaPrep™ RNA Cell Miniprep System following the manufacturer's protocol. The concentration and purity of RNA were assessed using a NanoDrop 2000 spectrophotometer. cDNA synthesis was performed using the GoScript™ Reverse Transcriptase kit (Promega) according to the manufacturer's instructions, which include the steps of primer annealing, DNA polymerization, and enzyme deactivation. As a negative control, nuclease-free water was substituted for RNA. The resulting cDNA was used for verification of the successful P2X4R KO cells. Details of the cDNA synthesis protocol can be found in the GoScript™ Reverse Transcriptase kit instruction book (Promega).

2.6.4 cDNA Primer design

The primer for cDNA amplification is as follows. There are 1215bp for the whole P2RX4 cDNA sequence, and the PCR product length is 493bp (Table 2.8) (Figure 2.10).

Table 2.8: Primer sequences

Primer	Sequences	TM(℃)	GC%
SgRNA-F	5' TCATCCGCAGCCGCAAAG 3'	63.6	61.1
SgRNA-R	5' TCATCCTCCACCGGGCACCA 3'	68.6	65.0

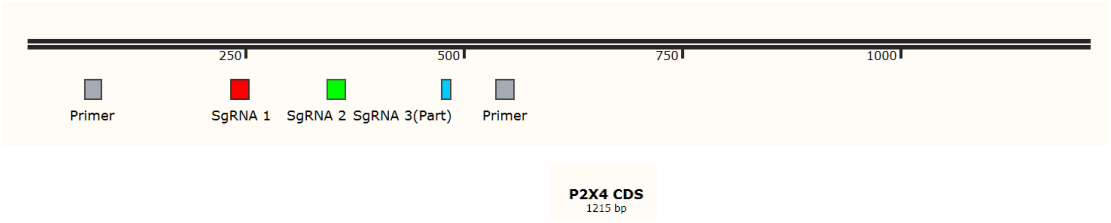

Figure 2.10: Primer location in P2X4R CDS. The location of designed primers for amplified the target P2X4R cDNA sequence.

2.6.5 Reverse transcription RT-PCR

Quantitative reverse transcription PCR (RT-qPCR) involves the conversion of RNA into its complementary DNA (cDNA) sequence using reverse transcriptase. This technique was used to verify P2X4R KO at the RNA transcription level (Rio, 2014). The RT-PCR system and assay used were the same in section 2.5.3.3.

2.6.6 qPCR using individual TaqMan® assays

TaqMan PCR is a real-time PCR technique that uses a nucleic acid probe complementary to an internal segment of the target DNA. Taq DNA polymerase synthesizes new strands using unlabelled primers and the template. When the polymerase reaches a TaqMan probe, its endogenous 5' nuclease activity cleaves the probe, separating the dye from the quencher.

One of the main strengths of qPCR is its ability to measure gene expression. In this study, the expression of P2X4R in PC3 WT and KO cells was measured using GAPDH as a housekeeping gene. The expression of other P2XR (P2X1R to P2X7R) and P2YR (P2YR, P2Y4R, P2Y11R, P2Y12R, P2Y13R, P2Y14R) was also measured.

Prior to the start of experiments, all pipettes, tips, tubes, the RT-PCR water, and the 384-well plates were irradiated with UV light for 20 minutes. The cDNA product was diluted 1:100 as a template and mixed with 50 µL of TaqMan® Universal Master Mix before being added to each fill port. The qPCR system presents in table 2.9.

Table 2.9: qPCR system

384-well standard	Compounds	Volume (ul)
qPCR positive	TaqMan® mix reagents	5
	Forward Primer	0.5
	Reverse Primer	0.5
	Template	2
	Nuclease-free water	2
	Total volume	10
qPCR negative	TaqMan® mix reagents	5
	Forward Primer	0.5
	Reverse Primer	0.5
	Nuclease-free water (As negative template)	2
	Nuclease-free water	2
	Total volume	10

The plate was centrifuged at 300 x g for 1 minute to collect the liquid at the bottom. The distribution channels on the plate were then sealed by the TaqMan® Array Micro Fluidic Plate Sealer. Finally, the plate was loaded onto the 7900HT Real-Time PCR system (Applied Biosystems, the USA) to measure the fluorescent signal in the samples with the following settings.

384-well standard run	Temperature (° C)	Time (mm:ss)
Hold	50	2
Standard Cycle (40 Cycles)	95	0:15
	60	1:00

2.6.7 qPCR data quantitative

Methods for quantifying qPCR data involve analyzing the differences in cycle threshold (Ct) values between the target gene (P2XRs) and a reference gene (GAPDH). Two formats, 1/ΔCt and $2^{-\Delta\Delta CT}$, can be used to represent the relative expression level of the target gene compared to the reference gene. The expression level of P2X4R was calculated using both 1/ΔCt and $2^{-\Delta\Delta CT}$ formats, while the expression of other P2XRs was calculated using 1/ΔCt.

2.7 *In vitro* assay

2.7.1 Proliferation

For the proliferation assay, CyQUANT™ Cell Proliferation Assay Kit (Life Technologies) was utilised using the CyQUANT™ GR dye. This dye binds to cellular nucleic acids, allowing cell numbers to be calculated by fluorescence measurement, and is a highly sensitive fluorescence-based method for quantifying cells and assessing cell proliferation and cytotoxicity. It was used to measure the difference in cell proliferation between PCa WT cells and P2X4R KO cells. The protocol for preparing the CyQUANT™ reagent can be found in the CyQUANT™ Cell Proliferation Assay Kit instruction manual (Promega).

PC3 WT and P2X4R KO cells were seeded at a density of 2,000 cells per well in a 96-well plate on Day 0, with the medium being changed daily. At 24-, 48-, 72-, and 96-hours post-seeding, the medium was removed, and 50 µL of 1X dye binding solution was added to each well. The plate was then incubated at 37°C for 60 minutes, and fluorescence intensity was measured in each well using an EnSight Multimode Plate Reader with an excitation of 485 nm and an emission of 530 nm.

2.7.2 Viability

The AlamarBlue Cell Viability Reagent is a quantitative method used to measure the viability of mammalian cell lines, including PCa cell lines used in this assay. The reagent contains an oxidation-reduction (REDOX) indicator that both fluoresces and changes colour in response to the chemical reduction due to cell growth. This makes it an effective method for measuring the viability of PC3 WT and KO cells *in vitro*.

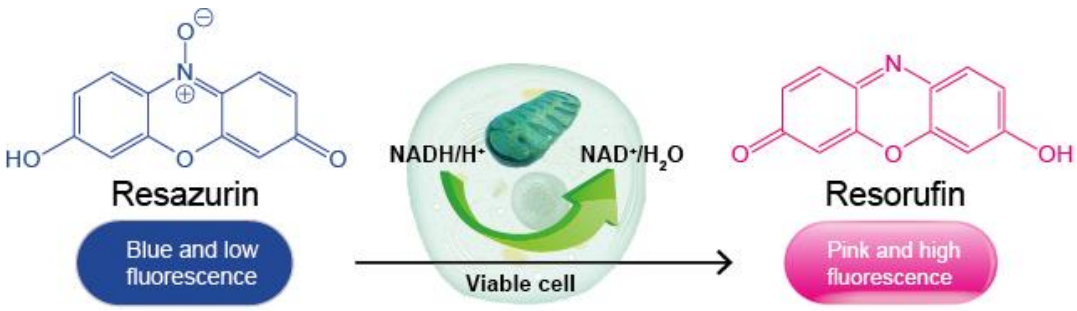

Figure 2.11: Principle of AlamarBlue™ cell viability reagent. Metabolic activity is reduced in viable cells. The Alamar Blue reagent can activate the process of resazurin reduced to resorufin, a compound that is pink in colour and highly fluorescent.

Cells were plated in a 96-well plate at a density of 3000 cells per well and allowed to incubate overnight, with clean PBS added to the surrounding wells. A blank medium without cells was prepared for every 96-well plate used. The medium was changed daily, and at each of the 24, 48, 72, and 96-hour time points, 10 µL of AlamarBlue™ cell viability reagent was added to each well. The plate was incubated at 37℃ for 3 hours and then read using a FlexStation 3 Multi-Mode Microplate Reader with excitation at 570 nm and emission at 600 nm. The AlamarBlue™ cell viability reagent was used to quantitatively measure the cell viability of mammalian and PCa cell lines in this assay.

2.7.3 Apoptosis assay

Apoptosis is a programmed cell death process that can prevent the development of cancer. However, if apoptosis is prevented, uncontrolled cell division can occur, leading to tumour development (Dang, 2012). The Caspase-Glo® 3/7 assay utilizes a proluminescent caspase-3/7 DEVD-aminoluciferin substrate and a proprietary thermostable luciferase in a reagent that is optimized for luciferase activity and cell lysis. When the Caspase-Glo® 3/7 Reagent is added to the cells, it induces cell lysis and releases the substrate, which is cleaved by caspases. This releases free aminoluciferin that is consumed by the luciferase, generating a luminescent signal that is proportional to caspase-3/7 activity.

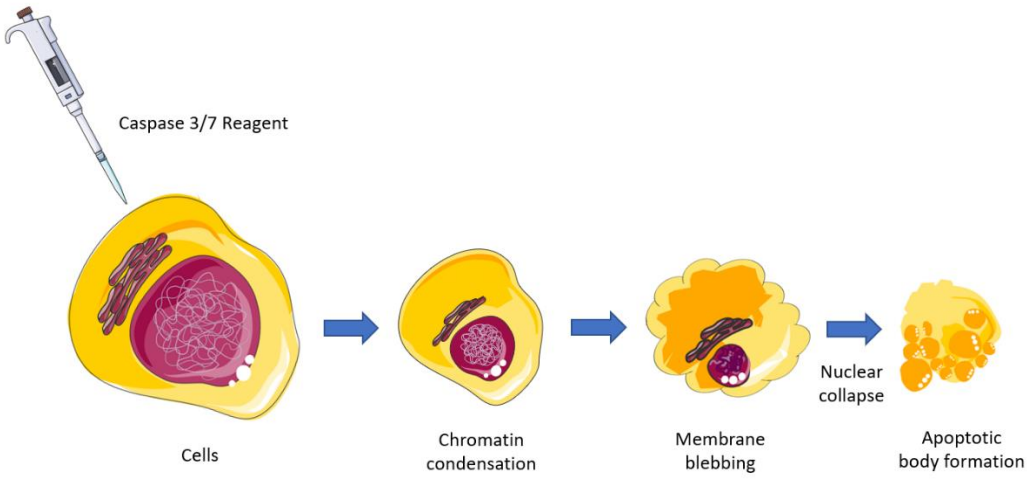

Figure 2.12: The apoptosis process of cells. After adding Caspase-Glo® 3/7 Reagent, first showing the chromatin condensation in cells, then the membrane is blebbing and nuclear collapse, and finally the cells become apoptotic body formation. The caspase cleavage of the substrate generates a luminescent signal that can be detected by a plate reader.

PCa cells were seeded in 96-well plates at a density of 1×10^4 cells per well and cultured for 24 hours. To examine the cell apoptotic activity, the Cell Meter™ Caspase 3/7 Activity Apoptosis Assay (Stratech Scientific, Ely, UK) was used following the manufacturer's instructions. Fluorescence was measured using an EnSight Multimode Plate Reader (PerkinElmer) with excitation at 490 nm and emission at 525 nm.

2.7.4 Cell migration by transwell assay

Due to the ease with which C4-2B4 monolayers were detached, a scratch assay was not suitable for testing cell migration. Instead, the Transwell method was employed. C4-2B4 cells were seeded onto Transwell cell culture inserts (6.5 mm with an 8-μm pore polycarbonate filter, Corning, New York, NY, USA) at a density of 2×10^5 cells per well in 200 μL of serum-free medium with or without antagonists. The lower chamber contained 500 μL of 10% FBS DMEM as a chemoattractant. After 16 hours of incubation, the inserts were fixed, stained, and mounted on slides. The slides were scanned, and the percentage of area covered by migrated cells was measured using ImageJ software.

2.7.5 Cell migration by scratch assay

A wound healing assay was conducted to evaluate cell migration in PC3 WT and P2X4R KO cells. The scratch assay is a commonly used method for investigating cell migration and can simulate the process of tissue repair *in vivo*. The repair of tissues and wounds can lead to a disordered extracellular matrix (ECM) and consequently impact cell migration (Schultz and Wysocki, 2009). Mitomycin C, which can crosslink DNA strands covalently, inhibits DNA synthesis and replication, thereby blocking cell proliferation and facilitating cell migration (Crooke and Bradner, 1976). The impact of P2X4R deficiency on cell migration was assessed by conducting a scratch assay. Cells were cultured in 24-well plates until confluence was reached, and a linear scratch was created using a pipette. Migration was monitored for 18 hours under an Olympus inverted CK2 microscope (Olympus) at 10x magnification. Changes in the wound area were determined using ImageJ analysis software, and cell migration was reported as the percentage of wound closure (Figure 2.13).

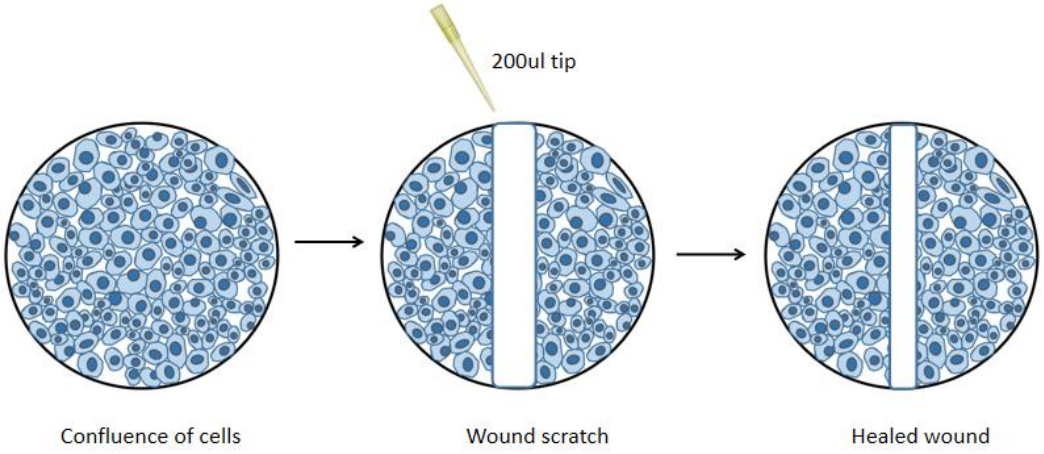

Figure 2.13: Scratch test for migration. Cells were full in 24-well plate before migration assay. Using 200ul tip to make a scratch in the middle of the well-plate. After 18h later, calculated the healing areas.

2.7.6 Invasion assay

Metastasis is the culmination of multiple changes in tumour cells and their microenvironment that enable cellular migration and invasion into healthy host tissue (Martin et al., 2013). The Transwell assay was used to evaluate the invasiveness of P2X4R inhibition or knockout in vitro. PCa cells were seeded at a density of $5x10^4$ cells per well and allowed to incubate for 72 hours. Non-invasive cells remained on top of the chamber, while invasive cells were attached to the membrane. Cells were stained with eosin and haematoxylin, and the resulting images were scanned by a digital scanner and analysed using the ImageJ software (Kramer et al., 2013).

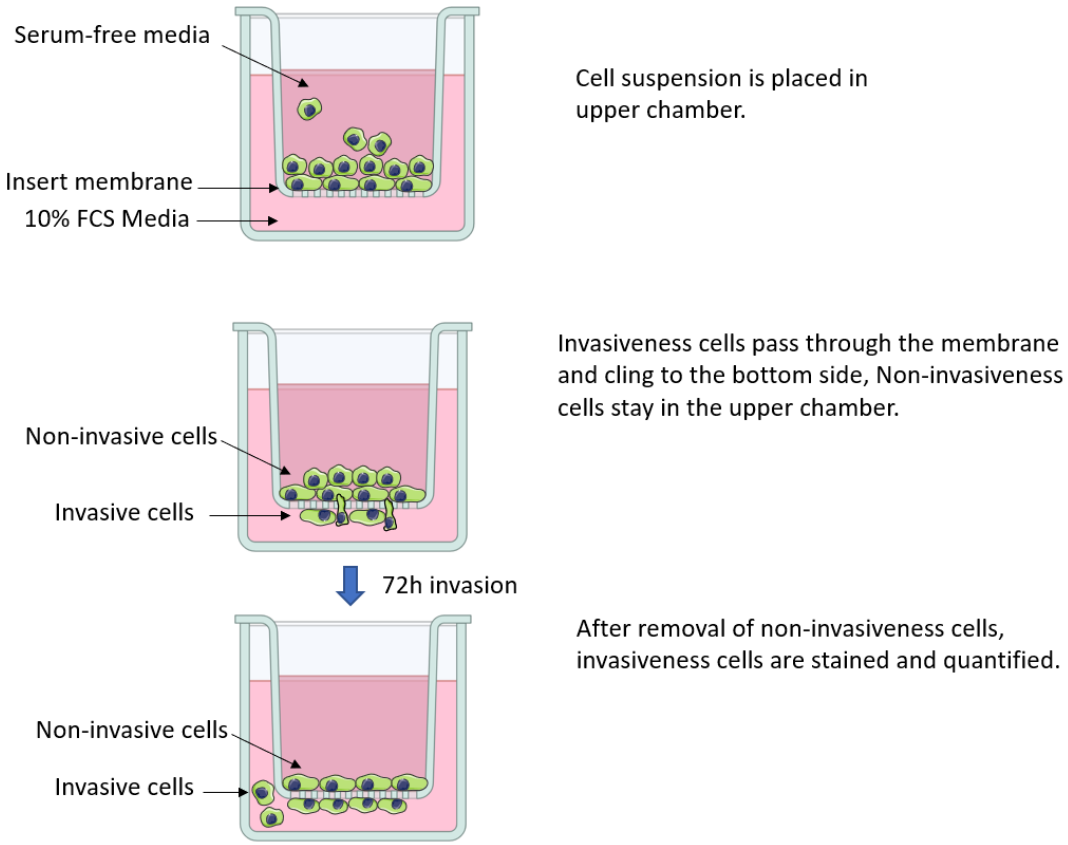

Figure 2.14: The Transwell chamber assay protocol. Plate 200μL of medium solution in the upper chamber, and plate 500μL of DMEM with 10% FCS to the lower chamber. The invasive cells can pass through the membrane and cling to the bottom side, while the non-invasiveness cells stay in the upper chamber. After 72 hours, the percentage of non-invasiveness cell can be quantified by staining and scanning the membrane. Elements in this figure were downloaded from the BioRender (Life Science Icons) or the Smart (Servier Medical ART) with copyright free (Kramer et al., 2013).

To evaluate the invasiveness of PCa cells with P2X4R inhibition or knockout *in vitro*, a Transwell invasion assay was employed. Matrigel was mixed with serum-free medium (SFM) to achieve a concentration of 0.5 μg/mL, and 20 μL of this solution was added to each Transwell. The Transwells were then placed in a 24-well plate and incubated at 37℃ for 2 hours to allow for the formation of a Matrigel membrane. PCa cells were seeded on the top of the chamber at a density of 5×10^4 cells per well in 200 μL of SFM with treatment. Mitomycin C was added to each well at a concentration of 5 μg/mL and incubated for 3 hours to block cell proliferation. After this, 500 μL of

DMEM with 10% FCS was added to the lower chamber and the cells were incubated for 72 hours. To stop the invasion assay, the reagents were removed from the insert with a cotton swab and the medium was cleaned off the chamber. The Transwells were then cleaned in 100% ethanol for 5 minutes, transferred into eosin for 1 minute, and then stained with haematoxylin for 5 minutes. After rinsing the Transwell in distilled water for 2 minutes, they were washed and dried for several minutes. Finally, the slides were scanned using the Pannoramic 250 Digital Scanner (3D HISTECH) at 1.2x magnification. The data was analyzed using Image J to calculate the percentage area covered by cells, and a t-test analysis was performed in the assay.

2.8 Inhibit P2X4R by 5-BDBD antagonists *in vivo*

Six-week-old male BALB/c AnNCrl immunocompromised (athymic nude) mice (Charles River, Kent, UK) were used in a xenograft model to study the effect of P2X4R antagonists on PCa tumourigenesis. The mice were housed in an environment with a 12-h light/dark cycle at 22°C and fed ad libitum with a rodent diet containing 18% protein and 1.01% calcium. Prior to treatment, the mice were kept in the animal house for 7 days. Tumour cells were prepared and mixed with Matrigel to a final concentration of 5×10^4/μl. Twenty-one mice were subcutaneously injected with 100 μL of PC3 cells suspension (5×10^6 cells in 50% PBS+ 50% Matrigel) in the right flank. The mice were then randomly divided into two groups (seven mice per group) and treatment was initiated one day after tumour cell inoculation. The two treatment groups received daily intraperitoneal injections of P2X4R antagonist 5-BDBD at 10 mg/kg dosages. The vehicle control group received daily injections of 20 μL of DMSO. The dosage of antagonist treatment was determined based on previously published *in vivo* usages (1–25 mg/kg). The injections were performed by Dr. Ning Wang (Srivastava et al., 2020, Long et al., 2020, Long et al., 2018). The procedure represents in Figure 2.15.

2.8.1 Tumour and weight measurement

Tumour sizes and weights were measured twice a week using vernier calipers. Tumour volumes were calculated as ellipsoids using the formula: Volume = πABC/6, where A represents the length, B represents the width, and C represents the height. Tumour growth was monitored for three weeks after cancer cell injection, and the animals were euthanized 21 days post-injection. All procedures were conducted in compliance with the UK Animals (Scientific Procedures) Act 1986 and were approved by the local Research Ethics Committees of the University of Sheffield Home Office (Sheffield, UK).

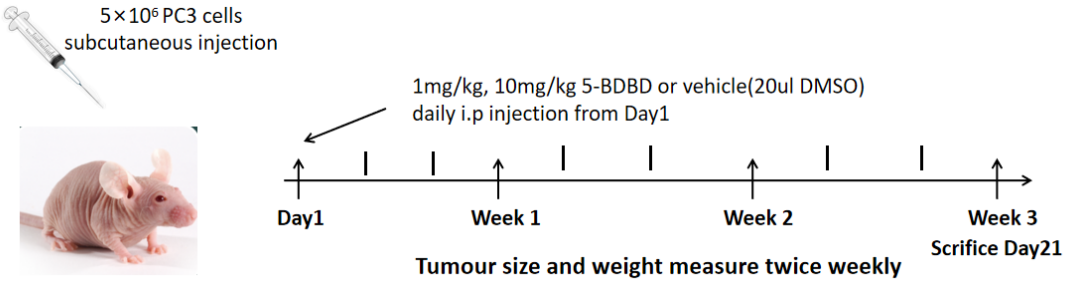

Figure 2.15: Procedure of P2X4R antagonist 5-BDBD treatment in vivo.

Schematic outline of the *in vivo* study. Briefly, the mice were subcutaneously (s.c) injected with 5 × 10^6 PC3 cells suspension with 50% PBS + 50% Matrigel. The mice were then daily intraperitoneally (i.p) injected with the P2X4R antagonist 5-BDBD at a dosage of 10 mg/kg or vehicle (20 µL DMSO), starting from day one until being euthanized three weeks post-tumour cell inoculation.

2.8.2 Ki67 antibody staining for immunohistochemistry

Ki67 staining is a commonly used method to estimate the proliferation index of tumours in oncology. Ki67 is a protein marker expressed during the S, G2, and M phases of the cell cycle. Formalin-fixed paraffin-embedded tumour samples were dissected and cut at a thickness of 3 µm and mounted on slides. Two antibodies, a primary and a

secondary, were used to detect and image Ki67 expression. Tissue samples were first subjected to antigen retrieval by immersing them in a 1x citrate buffer and incubating them in a pre-heated water bath at 80°C for 20 minutes. After cooling to room temperature, the samples were washed twice in PBST reagent and blocked with non-specific protein block (1% NGS in PBST) for 20 minutes at room temperature. Then, a serum block (1% NGS in PBST) was applied. The primary antibody against Ki67 was added and incubated for 1 hour at room temperature. The samples were washed with PBST twice to remove the primary antibody, followed by incubation with a biotinylated goat anti-rabbit secondary antibody for 20 minutes at room temperature. The samples were rewashed with PBST twice to remove the secondary antibody, and the ABC reagent (Elite-HRP) was added and incubated for 20 minutes at room temperature. The samples were washed in running water for 5 minutes, counter-stained with Gills haematoxylin for approximately 5 seconds, and gently washed in running tap water for 3 minutes.

2.8.3 Blood withdraw and multiplex cytokine assay

At the endpoint, the mice were euthanised, and their blood serum was collected. The serum was collected by Dr. Ning Wang and stored at a temperature of -80°C. The collected serum was subjected to a multiplex cytokine assay, which was performed by Dr. Hector Arredondo (The University of Sheffield).

2.9 *In vivo* assay of PCa bone metastasis

To investigate the role of P2X4R in PCa bone metastases, an intracardiac xenograft mouse model was utilized (Figure 2.16). Highly expressed in PCa (He et al., 2020), particularly in metastatic tissue (Maynard et al., 2022), P2X4R was studied using PC3 WT and KO cells in this *in vivo* assay. Six-week-old BALB/c nude mice were randomised into four cages of five mice each, kept in the animal house for seven days, and then intracardially injected with $1x10^6$ PC3 WT or KO cells. The mice were then kept warm (37°C incubator) for 40 minutes until they recovered from anaesthesia and

were subsequently observed in their cage. Among the PC3 P2X4R KO clones, PC3 KO-1 was chosen for the *in vivo*, which demonstrated a moderate impact on the cell aggressiveness. This decision was primarily based on the observation that PC3 KO-2 exhibited slow growth and even died after a few days *in vitro*. At the endpoint, the mice were sacrificed, and bone samples were collected from their lower limbs, which were then stored in 10% formalin for a week and subsequently in 70% ethanol for histological and micro-CT analysis.

To evaluate the tibias destruction induced by tumour, micro-CT scanning was performed, and tumour burden was calculated as the total amount of cancer in the mouse tibia. Tumour burden in the bone was determined by manually counting the PCa cells in the mouse's normal bone marrow cells. After TRAP and H&E staining, human tumour cells could be distinguished from bone marrow cells.

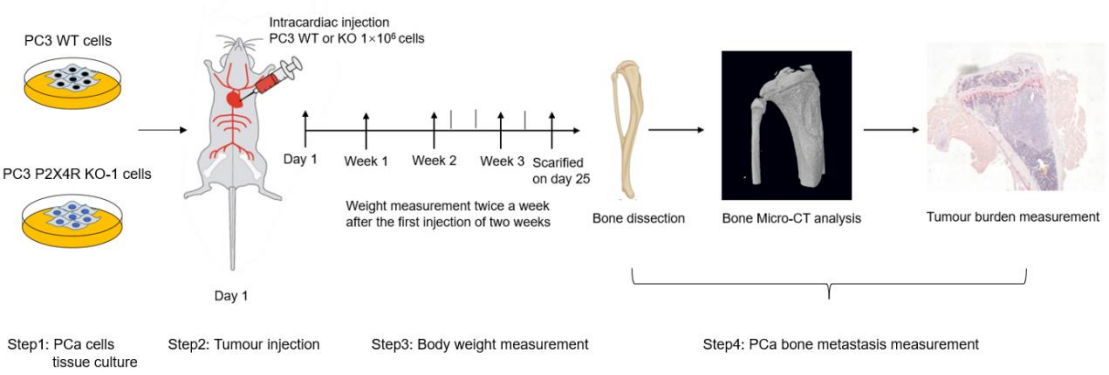

Figure 2.16: Process of PCa bone metastasis in xenograft mouse model. Mice were intracardiac injection with 1 x10^6 PC3 WT/KO cells on the first day. Weight measurement was performed twice a week during the experiment until the endpoint on day 25. Bones were collected and scanned by micro-CT scanning methods. After scanning, bone sections were cut and bone sections were prepared used used TRAP and H&E staining. Finally, tumour burden was measured using osteoMeasure software.

2.9.1 Micro-CT analysis

Micro-computed tomography (micro-CT) is a powerful imaging technique that can provide high-resolution images of bone structure with a voxel size as small as 10 μm. *In vivo* micro-CT allows for monitoring disease progression and treatment in living animals over time, making it a valuable tool for the preclinical assessment of bone architecture in the context of disease (Feldkamp et al., 1989).

The mouse tibia is a long bone comprised of various structures including the head of the tibia, tibia, lateral malleolus, and medial malleolus (Figure 2.17). It has a tubular shape and is composed of cortical bone on the outside and trabecular bone on the inside. Within the trabecular compartment, only 20% of the volume is composed of bone, while the remaining space is filled with marrow and fat.

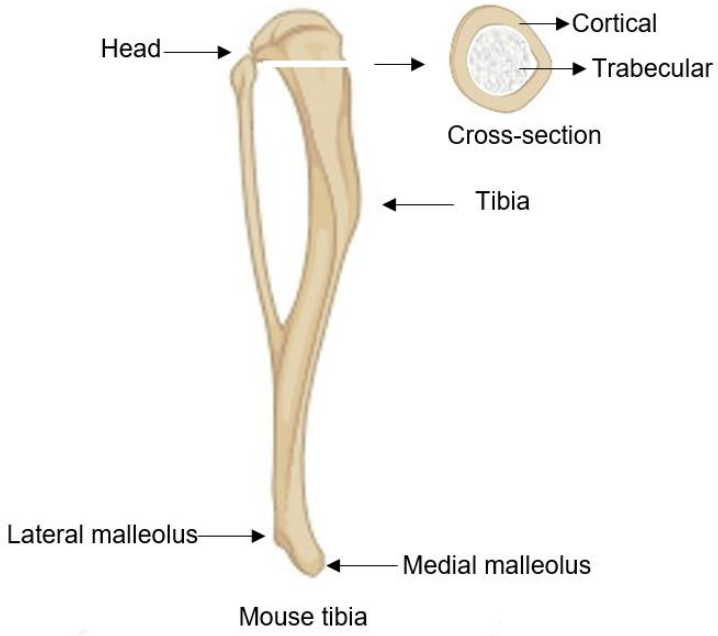

Figure 2.17: The structure of mouse tibia. Micro-CT can scan each cross-sections, which include cortical and trabecular. Then the region of interest (ROI) can be measured to obtain bone morphometry results.

Table 2.10: Bone morphometry analysis by Micro-CT

Abbreviation		Variable	Description	Standard unit
TV		Total volume	Volume of the entire region of interest	mm^3
BV		Bone volume	Volume of the region segmented as bone	mm^3
BV/TV	Trabecular	Bone volume fraction	Ratio of the segmented bone volume to the total volume of the region of interest	%
	Cortical		Ratio of the segmented bone volume to the total volume of the region of interest	%
Tb.N		Trabecular number	Measure of the average number of trabeculae per unit length	1/mm
Tb.Th		Trabecular thickness	Mean thickness of trabeculae, assessed using direct 3D methods	mm
Tb.Sp		Trabecular separation	Mean distance between trabeculae, assessed using direct 3D methods	mm
SMI		Structure model index	An indicator of the structure of trabeculae; SMI will be 0 for parallel plates and 3 for cylindrical rods	/

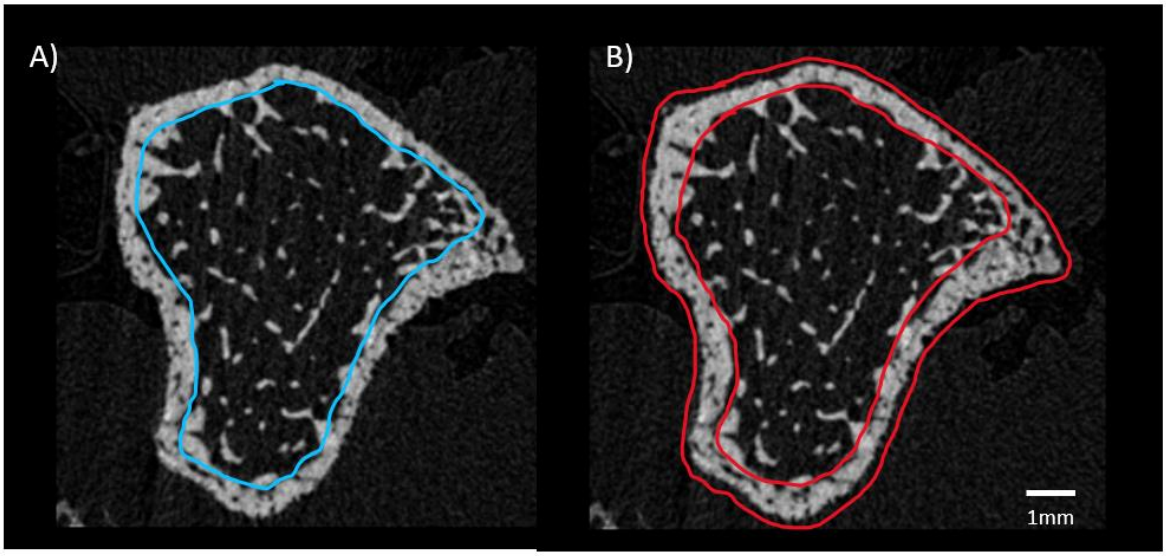

Figure 2.18: The ROI for trabecula and cortical in mice tibia. Schematic representation of ROI selected for trabecula and cortical tissue. The ROI for trabecula A) and cortical B) tissue, representing the colour in blue or red had a height of ~1mm and an offset of 0.2 and 0.5mm from the growth plate, respectively. The scale bar is 1mm.

The Skyscan 1272 scanner from Bruker in Billerica, Massachusetts, USA was used for bone structure analysis. The X-ray source emitted a voltage of 50 and a current of 200 µA, with a 0.5 mm aluminium filter. Approximately every 0.66°, a 2D picture sample was taken until 180°, resulting in a total of 272 2D images that were later reconstructed by the NRecon software. The settings of Micro-CT applied in the mice bone scanning represent in Table 2.11.

Table 2.11: Micro-CT settings applied in the mice bone scanning

Tibias	Scan resolution	Rotation	NRecon threshold	CTan threshold	ROI off set (mm)	ROI height (mm)
Trabecula	4.3 µm	180°	0-0.14	90-255	0.198mm	0.998
Cortical	4.3 µm	180°	0-0.14	90-255	0.499mm	0.998

2.10 Histomorphometry

2.10.1 Mice tibia sections

To compare the cellular events between PC3 WT and PC3 P2X4R KO cells, bone sections from mice tibias were stained to identify bone tissue and cells. The bone sections were prepared by Orla Gallagher (The University of Sheffield) using NBF to fix the mice tibias for a week. The samples were then transferred to 70% ethanol and decalcified using EDTA for 4 weeks, with the EDTA media changed every 3 days. After decalcification, the samples were embedded in paraffin wax and cut using a RM2265 microtome (Leica, Wetzlar, Germany) until the head of the tibia was revealed. The cut samples were kept on an ice block for an hour, and 3 um bone sections were cut using a Hand Operated Cutting Press. The section samples were immediately placed in a 45°C distilled water bath for 30 minutes to tighten the bone section. The bone sections were then mounted on Superfrost Plus Slides (Thermo Fisher), dried for 30 minutes, and kept in an oven overnight at 37°C. Finally, the bone sections were cooled to room temperature and stored in the fridge at 4°C.

2.10.2 TRAP staining

Tartrate-resistant acid phosphatase (TRAP) is an iron-containing enzyme common to bone and expressed in fully developed osteoclasts, the TRAP staining can stain tartrate-resistant acid phosphatase of osteoclasts. It can be a marker of osteoclast function. Bone mass is controlled by the balance between the activity of osteoblasts and the activity of osteoclasts (Janckila et al. 2001; Galão et al. 2011).

To assess the presence of tartrate-resistant acid phosphatase (TRAP) in bone samples, TRAP staining was performed by following the protocol (Janckila et al., 2001). The staining process was conducted by Orla Gallagher (The University of Sheffield). The bone sections were dewaxed through ethanol to distilled water and placed in an

acetate-tartrate buffer at 37°C for 5 minutes. The Acetate-tartrate buffer was prepared by adding sodium tartrate to an acetate buffer and warming it at 37°C for 2-3 hours. The sections were then incubated in Solution A, a mixture of Acetate-tartrate-buffer and naphthol/dimethylformamide solution, for 30 minutes at 37°C. Next, the bone sections were incubated in Solution B, a combination of 2 ml pararosaniline stock (50mg/ml, Sigma P-3750) and 2 ml of 4% sodium nitrite (Sigma S-2252) solution, for 15 minutes, and then washed twice in distilled water. Counterstaining was performed using Gill's II haematoxylin and blue for 20 seconds, followed by dehydration with ethanol, clearing in xylene, and mounting with DPX mounting medium. The presence of TRAP staining indicates the activity of osteoclasts, providing an insight into the balance between osteoblast and osteoclast activity in bone mass control.

2.10.3 H&E staining

The hematoxylin and eosin stain (H&E stain) is a commonly employed histological tissue stain and serves as one of the primary stains in the field of histology. The hematoxylin stains cell nuclei a purplish blue, and eosin stains the extracellular matrix and cytoplasm pink (Titford, 2005). The staining process was conducted by Orla Gallagher (The University of Sheffield). The H&E staining protocol is as follows: First, deparaffinize and rehydrate the slides to distilled water. Then, proceed to stain the slides in Mayer's Hematoxylin for 1 minute. Next, wash the slides with 4-5 changes of tap water or until the blue colour no longer comes off the slides. Afterward, submerge the slides in 1X phosphate-buffered saline (PBS) for 1 minute to enhance the blue colour of the nuclei. Following this, wash the slides with 3 changes of distilled water. Once washed, counterstain the slides in Alcoholic-Eosin for 1 minute without rinsing. Proceed to dehydrate the slides through 3 changes of 95% ethanol (EtOH) and 2 changes of 100% EtOH for 1 minute each. Clear the slides in 3 changes of xylene for 1 minute each change, and finally, mount the slides and apply coverslips.

2.10.4 Tumour burden measurement

To quantify the presence of tumour cells in bone after TRAP staining, the osteoMeasure assay was used. The bone sections were examined under a DMRB microscope (Leica, Wetzlar, Germany) at 20x magnification and the osteoMeasure7 v4.2.0.1 (osteoMetrics) software was used to manually measure the percentage of tumour cells. Tumour cells and bone marrow cells can be easily identified based on the colour and size of the cells (Figure 2.19).

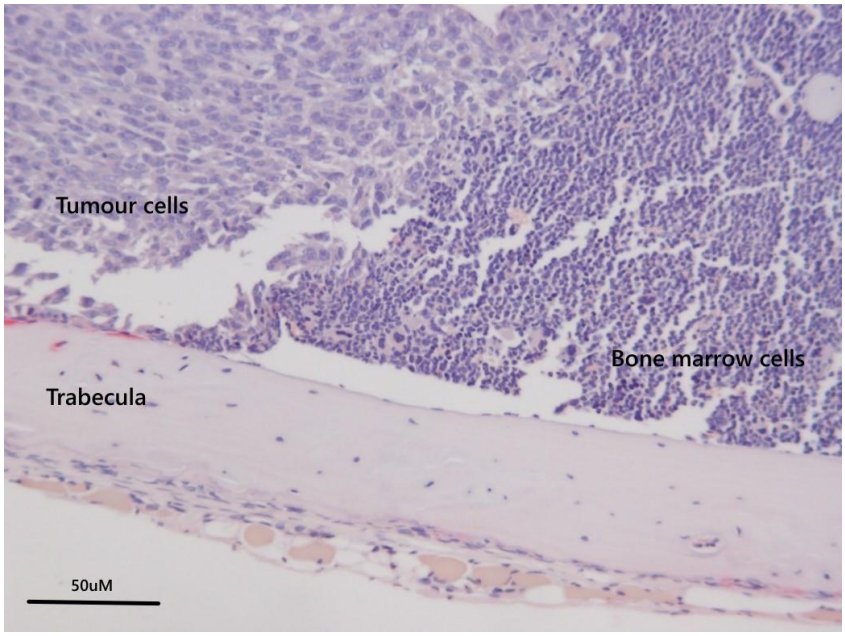

Figure 2.19: Bone sections after TRAP staining. The figure represents tumour cells and bone marrow cells in the mouse tibia. OsteoMeasure was used to manually measure the percentage of tumour cells manually by the DMRB microscope (Leica, Wetzlar, Germany) with the osteoMeasure7 v4.2.0.1 (osteoMetrics) software. Scale bar = 50uM.

2.11 RNA-seq bioinformatics analysis

RNA-seq analysis was carried out using four bioinformatics tools, namely Python, Galaxy Europe, David, and Gorilla (Table 2.12). To perform the principal component analysis (PCA) variance in samples, a scripting language for Python was downloaded from the website (https://pypi.org/), and the raw RNA-seq data was inputted into the script. Subsequently, the PCA result was generated. Galaxy Europe was carried out to identify differentiation expressed genes. In the David analysis, the ensymbols of differentiation genes were used to obtain gene ontology and KEGG pathways. Another analysis tool, Gorilla, was used to enrich the biological processes based on the differentially expressed genes.

Table 2.12: Bioinformatics tools used in RNA-seq analysis

Bioinformatics tools	Data sources	Results
Python	RNA-seq raw data	PCA variance
Galaxy Europe	RNA-seq raw data	Different expressed genes
David	Ensymbols of differentiation gene (Galaxy Europe)	Gene ontology KEGG pathway
Gorilla	Ensymbols of differentiation gene (Galaxy Europe)	Biological process enrichment

2.12 RNA-seq bioinformatics analysis by Galaxy Europe

Bioinformatics analysis was performed on the online platform Galaxy Europe (https://usegalaxy.eu/storage). Two pairs of RNA sequences (R1 and R2) for each sample were obtained from Company Source BioScience. Raw fastq files for both R1 and R2 sequences were uploaded onto Galaxy. The following tools were used for gene differential expression analysis in RNA-seq: trimmomatic, FastQC, featureCounts, and limma.

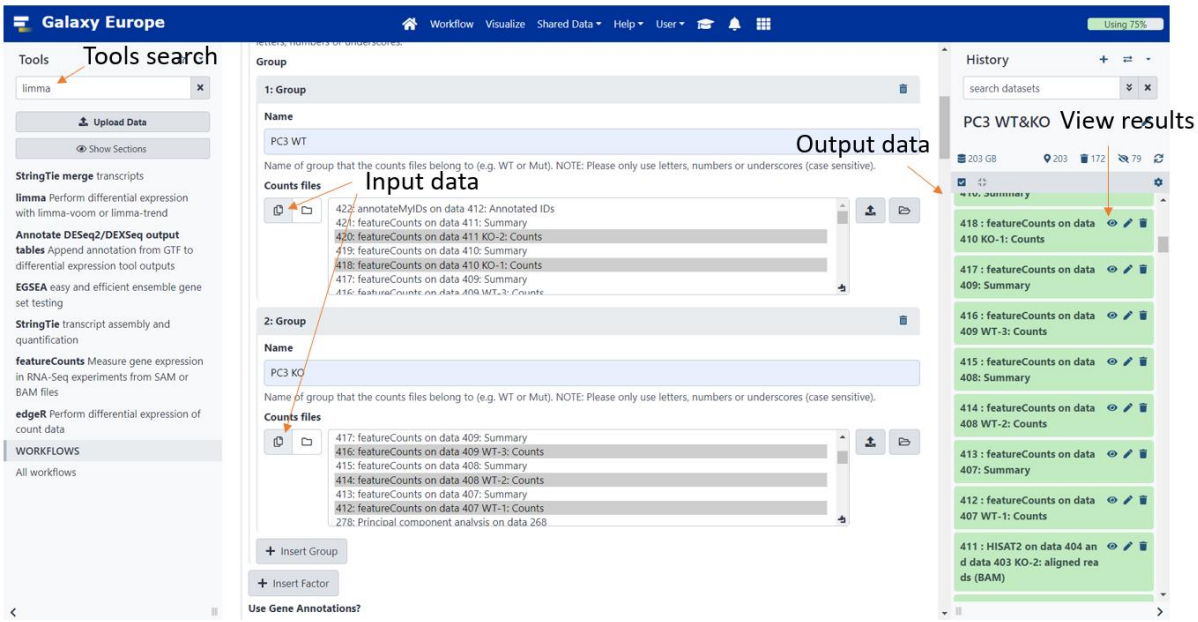

Figure 2.20: The Galaxy Europe web user interface. The figure displays a screenshot of limma analysis, which was used to analyze RNA-seq data. The red arrows pointed out the location of tools research, input data, output data and view results on the interface. The counts files were selected along with the gene annotation, and the contrast of interest was set as PC3 KO-PC3 WT with an exude option. The output of this analysis can be seen in the history list.

To ensure the quality of RNA sequence data, two tools, trimmomatic and FastQC, were used in the analysis. Trimmomatic was employed to remove low-quality reads and other artifacts, while FastQC was used to check the quality of the trimmed reads. In trimmomatic, paired-end reads and R1 and R2 sequences were selected, and the default options were used. The output of trimmomatic was then used as the input for FastQC. All the trimmomatic results were selected, and FastQC was executed with the default options. The FastQC report provided information on sequence counts, GC%, and quality values to assess the quality of the RNA sequence data.

To align all reads, the Hisat2 tool was used. A built-in genome with a reference genome called “Human Dec.12 (GRCh38/hg38)” was selected, and the previous trimmomatic results were used as input. The default options were kept, and the tool was executed to obtain the Hisat2 results. Feature counts were then used to create a

bam file for each gene read. The gene annotation file was selected as “featureCounts built-in, hg38”, and the previous Hisat2 results were used as input. The default options were kept, and the tool was executed. To annotate the gene IDs, the “annotateMyIDs” tool was searched and executed, and the results were generated with gene ID and aligned reads. Finally, the limma tool was used to create a gene differentiation expression table and report (Table 2.13). Control groups were selected as all the PC3 KO, and treatment groups were selected as all the PC3 WT. The contrast was set to “PC3 KO-PC3 WT” to generate the results (Jalili et al., 2020).

Table 2.13: Galaxy Europe setting

Tool	Functions	Parameters	Input	Output
Trimmomatic	Trim the reads	Paired-end reads	Raw fastq files	Trimmomatic fastq files
FastQC	Evaluate the quality of raw data	/	Trimmomatic fastq files	FastQC report
Hisat2	Reads alignment	Reference: “Human Dec.12 (GRCh38/hg38)”	Trimmomatic fastq files	Hisat2 aligned reads (BAM)
Feature counts	Calculate each gene reads	Built-in reference (hg38)	Hisat2 aligned reads (BAM)	Feature counts and summary report
Limma	Create a gene differentiation expression table and report	Treatment: PC3 KO; Control: PC3 WT; Contrast: PC3 KO-PC3 WT; Gene annotation option and set LogFC > 1	Feature counts	Differentiation genes expression and volcano plots

2.13 Statistical analysis

The experiments were conducted in triplicate, with each experiment performed independently three times. The exception is the apoptosis assay for P2X4R inhibition, which had two replicates. In *in vivo*, the P2X4R inhibition by 5-BDBD had a mouse number of 7 in each group, while the P2X4R knockout had 10 mice in each group. Differences between groups were analyzed using unpaired Student's t-tests, one-way ANOVA tests, or chi-square tests in GraphPad Prism 8 software. The results are reported as mean ± standard deviation (SD), and p-values are denoted as *p<0.05, **p<0.01, ***p<0.001, ****p<0.0001. For RNA-seq data statistical analysis, the built-in default test was used, considering p-values less than 0.05 as statistically significant.

CHAPTER 3:

RESULTS: Inhibiting P2X4R reduces the tumour growth *in vitro* and suppresses tumour formation *in vivo*

3.1 Introduction

P2XR are non-selective cation channels that open in response to ATP activity, it is mainly associated with secretory epithelia, allowing for direct transmembrane transport of ions such as Ca^{2+}, Na^{+} and K^{+} (Novak, 2011). P2X4R are found to be widely expressed in diverse physiological processes, such as synaptic transmission (Kawate et al., 2009a), inflammation (Paalme et al., 2019), nervous system disorders (Stokes et al., 2017) and sensing of taste and pain (Zhang et al., 2019). P2X4R is also expressed in many cancer types including breast cancer (Chadet et al., 2022), glioma (Huo and Chen, 2019), colon tumour (Schmitt et al., 2022), brain tumour (Guo et al., 2004) and most importantly to this study, PCa. P2X4R functionally in the process of tumour development, most studies suggest that P2X4R positively associates with tumourigenesis (Huo and Chen, 2019, Chong et al., 2010, Asif et al., 2019).

In the process of P2XR secretion in the epithelial cell, particularly the P2X4R in gland secretion, ATP-responsive and the increase in intracellular Ca^{2+} levels mediated by P2X4R is a vital part of the mechanism leading to exocytosis (Novak, 2011). Evidence showed that a P2X4R for an ATP-gated cation channel is predominantly expressed in human vascular endothelial cells and is involved in the ATP-induced Ca^{2+} influx (Yamamoto et al., 2000). Study showed that the antidepressant paroxetine, a P2X4R inhibitor, can induce free Ca^{2+} concentrations to rise in human PCa PC3 cells, suggesting a functional role of P2X4R in the process of PCa (Pan et al., 2010). Fluo-4 Direct™ Calcium Assay was performed in detecting changes of intracellular calcium release mediated by P2X4R.

Previously, to understand the transcriptional expression pattern of P2 receptors in PCa cells, an individual quantitative qPCR on total mRNA was measured using three different PCa cell lines including PC3, LNCaP and C4-2B4. The results demonstrated that P2X4R expressed the highest among P2 receptors including all the P2XR and P2YR (He et al., 2020). There are pharmacological tools targeted for P2X4R including selective antagonists (5-BDBD, PSB-12062, BX430) and positive modulators

(ivermectin, avermectins, divalent cations). The benzodiazepine derivative 5-BDBD (5-(3-bromophenyl)-1,3-dihydro-2H-benzofuro[3,2-e]-1,4-diazepin-2-one) was one of the commonly used P2X4R antagonists in recent years. Using two different concentrations of antagonist 5-BDBD resulted in ATP dose-response changes indicating that 5-BDBD acts as a competitive antagonist to P2X4R (Balázs et al., 2013). PSB-12062 (10-[(4-Methylphenyl)sulfonyl]-10H-phenoxazine) is a P2X4R antagonist, it has been used to pre-treat P2X7-deficient BV-2 cells to elucidate the roles of P2X4R (Trang et al., 2020). The selective P2X4R antagonists PSB-12062 have been used to investigate the role of this receptor in bone (Layhadi et al., 2018). Antagonist PSB-12062 inhibits ATP-mediated induction of CXCL5 gene expression and secretion of CXCL5 by primary macrophage. PSB-12062 can lose the function of the absence of extracellular Ca^{2+} to functionally inhibit P2X4R (Layhadi et al., 2018). In this study, P2X4R was inhibited by antagonists with different inhibition mechanisms, a competitive antagonist of 5-BDBD, and the antagonist PSB-12062 which could induce an ATP-mediated pathway to inhibit P2X4R expression.

Here, I comprehensively reveal the roles of P2X4R in PCa progression and test the hypothesis that P2X4R activity enhances tumour formation by PCa cells (He et al., 2020).

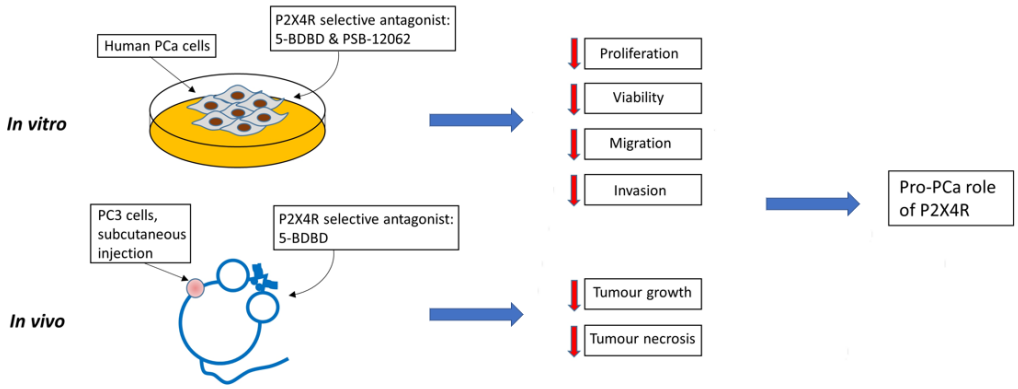

Figure 3.1: Graphical abstract. In this study, P2X4R inhibition by performing antagonist 5-BDBD or PSB-12062 treatment for testing PCa cellular changes *in vitro* including calcium influx, migration, invasion and apoptosis. Results showed inhibiting P2X4R reduced calcium intracellular release in PC3 cells, highly impacting the ability of invasion in both PC3 cells and C4-2B4 cells *in vitro*. Then PC3 cells were subcutaneously injected into BALB/c nude mice and treated with 5-BDBD antagonist, resulting in reduced tumour growth and necrosis compared to non-treatment *in vivo*. These data indicated that P2X4R has a pro-tumourigenesis role in PCa.

3.2 Inhibiting P2X4R reduced tumour growth *in vitro*

The previous study investigated the effects of P2X4R inhibition on the proliferation, viability, and migration of PCa cell lines PC3 and C4-2B4. Our preliminary data showed that the antagonists 5-BDBD and PSB-12062 significantly reduced cell proliferation in both cell lines, with a more significant impact on C4-2B4 viability. P2X4R inhibition also considerably reduced the ability of PC3 cells to migrate in a scratch assay. In this study, further investigated the effects of P2X4R inhibition using additional assays. I treated PC3 cells with 5-BDBD and PSB-12062 and used the Fluo-4 calcium kit to test calcium influx intracellularly. I also evaluated the migration of C4-2B4 cells using a transwell insert assay, and the invasion of PC3 and C4-2B4 cells using a transwell cell invasion assay. Finally, I measured apoptotic activity in both cell lines using the caspase 3/7 activity apoptosis assay.

3.2.1 Functional inhibition of P2X4R in PCa cells with specific antagonists

The Fluo-4 Assay Kit, which measures calcium influx associated with receptor activation or inhibition, was used to assess calcium mobilization in PCa cells and determine whether P2X4R are functionally expressed. This assay detects fluorescence from G-protein-coupled receptors (GPCRs) and calcium channels. Data analysis was performed using GraphPad Primer 8.

To investigate whether P2X4R is functionally expressed in PCa cells, PC3 cells were treated with antagonists 5-BDBD and PSB-12062, and calcium influx was assessed using Fluo-4 Assay Kit. Using ATP as an agonist and the antagonists at concentrations of 1.0 μM and 1.5 μM, respectively, the data demonstrated that P2X4R are functionally expressed in PCa cells. The peak intensity was absent in the vehicle control, indicating that no calcium signal was detected without agonist ATP. ATP dramatically activated P2X4R, while the antagonists 5-BDBD and PSB-12062 reduced the activation. Treatment with 5-BDBD and PSB-12062 reduced the calcium influx by around 9% (Figure 3.2 & 3.4) with a representative graph showing the calcium reduction (Figure 3.3 & 3.5). These results demonstrated that P2X4R was functionally inhibited in PCa cells by the inhibitors.

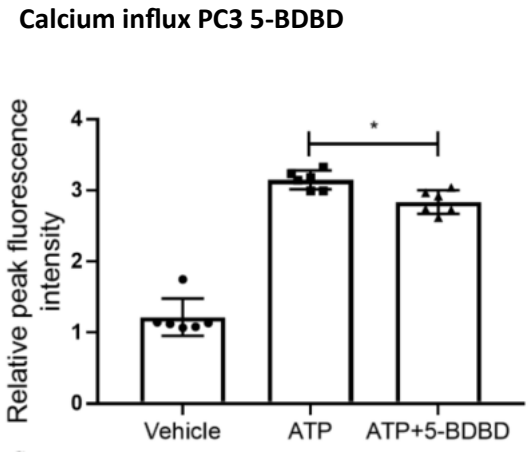

Figure 3.2: Antagonist 5-BDBD reduces calcium influx in PC3 cells. The activation of P2X4R was significantly reduced by treatment with the P2X4R-specific antagonist, 5-BDBD, which caused an 8.9% reduction in peak fluorescence compared to the treatment group with an agonist alone (ATP). The mean value of peak fluorescence in the ATP-only group was 3.07, while the mean value in ATP with 5-BDBD group was 2.74. The experiment was performed with six biological repeats and three technical repeats. Data are the mean ± SD, one-way ANOVA with post hoc Tukey, *$p < 0.05$.

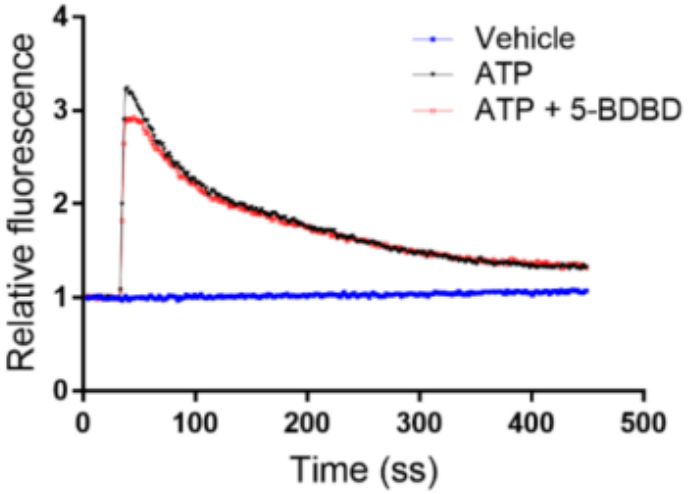

Figure 3.3: Representative graph of PC3 5-BDBD treatment. This figure shows the representative diagram of calcium assay in 5-BDBD antagonist treatment. The y-axis represents the fluorescence intensity, and the x-axis represents the time in seconds. The blue line represents the vehicle control, where no calcium signal is detected. The green line represents the treatment group with 50μM ATP, showing a calcium peak after ATP treatment, which confirms the activation of calcium influx in cells. The red line represents the treatment group with both ATP and 5-BDBD, where the peak is significantly reduced, indicating the functional inhibition of P2X4R in PCa cells by the antagonist 5-BDBD.

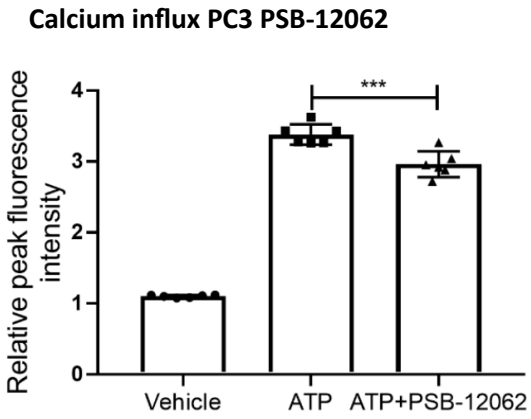

Figure 3.4: Antagonist PSB-12062 reduces calcium influx in PC3 cells. In the treatment group with both agonist and antagonist, the P2X4R-specific antagonist PSB-12062 decreased the activation of P2X4R by 9.2% compared to the treatment group with an agonist alone (ATP). The mean peak fluorescence value in the ATP-only group was 3.21, and the mean value in the PSB-12062 group was 2.94. The data were obtained from six biological repeats with three technical repeats. Data are the mean ± SD, one-way ANOVA with post hoc Tukey's test. ***$p < 0.001$.

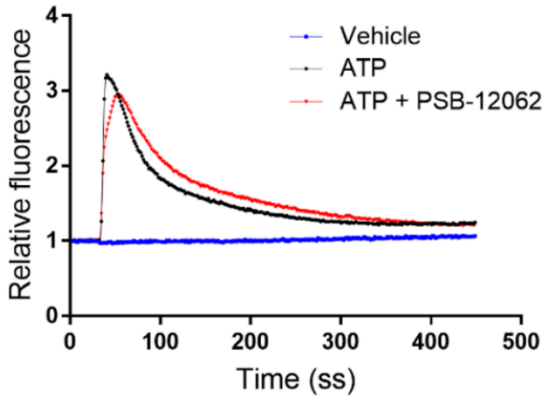

Figure 3.5: Representative graph of PC3 PSB-12062 treatment. The calcium influx peak was reduced by adding antagonist PSB-12062, confirming P2X4R has been functionally inhibited in PCa cells.

3.2.2 Inhibiting P2X4R did not affect apoptosis

The Caspase 3/7 activity apoptosis assay was utilized to measure the process of programmed cell death. PCa cells were treated with 1.0 μM 5-BDBD and 1.5 μM PSB-12062 antagonists, and the results demonstrated that inhibiting P2X4R with both antagonists for 24 hours did not impair the apoptosis of either the PC3 cells ($p > 0.05$) (Figure 3.6) or C4-2B4 cells ($p > 0.05$) (Figure 3.8). To confirm the effectiveness of the apoptosis assay, a positive control group was performed using doxorubicin. PCa cells were treated with a final concentration of 1.0 μM doxorubicin, and the results showed a significant increase in the doxorubicin treatment group compared to the vehicle control, with a 326% increase in PC3 cells (Figure 3.7) and a 386% increase in C4-2B4 cell lines (Figure 3.9).

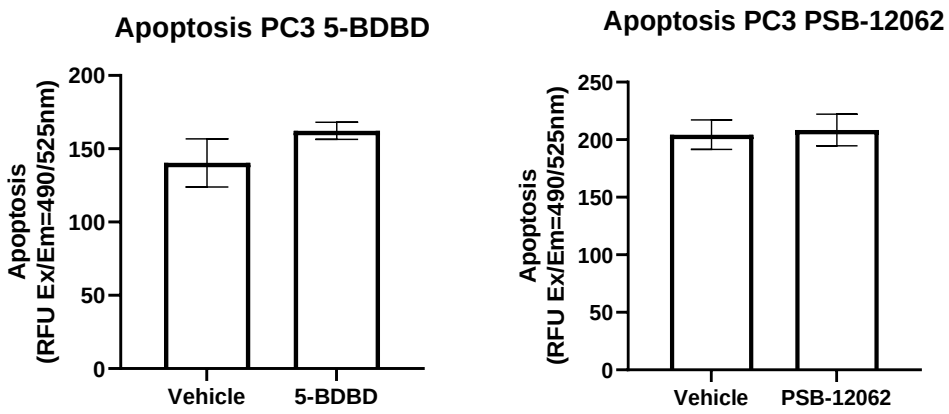

Figure 3.6: P2X4R antagonists did not affect PC3 apoptosis. After a 24h treatment of antagonists, the apoptotic activity was measured using the Cell Meter™ Caspase 3/7 apoptosis assay in PC3 cells. There was no significant difference observed between the vehicle control group and the treatment group with PC3 5-BDBD ($p = 0.22$) and PSB-12062 ($p = 0.79$). Data are the mean ± SD. N=2, Student's t-test, non-significant, $p > 0.05$.

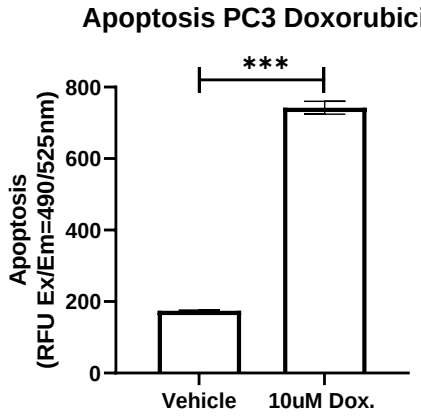

Figure 3.7: The apoptotic activity increased after doxorubicin treatment. The apoptotic activity after a 24h treatment of doxorubicin (as a positive control) was measured using the Cell Meter™ Caspase 3/7 apoptosis assay in PC3 cells. Results showed a significant increase in the doxorubicin treatment group compared to the vehicle control (p = 0.0005). Data are the mean ± SD. N=2, Student's t-test, *** p < 0.001.

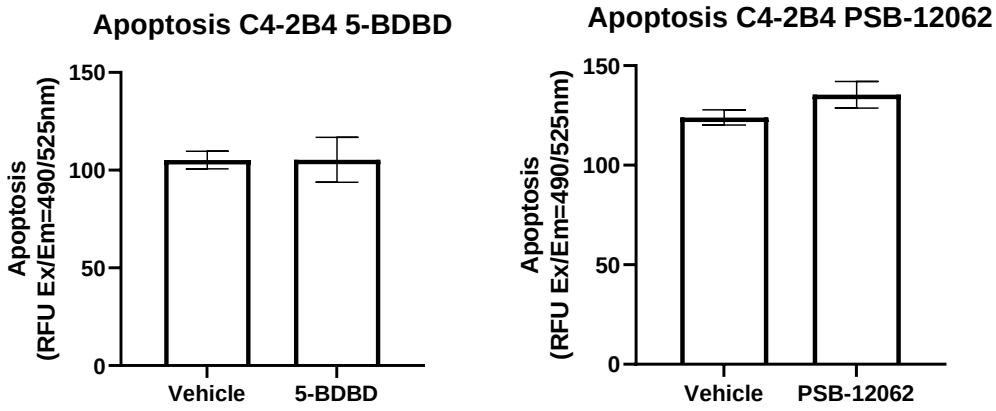

Figure 3.8: P2X4R antagonists have no effect on C4-2B4 apoptosis. After a 24h treatment of antagonists, the apoptotic activity was measured using the Cell Meter™ Caspase 3/7 apoptosis assay in C4-2B4. There was no significant difference observed between the vehicle control group and the treatment group with C4-2B4 5-BDBD (p = 0.98) and PSB-12062 (p = 0.17). Data are the mean ± SD. N=2, Student's t-test, non-significant, p > 0.05.

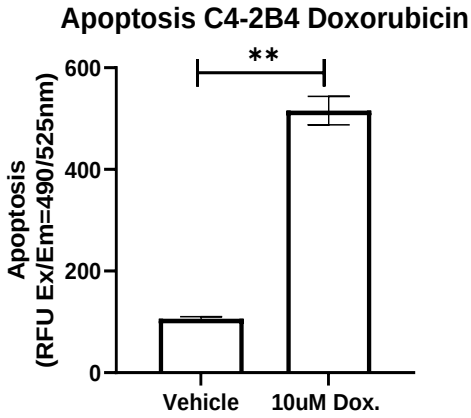

Figure 3.9: The apoptotic activity significantly increase after doxorubicin treatment. After a 24h treatment of antagonists or doxorubicin (as a positive control), the apoptotic activity was measured using the Cell Meter™ Caspase 3/7 apoptosis assay in C4-2B4 cells. Results showed a significant increase in the doxorubicin treatment group compared to the vehicle control ($p = 0.0024$). Data are the mean ± SD. N=2, student's t-test, ** $p < 0.01$.

3.2.3 Inhibition of P2X4R did not affect the migration of C4-2B4 cells

Due to technical limitations, the scratch assay was found to be an inappropriate method for testing the migration ability of C4-2B4 cells. Instead, the Transwell cell migration assay was used, in which C4-2B4 cells were seeded on top of the Transwell cell culture inserts with or without P2X4R inhibitors, and a chemoattractant was added to the lower chamber. After 16 hours, the migrated cells were stained and the percentage of areas covered by migrated cells was measured using ImageJ software. Results showed that 5-BDBD treatment led to a 13% reduction in migration ($p = 0.07$), meanwhile, PSB-12062 did not affect the migration of C4-2B4 cells ($p > 0.05$, Figure 3.10).

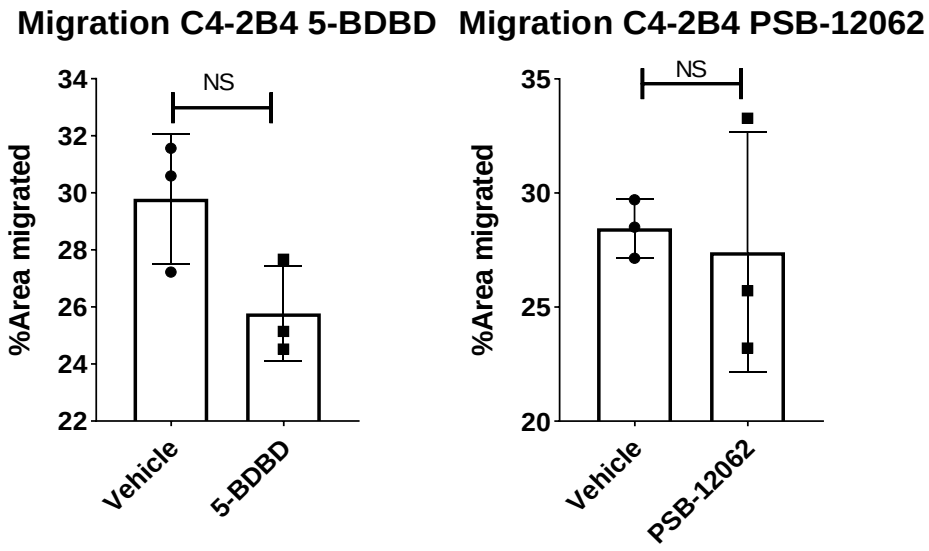

Figure 3.10: Migration ability of C4-2B4 cells did not affect with 5-BDBD treatment. A Transwell migration assay was performed to test the migration ability of C4-2B4 cells. Percentage areas that migrated within 16 h were measured and compared between 5-BDBD or PSB-12062 treated groups and vehicle groups. Data are the mean ± SD. N = 3, student's t-test, non-significant, $p > 0.05$.

3.2.4 Cell invasion assay

The Matrigel-based Transwell assays were employed to investigate the impact of P2X4R inhibition on the invasiveness of PC3 and C4-2B4 cells using specific antagonists. The assay involved adding PCa cells to the top chamber of the transwell with a density of $5x10^4$ cells per well and treating them with P2X4R inhibitors. During the invasion process, invasive cells attached to the membrane and were detected by eosin and haematoxylin staining. The invasive cells were then scanned using a digital scanner and analysed with Image J software to calculate the differences in the percentage area covered by cells between the vehicle control and antagonist-treated groups. As the following, inhibition of P2X4R reduced the invasion of both PC3 and C4-2B4 cells.

3.2.4.1 Inhibition of P2X4R reduce the invasion of PC3 cells

As shown in Figure 3.12, the invasiveness of PC3 cells was significantly reduced by 53% (p = 0.0436) under the treatment of 5-BDBD (1 μM) and 53% (p = 0.026) under the treatment of PSB-12062 (1.5 μM). T-test analysis showed a significant difference in invasiveness reduction between the antagonist's treatment and the vehicle control. Representative images of PC3 cell invasion are presented in Figure 3.11.

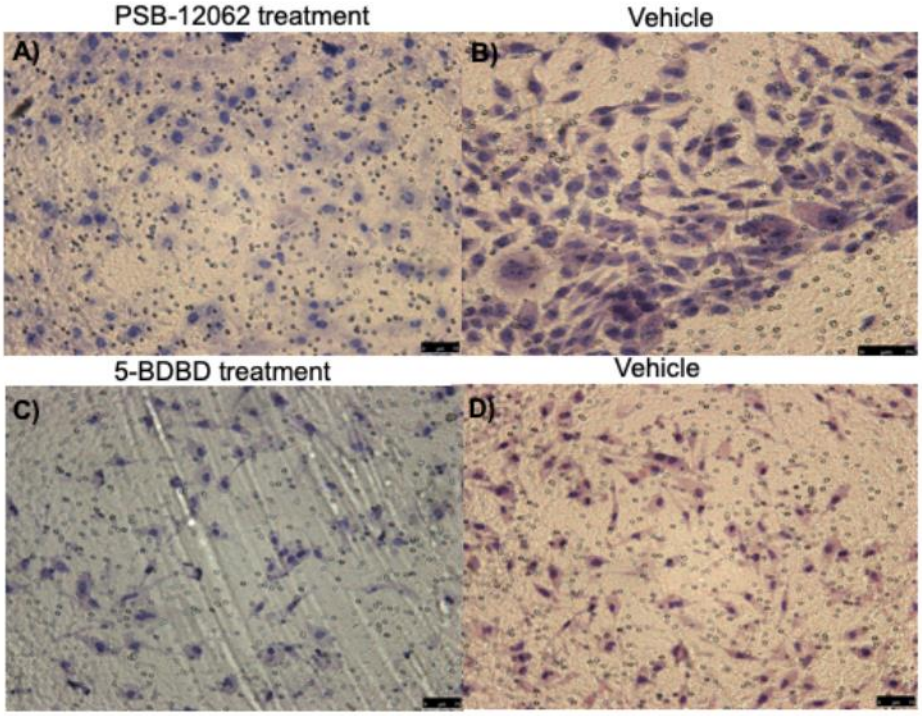

Figure 3.11: Representative images of PC3 cells invasion after antagonists' treatment for 72 hours. The number of invasive PC3 cells with 5-BDBD and PSB-12062 treatment is dramatically lower than the vehicle control. Scale bar = 75μm.

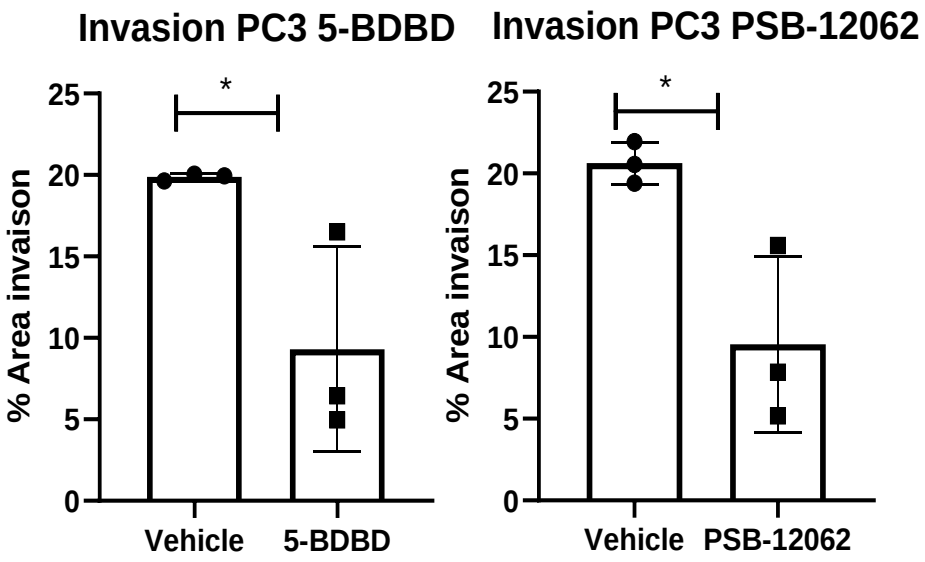

Figure 3.12: Invasion of PC3 cells decrease with P2X4R antagonist. These two P2X4R's antagonists, 5-BDBD and PSB-12062, significantly inhibited the invasion of PC3 cells, with a reduction of 53% by both 5-BDBD and PSB-12062. A t-test analysis found a significant difference between the vehicle control and treatment groups among the two antagonists. Data are the mean ± SD. N=3, unpaired t-test, * $p < 0.05$.

3.2.4.2 Inhibition of P2X4R reduce the invasion of C4-2B4 cells

As is shown in Figure 3.14, the treatment of PSB-12062 (1.5 μM) and 5-BDBD (1 μM) significantly reduced the invasiveness of C4-2B4 cells by 38% ($p = 0.032$) for 5-BDBD and 54% ($p = 0.037$) for PSB-12062 (Figure 3.14). The invasiveness reduction was calculated by analyzing the percentage area covered by cells in the transwell invasion assay using ImageJ software. These results demonstrated the effectiveness of P2X4R inhibition in reducing the invasiveness of C4-2B4 cells. Representative images of C4-2B4 cell invasion are presented in Figure 3.13.

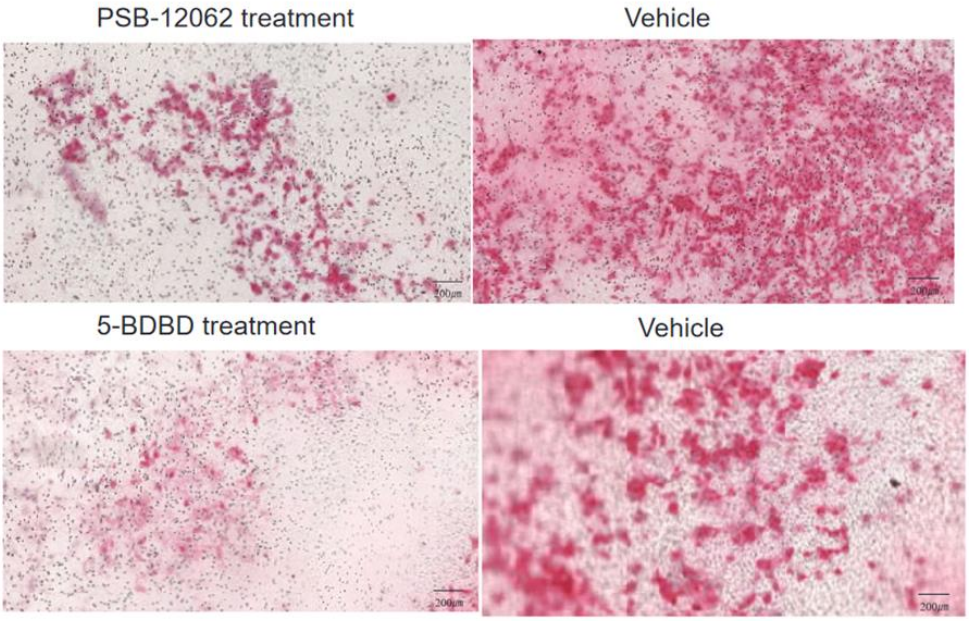

Figure 3.13: Representative images of C4-2B4 cells invasion after antagonists' treatment for 72 hours. The numbers of invasive C4-2B4 cells treated with 5-BDBD and PSB-12062 are dramatically lower than the vehicle control. Scale bar = 200 µm.

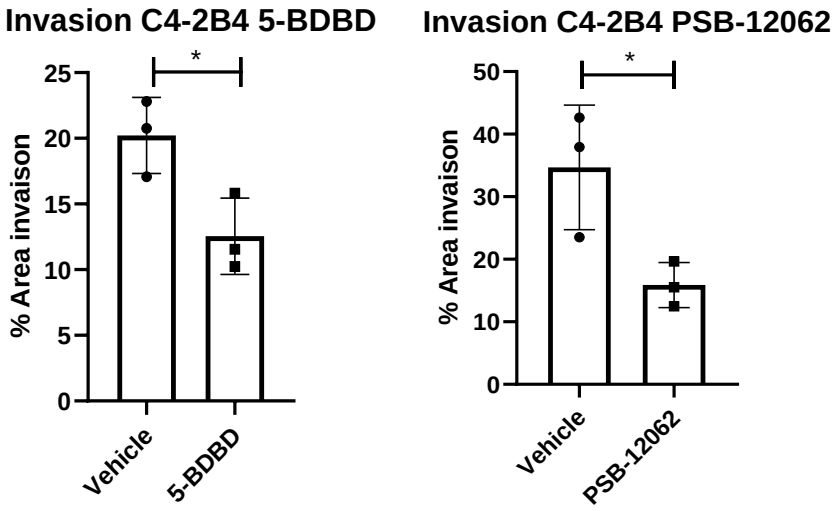

Figure 3.14: Invasion of C4-2B4 cells decrease with P2X4R antagonist. Both PSB-12062 and 5-BDBD significantly inhibited the invasion of PC3 cells, with reductions of 54% and 38%, respectively. A t-test analysis found a significant difference between the vehicle control and treatment groups among the two antagonists. Data are the mean ± SD. N=3, unpaired t-test, *$p < 0.05$.

3.3 Inhibiting P2X4R by 5-BDBD *in vivo*

3.3.1 Introduction

To study the interaction between tumour growth and the tumour microenvironment, cancer cell lines are commonly transplanted into immunodeficient mice (Murayama and Gotoh, 2019). In my study, the subcutaneous xenograft model was used, and the antagonist 5-BDBD was used to inhibit P2XR and understand its function in PCa. In Maynard's studies, 1×10^6 PC3 cells were mixed with 50% Matrigel diluted in PBS and subcutaneously injected into mice. Tumour size was measured using electronic calipers after subcutaneous injection, and tumour volumes were calculated as length × width × height × 0.5 (in mm^3) (Maynard et al., 2022, Mishra et al., 2021).

Previously, I found that the antagonist 5-BDBD can inhibit tumour cell proliferation and mobilization *in vitro*. To understand whether inhibiting P2X4R affects the progression of PCa *in vivo*, I used a BALB/c nude xenograft mouse model. Dr. Ning Wang subcutaneously injected PC3 cells into six-week-old BALB/c nude mice, followed by daily administration of 10 mg/kg 5-BDBD or vehicle (DMSO) for three weeks (Figure 3.15). Tumour sizes were measured twice a week using vernier calipers, and tumour volumes were calculated as ellipsoids and compared between treated and vehicle groups. At the endpoint, the mice were sacrificed by cervical dislocation, and the tumours were taken out from the mice.

3.3.2 P2X4R antagonist showed the anti-tumourigenic *in vivo*

The mice were first subcutaneously injected with 5 × 10^6 PC3 cells, which were suspended in 50% PBS and 50% Matrigel prepared fresh. Then the mice were randomly divided into two groups: 7 for 5-BDBD treatment and 7 for vehicle control. The reagent for 5-BDBD drugs was diluted in DMSO because it is not soluble in PBS, and DMSO was used as the vehicle control. The mice were intraperitoneally injected daily with 10mg/kg 5-BDBD for the treatment group and 10ul DMSO for the vehicle control group.

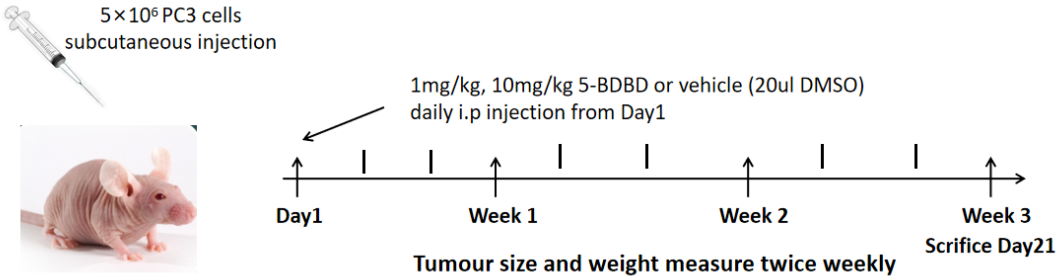

Figure 3.15: The process of in vivo assay for inhibiting P2X4R by antagonist 5-BDBD. Briefly, six-week-old BALB/c immunocompromised mice were subcutaneously (s.c) injected with 5 × 10^6 PC3 cell suspension with 50% PBS + 50% Matrigel. After randomization of the mice in the treatment group, the administration of 5-BDBD were daily intraperitoneally injected with a dosage of 10 mg/kg. In contrast, the vehicle group were injected with 10 ul DMSO. The injection started from day one until three weeks post-tumour cell inoculation at the endpoint.

3.3.3 5-BDBD treatment delays the tumour proliferation *in vivo*

The administration of 5-BDBD reduced the tumour growth compared to vehicle group. A significant reduction of about 40% was observed by day 14 ($p = 0.028$). It is important to note that while the statistical significance of the decrease in tumour volume was lost after two weeks of tumour cell injection, there was still a trend towards reduction in the

treatment group compared to the vehicle control group, with a 13% reduction (p = 0.086) in tumour volume at the end point. This suggests that the inhibition of P2X4R by 5-BDBD may have a delaying effects on early tumour proliferation *in vivo* (Figure 3.16).

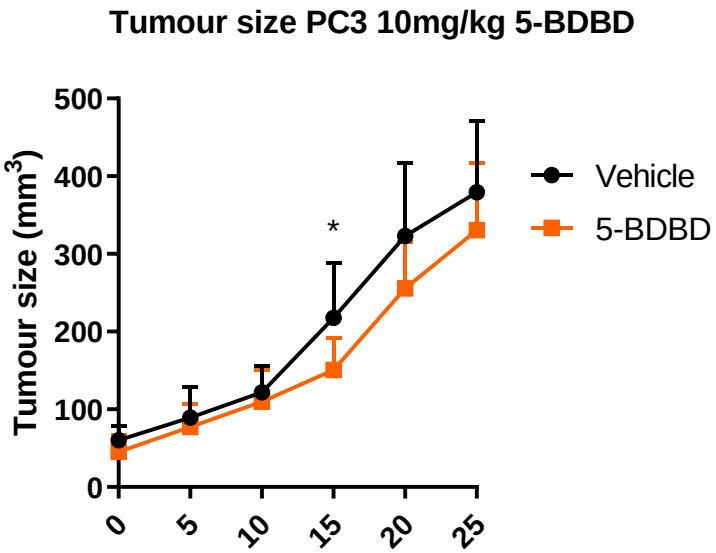

Figure 3.16: Tumour volumes reduced in 5-BDBD treatment tumour-bearing mice. Vernier calipers were used to measure the tumour size twice a week, and then tumour volumes were calculated as ellipsoids (volume = πABC/6; A = length, B = width, C = height) and compared between treated and non-treated groups. Data are the mean ± SD. N = 7, Student's t-test, * $p < 0.05$

The P2X4R antagonist treatment group suppressed tumour formation, leading to a significant 3.3-day delay until tumours reached the 200-mm3 volume, double the initial seeding volume. The tumour in the vehicle control group reached 200-mm^3 volume for 14.6 days while it took 17.9 days, a 3.3-day delay in the 5-BDBD treated group (p = 0.005, Figure 3.17). The representative images of tumour-bearing mice are shown in Figure 3.18.

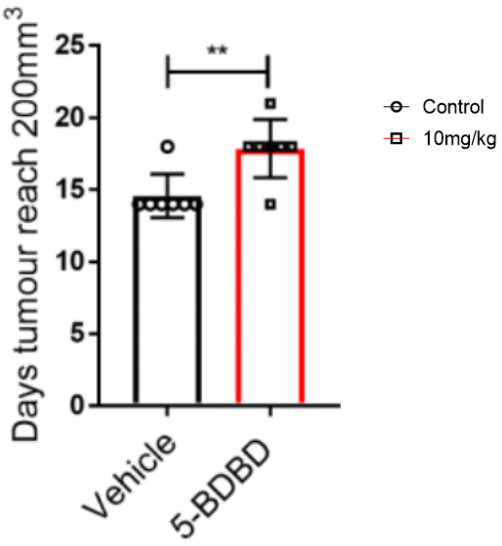

Figure 3.17: Time for tumour volume reached 200-mm3 significantly different from vehicle and treatment group. Days needed for tumours to reach 200 mm^3 were also compared between treated and vehicle groups. Data are the mean ± SD. N = 7, Student's t-test, $^{**}p < 0.01$.

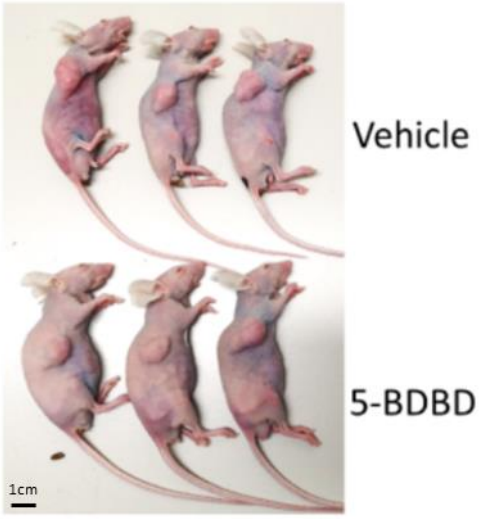

Figure 3.18: The representative images for 10mg/kg 5-BDBD treatment and vehicle control. After subcutaneous injection, the tumour can be observed growing under mice skin. Representative images of tumour-bearing mice tumour in 5-BDBD treatment and vehicle control at the endpoint. The scale bar = 1 cm.

3.3.4 There are more tumour necrosis in the vehicle control group compared to the 5-BDBD treatment

Dissected tumours were cut in half and examined for the presence of a necrotic center. Necrosis refers to the death of living tissues in tumour (Liu and Jiao, 2020). Histological staining revealed that the mouse number of vehicle control group had more necrosis compared to its of the 5-BDBD treatment group. Specifically, all seven tumour samples from the vehicle group had necrosis, while only two out of seven samples in the treatment group had necrosis. The tumour necrosis was observed in slides under microscope. This difference was found to be statistically significant (p = 0.0053, Chi-square test, Figure 3.19-3.20).

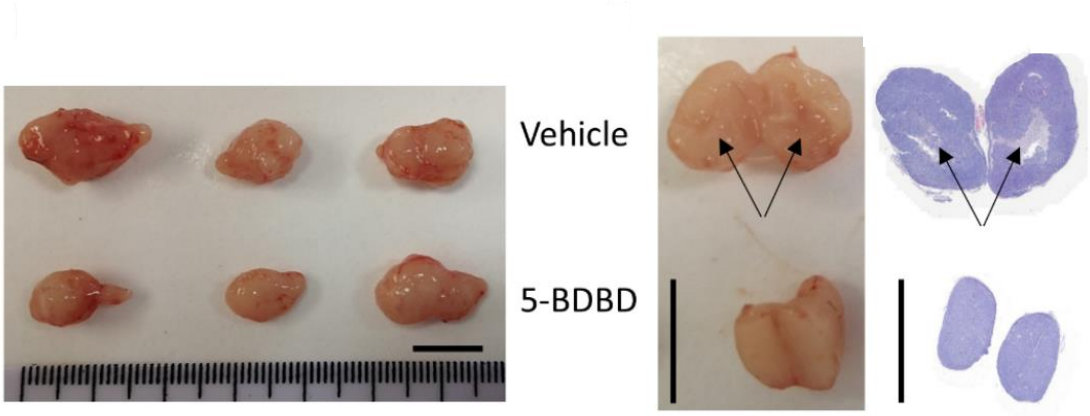

Figure 3.19: Representative images of mice dissected tumours. Representative pictures of dissected tumours, comparing treated and vehicle groups at the endpoint. The necrosis was further confirmed by H&E staining of the tumours, here are the representative images for tumour necrosis. The arrows indicated the necrosis in tumour and tumour sample slide. The scale bar = 1 cm.

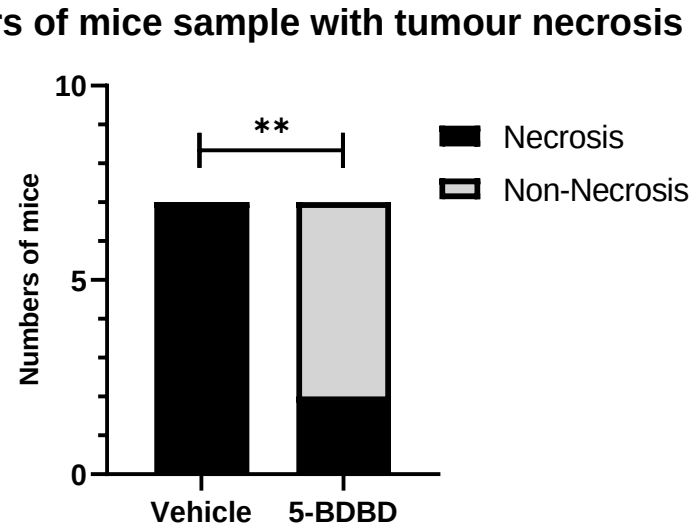

Figure 3.20: The number of mice samples with tumour necrosis are significantly higher in vehicle compared to 5-BDBD treatment. All tumours in the vehicle group have necrosis inside, while only two of seven observed necrosis in the treatment group. A statistical analysis with a Chi-square test suggested a significantly reduced presence of necrosis in the 5-BDBD-treated group compared to the vehicle. N = 7, ** $p < 0.01$.

3.3.5 No significant difference among the percentage of proliferating cells in tumours

The Ki67 protein has been widely used as a proliferation marker for human tumour cells for decades. Tumours were cut into sections and stained with a combination of Ki67 antibodies, and the positive proliferating cells were identified by the presence of brown nuclear (DAB) staining in tumour cells. The results of Ki67 staining demonstrated no significant difference in the number of proliferating cells between the 5-BDBD treatment and non-treatment groups (Figure 3.22). The representative images are presented in Figure 3.21. This may be due to the higher percentage of necrosis developed in the vehicle control group, leading to masses of cell death that cannot be accounted for.

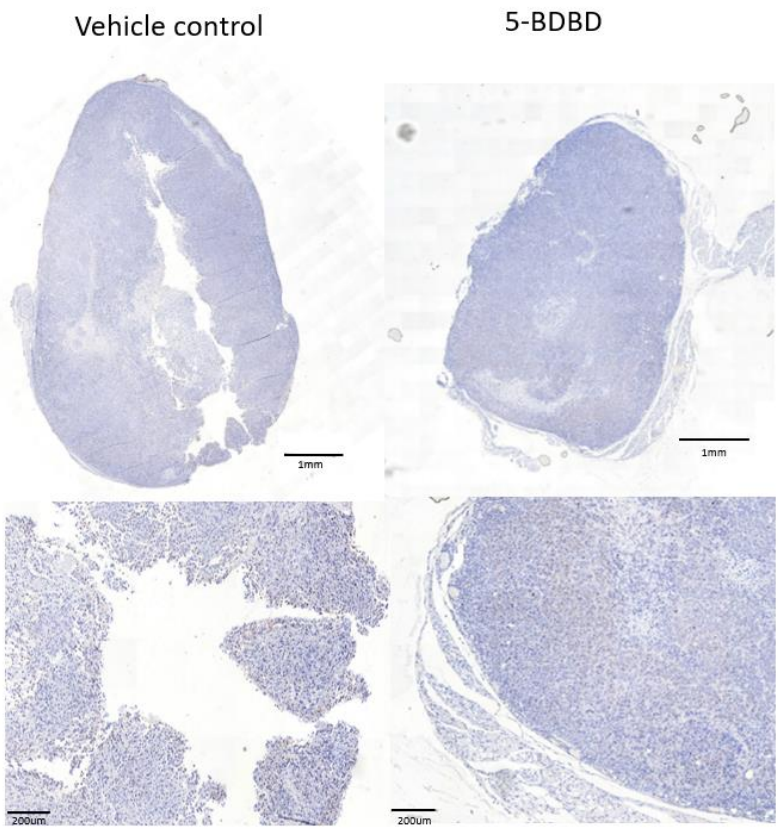

Figure 3.21: The representative images for Ki67. Briefly, the protocol of Ki67 staining is described as follows: the tumour samples were prepared for Ki-67 staining assay. First the tumour section was blocked with 1% NGS in PBST, and then incubated with primary antibody and secondary antibody, followed by counter staining with Gills haematoxylin and scanned by the Pannoramicoramic slide scanner machine.

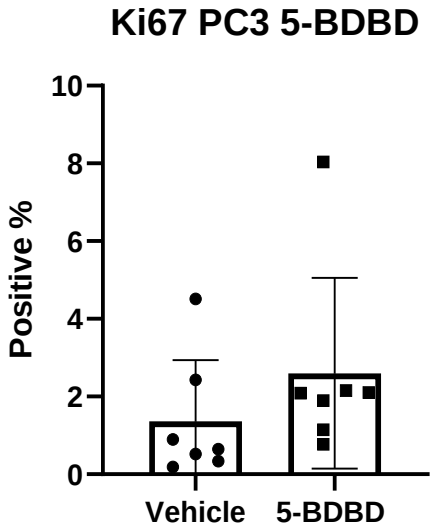

Figure 3.22: The percentage of proliferation cells in tumours are similar in vehicle and 5-BDBD treatment. The rate of proliferation cells in vehicle control group and 5-BDBD treatment group. Data are the mean ± SD. N = 7, Student's t-test, non-significant $p > 0.05$.

3.3.6 The Eotaxin, a related inflammation cytokine significantly lower after 5-BDBD treatment

The Bio-Plex® multiplex immunoassay system allows for the simultaneous analysis of up to 23 analytes using magnetic beads in a single experiment. The assay works by using magnetic beads that are coloured with two different fluorescent dyes in varying ratios. The beads are then attached to an antibody that is specific to the analyte of interest, and a secondary enzyme-conjugated antibody is used to detect the amount of analyte present in the sample. A flow cytometer with two channels is used to analyze the quantity of analytes in the beads, with one channel identifying the coloured beads and the other quantifying the analyte concentration (Graham et al. 2019; Houser 2012). This study used the Bio-Plex Pro Mouse Cytokine 23-plex Assay to analyze 23 cytokines in serum samples obtained from mice.

The results showed that, except for the cytokine Eotaxin, there were no significant differences among the other factors analyzed. Eotaxin is an important eosinophil-specific chemokine that is associated with the recruitment of eosinophils into sites of inflammation. Eotaxin was significantly decreased in the 5-BDBD treatment group, leading to a dramatic reduction in inflammatory response (p = 0.02) (Figure 3.22). These results indicate that 5-BDBD treatment can inhibit inflammatory activity *in vivo*, which may lead to suppression of tumour formation.

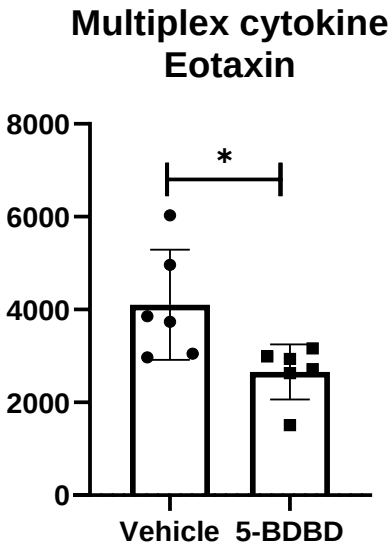

Figure 3.23: Eotaxin a related inflammation cytokine is significantly decreased with 5-BDBD. The Bio-Plex Pro Mouse Cytokine Assay showed cytokine Eotaxin significantly decreased in 5-BDBD treatment, suggesting the antagonist treatment inhibits animal inflammation activities. Data are the mean ± SD. N=6, unpaired t-test, * $p < 0.05$.

3.4 Discussion

In this study, a series of *in vitro* and *in vivo* experiments were performed using PCa models to investigate the role of P2X4R in PCa. Previous studies have reported the overexpression of P2X4R in PCa in publicly available gene datasets including Tomlins, Lapointe, Vanaja, Welsh, and Wallac (Maynard et al., 2022). Similarly, it has been suggested that P2X4R is significantly upregulated in PCa samples compared to benign prostate epithelium tissues using retrospective analysis in clinical datasets (He et al., 2020). These results demonstrate that P2X4R plays an essential role in PCa tumour progression, and inhibiting P2X4R supports my previous hypothesis that it positively affects PCa progression.

Results demonstrated that two P2X4R selective antagonists (5-BDBD and PSB-12062) could both significantly reduce the ATP-induced calcium influx in PC3 cells, indicating that P2X4R was functional in PC3 cells and also that these two antagonists could be used for subsequent tumour biology studies to determine the activities of P2X4R. Calcium assay was also performed in C4-2B4 cells; however, no extracellular ATP-induced calcium signalling was detected, suggesting that splice variants of the human P2X4R are known to lack a typical ATP-evoked channel activity (Dhulipala et al., 1998, Carpenter et al., 1999).

Previously, there was no significant difference between the treatment and non-treatment groups in viability assay *in vitro* in my study. However, a significant decrease in viability was observed in the Maynard study. This might be because they used a higher 5-BDBD concentration of 5 μM and 10 μM, or they used different cell types (Maynard et al., 2022). Inhibiting P2X4R with 5-BDBD and PSB-12062 significantly decreased the invasiveness ability in both PC3 and C4-2B4 cells. The results were quite similar to Maynard's study as they also treated PC3 cells with 5-BDBD (Maynard et al., 2022). Inhibiting P2X4R showed a significantly decreased ability of PC3 cells to migrate, and it also affected C4-2B4 cells but to a milder extent. The results were also similar to Maynard's study, even though they did not perform the assay in C4-2B4 cells.

Their study showed that inhibiting P2X4R affects cell mobility, PCa cells treated with 5 μM or 10 μM 5-BDBD significantly reduced migration and invasion *in vitro* (Maynard et al., 2022). The ex vivo results were consistent with findings by Ghalali's group that inhibiting P2X4R impairs the mobility of PCa cells (Ghalali et al., 2020).

These results suggest that P2X4R plays a crucial role in the tumour cell biology of PCa; however, the molecular and cellular mechanisms in PCa progression are still unknown. One of the potential candidate pathways mediating these effects could be the P2X4R Ca2+ influx-induced ATP release and activity of mitogen-activated protein kinases (MAPKs), p38 (Nandigama et al., 2006). p38 MAPK is associated with cell proliferation in both PCa cell lines and tumour samples derived from patients (Wang et al., 2022b, Porras and Guerrero Arroyo, 2011). p38 MAPK plays a dual role in regulating cell death; it can either mediate cell survival or cell death depending on different types of stimulations or specific cell types (Porras and Guerrero Arroyo, 2011). Surprisingly, the apoptosis results showed that treatment with antagonists did not decrease apoptotic activities, as P2X4R has also been suggested to have an anti-apoptotic role in glioblastoma multiforme (GBM) (Huo and Chen, 2019). Activating p38 promotes apoptosis, but this requires coordination with other signals, such as the PI3K/AKT pathway, to determine cellular outcomes. Studies have demonstrated that there is crosstalk between the PI3K-AKT-mTOR pathway and multiple interacting cell signalling cascades that positively affect the process of PCa (Shorning et al., 2020). Additionally, findings in breast cancer suggested that P2X4R modulates cell death by coordinating with other receptors/signalling pathways (such as P2X7R or Pannexin-1 channel), indicating that inhibiting only P2X4R may not be enough to affect PCa apoptosis (Draganov et al., 2015). Based on this evidence, one can speculate that the inactivation of p38 MAPK in PCa will resemble the *in vitro* observations. Furthermore, p38 is also known to be related to migration and invasion, which could result in the impaired migration and invasion ability in PCa cells when P2X4R is inhibited (Porras and Guerrero Arroyo, 2011).

The results of the invasion assay suggest that inhibiting P2X4R reduces invasiveness. It has been suggested that P2X4R has the ability to mediate the invasiveness and

EMT of PCa cells (Ghalali et al., 2014). Evidence suggests that EMT is a critical step in tumour progression. Cancer cells that have undergone EMT lose properties of cell-to-cell adhesion and polarity and gain cell motility and invasiveness, allowing them to migrate through the extracellular matrix (ECM) and have aggressive metastatic potential (Xu et al., 2009). The TGF-β signalling pathway is an important signalling pathway that induces EMT, while inhibition of the TGF-β pathway can induce the process of mesenchymal to epithelial transition (MET) and downregulate the invasiveness of PCa, possibly via coordination between TGF-β (Wang et al., 2014, Slater et al., 2004).

The *in vivo* data demonstrate that P2X4R is functional in tumour formation and PCa progression. Tumour size in mice subcutaneously inoculated with PC3 cells and daily administered 5-BDBD injections showed a significant reduction compared to vehicle control group on day fourteen. However, differences started to diminish in the final week, possibly because tumours in the control group became necrotic after two weeks, slowing tumour growth (He et al., 2020). Overall, these data indicate that inhibiting P2X4R *in vivo* delays the initiation and early growth of PCa tumours rather than causing cell death. These findings are consistent with the in vitro data that inhibiting P2X4R in PCa cells impairs proliferation but not apoptosis. In the xenograft model, the data suggest that the 5-BDBD inhibitor does not affect PC3 cell viability but significantly reduces proliferation by limiting DNA synthesis and proliferation through inhibition of p38 MAPK (Draganov et al., 2015).

The *in vivo* data also suggest that P2X4R inhibition reduces tumour necrosis, which may be a consequence of slower tumour initiation/early growth in the 5-BDBD treatment group. The results of Ki67 showed that the percentage of proliferating cells was similar among the treatment and non-treatment groups, considering the substantial number of dead cells around necrosis in tumours of the vehicle group cannot be detected. In PCa tumours, necrosis is associated with a poor prognosis (Acosta et al., 2018, Humphrey, 2017).

P2X4R has been shown to protect against polymicrobial sepsis-induced organ injury and inflammation (Csóka et al., 2018). Bio-Plex® multiple cytokine results demonstrated a reduced response of the inflammation factor Eotaxin in inhibiting P2X4R administered by 5-BDBD. The expression of P2X4R has been shown to be co-localized with many pro-inflammatory cytokines in renal tubule epithelial cells (Han et al., 2020, Chen et al., 2013). Maynard's study also showed that P2X4R responds to inflammatory reactions in PCa (Maynard et al., 2022).

A retrospective analysis of clinical datasets has suggested that the expression of P2RX4 may be associated with PCa malignancy. The researchers searched the Gene Expression Omnibus database and identified three clinical datasets that characterized the transcriptomic profile in PCa samples and benign prostate tissues. Results demonstrated that P2RX4 gene expression was upregulated compared to benign prostate tissues (He et al., 2020). These findings suggest that P2X4R may be a potential biomarker for PCa progression in clinical settings. The study found elevated expression of P2X4R in metastatic PCa, which was expressed in metastatic cancer cells. The mean P2X4R protein expression from the adrenal gland, lung, lymph node, and pancreas was significantly higher compared to benign prostate tissues (Maynard et al., 2022). P2X4R may serve as a potential therapeutic target for metastatic PCa.

Based on evidence that P2X4R is highly associated with malignant tumours, especially PCa, investigating the role of P2X4R in PCa bone metastasis would also be of great value which will be explored in Chapter 5. To understand the inside mechanism of the relationship between P2X4R and PCa, RNA-seq analysis will be explored in the Chapter 6.

3.5 Conclusion

In conclusion, my study has provided significant evidence for the functional role of P2X4R in the initiation and progression of PCa. The *in vitro* and *in vivo* assays have shown that P2X4R is crucial in promoting PCa cell proliferation, cell motility and invasiveness, and enhancing tumour formation and growth. The results of this study suggest that P2X4R could be considered a potential target for PCa therapy using already available inhibitors. Additionally, investigating the role of P2X4R in PCa bone metastasis could provide further insights into the mechanism of PCa progression. Overall, my study offers a foundation for further investigation into the potential of P2X4R as a therapeutic target in the treatment of PCa.

CHAPTER 4:

RESULTS: Knocking out P2XR4 in PCa cells

4.1 Introduction

Since its introduction in 2013, the CRISPR/Cas9 technology has become a powerful method for analyzing gene function in living cells (Ran et al., 2013a). It performs DNA cleavage with the help of guide RNAs (gRNAs) and the constitutive expression of Cas9 (Jin et al., 2020). It has been widely used in studying genes related to PCa incidence and aggressiveness, including the role of P2R family in tumour. For example, NANOG, a gene expressed in malignant cancer stem cells, was successfully knocked out in PCa cells in 2015, which led to a decrease in their malignant potential (Kawamura et al., 2015). In 2017, the knockout of GPRC6A, a gene related to the pathogenesis of PCa, using CRISPR/Cas9, was shown to suppress PCa tumourigenesis *in vivo* (Ye et al., 2017). CRISPR/Cas9 has been used to understand the role of P2Y14R in osteoblasts, and results demonstrated that P2Y14R in osteoblasts can modulate its differentiation in murine (Mikolajewicz and Komarova, 2020). In addition, P2Y2R knockout using CRISPR/Cas9 reduced tumour growth in a xenograft model of head and neck squamous cell carcinoma (Woods et al., 2020).

The P2RX4 gene was blocked using the CRISPR/Cas9 gene editing system. The plasmid was prepared at a concentration of 2ug/ul, and 20ng of plasmid was used for transfection of 200,000 cells seeded in a 6-well plate. A GFP selecting reporter was used for quick detection of transfection efficiency, and the strongest signal was observed 48 hours after transfection by LipofectamineTM 3000 reagent. Once successfully transfected into the cells, the plasmid was sorted using a GFP sorting machine. The transfected cells were imaged using the EVOS imaging system and sorted using a flow cytometer. A single GFP+ cell was selected in a 96-well plate using the cell sorting machine and then cultured to verify whether P2RX4 was knocked out in the cells. To confirm that the P2RX4 gene was depleted from the PCa cells, the KO cells were first subjected to DNA extraction, and gene sequencing was performed using PCR amplification. Next, RNA was extracted from the KO cells and analyzed for P2X4R expression at the transcriptional level using the RT-PCR method. Then Fluo-4 Direct™ Calcium assay was carried out to test the function loss in P2X4R deficient cells.

This project aims to use CRISPR/Cas9 gene editing technology to create PC3 cells that lack the P2RX4 gene. The hypothesis is that knocking out P2X4R in PC3 cells will provide direct insights into its role in PCa progression. The PC3 P2X4R KO cells will be prepared and used in the Chapter 5 study.

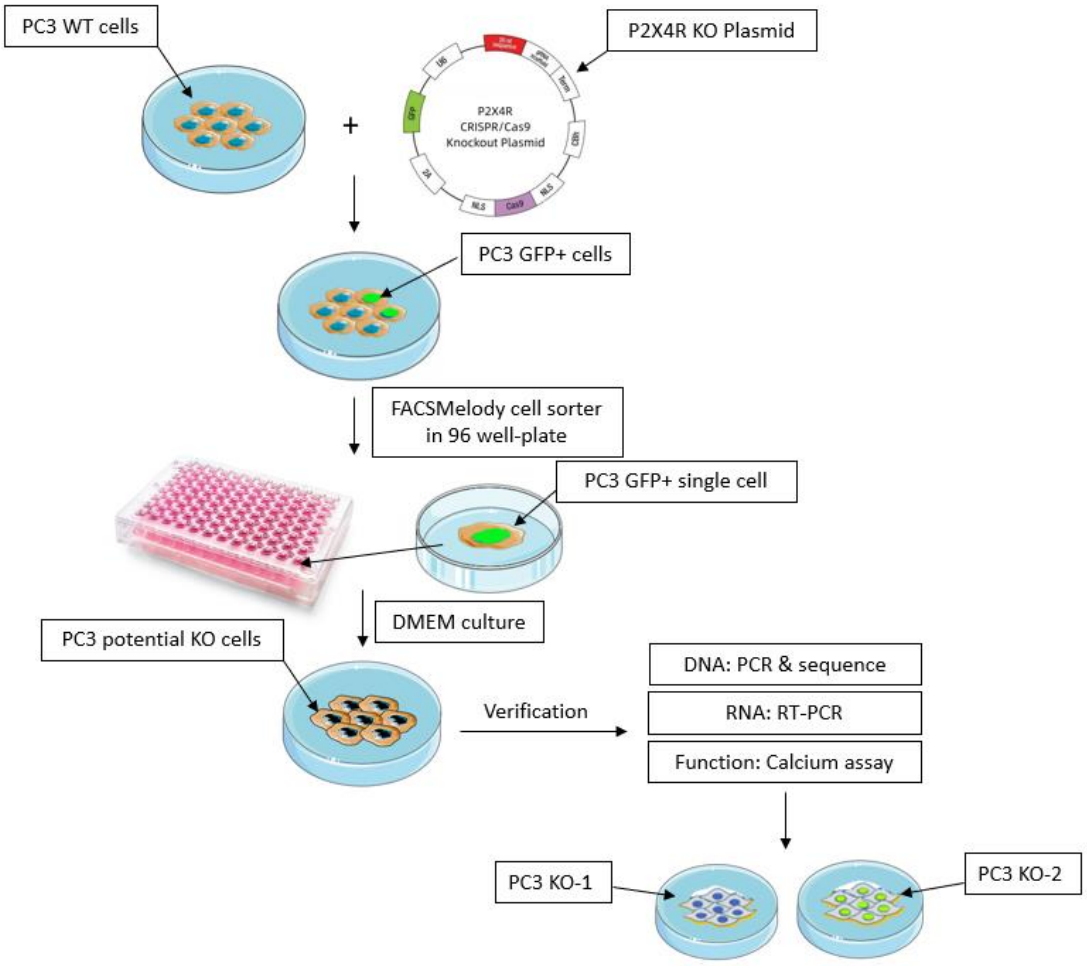

Figure 4.1: Graphical abstract. To obtain PC3 P2X4R KO cells, CRISPR/Cas9 technology was used to deplete P2RX4 in living cells. The P2RX4 KO plasmid was transfected into cells with a GFP+ signal, and the GFP+ single cells were selected by cell sorting and cultured in a 96-well plate. Sequencing, RT-PCR, and calcium assay verified the potential KO cells. Finally, two PC3 P2X4R KO cell lines were successfully generated.

4.2 PC3 P2X4R KO in cell sorting

The P2RX4 KO plasmid was transfected into PC3 WT cells using LipofectamineTM 3000 transfection assay for cell sorting. The successful transfection was confirmed by detecting the GFP+ signal using fluorescence microscopy (Figure 4.2). After 48 hours of transfection, cells were treated with trypsin-ethylenediaminetetraacetic acid in a 6-well plate to obtain single cells. A negative control group was prepared by changing the plasmid to PBS to blank the fluorescence background while using flow cytometry. Cells with P2RX4 KO plasmid were detected and selected (Figure 4.3) using the FACS sorting technique. Approximately 0.1% of the GFP+ cells were isolated and seeded in a 96-well plate for *in vitro* culture until a sufficient quantity of cells was available.

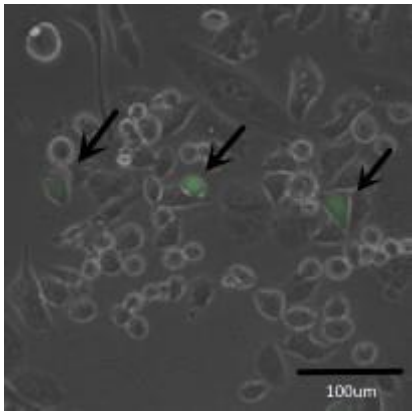

Figure 4.2: Representative image of GFP+ cells. The picture was taken with EVOS FL Auto Cell Imaging System after 48 transfections by Lipofectamine^{TM} 3000, representative GFP+ cells were shown and pointed by black arrows.

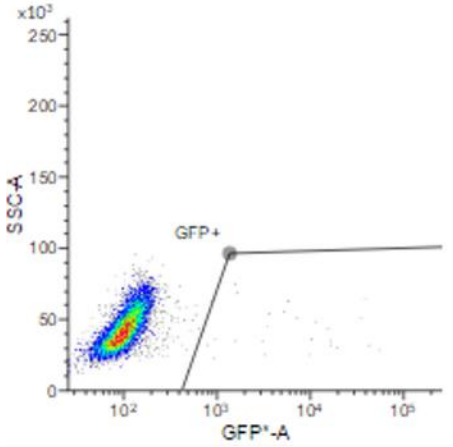

Figure 4.3: Transfection of PC3 WT cells with P2X4R KO plasmid GFP+ signal. The transfection rate is around 0.1% measured by flow cytometry, dot plot showed PC3 WT GFP+ cells.

4.3 PCR results of PC3 WT and KO

The blockage of the P2RX4 gene region by CRISPR/Cas9 was assessed through gel electrophoresis. The PCR product was purified and sequenced using three different sgRNAs designed in the plasmid. DNA was extracted and its quality and quantity were measured by the NanoDrop™ system, and the DNA nuclease concentration was above 15 ng/µl. Specific gene sequences were amplified at different annealing temperatures and extension times (1 min/kb) for the WT and KO cells. 8ul of PCR products were run in 1% agarose gel electrophoresis at 100V, 100mA for 30 minutes. The length of SgRNA1 is 994bp; SgRNA2 is 511bp, and SgRNA3 is 1427bp (Figure 4.4). Using PC3 WT as a positive control, the results showed that all target sequences were successfully amplified, except for PC3 P2X4R KO-2 SgRNA2.

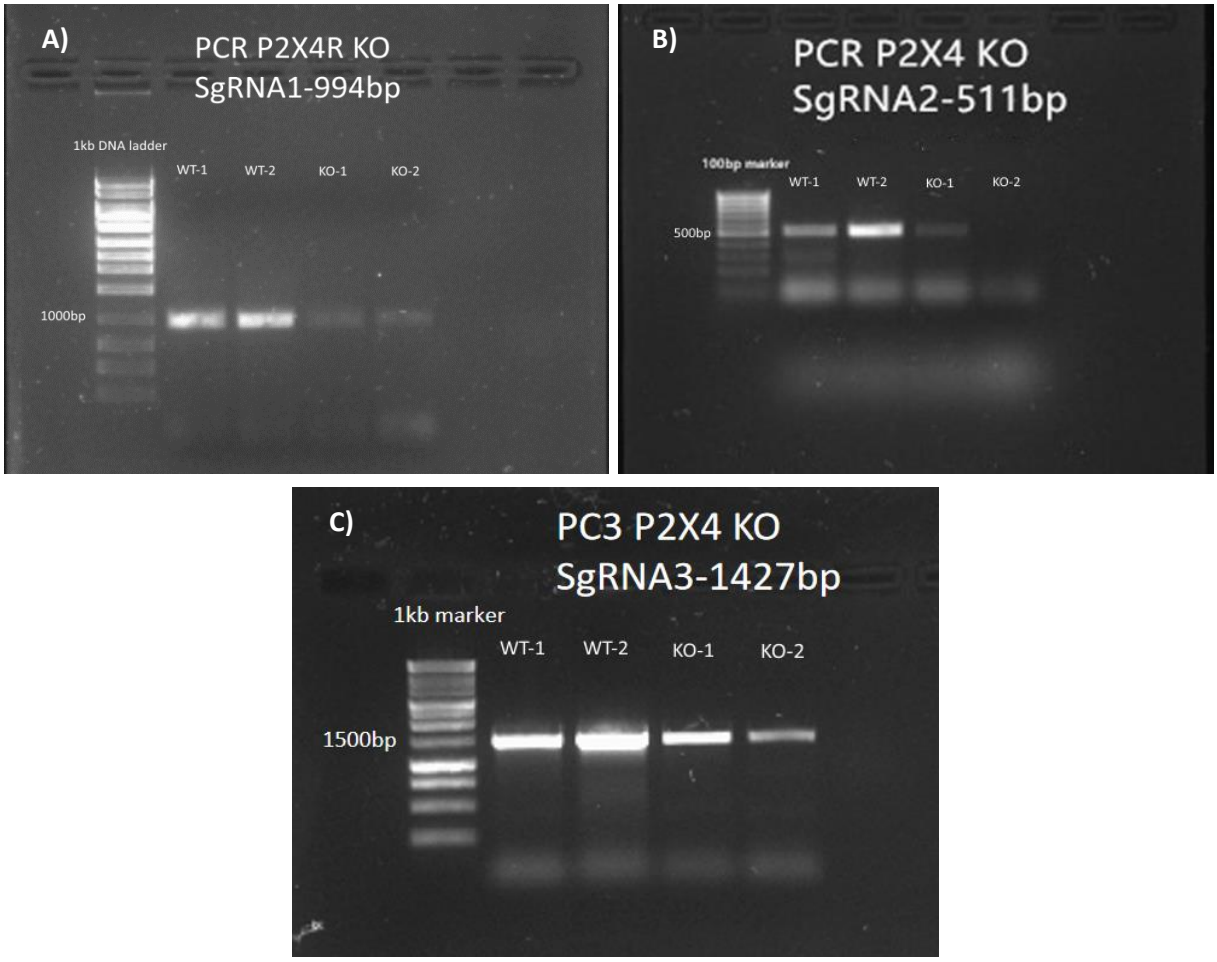

Figure 4.4: The PCR results for SgRNA sequence amplification. The PCR products ran in the 1% gel Electrophoresis for 30 minutes. And then, gel assessment is performed via Gel Doc XR +Imaging System (BIO-RAD). A) The primer annealing temperature for SgRNA1 is 57℃, and the PCR extension cycle took 1 minute to reach 994bp. B) The primer annealing temperature for SgRNA2 is 55℃, and the PCR extension cycle took 40 seconds to reach 511bp. Using 100bp DNA ladder as a marker for SgRNA1 and SgRNA2. C) The primer annealing temperature for SgRNA3 is 55℃, and the PCR extension cycle took 1 minute and 30 seconds to reach 1427bp. Using 1kbp DNA ladder as a marker for SgRNA3.

4.4 Sequence results showed DNA modification in PC3 P2X4R KO cells

Sanger sequencing was used to evaluate the efficiency of the gene knockout in the KO cells. PCR products were cleaned up using the Wizard® SV Gel and PCR Clean-Up System, and the DNA was diluted in nuclease-free water to avoid inhibition by EDTA. The quality and quantity of the DNA were assessed by the NanoDrop™ system, with a concentration of DNA above 10ng/ul and a 260/280 ratio of ~2.0 and a 260/230 ratio of ~2.0. The concentration of the providing primer was 10uM. The samples were sent to Azenta Life Sciences Company for sequencing. The sequencing analysis confirmed the successful knockout of the P2X4R gene in PC3 cells (PC3 KO-1 and KO-2) (Table 4.1). The DNA sequencing revealed significant modifications in KO-1 SgRNA2 (Figure 4.5), and sequencing failure in KO-2 SgRNA1 with an early termination signal.

Table 4.1: sequencing results for PC3 P2X4R KO cells

P2X4R KO clones	Targets to be modified	Mutation
PC3 P2X4R KO-1	SgRNA2	Sequence has been largely modified
PC3 P2X4R KO-2	SgRNA1	Early termination

Figure 4.5: The sequence results showed the SgRNA target sequence has been successfully modified in PC3 P2X4R KO-1. Sequence has been largely modified in PC3 P2X4R KO-1 after targeting SgRNA2.

4.5 RT-PCR results showed P2RX4 had been disrupted in the RNA level

The RNA from PC3 WT and KO cells was extracted using the ReliaPrep™ RNA Cell Miniprep System, and then fresh cDNA was synthesized using the First Strand cDNA Synthesis Kit. The RT-PCR results for PC3 WT, PC3 P2X4R KO-1 and KO-2 have been shown in Figure 4.6. There is a clear band in PC3 WT as a positive control, while no target bands in PC3 P2X4R KO-1 and KO-2, indicating that there was no RNA transcription after knocking out P2RX4. Therefore, PC3 P2X4R KO cells have been verified at the RNA transcription level. The GAPDH house-keeping gene was used to test the quality of cDNA to confirm the quality of the samples' cDNA in the system can be performed by the RT-PCR assay. The length of the RT-PCR products was 493bp for P2RX4 and 388bp for GAPDH.

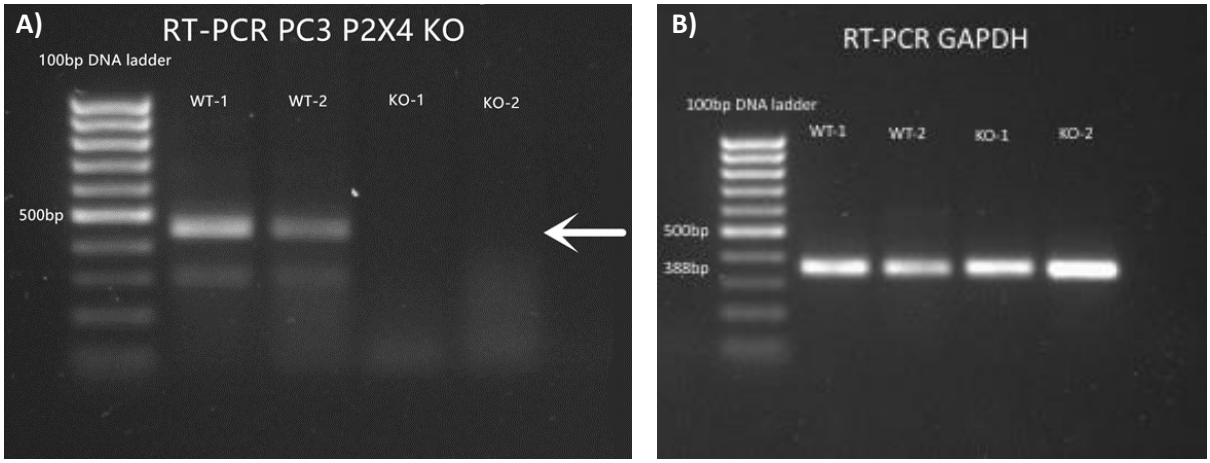

Figure 4.6: Results of RT-PCR. A) The primer annealing temperature for SgRNA-KO is 56°C, and the PCR extension cycle took 40 seconds to reach 493bp. Using 100bp DNA ladder as a marker. B) The primer annealing temperature is 58 °C, and the PCR extension cycle took 40 seconds to reach 388bp. Using 100bp DNA ladder as a marker.

4.6 q-PRC results showed rarely P2RX4 expressed in PC3 KO cells

To assess the expression level of P2RX4 in PC3 KO cells, TaqMan assays were used for qPCR analysis. RNA was isolated from the WT and KO cells and cDNA was synthesized using 1 µg of total RNA, following the manufacturer's instructions. Primers were designed and synthesized, with GAPDH as the housekeeping gene. The target gene's relative mRNA expression level quantification (2-ΔΔCT) was calculated by relative expression, with the PC3 WT P2RX4 expression as a baseline of 1.0. Expression of P2RX4 in PC3 KO was compared to WT. The results showed that the expression of P2RX4 was dramatically decreased to 0.11 in PC3 P2X4R KO-1 (Figure 4.7), suggesting successful disruption of P2X4R in RNA transcription. The analysis of 1/ΔCT results also indicated P2RX4 deficiency in PC3 KO-1 cells (Figure 4.8).

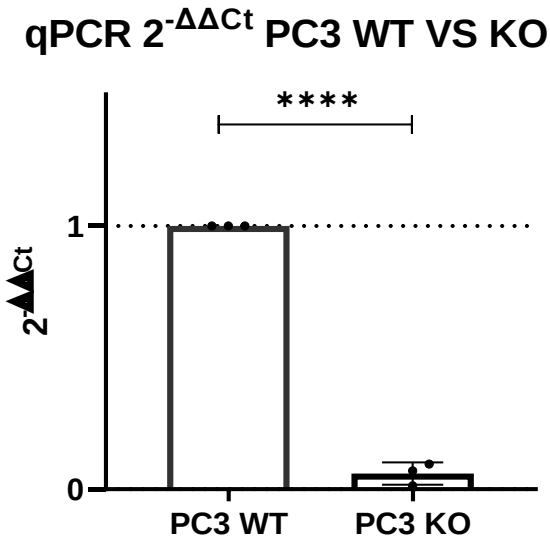

Figure 4.7: Expression of P2RX4 significantly reduced in PC3 KO cells by 2-ΔΔCT analysis. P2RX4 expression in PC3 WT and KO cells by Taq-man qPCR assay, the $2^{-\Delta\Delta CT}$ results showed there is rarely P2RX4 expression in PC3 KO-1 cells compared to PC3 WT cells, suggesting that P2RX4 has been intensely disrupted in RNA level. Data are the mean ± SD. N = 3, Student's t-test, **** $p < 0.0001$.

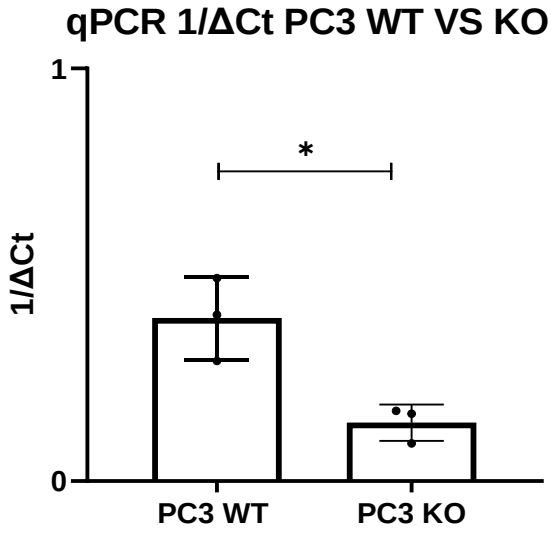

Figure 4.8: Expression of P2RX4 significantly reduced in PC3 KO cells by 1/ΔCT analysis. Analysis results of qPCR, 1/ΔCT data demonstrated the P2RX4 expression significantly reduced in KO-1 cells compared to WT cells. Data are the mean ± SD. N = 3, Student's t-test, * $p < 0.05$.

4.7 P2RX4 is functionally KO in PCa

As P2X4R functions through the influx of calcium as an ATP-gated ion channel, measuring ATP-induced calcium influx changes in KO cells can indicate whether P2RX4 has been functionally knocked out in PC3 cells. A Fluo-4 Direct™ calcium influx detection assay was performed on PC3 WT and KO cells. Results showed that the calcium influx was significantly reduced in PC3 P2X4R KO cells (KO-1 and KO-2) when treated with an ATP concentration of 50 μM. The calcium influx was reduced by 13% for PC3 KO-1 (p = 0.038), and 54% for PC3 KO-2 (p = 0.0006) respectively, demonstrating the successful functional knockout of P2RX4 in PC3 cells (Figure 4.13).

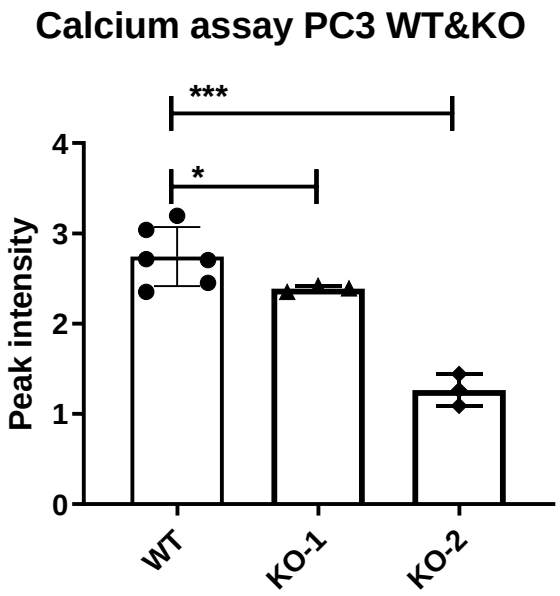

Figure 4.9: The calcium influx was significantly decreased in PC3 P2X4R KO cells compared to WT cells. Calcium release was performed by Fluo-4 Direct™ assay. Data are the mean ± SD. N = six biological repeats for WT. N = three biological repeats for KO, Student's t-test, *p < 0.05, ***p < 0.001.

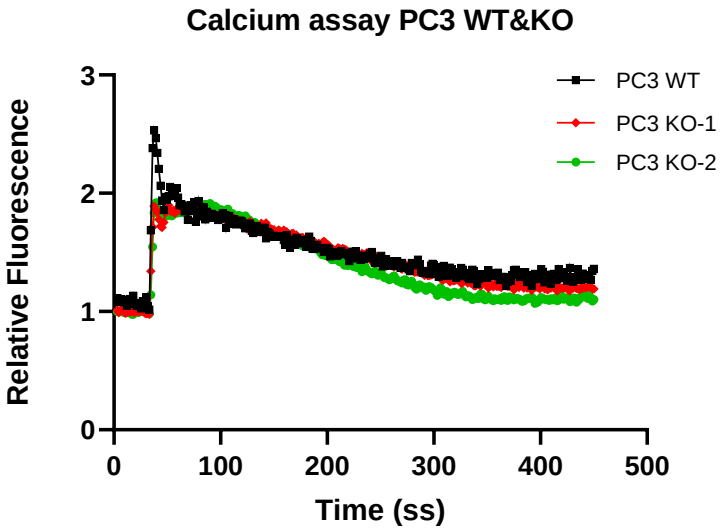

Figure 4.10: The representative curve of calcium influx in PC3 WT and KO cells. The representative graph of calcium influx in PC3 WT and KO cells by 50μM ATP activation. There were dramatically decreased in PC3 KO calcium influx compared to PC3 WT. The calcium influx peak reduced proves P2X4R has been functionally knocked out in PC3 KO cells.

As there is still calcium detected in the assay, it is considered ATP also active in other P2 receptors (Surprenant and North, 2009). Different concentrations of ATP active different P2R. To confirm the reduction between PC3 WT and KO cells was caused by P2X4R deficiency, using the antagonist 5-BDBD to treat PC3 KO cells. Results showed it reaches the same level of reduction as the antagonist treated in PC3 KO cells, confirming that the fall in calcium influx was caused by P2X4R deficiency (Figure 4.11). Data was analysed by GraphPad Primer 8.

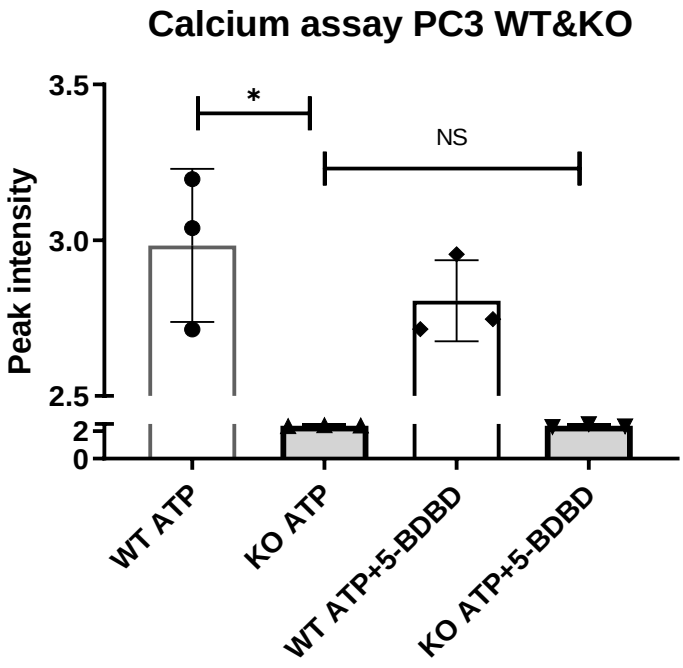

Figure 4.11: There is no difference in calcium influx results of PC3 KO-1 cells with 5-BDBD treatment. There is a significant difference between PC3 WT and KO-1, suggesting gene P2RX4 has been blocked in KO-1 cells (p = 0.014), even lower than 5-BDBD inhibiting treatment previously, suggesting more intensely interruption in PC3 P2X4R KO RNA expression (p = 0.0057). The calcium influx is similar in PC3 KO-1 with or without 5-BDBD treatment, suggesting calcium is reduced by P2X4R deficiency instead of other P2R. Data are the mean ± SD. N=3, Student's t-test, * p < 0.05, non-significant p > 0.05.

4.8 Discussion

In this study, the role of P2X4R in PCa bone metastasis was investigated using CRISPR/Cas9 technology for genetically knocking out P2X4R in PCa cells. Verification of successful depletion of P2X4R in KO cells was achieved at the genomic, transcriptional and functional levels. Sequencing results demonstrated genetic modification of P2RX4 in the genomic DNA. Also, RNA expression analysis revealed a significant reduction of P2X4R in PC3 KO compared to PC3 WT cells. Electrophoresis results showed P2RX4 RNA disruption in KO cells. Additionally, declining calcium influx release in KO PC3 cells confirmed P2X4R functional knockdown in PCa cells. These findings indicated two different PC3 P2X4R KO single clones have been obtained.

Other P2XR subtypes can also be activated by ATP, UTP, or BzATP agents, but at different concentrations (Surprenant and North, 2009). An optimum ATP concentration of 50 μM was selected for P2X4R activation. This is much higher than that required for other P2XR subtypes such as P2X1R (~0.1 μM), P2X2R (~1 μM), P2X3R (~0.1 μM), P2X5R (~5 μM), and slower than P2X7R (>300 μM) (Xing et al., 2016). All P2YR activation requires a low ATP concentration of approximately 0.1 μM ATP (Xing et al., 2016). Based on my previous optimal ATP concentration assay, 50 μM of ATP can significantly activate ATP-mediated calcium influx by P2X4R, as shown by the considerably reduced calcium influx in PC3 KO cells. The assay compared calcium release between PC3 WT and KO cells both treated with the P2X4R-specific antagonist 5-BDBD. The results showed that KO cells reached the same level of reduction as cells treated with the inhibitor, confirming that the decline in calcium influx in PC3 KO cells was indeed caused by P2X4R deficiency.

Despite a declining trend in the intracellular calcium release in both PC3 KO clones, the reduction of calcium influx was different between these two cells, showing slightly reduction in PC3 KO-1 but dramatically decreased in PC3 KO-2. This could be due to

the differently modified sgRNA targets, with KO-1 being impaired by target SgRNA2 and KO-2 was being impaired by target SgRNA1.

It is important to note that the CRISPR/Cas9 technique used in this study has a low efficiency in P2X4R plasmid transfection, with a transfection rate of around 0.1%. Additionally, there may be off-target effects, which are considered the main limitation of CRISPR/Cas9 technology (Jin et al., 2020). However, despite that screening singular clones for successful CRISPR/Cas9 P2RX4 knockouts was challenging due to inefficiencies and off-target effects(Kim et al., 2018), I ultimately obtained two different P2X4R deficient PC3 cells.

I primarily intended to use C4-2B4 cells as a compensation cell line for PC3, but unfortunately, I had to desist because C4-2B4 cells cannot survive as single cells. Previous studies have shown that C4-2B4 cells have difficulty attaching to the bottom of tissue culture flasks, which prevents the performance of scratching migration assays. Additionally, they have a longer doubling time compared to PC3 and LNCaP cells. These findings are consistent with Testa's study, which implying that C4-2B4 cells grow slower than PC3 and LNCaP cells (Testa et al., 2019).

4.9 Conclusion

In conclusion, two different PC3 P2X4R KO cells were obtained by CRISPR/Cas9 gene editing technology to investigate the role of P2X4R in the process of PCa. The deficiency of P2X4R in PC3 cells was verified in genomic, transcriptional and functional levels. Two PC3 P2X4R KO cells were used *in vitro* and RNA-seq analysis, and a mild P2X4R KO-1 cell was selected for further *in vivo* experiment. Overall, this study, at the above stage, provides a proper model for investigating the role of P2X4R in PCa bone metastasis and paves the way for further research in this area.

CHAPTER 5:

RESULTS: Knocking out P2X4R reduces the tumour growth *in vitro* and prevents bone metastasis *in vivo*

5.1 Introduction

In Chapter 3, the pro-tumourigenic function of P2X4R in PCa progression was established. In Chapter 4, two different PC3 P2X4R KO single cell clones, PC3 KO-1 and PC3 KO-2, were obtained using the CRISPR/Cas9 gene editing system. To gain a deeper understanding of P2X4R's function in PCa cells *in vitro* and the process of PCa bone metastasis *in vivo*, P2X4R-deficient PCa cells (KO1 and KO2) were used for *in vitro* experiments, while PC3 KO-1 was selected for *in vivo* research. The graphical abstract (Figure 5.1) illustrates the main findings and processes described in this chapter.

I focused on the process of bone lesions in metastatic PCa, as mortality rates increase in advanced PCa. In the early stages of PCa, the disease is nonlethal and can be effectively treated (Rawla, 2019, Scardino, 1989) However, metastatic disease is the principal cause of prostate-cancer-related mortality (Berish et al., 2018). PCa frequently metastasizes to bone; studies have found that over 70% of PCa cases result in bone metastasis (Bubendorf et al., 2000). According to an autopsy study, about 90% of men who had hematogenous metastases of PCa and had died were found to have bone metastases (Wong et al., 2019). An important factor contributing to advanced PCa in patients is the preferential metastatic spread of tumour cells to lymph nodes or the strong proclivity to bone (van Weerden and Romijn, 2000, Berish et al., 2018). Once the disease has been confirmed to have developed metastases, it represents an incurable form of PCa (de Bono et al., 2010, 2011; Halabi et al., 2016; Petrylak et al., 2004; Tannock et al., 2004). Therefore, the complex pathology of bone lesions in metastatic PCa must be revealed and new targets for preventing metastasis must be discovered to provide novel therapeutic strategies for metastatic clinical studies.

Our previous study found that P2X4R was the most highly expressed P2 receptor in PCa cell lines using RT-PCR assay (He et al., 2020). A recent study by Maynard et al. examined P2X4R expression profiles in PCa tissues, including normal prostate tissue, primary PCa, metastatic PCa, and mouse PCa tissues. Their results demonstrated that P2X4R expression was elevated in metastatic PCa by analyzing tissue

microarrays from autopsy specimens using IHC analysis (Maynard et al., 2022). Furthermore, P2X4R protein expression was significantly higher in the adrenal gland, lung, lymph node, and pancreas compared to benign prostate tissues (Maynard et al., 2022). These results suggest that P2X4R expression is closely related to the process of PCa metastasis. However, the specific role of P2X4R in PCa bone metastasis progression is still unclear and needs to be further investigated.

To assess the impact of P2X4R deficiency on PCa cells, several *in vitro* assays were conducted on three different cell types: PC3 WT, PC3 KO-1, and PC3 KO-2. Cell proliferation, viability, and apoptosis were measured using CyQuant, Amalarblue, and caspase 3/7, respectively. Migration and invasion were assessed through a scratching assay and a matrigel-based transwell insert assay. The hypothesis was that P2X4R contributes to PCa metastasis and targeting it could slow down bone metastasis progression.

To better understand the function of P2X4R in PCa metastasis, a translational xenograft model was utilized to gain a deeper understanding of advanced PCa. Micro-CT was employed to evaluate bone destruction in tumour-bearing mice, and parameters such as trabecular bone volume fraction (BV/TV), trabecular thickness (Tb.Th), trabecular number (Tb.N), trabecular separation (Tb.Sp), trabecular bone pattern factor (Tb.Pf), structure model index (SMI), degree of anisotropy (DA), and cortical bone volume were analysed (Cooper et al., 2008). To measure tumour burden in bones histologically, osteoMeasure was performed on bone sections, and the percentage of tumour cells in the mouse tibia was used to quantify tumour burden. This study is the first to describe the association between P2X4R function and PCa bone metastasis.

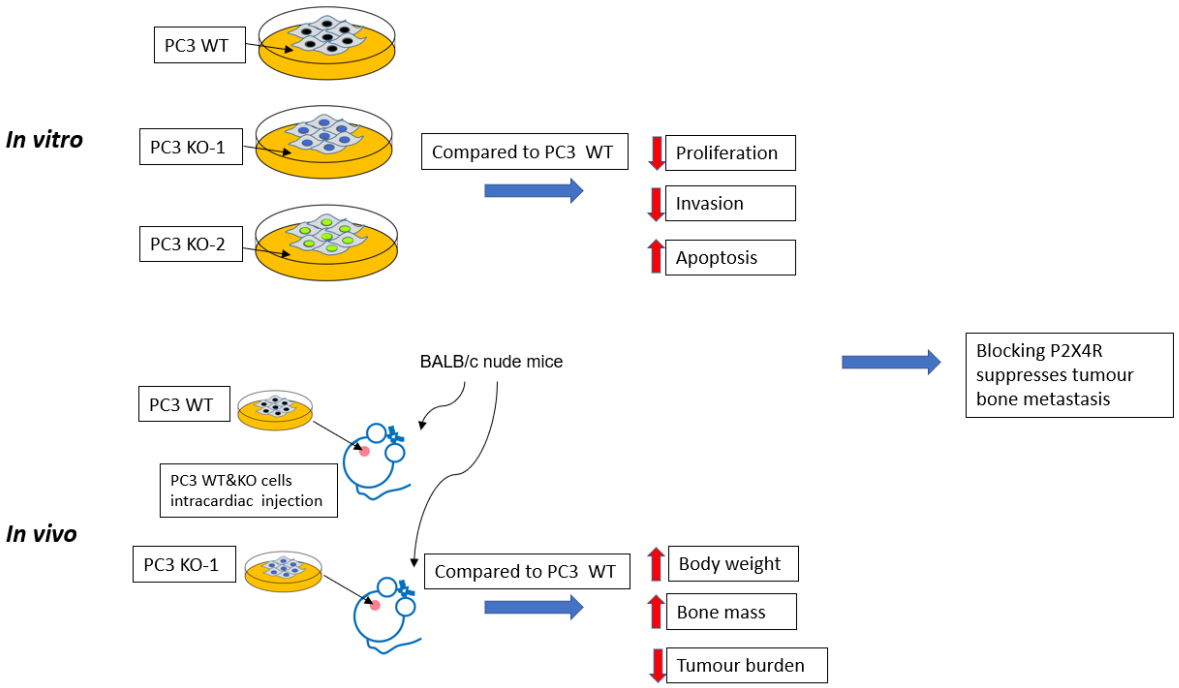

Figure 5.1: Graphical abstract for P2X4R deficiency in PCa in vitro and in vivo. PC3 WT & KO cells were tested by a series of *in vitro* assays, results showed the ability of proliferation and invasion has been significantly decreased, while enhanced the apoptotic activities compared to PC3 WT. PC3 WT & KO cells were intracardiac injected into BALB/c nude mice respectively, results showed the bone mass is also higher than WT. The percentage of tumour burden in KO tumour-bearing mice keeps low level compared to the WT. The body weight of KO tumour-bearing mice is higher than the WT. Both *in vivo* and *ex vivo* results suggested that blocking P2X4R can suppress tumour metastasis in mouse tibias.

5.2 P2X4R deficiency impacts tumour growth and mobility *in vitro*

To further reveal the role of P2X4R in PCa progression *in vitro*, two different single PC3 P2X4R KO clones PC3 KO-1 and PC3 KO-2 were performed in *in vitro* study. To understand the growth and mobilization compared with PC3 WT and PC3 P2X4R KO cells, a series of assays were performed including proliferation, viability, migration, invasion and apoptosis.

5.2.1 Knocking out P2X4R significantly reduces PCa proliferation

The CyQuant proliferation assay was performed to investigate the effect of P2X4R on PCa cells growth. The results indicated that knocking out P2X4R significantly reduced the proliferation ability of both PC3 P2X4R KO cells, with a 47% reduction of KO-1 (p = 0.044), and a 33% of KO-2 (p = 0.056) at 72 hours; it also reduced around a 60% in both KO-1 (p = 0.044) and KO-2 (p = 0.049) at 96 hours (Figure 5.2).

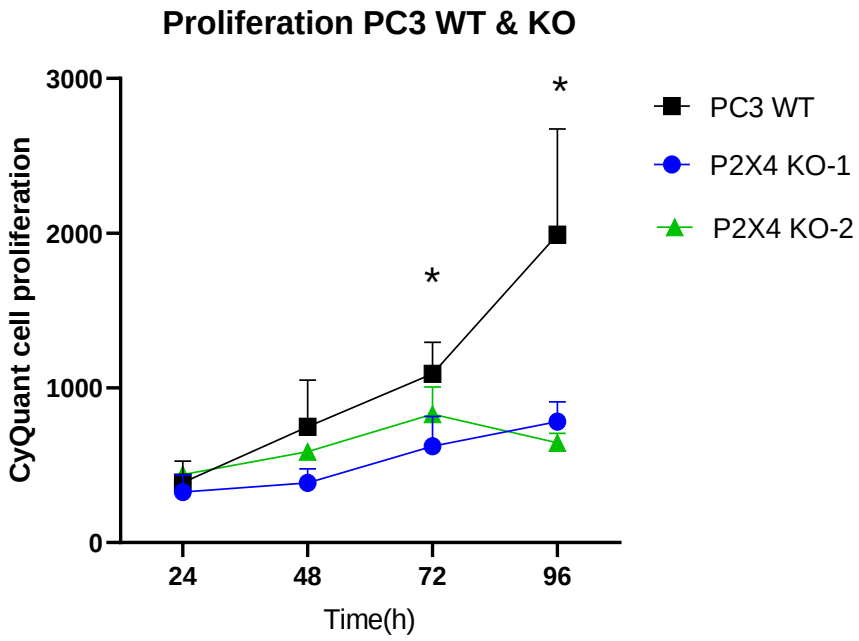

Figure 5.2: The ability of proliferation in KO cells is significantly reduced compared to WT. Cell proliferation was analyzed using CyQuant proliferation assay for PC3 WT & KO cells incubated for 24- ,48- , 72- and 96 h in DMEM. Plate cells in 96 well-plate at a density of 2000 cells each well overnight, change to CyQuant reagent the next day and incubate an hour, the fluorescence was then measured by EnSight Multimode Plate Reader at 485 nm excitation and 530 nm emission. Data are the mean ± SD. N = 3, Student's t-test, * p < 0.05.

5.2.2 Depleting P2X4R did not affect PCa cells viability

The AlamarBlue viability assay was performed to assess the function of P2X4R in PC3 cell viability. To evaluate the change in viability, the data were normalized, with PC3 WT at 24 hours set to 1.0, and the changes in PC3 WT and KO cells at different time points were compared to PC3 WT at 24 hours (Figure 5.3). The results showed that knocking out P2X4R had no significant effect on cell viability between PC3 WT and PC3 KO cells for all time points ($p > 0.05$).

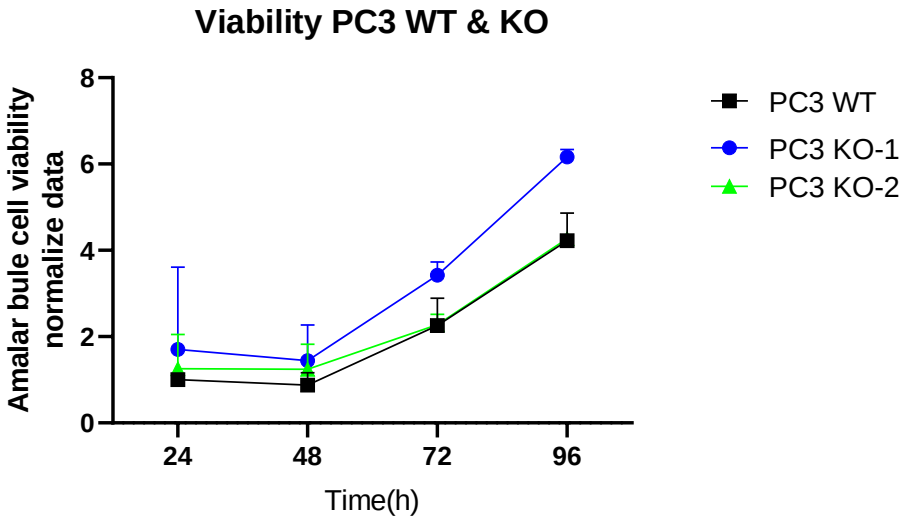

Figure 5.3: There is no significant difference between PC3 WT & KO cells on cell viability. Cell viability was analyzed using Amalrblue assay for PC3 WT & KO cells incubated for 24-, 48-, 72-, 96 h in DMEM. Plate cells in 96 well-plate at a density of 3000 cells each well overnight, change to Amalrblue reagent the next day. After 3 hours Amalrblue reagent incubation, the absorbance was measured in an EnSight Multimode Plate Reader at 570 nm excitation and 600 nm emission. Data are the mean ± SD. N =3, student's t-test, non-significant, $p > 0.05$

5.2.3 Depleting P2X4R did not affect PCa cells migration

The scratch-wound assay was performed to test the migration ability of PC3 WT and KO cells. Representative figures are presented in Figure 5.4. The average areas of migration closure for each group were 38% for PC3 WT, 41% for PC3 KO-1, and 36% for PC3 KO-2, respectively (Figure 5.5). The results showed that there were no significant differences in migration between each group ($p > 0.05$). Representative images of migration were shown in Figure 5.4.

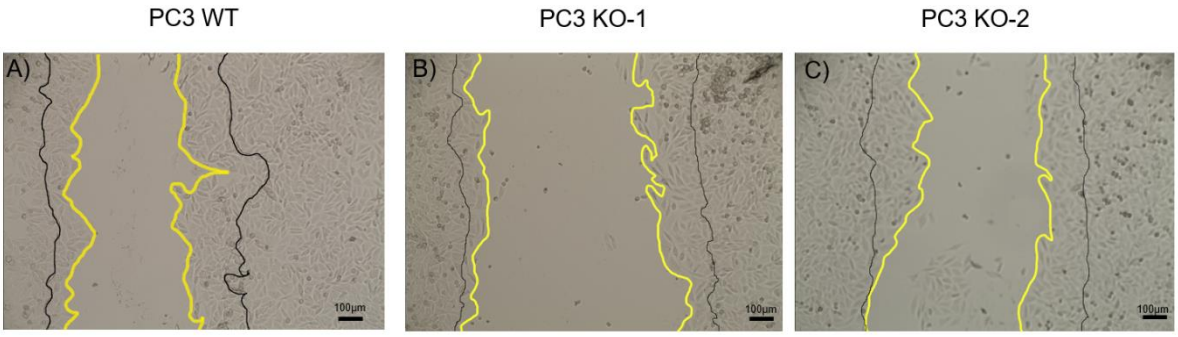

Figure 5.4: Representative migration images for PC3 WT, PC3 KO-1 and PC3 KO-2. Black lines represent cells' initial positions at 0 hour, yellow lines represent the final position at 18 hours. There is no significant difference in migration areas between PC3 WT, PC3 KO-1 and PC3 KO-2. Scale bar = 100μm.

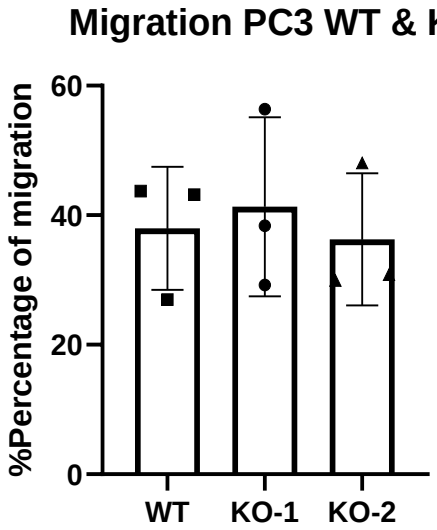

Figure 5.5: There is no significant difference between PC3 WT & KO cells on cell migration. A scratch migration assay was adopted for testing the migration ability in PC3 WT & KO cells. Seeding a density of 200,000 cells per well, cells were attached to the well plate bottom. The pipette was used to scratch a line in the middle of the confluence cells. Percentage areas that migrated within 18 h were recorded by EVOS microscope and then measured by Image J software. The area of wound closed was compared between PC3 WT & KO. Data are the mean ± SD. N = 3, student's t-test, non-significant, $p > 0.05$.

5.2.4 Blocking P2X4R reduced the invasion ability

The matrigel-based membrane chamber-mediated invasion assay was performed to assess the role of P2X4R in PCa metastasis potential. The results showed that knocking out P2X4R affects the invasiveness of PCa cells. Representative images for PC3 WT and KO cells in the insert membrane were presented in Figure 5.6. Knocking out P2X4R resulted in a decrease in invasiveness in both P2X4R-deficient clones KO-1 and KO-2, with the percentage of invaded areas being 61% for PC3 WT, 30% for PC3 KO-1 ($p > 0.05$), and 5% for PC3 KO-2 ($p = 0.027$) (Figure 5.7). The invasiveness area was reduced by approximately 50% in KO-1 and by approximately 90% in KO-2 compared to WT.

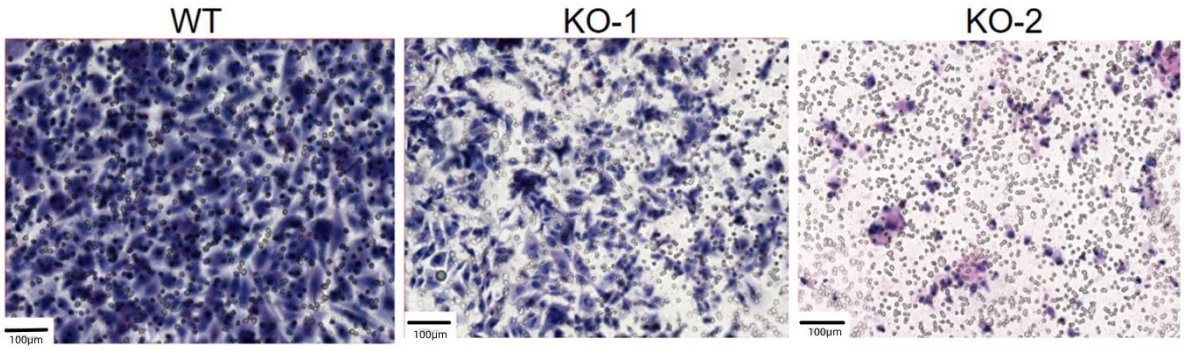

Figure 5.6: Representative images of invasion assay for PC3 WT, KO-1 and KO-2. Cells were seeded at a density of $5x10^4$ cells per well in the upper chamber. Cells were allowed to invade through matrigel insert for 72 hours. Then the percentage of non-invasiveness cells can be quantified by H&E staining and scanning the membrane using the Pannoramic 250 Digital Scanner. Data were analysed by Image J to calculate the percentage area coved by cells. Scale bar=100µm.

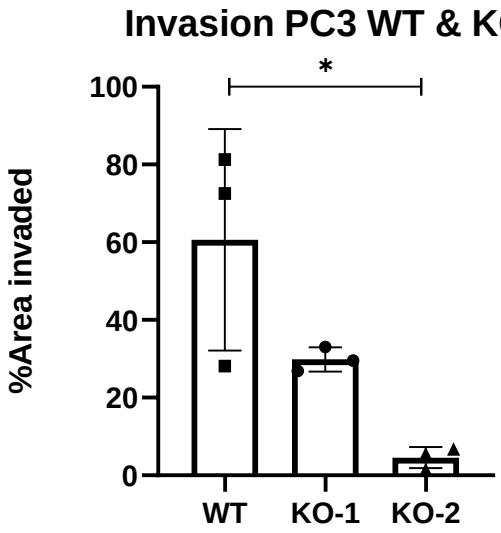

Figure 5.7: Knocking out P2X4R reduced the cell invasion. Matrigel-based membrane chamber-mediated invasion assay was performed in PC3 WT& KO cells. Data showed the invaded area is 61% for PC3 WT, 30% for PC3 KO-1 ($p > 0.05$) and 5% for PC3 KO-2 ($p = 0.027$). Data are the mean ± SD. N=3, Student's t-test, * $p < 0.05$.

5.2.5 Blocking P2X4R significantly enhanced apoptosis

The caspase 3/7 activity apoptosis assay was used to measure the process of programmed cell death compared it between PC3 WT, PC3 KO-1 and PC3 KO-2 cells. The results demonstrated that knocking out P2X4R significantly enhance the apoptotic activities in both P2X4R KO cells with a 106% increase in PC3 KO-1 (p = 0.041) and a 196% increase in PC3 KO-2 cells (p = 0.0034) (Figure 5.9).

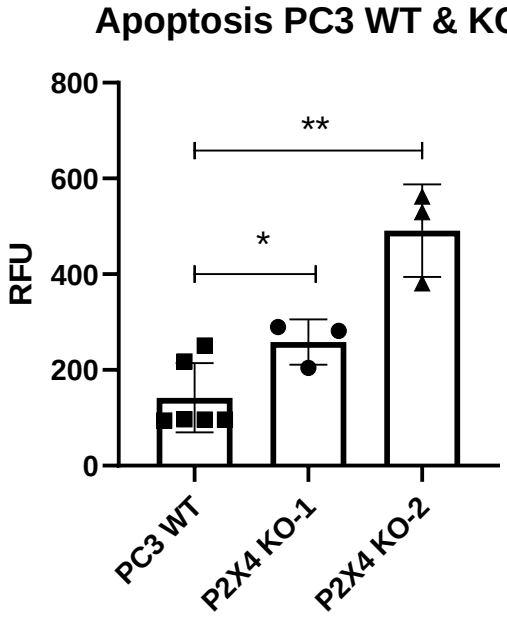

Figure 5.8: Knocking out P2X4R significantly enhanced PCa cells apoptosis. The 3/7 caspase assay was used to measure the apoptotic activity of PC3 WT&KO cells. Cells were seeded at a density of 1×10^4 cells per well in 96-well plates and incubated overnight. After an hour of incubation with 3/7 caspase reagents, the apoptotic activity was measured. The fluorescence was measured using an EnSight Multimode Plate Reader (PerkinElmer) with excitation at 490 nm and emission at 525 nm. Data are the mean ± SD. N=3, Student's t-test, * $p < 0.05$, ** $p < 0.01$.

5.3 Knocking out P2X4R prevent PCa bone metastasis *in vivo*

Previous data have shown that P2X4R is highly expressed in PCa, especially in metastatic tissue (Maynard et al., 2022). To further understand the role of P2X4R in PCa bone metastasis, an intracardiac xenograft mouse model was used in this study. Twenty-six-week-old BALB/c nude mice were injected with a mild PC3 P2X4R KO cell line called PC3 KO-1 to understand the effect of P2X4R deficiency in PCa bone metastasis. PC3 WT and PC3 KO-1 cells were separately injected intracardiacally at 1 x10^6 cells under general anaesthesia. At the endpoint, mice were killed and bones were collected to measure the damage caused by tumours. The process of procedures is presented in Figure 5.9. To evaluate the tumour volume in tibias, right tibias were subjected to micro-CT scanning to measure tumour lesions. Parameters used for micro-CT scanning were presented in Chapter 2, section 2.9.1. Tumour burden was assessed using the osteMeasure to count the tumour area in the bone tissue.

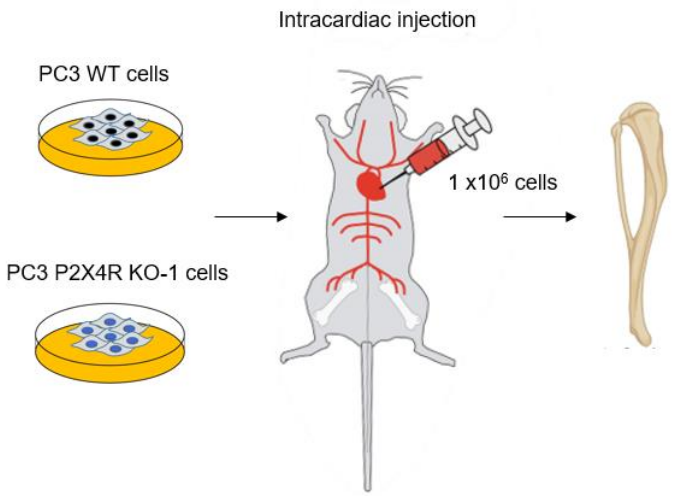

Figure 5.9: Process of PCa bone metastasis xenografts assay in vivo. Mice were injected intracardiacally with 1 x10^6 PC3 WT or KO cells separately on the first day. Mice were sacrificed at the endpoint on day 25, the bone samples were collected and scanned by micro-CT scanning. Once the micro-CT scanning has been done, the bone was cut into sections and then preparing the sections using TRAP and H&E staining. Finally, tumour burden was measured by osteoMeasure.

5.3.1 Micro-CT scanning results showed knocking out P2X4R increased trabecula and cortical bone mass in mice tibia

The micro-CT technique allows for the measurement of bone destruction in tumour-bearing mice. Micro-CT results evidence that P2X4R KO cells caused higher bone mass compared to WT group, and representative 3D models of PC3 WT and PC3 KO are presented in Figure 5.11. Figure 5.10 showed a graph comparing each individual analysis, suggesting that KO cells caused less bone destruction than WT cells, including higher trabecular BV/TV (161%, $p < 0.0001$), Tb.Th (12%, $p = 0.0072$), Tb.N (132%, $p < 0.0001$), Tb.Sp (15%, $p = 0.0031$), and cortical bone volume (25%, $p < 0.0001$), while there was no significant difference between PC3 WT and KO in SMI ($p > 0.05$) and DA ($p > 0.05$).

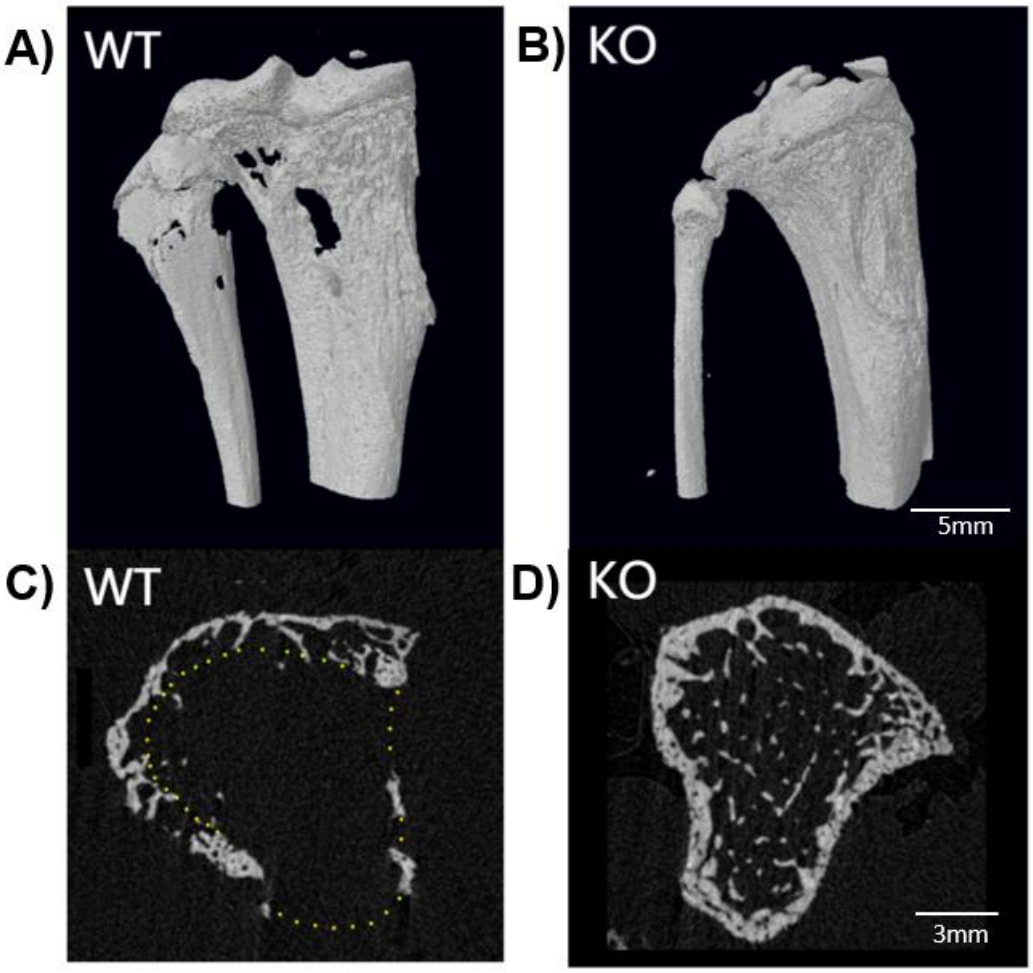

Figure 5.10: Representative images for Micro-CT results of PC3 WT and PC3 KO. 3D models of mouse right tibias were created by CTvol software. Images A) and B) show the tibias of WT & KO respectively; images C) and D) show the section of tibias of WT & KO respectively. The lesion showed in WT group tibia and the section of trabecular tissue suggested bone marrow have been destroyed compared to KO group. The scale bar is 5mm and 3mm separately.

The quantitative data of trabecular and cortical parameters are presented in Table 5.1.

Table 5.1 : Quantitive data of mouse right tibial by Micro-CT analysis

Parameter	PC3 WT	PC3 KO	P value
	N=10	N=10	
Trabecular BV/TV (%)	4.19 ± 2.21	10.76 ±1.48	<0.0001
Tb.Th (mm)	0.03 ± 0.003	0.03 ±0.002	=0.0072
Tb.N (1/mm)	1.28 ± 0.06	2.97 ± 0.01	<0.0001
Tb.Sp (mm)	0.28 ± 0.65	0.15 ± 0.37	<0.0001
Tb. Pf (1/mm)	50.08 ± 6.16	41.99 ± 3.51	=0.0031
SMI	2.41 ± 0.24	2.30 ± 0.10	=0.2279 (NS)
DA	2.00 ± 0.30	2.09 ± 0.22	=0.4810 (NS)
CORTICAL BV	0.55 ± 0.08	0.69 ± 0.03	<0.0001

Values are mean ± SEM

NS: Non-significant

* $p<0.05$

** $p<0.01$

*** $p<0.001$

**** $p<0.0001$

All of data is tested by unpaired Student's t-test.

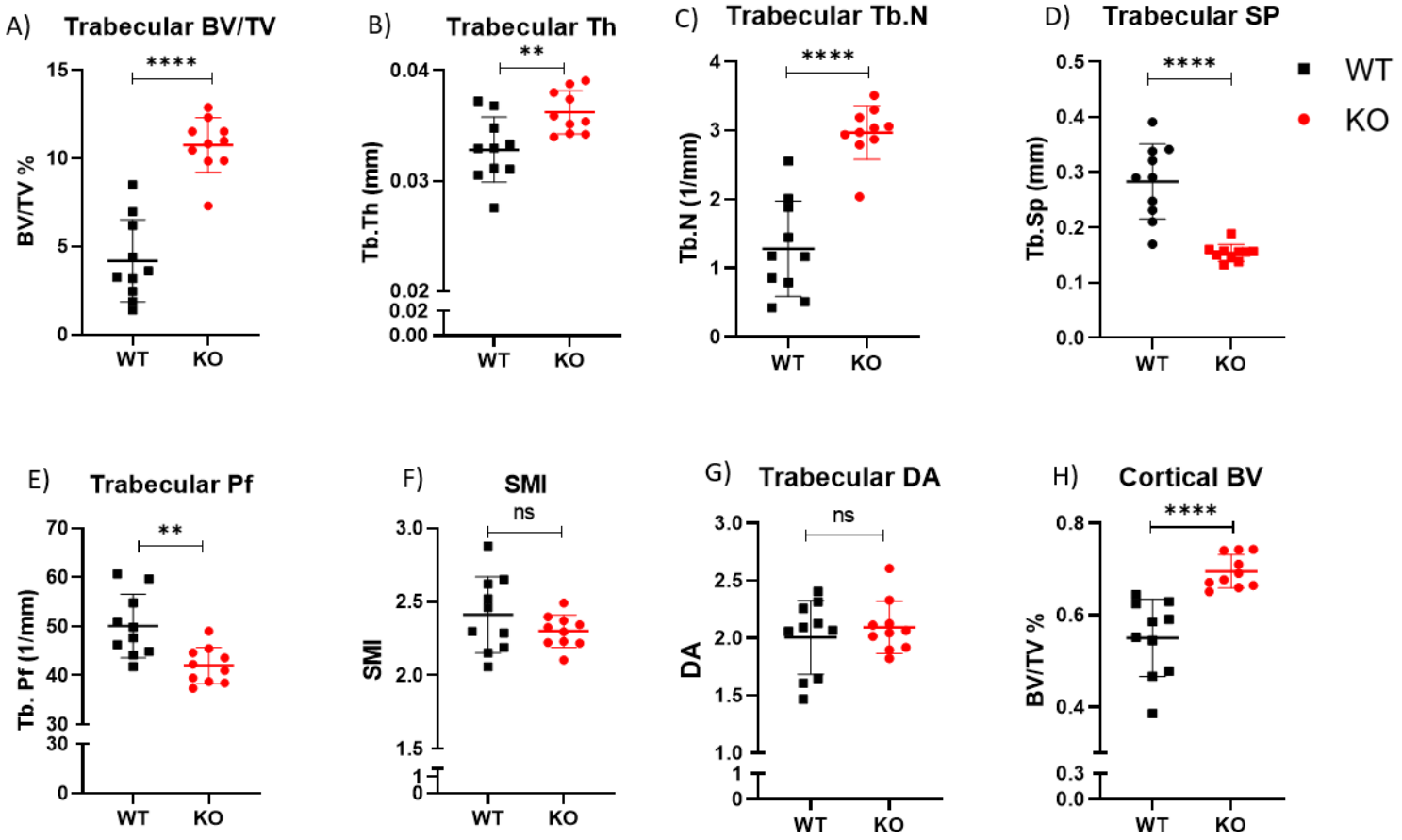

Figure 5.11: The CT analysis of bone morphometry of an intracardially injected with PC3 WT or KO xenograft mouse model. 6-week-old BALB/c nude mice were intracardially injected with either PC3 WT or KO cells and sacrificed on day 25 to collect bone samples. Right tibias were scanned using a Skyscan 1172 X-ray-computed microtomography scanner equipped with an X-ray tube and a 0.5-mm aluminium filter. Each graph in Figure 5.11 showed the quantitative analysis of trabecular and cortical bone parameters, including A) BV/TV, B) Tb.Th, C) Tb.N, D) Tb.SP, E) trabecula pattern factor (Tb.Pf), F) SIM, G) degree of anisotropy, and H) cortical bone volume was analyzed. N=10, Student's t-test, ns: non-significant, * $p < 0.05$, ** $p < 0.01$, *** $p < 0.001$, **** $p < 0.0001$

5.3.2 P2X4R deficiency of PCa cells significantly reduced tumour formation in mouse tibias

To measure tumour burden in bones, osteoMeasure was performed in bone sections. The tumour burden in mouse tibia was measured using osteoMeasure assay under a DMRB microscope (Leica, Wetzlar, Germany) at 20x magnification with the osteoMeasure7 v4.2.0.1 (OsteoMetrics) software to quantify the tumour percentage in mouse tibias.

In the intracardiac xenograft model, P2X4R-deficient PCa cells showed a significant reduction in the onset of PCa bone metastasis. None of the tumours were detected in the mouse tibias injected with KO cells, while 53% of the bone marrow areas were occupied by WT PCa cells ($p < 0.0001$) (Figure 5.13). Representative images present in Figure 5.12.

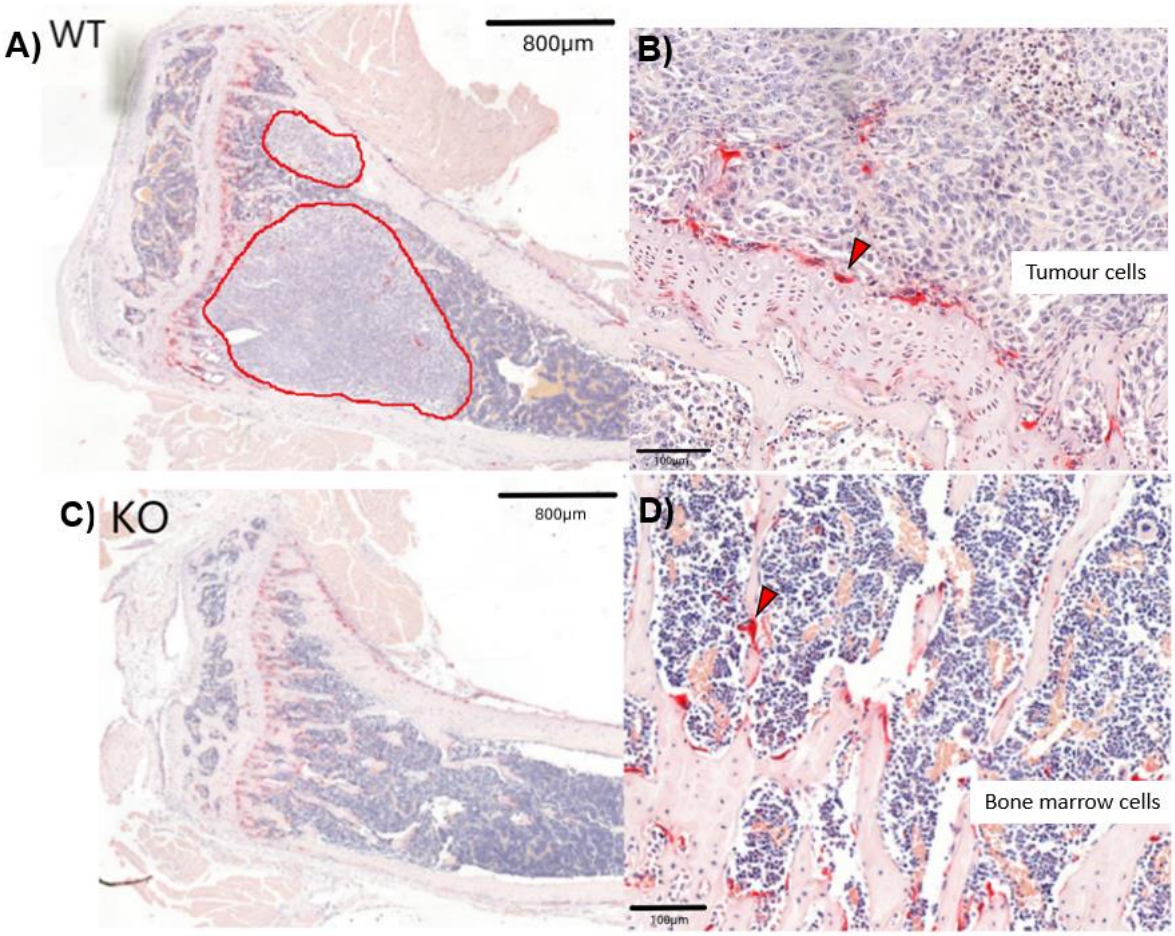

Figure 5.12: Representative images for the tumour burden in PC3 WT&KO. Images WT A) & B) represent the PC3 WT group mouse right tibias bone section while images KO C &D) represent the PC3 KO. As it is shown in the images, differences between tumour cells and bone marrow cells can be identified from the colour and cell size in tibia sections in images B) & D). Red arrows indicate pink TRAP-stained osteoclasts cells in the trabecula surface. Red areas shown in image A) represent tumour cells in tibial section. Scale bar=800µm in images A) & C); scale bar=100µm in images B) & D).

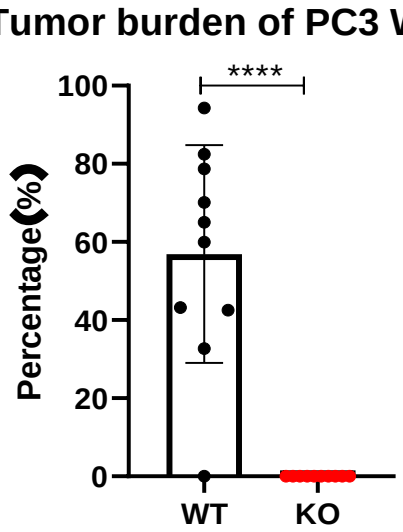

Figure 5.13: PCa bone metastasis area measurement in PC3 WT and PC3 KO mouse right tibias. The PC3 WT&KO tumour-bearing mice bone samples were cut into sections, and bone sections were stained by TRAP staining to identify bone mass. The effect of P2X4R deficiency in PCa bone metastasis progression at a histologic level was measured manually using the osteoMeasure bone histomorphometry software, results have found a significant reduction of tumour area in KO group with 53% in WT and none in KO ($p < 0.0001$). Data are the mean ± SD. N=10, student t-test. **** $p < 0.0001$.

5.3.3 The P2X4R deficient cells cause less adverse effects in animals

To investigate the pathophysiological consequences of tumour development in mice, the body weight was evaluated twice a week after 14 days of tumour cell injection. On day 18, the body weight had decreased compared to the PC3 P2X4R KO group, indicating that PC3 WT cells are more aggressive *in vivo*. The mice were sacrificed on day 25, and the P2X4R KO cells group had a body weight around 20% higher than that of the PC3 WT group. There was a significant difference in body weight between the PC3 WT and PC3 KO groups from day 21 (Figure 5.14). The percentage change in body weight in PC3 KO tumour-bearing mice was significantly higher than its in the PC3 WT group, with a comparison between day 25 and day 23. The body weight

decreased by approximately 20% in PC3 WT group meanwhile it increased approximately 5% in PC3 KO group (p = 0.0003) (Figure 5.15).

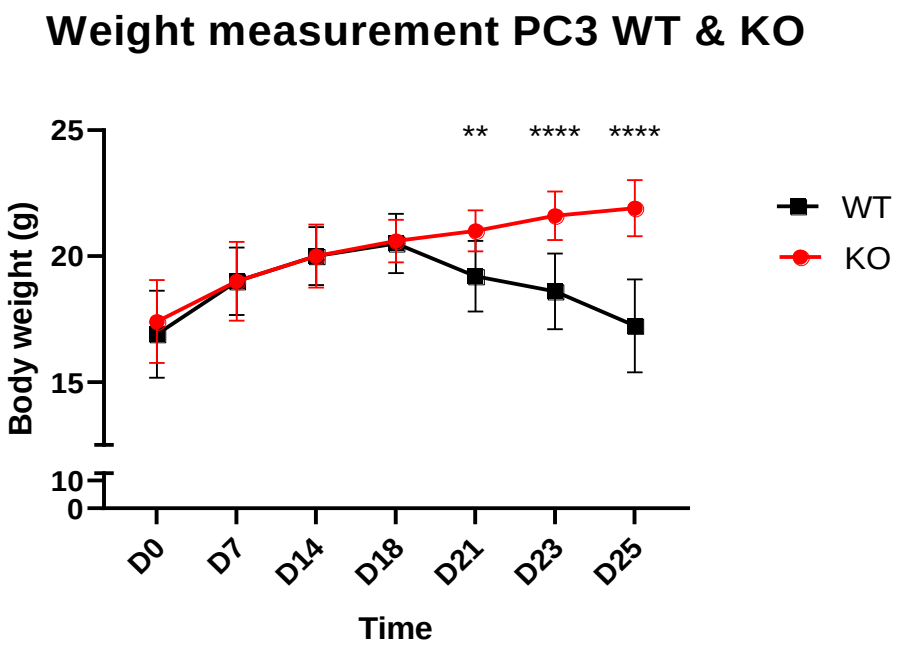

Figure 5.14: The body weight of PC3 KO group tumour-bearing mice is significantly higher than PC3 WT group. Body weight of mice with PC3 WT or KO cells intracardiac tumour cells injection, there is significantly higher body weight in the KO group compared to WT group. Body weight was measured once a week in the first 14 days, then it was measured twice a week. Twenty BALB/c nude mice were subjected to this assay with 10 mice in each group. Data are the mean ± SD, n = 10, Student's t-test, non-significant, ** p<0.01, *** p<0.001, **** p<0.0001.

5.4 Discussion

The present results also demonstrated the anti-tumour effect of P2RX4 gene depletion using CRISPR/Cas9 in human PCa cells through a series of *in vitro* and *in vivo* assays. My data showed that P2X4R deficiency led to a consistent decrease in detectable bone metastases *in vivo* and impaired tumour growth and cells' mobility *in vitro*. Specifically, negative effects of P2X4R blockade were also observed on PCa cells proliferation, survival, and invasion in both PC3 P2X4R KO selected clones. Additionally, knocking out P2X4R in PCa cells caused less destruction on tumour-bearing mouse bone lesions, and tumour burden areas in mouse tibia. Despite the use of different PCa models in Marynard's study in a subcutaneous injection allograft mouse model, their results were consistent with mine (Maynard et al., 2022). Therefore, both of our finding agreed that knocking out P2X4 significantly suppresses tumour formation *in vivo*. These results confirm that P2X4R is involved in tumorigenesis during PCa progression. Furthermore, in my study, it was found that P2X4R depletion has an anti-tumour effect on PCa progression in advanced stages with bone metastasis.

The present data from *in vitro* examinations showed that P2X4R deficiency significantly decreases invasion ability of PCa cells. The underlying mechanism can be EMT process, PHLPPs and PTEN crosstalk, or matrix metallopeptidase secretion. Recently, Chadet et al. demonstrated that P2X4R is overexpressed in breast cancer biopsies obtained from patients. Their discussed that P2X4R promotes invasion *in vitro* and enhances mammary tumour growth and metastasis in *vivo*. P2X4R exerts its pro-malignant effects by regulating lysosome acidity, promoting autophagy, and enhancing cell survival. On top of that, we found that autophagic activity is associated with the induction of EMT, and this effect of P2X4 enhances under metabolic stress conditions (Chadet et al., 2022).

The crosstalk between PHLPPs and PTEN mediated by P2X4R might be the mechanism explaining the invasiveness and tumour metastasis reduction. Some literature evidence that P2X4R receptor could reduce the crosstalk between PHLPPs

and PTEN and increase cell invasiveness in PCa (Ghalali et al., 2020). However, there is limited evidence about the contribution of P2X4R in PHLPPS and PTEN interaction.

Aberrant cell proliferation during cancer initiation and progression to metastasis is controlled by cell cycle progression. Tumour protein p53 is a critical player during the process downstream effectors, such as p21 (induces cell cycle arrest) and PUMA (p53 upregulated modulator of apoptosis) which blocks anti-apoptotic players leading to apoptosis induction (Fiandalo and Kyprianou, 2012). The apoptotic activities enhanced in P2X4R deficient PCa cells in this study may be activated by p53 and promote cell cycle progression (Chen, 2016).

Interestingly, the *in vitro* results demonstrated it affected cell growth and invasion, however, it did not affect viability and migration in P2X4R deficient PCa cells. Maynard et al reached similar data that migrate ability had no significant changes in P2X4R KO of PCa cells blocking by CRISPR/Cas9.

In this study, the intracardiac injection xenograft model in BALB/c nude mice was utilized to investigate the role of P2X4R in PCa bone metastases. Compared to other mouse models of PCa, such as subcutaneous or orthotopic (van Weerden and Romijn, 2000), the intracardiac injection model is considered superior in mimicking the clinical process of PCa cells invading the bone. The effectiveness of this approach is believed to be attributed to the ability of tumour cells to bypass the lung capillaries and directly enter the left ventricle of the heart via injection (Berish et al., 2018).

Unfortunately, we were unable to detect any luciferase signal in the group of mice that received injections of PC3 P2X4R KO cells for in vivo studies. One possibility is that the luciferase gene was lost during the process of knocking out P2X4R in PC3 cells. Alternatively, the cell sorting process may have resulted in the selection of a GFP+ single clone without luciferase. The absence of the luciferase signal makes it difficult to directly observe the metastasis of PCa tumors in the mouse body during the animal

experiment, which adds to the challenge of tracking tumor metastasis (Cunningham and You, 2015).

5.5 Conclusion

In conclusion, the findings demonstrate that P2X4R plays a crucial role in the growth and mobility of PCa cells *in vitro* and *in vivo*. Knocking out P2X4R in PC3 cells led to a significant reduction in tumour cell growth and mobility *in vitro*, as well as a dramatic attenuation of bone metastasis in intracardiac injected BALB/c nude mice. These results suggest that P2X4R promotes the aggressive process of PCa bone metastasis and may represent a promising therapeutic target.

CHAPTER 6:

RESULTS: RNA-seq analysis suggested knocking out P2X4R increased cell adhesion and up-regulated anti-tumour genes

6.1 Introduction

RNA-seq (short for RNA sequencing) is a next-generation sequencing (NGS) technique used to determine the presence and quantity of RNA in a biological sample, providing insights into the constantly changing cellular transcriptome. The transcriptome refers to the complete set of transcripts in a cell, and understanding it is critical for interpreting the functional elements of the genome and understanding the development of PCa in the context of P2X4R deficiency. RNA-seq allows for differential expression analysis and functional annotation. By quantifying the relative abundance of each transcript, RNA-seq enables the measurement of gene expression levels. In this study, by comparing transcriptomes between PC3 WT and KO cells, RNA-seq revealed differentially expressed transcripts that can be used to annotate the function of shared transcripts or predict potential biological processes (Khatoon et al., 2014, Kukurba and Montgomery, 2015).

The data presented in Chapters 3 and 5 demonstrate the significant impact of P2X4R inhibition and knockout on cell proliferation, migration, invasion, and tumour formation *in vitro* and *in vivo*. To elucidate the underlying mechanisms, RNA-seq was used to identify differentially expressed genes and signalling pathways involved in the observed effects. The results provide valuable insights into the changes in gene expression contributing to the biological effects of P2X4R deficiency.

The study used RNA-seq to determine gene expression differences and the underlying biological processes affected by P2X4R deficiency in PC3 cells. Total RNA was extracted from three PC3 WT cultures and two PC3 KO clones, and RNA quality was evaluated using Nano-drop. The RNA samples were then sent to Source BioScience for RNA sequencing, and the resulting data were analysed using three bioinformatics tools: Galaxy European, David, and Gorilla. Galaxy European was used to determine gene expression differences, while David and Gorilla were employed for gene ontology and biological process enriched analysis, respectively. The expression of other P2XRs was also examined by gene expression in RNA-seq, and q-PCR was performed to

verify the RNA-seq data and test the impacts of P2X4R deficiency on other P2Rs. Overall, these analyses provided a comprehensive understanding of the gene expression changes and biological processes affected by P2X4R deficiency in PC3 cells. Process of RNA-seq analysis presents in Figure 6.1.

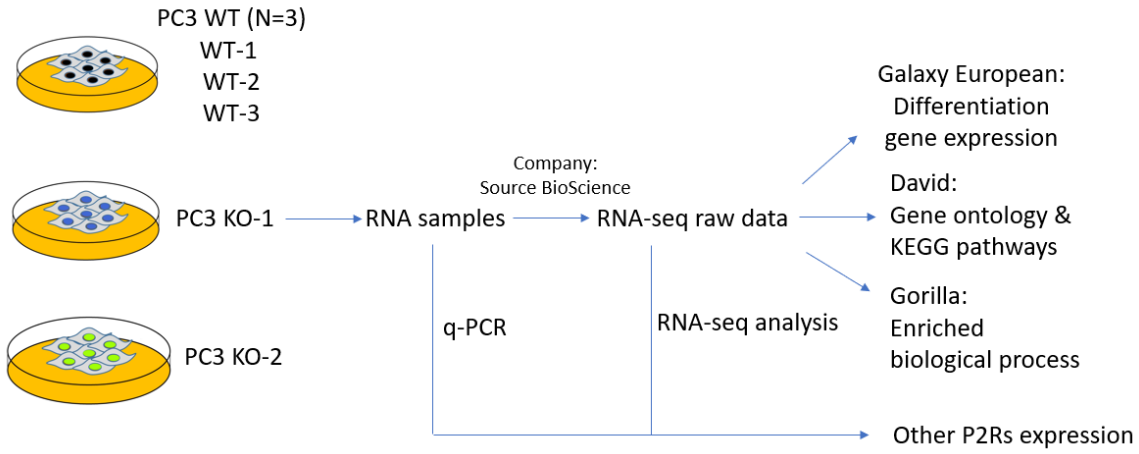

Figure 6.1: The process of RNA-seq. RNA sequencing was performed on PC3 WT and PC3 KO cells, and bioinformatics tools such as Galaxy European, David and Gorilla were used to analyse the RNA-seq data. Additionally, q-PCR and RNA-seq analysis were performed to assess the expression of other P2Rs.

6.2 The quality of RNA sample for RNA-seq

The quality of RNA samples is critical for RNA sequencing, and therefore, quality control measures were taken to ensure that the samples met the requirements for sequencing (Table 6.1). The samples were tested for quantity and quality using Nano-drop and Bioanalyzer, with the results meeting the minimum concentration for sequencing and demonstrating adequate RNA integrity. The RIN values of the samples were above 9.5, indicating high RNA integrity. The Nano drop testing was performed by NanoDrop 2000 (Themo Scientific) in my lab while the value of RIN was provided by company Source Bioscience. FastQC was also used to evaluate the quality of the sequencing data, which indicated adequate sequencing quality. These

measures ensured that the RNA-seq analysis could be performed accurately and effectively (APPENDIX A Figures A1.2).

Table 6.1: Values of RNA quality and quantity for PC3 WT&KO cells

Sample ID	Conc. (ng/µl)	260/280	260/230	RIN
PC3 WT-1	625	2.16	2.18	9.7
PC3 WT-2	408	2.07	2.12	9.8
PC3 WT-3	1800	2.05	2.11	9.7
PC3 KO-1	2210	2.08	2.15	9.5
PC3 KO-2	500	2.11	2.16	9.7

6.3 PCA variance

The variance in each biological replicate of PC3 WT and PC3 KO cells was analyzed by conducting principal component analysis (PCA) (Figure 6.2). The results showed minimal variance in the three biological replicates of PC3 WT cells, whereas there was considerable variance between PC3 KO-1 and PC3 KO-2 cells. During the CRISPR/Cas9-mediated P2X4R knockout, three different SgRNAs were designed to target distinct regions of P2X4R exons. DNA sequencing results in Chapter 4, section 4.4, revealed that a mutation occurred in the target SgRNA2 in PC3 KO-1, whereas the mutation in PC3 KO-2 occurred in the target SgRNA1. Variations were expected in these two P2X4R PC3 KO cells.

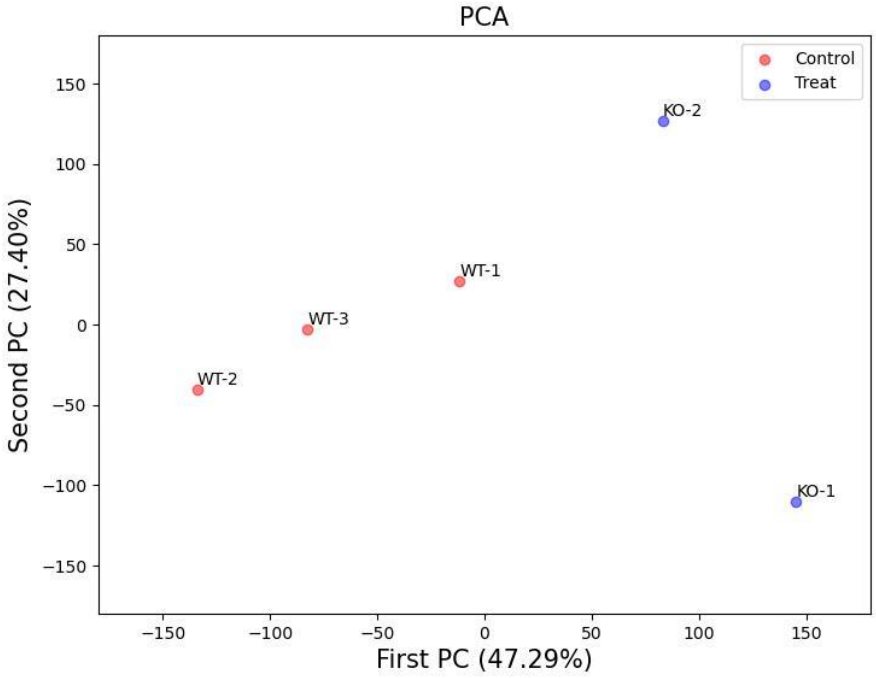

Figure 6.2: Expression variance between sample biological replicates. PCA was analysed by Python programming language. Three PC3 WT replicates have been examined, including WT-1, WT-2 and WT-3; while two PC3 KO have been examined, including KO-1 and KO-2.

6.4 Differentiation genes expression in PC3 WT&KO

RNA-seq was utilized to identify differentially expressed genes in PC3 cells with or without P2X4R using the Galaxy European website. Approximately 28,000 genes were identified, and 417 genes were significantly upregulated, while 40 genes were significantly downregulated in PC3 KO cells compared to PC3 WT. The volcano plot demonstrated the most significant differential up-regulated or down-regulated genes, and the top 15 up-regulated or down-regulated genes were listed in Tables 6.3 & 6.4 respectively, along with their gene symbols, gene names, *p* values, logFC values and functions.

Table 6.2: Number of differentiation genes in PC3 P2X4R KO

Differentiation genes	Up-regulate	Flat	Down-regulate
PC3 KO-PC3 WT	417	27506	40

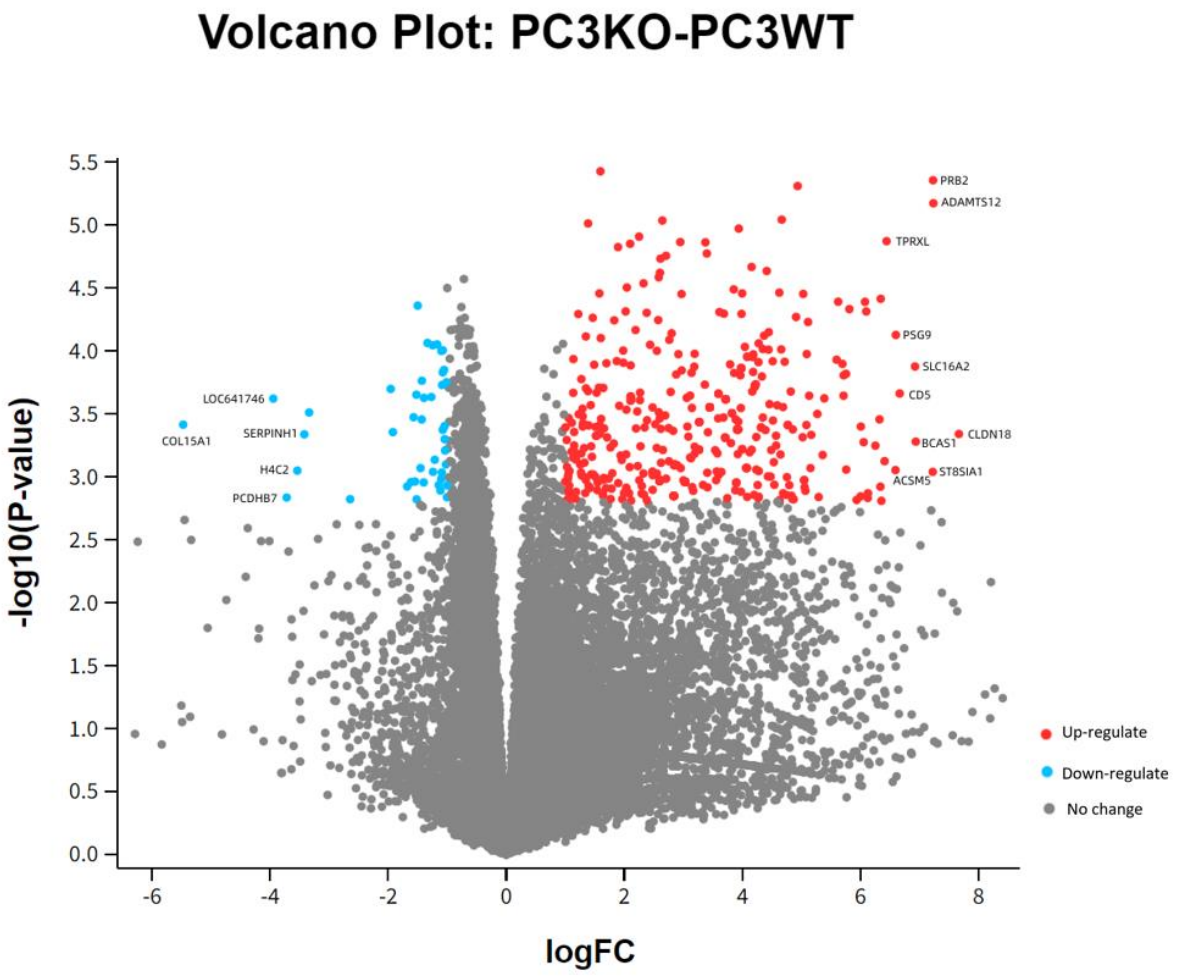

Figure 6.3: The differentiation gene expression was performed in the volcano plots. The volcano plots were generated by Galaxy European "Limma" results. The red points represent significantly up-regulated genes, while the blue points represent significantly down-regulated genes. The parameter is set as logFC > 1 and $p < 0.05$.

6.4.1 Up-regulated genes

In the present study, I identified 417 significantly up-regulated and 40 down-regulated genes in PC3 cells with P2X4R deficiency using RNA-seq data and Galaxy European. The top 15 up-regulated genes were listed in Table 6.3 with their logFC values, *p* value, gene functions and references. Among these genes, 13 were related to tumourigenesis, with 7 showing anti-tumour functions, including CLDN18, ADAMTS12, PRB2, BCAS1, ACSM5, RNF182, and THSD7B. CLDN18 (logFC = 7.23, *p*= 0.04) was the leading up-regulated gene, followed by ADAMTS12 (logFC=7.24, *p*=0.03) and PRB2 (logFC=7.23, *p*=0.03). Three of the up-regulated genes contribute to tumour promotion among the 15 genes, while the function of IGFN1 remains unclear. CD177 and SLC16A2 were found to be related to cancer risk with limited evidence. Gene CLDN18, ADAMTS12 and CD177 have been involved in cell adhesion function. The up-regulated genes were functionally categorized into anti-tumour, tumour-promoting, related to tumour risk, and non-cancer-related.

6.4.2 Down-regulated genes

The study identified the top 15 down-regulated genes in P2X4R-depleted PC3 cells, including their gene symbol, gene name, logFC value, *p* value, and gene functions (Table 6.4). Out of the 13 genes related to cancer, seven down-regulated genes were found to promote tumour progression, suggesting that their downregulation could suppress tumour growth or mobility. The leading tumour-promoting genes were PCDHB7 (log FC = -3.72, *p* = 0.04), SERPINH1 (log FC = -3.42, *p* = 0.03), and MIR611 (log FC = -2.64, *p* = 0.04). Additionally, PCDHB7 was found to be related to cell adhesion. The down-regulated genes were categorized into anti-tumour, tumour-promoting, related to tumour risk, and no cancer-related. Two genes were found to be involved in ion channels functions, including KCNK10, which is related to potassium channels, and CACNB4, which is in the calcium channel.

Table 6.3: Top 15 up-regulated genes and functions

Gene functions	Symbol	Gene name	Log FC	P Value	Reference
Anti-tumour	CLDN18	claudin 18	7.67	0.04	(Yao et al., 2015, Singh et al., 2017, Cao et al., 2022)
	ADAMTS12	ADAM metallopeptidase with thrombospondin type 1 motif 12	7.24	0.03	(Mohamedi et al., 2021, Beristain et al., 2011)
	PRB2	Proline-rich protein BstNI subfamily 2	7.23	0.03	(Giordano et al., 2007)
	BCAS1	brain enriched myelin associated protein 1	6.94	0.04	(Collins et al., 1998, Correa et al., 2000) (Munir et al., 2017)
	ACSM5	acyl-CoA synthetase medium chain family member 5	6.59	0.04	(Yazdani et al., 2021)
	RNF182	ring finger protein 182	6.35	0.05	(Okamoto et al., 2020, Liu et al., 2022)
	THSD7B	thrombospondin type 1 domain containing 7B	6.32	0.04	(Yao et al., 2022)
Tumour-promoting	ST8SIA1	ST8 alpha-N-acetyl-neuraminide alpha-2,8-sialyltransferase 1	7.23	0.04	(Nguyen et al., 2018)(Mabe et al., 2022)
	CD5	CD5 molecule	6.67	0.03	(Brown and Lacey, 2010, Tabbekh et al., 2011) (Zhang et al., 2016)
	PSG9	pregnancy specific beta-1-glycoprotein 9	6.60	0.03	(Jones et al., 2016, Xiong et al., 2021)
Tumourigenesis risk	SLC16A2	solute carrier family 16 member 2	6.92	0.03	(Sohrabi et al., 2021)
	IGFN1	immunoglobulin like and fibronectin type III domain containing 1	6.41	0.04	(Verma and Das, 2018, Lefebvre et al., 2016) (Cracknell, 2019)
	CD177	CD177 molecule	6.34	0.05	(Stroncek et al., 2004, Sachs et al., 2007)
None cancer-related: Early embryonic development	TPRXL	tetrapeptide repeat homeobox like (pseudogene)	6.44	0.03	(Booth and Holland, 2007)
None cancer-related: Long Intergenic Non-Protein Coding RNA	LINC01920	long intergenic non-protein coding RNA 1920	6.34	0.03	GeneCards (website)

Table 6.4: Top 15 down-regulated genes and functions

Gene functions	Symbol	Gene name	logFC	*P* Value	Reference
Tumour-promoting	PCDHB7	protocadherin beta 7	-3.72	0.04	(White et al., 2013)
	SERPINH1	serpin family H member 1	-3.42	0.03	(Wang et al., 2022a, Kawagoe et al., 2020)
	MIR611	microRNA 611	-2.64	0.04	(Chen et al., 2019)
	HIC1	HIC ZBTB transcriptional repressor 1	-1.54	0.04	(Wu et al., 2022)
	FAM27B	family with sequence similarity 27 member B	-1.52	0.03	(Fang et al., 2021)
	LINC00261	long intergenic non-protein coding RNA 261	-1.51	0.04	(Eke et al., 2021)
	APLN	apelin	-1.50	0.03	(Chen et al., 2021)
Anti-tumour	COL15A1	collagen type XV alpha 1 chain	-5.47	0.03	(Martínez-Nieto et al., 2021) (Sevgul and Karakok, 2016)
	FAM43B	family with sequence similarity 43 member B	-1.92	0.03	(Xu et al., 2011)
	KCNK10	potassium two pore domain channel subfamily K member 10	-1.68	0.04	(Innamaa et al., 2013)
	CACNB4	calcium voltage-gated channel auxiliary subunit beta 4	-1.61	0.04	(Shiozaki et al., 2021)
	TMEM52	transmembrane protein 52	-1.57	0.04	(Mao et al., 2017, Yu et al., 2017)
Tumourigenesis risk	TEX15	testis expressed 15, meiosis and synapsis associated	-1.95	0.03	(Lin et al., 2017)
None cancer-related: Pseudogene	LOC641746	glycine cleavage system protein H (aminomethyl carrier) pseudogene	-3.94	0.03	GeneCards (website)
None cancer-related: Low cancer specificity	H4C2	H4 clustered histone 2	-3.54	0.04	GeneCards (website)

6.5 Gene ontology

David bioinformatics tool was used for gene functional annotation, allowing the grouping of genes with similar functions and the annotation of large gene sets. Gene ontology (GO) was generated from the differential expression of genes in PCa P2X4R deficient cells. GO terms were selected based on the criteria of having more than 5 genes accounting for over 1.5% of total up-regulated genes, and the top 20 GO terms were chosen for up-regulated genes. Due to the limited number of down-regulated GO process, all down-regulated GO processes were shown. The top three GO terms in up-regulated genes were signal transduction (33 genes, 7.9%), cell adhesion (23 genes, 5,5%), and inflammation (16 genes, 3.8%). The down-regulated genes were involved in the regulation of angiogenesis and vascular endothelial cell proliferation, both related to blood vessel formation. Other GO terms included immunity, angiogenesis, and lipopolysaccharide. The results indicate that P2X4R is involved in several biological processes. The details of the GO terms and their associated genes are provided in Table 6.5.

Table 6.5: Gene ontology terms in biological process

Gene regulation	Similar terms	Term	Count	%
Up-regulated gene	Signal transduction	**Signal transduction**	33	7.9
		Cell surface receptor signalling pathway	10	2.4
		Transmembrane transport	9	2.2
		Calcium-mediated signalling	8	1.9
		Modulation of synaptic transmission	7	1.7
	Cell adhesion	**Cell adhesion**	23	5.5
		Positive regulation of cell migration	12	2.9
		Cell-cell adhesion	10	2.4
		Cell-matrix adhesion	9	2.2
		Cell migration	9	2.2
		Regulation of cell adhesion	8	1.9
		Regulation of cell migration	7	1.7
	Inflammation	**Inflammatory response**	16	3.8
		Regulation of inflammatory response	9	2.2
	Immunity	Immune response	14	3.4
	Angiogenesis	Angiogenesis	12	2.9
	Lipopolysaccharide	Cellular response to lipopolysaccharide	11	2.6
	Others	Negative regulation of endopeptidase activity	9	2.2
		Positive regulation of protein phosphorylation	8	1.9
		Extracellular matrix organisation	8	1.9
Down-regulated gene	Angiogenesis	Angiogenesis	3	7.5
		Positive regulation of vascular endothelial cell proliferation	2	5
	Others	Positive regulation of heat generation	2	5
		Positive regulation of protein localisation to nucleolus	2	5
		Positive regulation of heart rate	2	5
		Positive regulation of pri-miRNA transcription from RNA polymerase II promoter	2	5
		Collagen fibril organisation	2	5

David bioinformatics tool was used to enrich the functional annotation GO terms in the biological process. All differentiation genes were input to avoid irrelevant GO enriched biological processes, and the top enriched GO terms included cell adhesion (5.3%, p = 0.00001), angiogenesis (2.0%, p = 0.0029), prostaglandin metabolism (0.7%, p = 0.021), and ion transport (4.4%, p = 0.022). Other enriched terms included immunity (5.5%, p = 0.027), potassium transport (1.3%, p = 0.062) and lipid metabolism (4.2%, p = 0.097). The p value associated with each annotation term was inversely proportional to its relevance. Notably, prostaglandin metabolism was found to be an enriched biological process in P2X4R depletion, which may be related to Prostaglandin E2 (PEG2) release. The analysis was separated into up-regulated and down-regulated genes, with the up-regulated genes involved in cell adhesion, immunity, prostaglandin metabolism, lipid metabolism, angiogenesis, innate immunity, and ion transport. The down-regulated genes were involved in angiogenesis and differentiation (Table 6.6).

Table 6.6: Gene ontology enrichment of biological process

Biological process	Related genes	Count	%	*P* value
Cell adhesion	CD177,CD33,NUAK1,ADA,APLP1,COL6A2,COL6A3,COL13A1,COL15A1,DSG3,DSG4,ITGA2,ITGA5,ITGB4,LAMA3,LAMA4,LAMB3,LAMC2,MEGF10,PECAM1,PCDHB7,RELN,SIRPG,SRPX2	24	5.3	0.00001
Angiogenesis	NOX5,APLN,COL15A1,FGF1,PDE3B,RHOJ,SRPX2,THSD7A,TIE1	9	2.0	0.00287
Prostaglandin metabolism	HPGD,PTGS1,PTGS2	3	0.7	0.02083
Ion transport	ATP1B4,CFTR,NOX5,CACHD1,CACNB4,CACNA1A,GABRB1,GRIK2,HEPHL1,KCTD12,KCNJ15,KCNJ9,KCNK10,KCNG1,KCND1,RYR2,SLC24A5,SLC4A8,SLC5A7,SLC9A4	20	4.4	0.02180
Immunity	CX3CR1,CD177,CD3E,CYLD,FCGR1BP,FCMR,TRAV13-2,TRAV30,TRAV39,TRAV8-4,TRBJ2-3,TRBJ2-7,TXK,ADGRE1,BPI,CLU,C1S,GBP1,IDO2,LILRB3,MARCO,OPTN,SLPI,SAMD9,TRIM5	25	5.5	0.02690
Potassium transport	KCNJ15,KCNJ9,KCNK10,KCNG1,KCND1,SLC24A5	6	1.3	0.06237
Lipid metabolism	HPGD,ST8SIA1,ACSM5,ADTRP,ASPG,CERS4,CYP11A1,CYP2C19,CYP3A5,DGKG,DGKK,HSD3B2,HSD17B2,MGLL,PLCXD2,PLA1A,PTGS1,PTGS2,RDH8	19	4.2	0.09747

Biological process in up-regulated genes	Cell adhesion; Immunity; Prostaglandin metabolism; Lipid metabolism; Angiogenesis; Innate immunity; Ion transport.
Biological process in down-regulated genes	Angiogenesis; Differentiation (COL15A1,NGEF,PEG10,TEX15,TLL1)

The activity of a gene product that interacts with receptors effect changes in the activities of the receptor. Ligands may be produced by the cell that expresses the receptor. Ligands may diffuse extracellularly from their point of origin to the receiving cell or remain attached to an adjacent cell surface. Interactions ligand results of P2X4R deficiency showed calcium count for 38 related genes with 8.3% in total detecting genes (p = 0.00027). Heme count for 8 related genes with 1.8% (p = 0.034) (Table 6.7). The P2X4R is a ligand-gated ion channel related to calcium influx in the intro-cellular. The Ligand of Heme might involve in the process of angiogenesis.

Table 6.7: Interaction ligands with P2X4R

Category	Term	Count	%	*P* Value
Ligand interaction	Calcium	38	8.3	0.00027
Ligand interaction	Heme	8	1.8	0.03400

6.6 KEGG pathway

The KEGG pathway is a comprehensive database covering molecular interactions, reaction, and relation networks. It includes metabolism, genetic information processing, environmental information processing, cellular processes, organismal systems, human diseases, and drug development (Kanehisa et al., 2016). The results of the KEGG pathways are presented in Table 6.8, which includes GO term, gene count, percentage in genes, and *p* value. The *p* value associated with each enriched annotation term was inversely proportional to its relevance. The supplement information of genes related to each KEGG pathways represents in APPENDIX Table A1. The top three KEGG pathways are ECM-receptor interaction (2.41%, $p = 0.00001$) (Figure 6.4), focal adhesion (3.51%, $p = 0.00001$) (Figure 6.5), and human papillomavirus infection (3.51%, $p = 0.002$) (Figure 6.6).

Several factors have been reported to be associated with PCa or P2X4R in these pathways, such as WNT (Zhan et al., 2017) or PTEN/PHLPP (Ghalali et al., 2020). KEGG pathway annotations were performed, focusing on these potential P2X4R or cancer-related factors (APPENDIX A, Table A3). Four selected KEGG pathways were analysed to understand the mechanism of P2X4R depletion leading to tumour suppression, including ECM-receptor interaction, human papillomavirus infection (3.51%, $p = 0.002$) (Figure 6.7), the PI3K-Akt signalling pathway (3.29%, $p = 0.0091$) (Figure 6.8), and the cytokine-cytokine receptor interaction (2.41%, $p = 0.062$) (Figure 6.9).

Table 6.8: KEGG pathways

Term	Count	%	*P* Value
ECM-receptor interaction	11	2.41	0.00001
Focal adhesion	16	3.51	0.00001
Human papillomavirus infection	16	3.51	0.00197
Small cell lung cancer	7	1.54	0.00899
PI3K-Akt signalling pathway	15	3.29	0.00913
Protein digestion and absorption	7	1.54	0.01515
Gastric acid secretion	6	1.32	0.01611
Serotonergic synapse	7	1.54	0.02469
Regulation of lipolysis in adipocytes	5	1.10	0.02617
Steroid hormone biosynthesis	5	1.10	0.03242
Hematopoietic cell lineage	6	1.32	0.04385
Viral protein interaction with cytokine and cytokine receptor	6	1.32	0.04547
Amoebiasis	6	1.32	0.04879
NF-kappa B signalling pathway	6	1.32	0.05226
Cytokine-cytokine receptor interaction	11	2.41	0.06247
Arrhythmogenic right ventricular cardiomyopathy	5	1.10	0.06309
Axon guidance	8	1.75	0.06503
Ovarian steroidogenesis	4	0.88	0.07689
Complement and coagulation cascades	5	1.10	0.08683
Hypertrophic cardiomyopathy	5	1.10	0.09859

6.6.1 Cell-adhesion molecules were regulated in ECM-receptor interaction pathways

The ECM-receptor interaction pathway was found to be the most upregulated gene-enriched signaling pathway. The ECM-receptor has an important role in tumour shedding, adhesion, degradation, movement, and hyperplasia (Bao et al., 2019). The results indicated that many receptors were regulated and had molecular interactions with proteins, including α2 and α5 of VLA proteins and β4 of other combinations. VLA proteins are members of the β-integrin family of cell-surface adhesion molecules that are involved in cell adhesion functions (Figure 6.4).

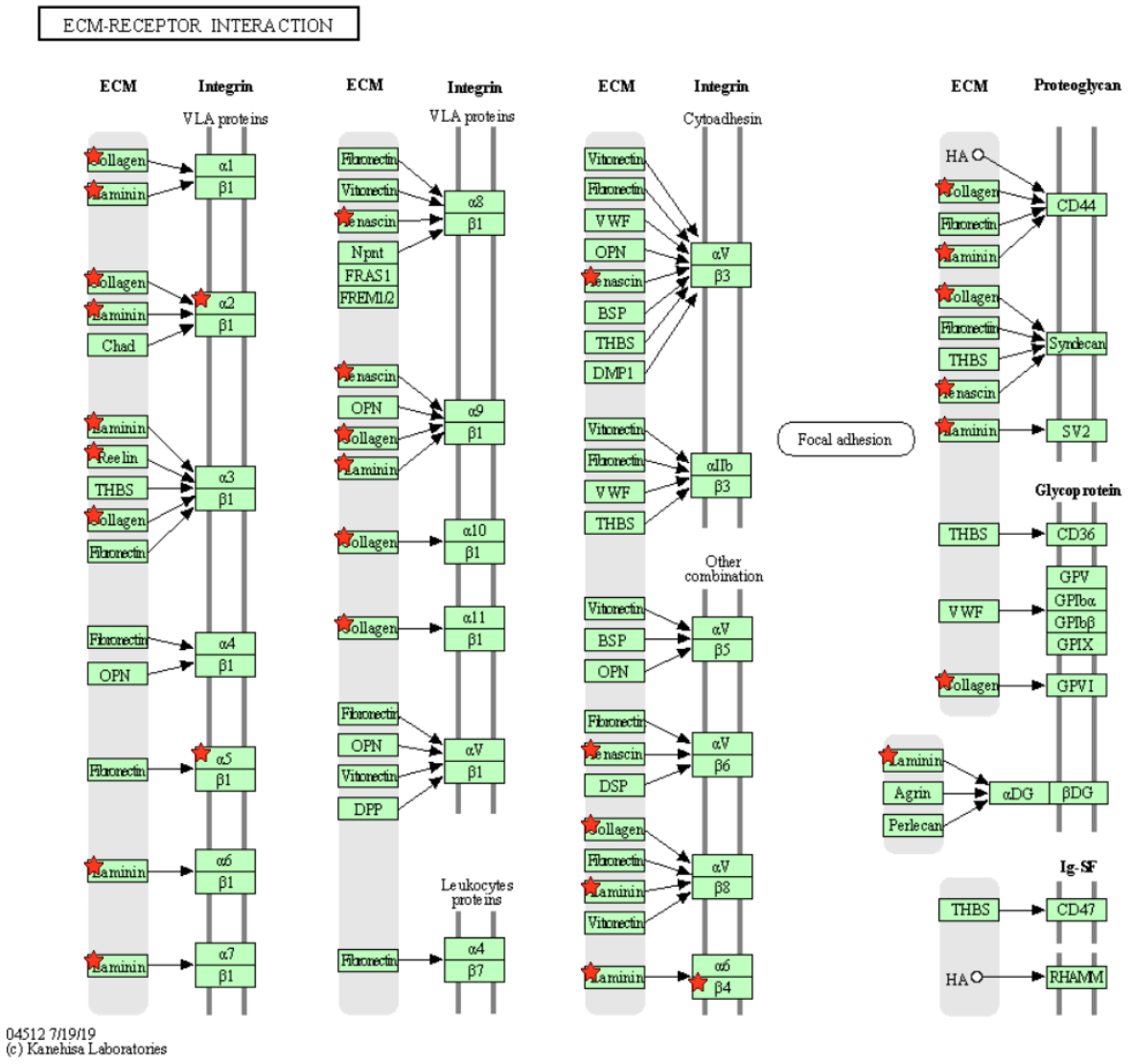

Figure 6.4: ECM-receptor interaction pathways. The pathways were generated from David. Regulated genes were marked in red stars.

6.6.2 Cell-adhesion related genes in the focal adhesion pathways

The focal adhesion complexes are transmembrane clusters of proteins that connect intracellular stress fibres and ECM molecules on the substrates in contact with cells. The stress fibres, primarily consisting of actin molecules, actively pull the focal adhesion complexes. Cell-matrix adhesions play essential roles in important biological processes, including cell motility, cell proliferation, cell differentiation, regulation of gene expression and cell survival (Berrier and Yamada, 2007). Results showed that ECM, ITGA, and ITGB had been regulated which was involved in the cell adhesion (Figure 6.5).

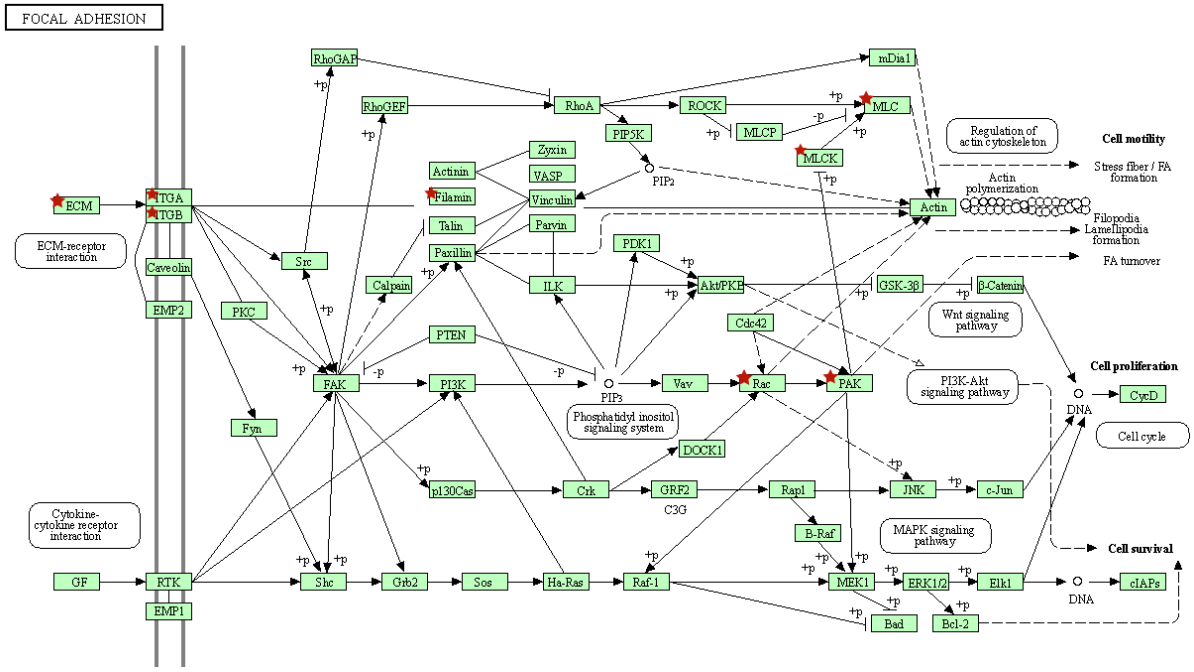

Figure 6.5: Focal adhesion pathways. The pathways were generated from David. Regulated genes were marked in red stars.

6.6.3 WNT and COX-2 were regulated in human papillomavirus infection pathways, PGE2 may be the downstream signal of P2X4R to slow down PCa progression

In the human papillomavirus infection pathways, WNT and COX-2 were regulated, and PGE2 may act as the downstream signal of P2X4R to slow down PCa progression. Notably, the WNT and COX-2 pathways were regulated in these pathways (Figure 6.6). WNT signaling is a critical cascade that regulates development and stemness and is tightly associated with cancer (Shorning et al., 2020). Prostaglandin-endoperoxide synthase 2, or COX-2, is an enzyme involved in the biosynthesis of prostaglandins (Hla and Neilson, 1992), and Prostaglandin E2 (PGE2), also known as dinoprostone, is a naturally occurring prostaglandin (Abrahao et al., 2010). COX-2 promotes the release of the pro-inflammatory mediator PGE2. The expression of COX-2 is regulated, leading to the release of PGE2, indicating that PGE2 might be the downstream signal of P2X4R (Figure 6.7).

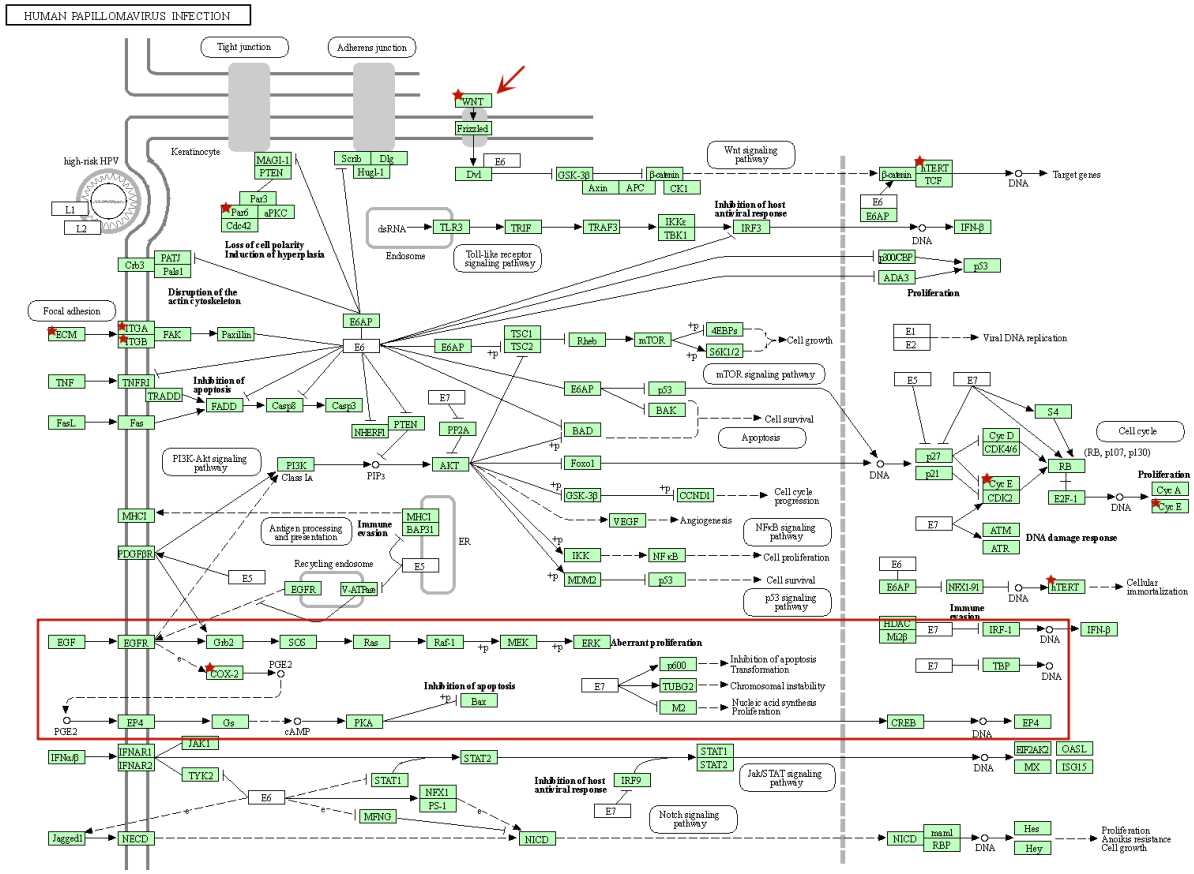

Figure 6.6: Human papillomavirus infection pathways. The pathways were generated from David. Regulated genes were marked in red stars. The red arrow pointed out gene WNT.

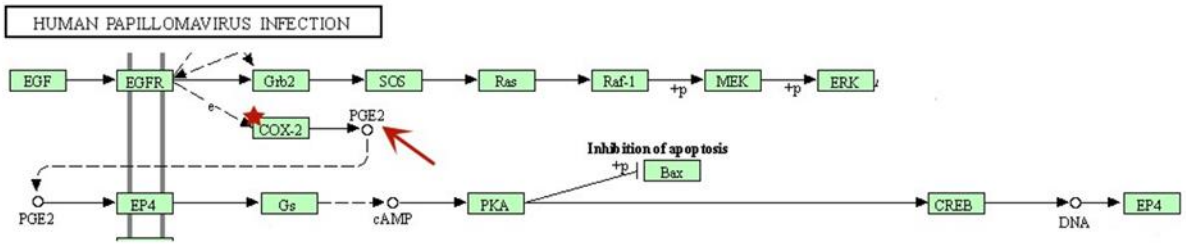

Figure 6.7: PGE2 might be the downstream signal of P2X4R. Knocking of P2X4R showed the regulated gene COX-2, which releases PGE2. Figure 6.7 was taken as part of the marked part in Figure 6.6. Gene COX-2 was regulated and marked in a red star. The red arrow pointed out gene PG2.

6.6.5 There is no interaction between P2X4R and PTEN/PHLPP

PTEN has been proven to lead to the development of cancerous tumours. There is limited evidence suggesting a relationship between P2X4R and PTEN/PHLPP. However, results in my study showed knocking out of P2X4R did not affect the expression of either PTEN or PHLPP (Figure 6.9).

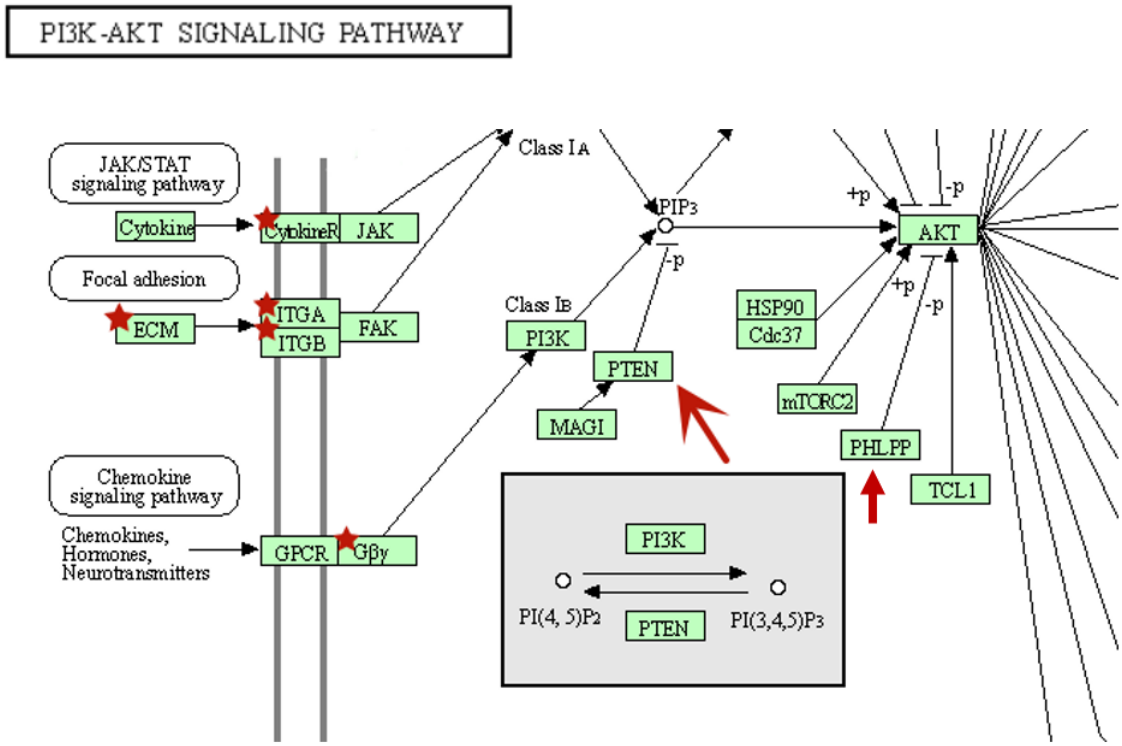

Figure 6.8: There is no affecting on the expression of PTEN or PHLPP after depleting P2X4R. The red arrows pointed out the PTEN and PHLPP in the PI3K-Akt signalling pathway. Figure 6.8 was taken as part of the PI3K-Akt signalling pathway, and the pathway was generated from David. Regulated genes were marked in red stars.

6.6.6 No TGF-β cytokines change after depleting P2X4R

Researchers have established a close relationship between P2XRs and TGF-β (Schenk et al., 2011), particularly the P2X7R and TGF-β (Huang et al., 2022). They have suggested that TGFβ-1 enhances the PHLPP levels (Bradley et al., 2013). Moreover, it has been shown that P2X4R plays a crucial role in invasiveness induced by TGFβ-1 and epithelial-mesenchymal transition (Ghalali et al., 2020). The transforming growth factor beta (TGF-β) superfamily is a large group of structurally related cell regulatory proteins. Although there is a close relationship between P2XRs and TGF-β (Schenk et al., 2011), no research has found a direct relationship between P2X4R and TGF-β. Results indicated that knocking out P2X4R did not affect the expression of TGF-β cytokines (Figure 6.10).

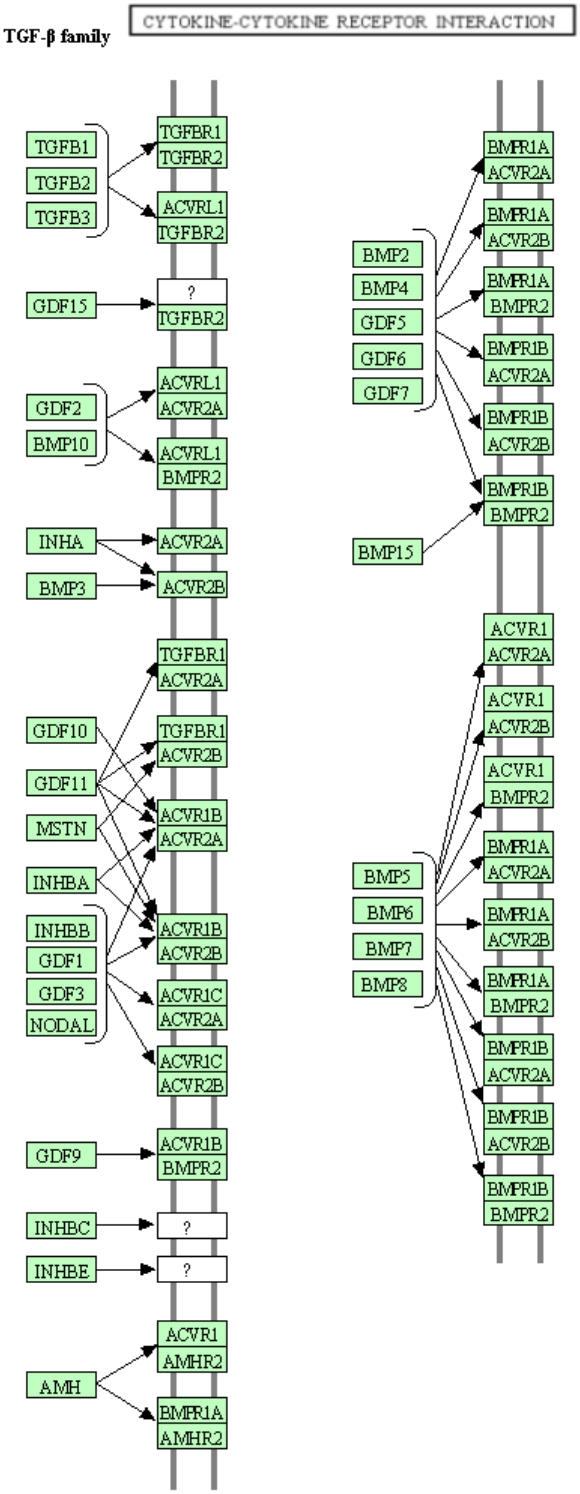

Figure 6.9: Blocking of P2X4R did not affect the TGF-β family. Results showed there are no TGF-β cytokines changed after P2X4R depletion. Figure 6.9 was taken as part of the cytokine-cytokine receptor interaction map, and the map was generated from David.

6.7 GO biological process enriched to glycoprotein metabolic

The Gorilla application was used to analyze the specific enriched GO biological patterns. The results showed enrichment in the glycoprotein metabolic process (Figure 6.11). This process involves chemical reactions and pathways that affect glycoproteins, which are proteins that contain covalently bound monosaccharide residues. The two critical genes involved in this process are ADAMTS12 and ST8SIA1.

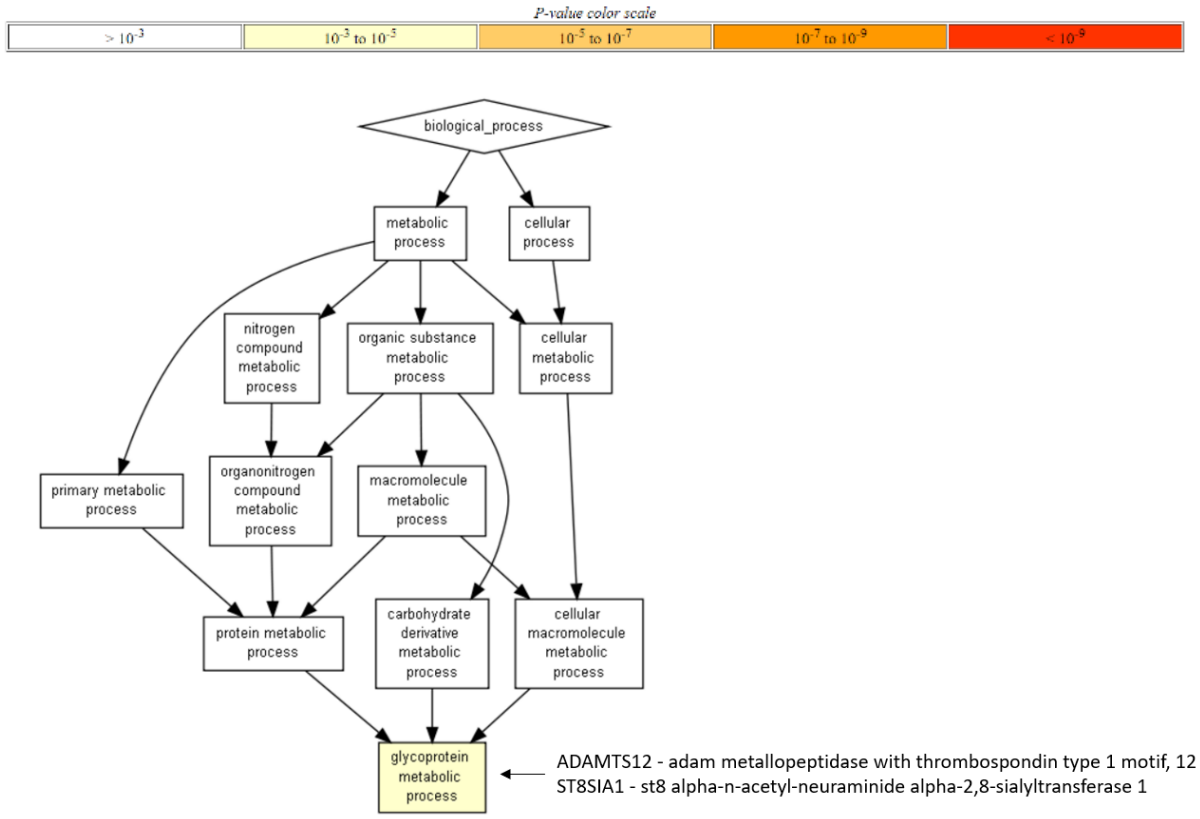

Figure 6.10: GO biological process enriched to glycoprotein metabolic process. GO enrichment analysis was used in the web-based Gorilla application.

6.8 Depleting P2X4R did not affect other P2Rs expression

P2X4R is a typical member of the P2XR family that can form heterotrimers with P2X2R, P2X5R, P2X6R, or P2X7R, which is crucial for co-expression and functional ATP-binding activity (Nicke et al., 2005, Lê et al., 1998, Boumechache et al., 2009, Craigie et al., 2013). It is common and essential for the P2XR family to form homotrimer receptor units. To explore the expression of other P2Rs after P2X4R knockout in PCa cells, RNA-seq was used to measure the expression level of P2Rs, including P2XRs and P2YRs. The expression of other P2XRs was found to be barely affected by P2X4R knockout, which is consistent with the q-PCR results obtained by comparing the expression of other P2Rs in PC3 WT and PC3 KO cells.

6.8.1 Other P2Rs expression analysis by RNA-seq

The expression of other P2Rs in P2X4R-deficient cells was analyzed by RNA-seq, and the results are presented in Table 6.9, including the logFC value and adjusted *p* value. The RNA-seq data showed that the expression of P2X4R was reduced in PC3 KO cells compared to PC3 WT, although no significant difference was detected. It is possible that the incomplete P2X4R mRNA encoded a non-functional protein and could not represent a significant reduction in P2X4R in PC3 P2X4R KO cells. The expression of P2X5R was significantly reduced in the RNA-seq results. However, the expression of other P2Rs remained at the same level in P2X4R-depleted PC3 cells compared to PC3 WT.

Table 6.9: Other P2Rs expression in RNA-seq

P2R	SYMBOL	logFC	adj.P.Val
P2XR	P2RX1	2.49	0.26
	P2RX2	0.92	0.62
	P2RX3	1.77	0.48
	P2RX4	-0.79	0.09
	P2RX5	-0.79	0.04
	P2RX6	1.81	0.41
	P2RX7	0.27	0.62
P2YR	P2RY1	0.14	0.62
	P2RY2	0.17	0.62
	P2RY4	4.18	0.16
	P2RY6	1.12	0.67
	P2RY8	-0.47	0.77
	P2RY10	0.28	0.62
	P2RY11	-0.27	0.38
	P2RY12	1.51	0.62
	P2RY13	1.89	0.39
	P2RY14	-0.87	0.62

6.8.1 Other P2XRs expression analysis by q-PCR

The q-PCR relative gene expression test was performed using the Taq-man assay. The housekeeping gene GAPDH was used to normalize Ct values and generate delta Ct values to calculate the relative expression levels of P2XRs. Values of 1/ΔCt for each sample are presented in Figure 6.11. The results showed that the expression of P2X4R significantly decreased by 59% in PC3 P2X4R KO-1 cells ($p < 0.05$), while there was no significant difference in gene expression for other P2XRs. The relative mRNA expression level quantification ($2^{-\Delta\Delta CT}$) between PC3 KO-1 and PC3 WT was significantly reduced by over 90% ($p < 0.001$) (Chapter 4, section 4.6).

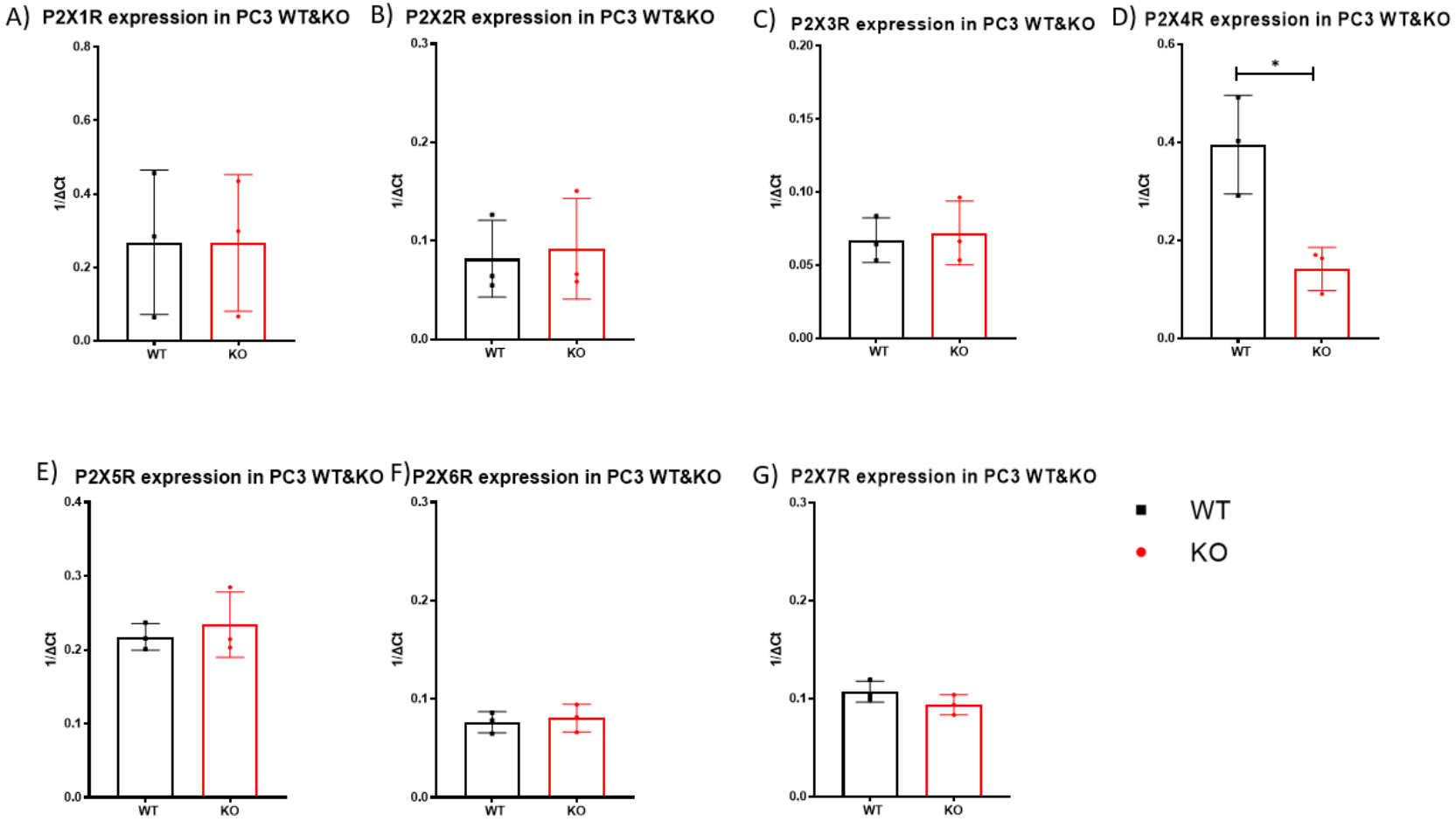

Figure 6.11: There are no significant changes in P2XRs expression through P2X4R deficiency. Total RNA was isolated from the WT and KO cells using the RNA Miniprep Systems protocol, and the first complementary DNA (cDNA) strand was synthesized. Primers were designed according to the PubMed GenBank database and synthesized by the company Azenta. qPCR was performed using Taq-man qPCR assay, and ΔCt values were read by the Applied Biosystems 7900 Real-Time PCR machine. Relative expression was then calculated and presented in the graph. Data are the mean ± SD. N=3, students' t-test. *$p < 0.05$.

6.9 Discussion

P2X4R deficiency was found to have a tumour-suppressive effect on PCa cells. Our observations reveal that inhibiting P2X4R by its specific antagonists could impair the growth and mobility of PCa cells *in vitro* and suppress tumour formation *in vivo*. Furthermore, blocking P2X4R in PCa cells significantly reduced cell growth, survival and invasion *in vitro*. PCa cells with P2X4R deficiency showed suppressed tumour growth and prevented bone metastasis *in vivo*.

RNA-seq was performed to understand the mechanism of how P2X4R deficiency significantly reduces the progression of PCa. The gene ontology analysis based on RNA-seq revealed that the absence of P2X4R resulted in significant enrichment of biological processes related to cell adhesion, angiogenesis, and prostaglandin metabolism among the differentially expressed genes. These findings suggest that the absence of P2X4R may have anti-tumor effects by impacting these processes. The RNA-seq analysis also revealed a significant increase in cell adhesion activity upon P2X4R KO in PCa cells. KEGG pathway analysis showed that the potential downstream signal of P2X4R, PGE2 can affect WNT expression levels, indicating that P2X4R blockade might affect WNT signaling pathways, which is critically involved in tumour progression. Finally, our results evidenced no effect on other P2Rs expression by P2X4R depletion.

Identifying the expression of differentiation genes showed that anti-tumour genes were regulated after targeting P2X4R. The top three up-regulated genes are all tumour suppressors, including CLDN18, ADAMTS12, and PRB2. These three genes have the following functions:

- CLDN18 gene is linked to abnormal expression during the occurrence and development of various malignant tumours such as gastric and breast cancer (Cao et al., 2022). CLDN18 has been specifically associated with prognosis in gastric cancer, and CLDN18.2 is an anti-tumour target for advanced gastric

cancer (Singh et al., 2017). CLDN18 also plays a significant role in tight junction-specific, calcium-independent cell-adhesion activity (Yao et al., 2015).

- ADAMTS-12 is a novel anti-tumour protease that reduces the proliferative properties of tumour cells (Mohamedi et al., 2021). ADAMTS12 may potentially participate in the tumorigenesis of pulmonary cells through its proteolytic activity or as a molecule that could regulate cell adhesion (Beristain et al., 2011).
- PRB2 is a known cancer suppressor gene (De Falco and Giordano, 2006). Human PRB2 can induce growth suppression in human glioblastoma cell lines (Giordano et al., 2007).

The top five down-regulated genes include COL15A1, LOC641746, PCDHB7, H4C2, and SERPINH1. PCDHB7 and SERPINH1 are tumour-promoting genes, and their down-regulation can prevent tumour progression. These four genes have the following functions:

- COL15A1 is an anti-tumour gene and its inactivation in mice leads to changes in the fibrillar tumour matrix and increased mammary tumour growth (Martínez-Nieto et al., 2021). there is a correlation or association between COL15A1 and the density of microvessels in a tissue (promoting angiogenesis) as well as the development of carcinoma cells (Sevgul and Karakok, 2016).
- PCDHB7 is a cell surface protein involved in cell-cell communication and adhesion most likely playing a critical role in establishing and functioning specific cell-cell neural connections. Correlation of PCDHB7 to calcium ligands and cancer suggests it as a possibly calcium-dependent cell-adhesion protein (White et al., 2013).
- SERPINH1, when expressed by anti-tumour miR-148a-5p, inhibits cancer cell aggressiveness in gastric cancer (Kawagoe et al., 2020).
- LOC641746 is a pseudogene with low cancer specificity which means that is not only found in cancer cells and is also expressed in normal cells. This makes LOC641746 less useful as a target for cancer therapies (Poliseno et al., 2010).

In general, many differentially expressed genes are involved in cell adhesion, and the GO term for biological processes is also enriched in cell adhesion. As discussed in Chapters 3 and 5, P2X4R inhibition significantly reduced cell migration, while P2X4R knockout did not; however, both P2X4R inhibition and knockout significantly reduced invasion. The *in vivo* experiments demonstrated a significant reduction in PCa bone metastasis upon injection of P2X4R-deficient PCa cells. RNA-seq analysis indicates an increase in cell adhesion activity in PCa P2X4R KO cells. Cell adhesion activity, mediated by cell adhesion molecules (CAMs), commonly plays a central role in cancer progression and acquisition of a metastatic phenotype (Wai Wong et al., 2012). CAMs act as membrane receptors, which facilitate cell-cell and cell-matrix interactions, and are crucial for transmitting intracellular signals related to adhesion, migration, invasion, angiogenesis, and organ-specific metastasis (Li and Feng, 2011). A study has demonstrated that inhibiting CAMs, has the potential to be a therapeutic target for breast cancer metastasis (Li and Feng, 2011).

CLDN18 is a crucial gene expressed in epithelial cells and is the top up-regulated gene in P2X4R knockout cells. The EMT is a process by which epithelial cells lose their cell polarity, cell-cell adhesion, and acquire migratory and invasive properties. The process of EMT has been shown to be associated with cancer metastasis (Bhanoat and Levine, 2012, Heerboth et al., 2015, Bakir et al., 2020). The results suggest that P2X4R might mediate the EMT process, slowing down tumour migration and invasion *in vitro* and preventing tumour bone metastasis *in vivo*. In breast cancer, the upregulation of P2X4R promotes cancer progression by regulating lysosome acidity, promoting autophagy and cell survival. Additionally, this receptor is associated with the induction of EMT, which is further enhanced under metabolic stress conditions. Inhibition of P2X4R by both gene silencing and pharmacological means led to decreased autophagy and EMT resulted in disrupting the aggressive cancer phenotype (Chadet et al., 2022). However, currently, there is no evidence indicating the involvement of P2X4R in the progression of PCa or PCa bone metastasis.

P2X4R is not only expressed in prostate cells but also in immune cells and has been shown to be involved in the inflammatory response (Li et al., 2014, Boumechache et

al., 2009). Inflammatory GO terms were identified as enriched in a biological process that can explain the decreased levels of the inflammation cytokine Eotaxin after inhibiting P2X4R *in vivo*. P2X4R is known to be involved in various inflammation-related activities as ATP is a pro-inflammatory molecule. Pathological events associated with cellular destruction can result in a massive accumulation of ATP, including cell stress, injury, and death, which exacerbate the inflammatory response and lead to an inflammatory cascade (Suurväli et al., 2017). Increased extracellular ATP concentrations can act as powerful chemotactic stimuli for host innate immune cells, many of which express P2 purinergic receptors. Studies have shown a close relationship between P2X4R and inflammation in the brain post-ischemic, rheumatoid arthritis, and neuroinflammation (Suurväli et al., 2017, Maynard et al., 2022). Additionally, P2X4R protein has been shown to be primarily expressed in epithelial cells and immune cells in the prostate (Maynard et al., 2022).

Inhibition of P2X4R signaling may lead to anti-tumor effects in prostate cancer. This may occur through the modulation of inflammation by regulating the expression of WNT and PGE2, which subsequently slows down the progression of the disease. In peripheral macrophages, expression of P2X4R can contribute to pain pathways by releasing PGE2 (Basbaum et al., 2009), which indicate PGE2 as the downstream signal pathway of P2X4R. The COX-2/PGE2 pathway has been shown to play a key role in the development of colorectal cancer. Deregulation of COX-2 expression and increased levels of PGE2 have been linked to various aspects of colorectal tumourigenesis, including tumour maintenance and progression, metastatic spread, and possibly even tumour initiation (Greenhough et al., 2009). Greenhough et al. also demonstrated that there is a relationship between the WNT signalling pathway and COX-2 within the tumour microenvironment, targeting WNT and PGE2 have been involved in the regulation of cell proliferation, apoptosis, and angiogenesis. This evidence explains the observation that targeting P2X4R can contribute to PCa anti-tumourgenesis. Its mechanism may be through inhibiting inflammation by regulating the expression of PGE2 resulting in slowing down the PCa progression.

The P2X4R is a ligand-gated cation channel that opens in response to binding to ATP (White et al., 2013). It is abundantly expressed in the cell membrane to allow Ca^{2+} and Na^{+} influx and K^{+} efflux through the transmembrane (Kawate et al., 2009). Based on the known function of P2X4R, the leading GO term is signal transduction, which includes cell surface receptor signalling pathways, transmembrane transport, and calcium-mediated signalling. P2X4R is also abundantly expressed in central nervous cells and is associated with the modulation of synaptic transmission (Ostrovskaya et al., 2011).

Angiogenesis has been shown to positively impact tumour invasion (Florencio-Silva et al., 2015). GO analysis results showed that the blockage of P2X4R significantly impacts angiogenesis in PC3 cells, which may lead to preventing tumour bone metastasis *in vivo*.

Ghalali et al. (2020) argued that P2X4R might mediate the crosstalk between PTEN and PHLPP in PCa cancer (Ghalali et al., 2020). Maynard et al. demonstrated a relationship between PTEN and P2X4R in PCa tissues (Maynard et al., 2022). However, my study found no interaction between P2X4R and PTEN/PHLPP. TGF-β functions as a tumour suppressor by mediating its antiproliferative effects in a large variety of cell types, including PCa cells (Bello-DeOcampo and Tindall, 2003). Evidence has shown a close relationship between P2XRs and TGF-β (Huang et al., 2022); however, there is no interaction between P2X4R and TGF-β in PCa cell lines PC3.

While RNA-seq analysis provides the potential mechanism for knocking out P2X4R in PC3 cells and differentiating gene expression at the transcriptional level, there are still limitations to consider, including experimental design, cell cycling, and the inherent limitations of RNA-seq techniques. First, one limitation is that only two PC3 knockout clones have been generated using the CRISPR/Cas9 system, which falls below the recommended three biological replicates for RNA-seq analysis. Then using only the PC3 cell line may not adequately represent the progression of PCa disease.

Furthermore, the different stages of the cell cycle may also affect the accuracy of gene expression when applying RNA-seq analysis, for example, PCa cells exhibit cell-cycle-related transcriptional changes and variations in their response to androgen stimulation (Horning et al., 2018). Moreover, RNA-seq itself possesses limitations, such as the method of RNA-seq library construction, accuracy of gene splicing and Incomplete annotation (Pertea et al., 2015). RNA-seq is a hypothesis-generating exercise that provides a potential direction for further investigation, allowing for the identification of potential genes or pathways. Subsequent validation experiments, such as the verification of signal pathways through western blotting, are necessary to enhance the reliability of RNA-seq results (Dai et al., 2021).

6.10 Conclusion

In conclusion, my study showed that depleting P2X4R in PCa cells can significantly reduce tumour growth and prevent PCa bone metastasis *in vivo* by upregulating genes that may have an anti-tumour effect or epithelial associated gene. Meanwhile, PCa cells deficient of P2X4R demonstrated a higher activities in cell adhesion compared to PCa WT cells. This mechanism may be attributed to the regulation of WNT and PEG2 signals, resulting in reduced cell proliferation, enhanced apoptosis, and affect angiogenesis.

Chapter 7:

GENERAL DISCUSSION

7.1 Discussion

A growing evidence show that P2X4R play a significant role in cancer. Research has shown that P2X4R expression is upregulated in various types of cancer, including breast cancer (Chadet et al., 2022), colon cancer (Schmitt et al., 2022), and glioblastoma (Guo et al., 2004). In some studies, higher P2X4R expression was associated with poor prognosis and decreased survival in cancer patients (Correa et al., 2000, Collins et al., 1998).

In my project, to investigate the role of P2X4R in PCa aggressiveness, P2X4R was inhibited by antagonist 5-BDBD or genetically knocked out in PCa cells in a series of *in vitro* and *in vivo* studies. As observed, P2X4R inhibition and knockout contributes to anti-tumourigenesis in PCa. Further RNA-seq analysis-based mechanistic study indicated that several anti-cancer genes were dramatically up-regulated in P2X4R KO cells, and cell adhesion activities was increased.

According to my results, the current findings firstly show targeting P2X4R by the specific antagonist, PSB-12062 or 5-BDBD, inhibits PCa cells proliferation, migration, and invasion *in vitro*. *In vivo* studies using a subcutaneously injected mouse model showed that treatment with 5-BDBD led to reduced tumour size and decreased inflammation factors Eotaxin. Although Maynard et al. used an allograft mouse model and mouse PCa cell lines Myc-CaP, their study demonstrated that knocking out P2X4R significantly reduced tumour formation *in vivo* (Maynard et al., 2022). These findings support that P2X4R is a potential therapeutic target for PCa (He et al., 2020, Maynard et al., 2022).

Secondly, the role of P2X4R deficiency in PCa bone metastasis was studied here for the first time using P2X4R KO cells which showed that blockage of P2X4R significantly decreased tumour cell growth and invasion while enhancing apoptosis *in vitro*. Similarly, *in vivo* studies using an intracardiac xenografts bone metastasis model in

BALB/c nude mice demonstrated that knocking out P2X4R significantly reduced PCa cells metastasis in mouse tibias. The rationale for focusing on PCa bone metastasis in this study is due to its association with poor patient outcomes (Sturge et al., 2011). Our findings strongly suggest that P2X4R plays a critical role in the aggressiveness of PCa bone metastasis and may be a potential therapeutic target.

Thirdly, the RNA-seq analysis provides the first comprehensive understanding of the molecular mechanism by which P2X4R contributes to PCa development. Knocking out P2X4R was found to dramatically increase cell adhesion function and the characteristic of epithelial cells, which reduced the progression of PCa. RNA-seq analysis showed that knocking out P2X4R up-regulated epithelial and anti-cancer genes, although the mechanism behind this up-regulation is currently unclear. One possible explanation for this is the EMT process, which is known to be involved in PCa progression (Zhou, 2019). Inhibiting the process of EMT can also increased cell-cell recognition and adhesion, and decreased cell motility (Heerboth et al., 2015). The mechanism underlying this effect may apply in the up-regulation of anti-tumour genes, which in turn can mediate the WNT and PGE2 signalling pathways (Greenhough et al., 2009, Abrahao et al., 2010).

Of notice, P2X4R is a type of purinergic receptor that can bind to ATP. When ATP binds to P2X4R, they open up and allow the flow of positively charged ions, such as calcium and sodium, into the cell (Chen et al., 2013). This can trigger a cascade of intracellular signalling pathways, leading to various cellular responses (Hattori and Gouaux, 2012). For example, activating P2X4R in immune cells can trigger the release of pro-inflammatory cytokines, which are essential for fighting infections (Han et al., 2020). These inflammation responses can affect cancer progression. However, in this study, BALB/c nude mice was used *in vivo* with elimination of T cells still with B and NK cells. The BALB/c nude mice are with low immune system that dramatically decrease the immunity responses (Berish et al., 2018). In order to understand the function of P2X4R in PCa bone metastasis in this study, I utilized a xenograft mouse intracardiac injection model. By comparing xenograft data to cell-based i*n vitro* studies, I can get a relatively accurate understanding of the development of a particular tumour

and the efficacy of drugs used to treat it. A further allograft mouse model, e.g. murine RM1 or TRAMP C2 models, can be used to strengthen my PCa bone metastasis research. P2X4R has been shown to play a significant role in immunity and inflammation. These receptors are expressed on various immune cells, including T cells, B cells, natural killer cells, dendritic cells, and macrophages (Boumechache et al., 2009). In addition, the role in producing pro-inflammatory cytokines and chemokines, P2X4R has also been shown to play a role in the phagocytosis of bacteria by immune cells (Csóka et al., 2018). Activation of P2X4R on macrophages has been shown to enhance the phagocytosis of bacterial pathogens, leading to their clearance. In patients' samples, there is a relationship between P2X4R and Macrophages, indicating that P2X4R was involved in the inflammation response (Maynard et al., 2022). These findings suggest that P2X4R expression may be involved in the development and progression of PCa, possibly through its role in inflammation and immune cell function. However, more research is required to understand these associations' mechanisms fully. Future studies can be focused on the inflammatory response to anti-tumour cancer by P2X4R deficiency.

An obvious limitation is that only two PC3 knockout clones have been generated using the CRISPR/Cas9 system, which is below the recommended three biological replicates for RNA-seq analysis. Additionally, to achieve a more comprehensive understanding of P2X4R function, it is crucial to include at least two different PCa cell lines with distinct characteristics, such as varying levels of metastatic potential or androgen dependent or independent. The PCa cell lines PC3, DU145, and LNCaP are commonly employed in xenograft models (Shi et al., 2019), and each is derived from a distinct anatomical location, namely bone for PC3, brain for DU145, and lymph node for LNCaP (van Weerden and Romijn, 2000). These cell lines demonstrate varying levels of metastatic potential. In terms of androgen response, PC3 and DU145 are androgen-independent, whereas LNCaP is androgen-dependent (Shi et al., 2019). Conducting another PCa cell lines for *in vitro* studies, or consider the different stages of cell cycling and heterogeneity of samples could provide a better understanding of P2X4R's functions in the disease.

5-BDBD is a potent and selective antagonist for P2X4R and has been used in numerous studies to inhibit cancer (Bidula et al., 2022), neurological (Srivastava et al., 2020), or inflammation responses (Schneider et al., 2022). However, 5-BDBD can also inhibit other P2 receptors, such as P2X1R and P2X3R (Coddou et al., 2019), which may explain the differences in P2X4R inhibition and knockout data. For instance, while P2X4R deficiency enhances apoptosis, this effect is not observed with its inhibition. Similarly, inhibition of P2X4R decreases cell migration, but this is not always observed in P2X4R knockout data.

Previous studies demonstrated that P2Rs might play a critical role in PCa, especially P2X7R (Adinolfi et al., 2015). P2X7R is a member of the P2XR family, Qiu (Qiu et al.2014) demonstrated that silencing P2X7R expression using siRNA can inhibit the migration and invasion of PCa cells driven by ATP and BzATP *in vitro*. Additionally, silencing P2X7R significantly reduced the expression of genes associated with EMT (Shieh et al. 2014), a process closely linked to cancer progression. Interestingly, the characters are similar between P2X4R and P2X7R as they share similar functions (Adinolfi et al., 2015). Both subunit isoforms are widely co-expressed, particularly in secretory epithelial cells and cells of the immune and inflammatory system (Schneider et al., 2017). Further study could double knock out P2X4R and P2X7R together. The P2X receptor family can form heterotrimeric P2X4R/P2X7R. In the context of PCa, the knockdown of P2X4R or P2X7R may potentially have a role in regulating cancer cell growth, migration, or metastasis, given that both receptor subtypes have been implicated in processes such as cell proliferation and invasion. Further research is needed to fully elucidate the role of P2X4R and P2X7R in PCa and to determine the potential therapeutic implications of targeting these receptors in cancer treatment (Boumechache et al., 2009, Adinolfi et al., 2015).

Further research can also be combined the P2X4R deficiency with PCa therapies such as bisphosphonates, denosumab or docetaxel to see the effect on preventing PCa bone metastasis (Pienta, 2001). Docetaxel is a chemotherapy drug that is used to treat advanced PCa that has spread beyond the prostate gland and is resistant to hormone therapy. It works by inhibiting the growth and division of cancer cells, ultimately leading

to their death (Pienta, 2001, Hwang, 2012). Bisphosphonates and denosumab have been evaluated in clinical trials for the treatment of bone metastases in cancer patients (Farrell et al., 2018). However, docetaxel has limited studied for this indication due to its toxicity profile (Di Gregorio et al., 2023). Focusing on the combination of drug therapies could provide better treatments for PCa bone metastasis.

Clinically, there is still a significant journey ahead in targeting P2X4R for the treatment of localized or metastatic PCa. P2X4R is abundantly expressed in different cell types and regions in the central nervous system (CNS) (Montilla et al., 2020). Among ionotropic receptors, P2X4R has emerged in the last decade as a potential target for CNS disorders such as epilepsy, ischemia, chronic pain, anxiety, multiple sclerosis and neurodegenerative diseases and complicated P2X4R function (Gofman et al., 2014, Burnstock, 2016). Despite the general overexpression of P2X4Rs in various neurological conditions, both acute and chronic (Domercq et al., 2013, Beggs et al., 2012), their role in inflammatory cascades and secondary brain damage could vary in each condition. In fact, the P2X4R has a dual role in the inflammatory cascade of brain pathologies, and thus, potential future therapies may range from receptor potentiation to its blockage (Montilla et al., 2020). Additionally, studies have shown that P2X4R-deficient mice are at a higher risk of developing hypertension disease (Chen et al., 2013) and exhibit cell senescence in the hippocampus, potentially contributing to neural stem cell disorder (Srivastava et al., 2020). Moreover, P2X4R deficiency in mice negatively impacts various aspects of sensory and social functions. Specifically, P2X4R knockout mice showed marked deficits in acoustic startle reflex amplitude, sensorimotor gating impairments, enhanced tactile sensitivity, and reduced social interaction and maternal separation-induced ultrasonic vocalizations in pups (Wyatt et al., 2013). Targeting P2X4R may have side effect at the early developmental stage (Xiang and Burnstock, 2005) but unlikely affect adult. Conversely, inhibiting P2X4R has been shown to prevent depression in animals (Pan et al., 2010). Notably, a phase 1 clinical trial has been conducted for a P2X4R antagonist specifically designed for the treatment of neuropathic pain (Matsumura et al., 2016).

It is notable that PCa is a disease associated with ageing; therefore, it is imperative to minimize the potential for adverse effects (Minelli et al., 2009). No side effects have been identified from existing references for targeting P2X4R in breast cancer (Chadet et al., 2022) or PCa (Zhou, 2019) *in vivo*. In general, before the development of clinical trials, there needs to be more research into targeting P2X4R in PCa without affecting the CNS and the development of more specific and safe drugs.

Currently, the treatment of PCa depends on various factors, including the stage and grade of the cancer, the overall health of the patient, and their personal preferences. Tissue biopsy continues to be the established diagnostic standard for suspected cases of PCa. Active surveillance is commonly recommended for low-risk and early-stage prostate cancer, particularly in cases classified as TX or T0 stage according to the TNM classification. Existing studies have shown higher expression of P2X4R in localized PCa tissue compared to benign tissue (Maynard et al., 2022). However, there is currently no evidence indicating its expression in suspicious or early-stage PCa tissue. Further studies could focus on identifying and validating tumour markers of P2X4R in the early stages of PCa. Androgen deprivation therapy is a commonly used treatment in advanced prostate cancer, aimed at reducing serum testosterone levels. However, the direct relationship between the P2X4R and androgen signalling remains poorly understood. One study observed that ATP treatment inhibited the growth of androgen-independent prostate cancer cells, but the specific receptor involved was not identified (Fang et al., 1992). Another study found that synthetic testosterone derivatives could modulate the channel gating of the rat P2X4R, suggesting potential interplay between these two pathways (Sivcev et al., 2019). Future studies could focus on investigating the relationship between P2X4R signaling and androgen signaling in order to gain further insights into their interactions. No evidence has established a relationship between P2X4R and other typical PCa treatments, such as surgery, radiation, or immunotherapy (Litwin and Tan, 2017).

P2X4R inhibition can be considered as a potential strategy to combine with the most relevant bone-directed therapies in advanced PCa. Three therapies are available for treating bone diseases resulting from cancer, which is also considered therapies for

advanced PCa. The most commonly used drugs for bone-specific drug targeting include bisphosphonates, denosumab, and radiation therapy. Novel therapies include bisphosphonate conjugates with antineoplastic agents and nanoparticles (Farrell et al., 2018). Combining these clinical methods such as bisphosphonates for bone disease with P2X4R expression inhibition can potentially enhance the effectiveness of inhibiting bone metastasis in prostate cancer.

Bisphosphonates have emerged as effective adjuvant therapies for cancer-associated bone disease, relieving pain and skeletal complications (Farrell et al., 2018). Since bone metastasis is a common occurrence in cancer, it is noteworthy that patients with PCa have bone metastases in over 70% of cases (Cancer Research, UK), while it is approximately 70% of cases in breast cancer (Kuchuk et al., 2013). In addition to reducing pain, bisphosphonate treatment can delay bone metastasis and even reduce tumour growth in some metastatic cancers. Bisphosphonates also prevent bone metastasis in prostate cancer, with studies showing a reduced incidence of skeletal metastasis, increased time to SREs, and improved disease progression (Corey et al., 2003, Russell et al., 2011). Similarly, Bisphosphonates have been shown to improve bone density, prevent osteolytic lesions in breast cancer patients, and are considered standard of care (Van Acker et al., 2016). Bisphosphonates possess a high affinity for bone and specific binding, which has led to the development of bisphosphonate conjugates for targeted drug delivery to the bone. These conjugates have been used for cancer, osteomyelitis, osteoporosis, radiation therapies, and imaging. Various molecules, including antineoplastic drugs, small molecules, proteins, antibiotics, and imaging agents, have been conjugated to bisphosphonates for bone targeting (Gittens et al., 2005, Herczegh et al., 2002, Reinholz et al., 2010). Considering the positive effects on delay PCa bone metastasis, it is worthy to be considered combined the P2X4R inhibitor with bisphosphonates. Despite the demonstrations of bone targeting and efficacy, conjugate applications are mostly limited to preclinical stages and have not yet progressed to human trials or clinical use (Farrell et al., 2018).

Furthermore, the latest developments in bone metastasis therapy have demonstrated that bisphosphonates can also be utilized in nanoparticles, where they can act as

targeting moieties for drug delivery to bone (Farrell et al., 2018). A study proposed a new design for a bone morphogenetic protein delivery system using polyelectrolyte Alen-MHA MBs, which can control the loading and release of the bone morphogenetic protein through ionic interaction. The authors suggest that the conjugation of bisphosphonate could be extended to further tune the loading and release of the bone protein (Jenjob et al., 2021). One major challenge of this therapy is to optimise the delivery of bone morphogenetic protein. It requires a system that can precisely apply the titrated dose to bone defects and release BMP2 only at the site of implantation without causing detrimental leakage to surrounding tissues (Huang et al., 2017). These novel approaches with the potential for synergistic effects when combined with P2X4R inhibition, to enhance the management of bone metastasis in advanced PCa. Additionally, the direct injection of P2X4R inhibitors into the bone through nanoparticle-based methods provides possibilities for directly targeted PCa bone metastasis.

Based on the references (He et al., 2020, Maynard et al., 2022) and my study on PCa progression, it is suggested that inhibiting P2X4R in the early metastasis stage of PCa or localized PCa may yield better effects compared to other stages of the disease. Solely targeting the inhibition of P2X4R in tumour growth may have limited efficacy. To enhance the management of the disease, combining P2X4R inhibition with other PCa treatments it is considered such as taxane or antiandrogen therapies. Antiandrogen therapies and taxane chemotherapy are standard of care treatments for PC (Rice et al., 2019). Compared to the current standard of care for PCa, targeting P2X4R specifically for bone metastasis has the potential to offer advantages with fewer side effects. However, the efficacy and safety of this approach still require extensive testing and validation. While P2X4R presents a potential target that is specific to PCa bone metastasis, its integration into clinical trial will require further development.

7.2 Conclusion

In conclusion, targeting P2X4R is a novel potential therapeutic strategy for PCa bone metastasis. By inhibiting P2X4R activity, it may be possible to reduce the growth and spread of cancer cells in the bone, ultimately improving patient outcomes. Combining it with current bone disease treatments may also provide new ideas for treatment, potentially enhancing the management of advanced PCa. While there is still much to learn about the safety and efficacy of targeting P2X4R, these findings represent an essential step forward in the development of novel therapeutic strategies for treating bone metastasis in cancer patients.

APPENDIX

A1: RNA-seq supplement data

A1.1The Bio-analyzer result

The RNA samples were qualified using electrophoretic separation on the Agilent BioAnalyzer 2100. The quality figures from these analyses are presented below. Results of Bio-analyzer were provided by Source BioScience company.

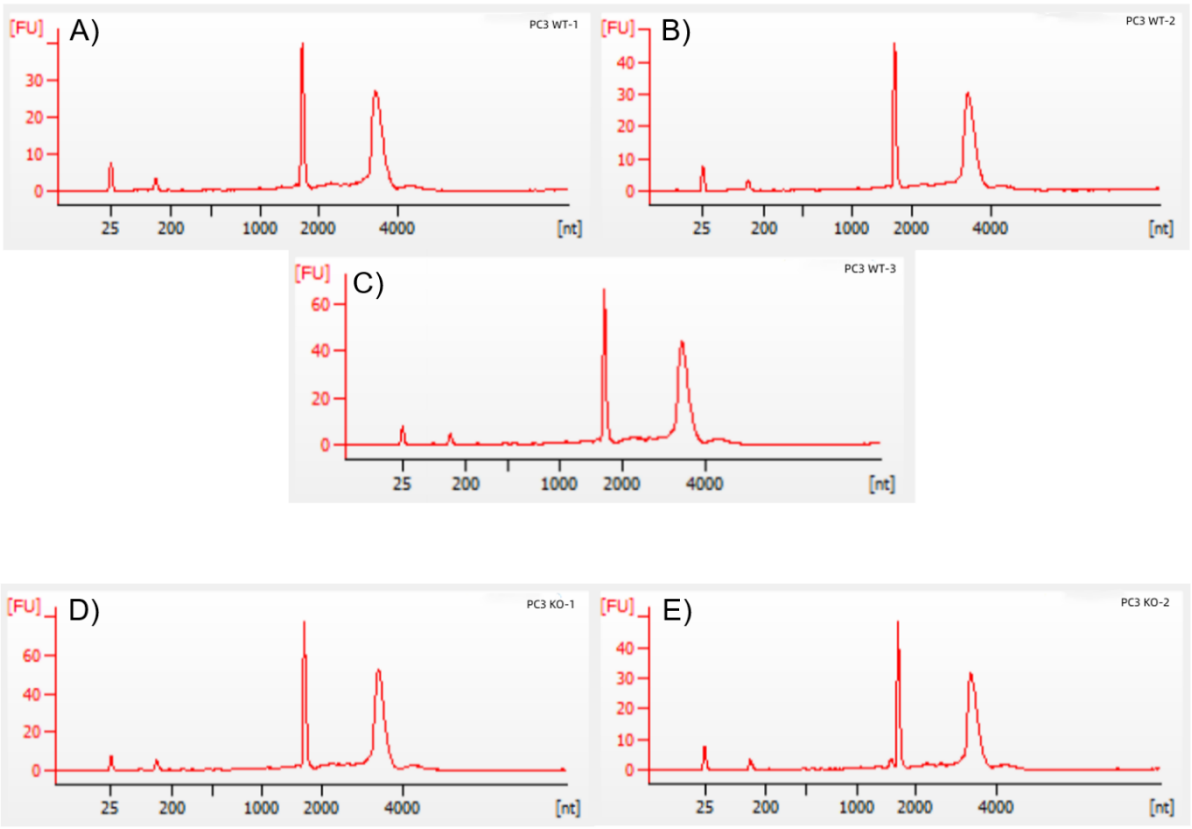

Figure A1.1: RIN figures for PC3 WT and KO samples

A1.2: FastQC results

FastQC results is the sequence scores for each RNA-seq samples.

A)

Sample Name	% Dups	% GC	M Seqs
PC3_KO-1_R1	54.7%	50%	42.6
PC3_KO-1_R2	16.1%	51%	42.6
PC3_KO-2_R1	57.7%	50%	40.9
PC3_KO-2_R2	16.4%	51%	40.9
PC3_WT-1_R1	57.9%	50%	43.1
PC3_WT-1_R2	16.1%	51%	43.1
PC3_WT-2_R1	61.4%	50%	56.8
PC3_WT-2_R2	18.0%	51%	56.8
PC3_WT-3_R1	60.8%	50%	54.3
PC3_WT-3_R2	18.7%	51%	54.3

B)

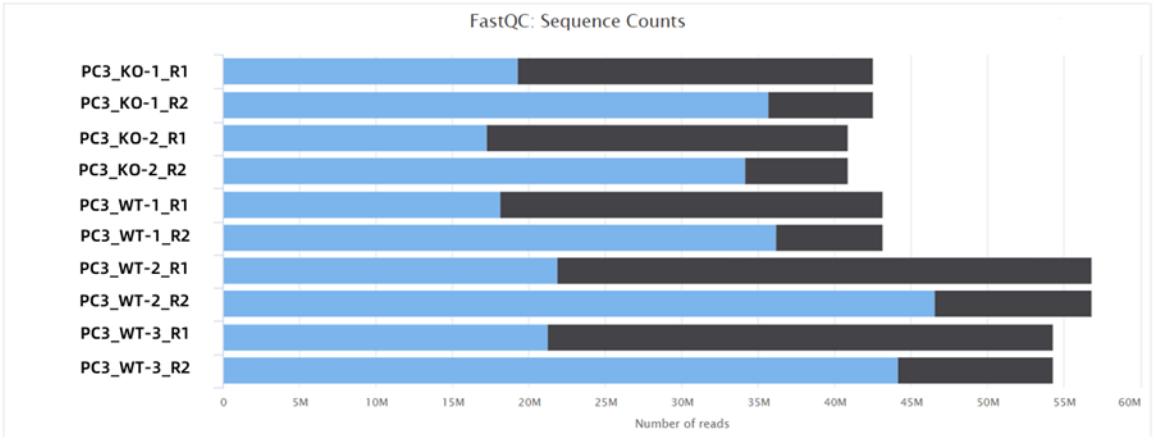

C)

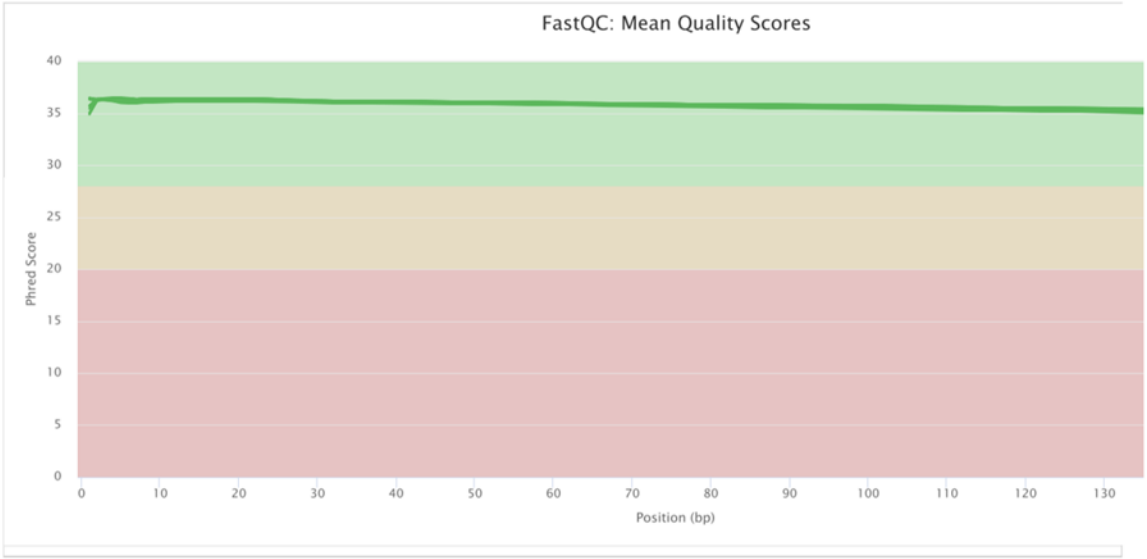

Figure A1.2: FastQC results. A) Overview of RNA-seq samples; B) Sequence counts for RNA-samples; C) Quality scores of RNA-seq samples

A1.3: KEGG pathway related genes table

Table A1: Supplement table for Table 6.8

Term	Count	Gene
ECM-receptor interaction	11	COL6A2, COL6A3, ITGA2, ITGA5,ITGB4,LAMA3,LAMA4,LAMB3,LAMC2,RELN, TNN
Focal adhesion	16	RAC3,COL6A2,COL6A3,FLNC,ITGA2,ITGA5,ITGB4, LAMA3,LAMA4,LAMB3,LAMC2,MYL9,MYLK,PAK3,R ELN,TNN
Human papillomavirus infection	16	WNT7A,COL6A2,COL6A3,CCNE1,ITGA2,ITGA5,ITG B4,LAMA3,LAMA4,LAMB3,LAMC2,PARD6G,PTGS2, RELN,TERT,TNN
Small cell lung cancer	7	CCNE1,ITGA2,LAMA3,LAMA4,LAMB3,LAMC2,PTGS 2
PI3K-Akt signalling pathway	15	GNGT2,COL6A2,COL6A3,CCNE1,FGF1,ITGA2,ITG A5,ITGB4,LAMA3,LAMA4,LAMB3,LAMC2,PRLR,REL N,TNN
NF-kappa B signaling pathway	6	CXCL8,CYLD,TNFAIP3,IL1B,PLAU,PTGS2
Cytokine-cytokine receptor interaction	11	CCR2,CCR9,CXCL8,CX3CR1,TNFSF4,IL1B,IL13RA 2,IL22,IL24,IL37,PRLR

APPENDIX

A2 : The optimal concentration of FCS in three PCa cell lines

A2.1 Introduction

"Fetal calf serum (FCS) is a common growth medium for *in vitro* cell culture. It is a natural compound that contains most of the factors required for human cell attachment, growth, and proliferation (Jochems et al., 2002). Most cells cannot survive without FCS due to nutrient deprivation. FCS promotes stable and rapid cell growth *in vitro*, which is important for further *in vitro* and *in vivo* assays in this study (Guehring et al., 2009).

Three types of PCa cells derived from different metastasis tissues were selected, including PC3, LN-CaP, and C4-2B4. PC3 cells are a human PCa cell line derived from bone metastasis with high metastatic potential. It is one of the most commonly used PCa cell lines in xenograft models, and studies have shown that it is an appropriate model for investigating PCa bone metastasis (Wu et al., 2013, Meng et al., 2018, Dey et al., 2012). C4-2B4 is a lineage-derived human PCa cell line that acquires androgen independence and bone metastatic potential *in vivo* (Wu et al., 1998). LNCaP was derived from lymph node metastasis with lower metastasis potential and is included as compensation for using only high metastasis cell lines PC3 and C4-2B4 (Horoszewicz et al., 1983).

According to multiple studies, bone marrow is an important site for dormant tumour cells, as indicated by the frequency of bone metastases and the presence of disseminated tumour cells in patients with localized disease (Cackowski and Heath, 2022, Bubendorf et al., 2000b, Van der Toom et al., 2016). PCa cells have been shown to reside in bone for an extended period, which may explain why second-time invasions of PCa are often more aggressive. 'Cellular dormancy' refers to tumour cells that are likely in the G0 phase of the cell cycle (Van der Toom et al., 2016). In this study, cells were subjected to a low-nutrient environment to simulate a shortage of cell growth substances related to the bone microenvironment. Subsequently, the cells were transferred to normal media to determine whether the PCa cells could recover from dormancy. Using cell lines with dormancy characteristics could improve predictions for future clinical investigations.

To maintain the optimal growth of PCa cell lines, the concentration of FCS in the growth medium was carefully determined. Various concentrations of FCS (2%, 5%, 10%, 15%, and 20%) were tested to determine the optimal concentration for each cell line. To test whether the cells could recover from the low-nutrient condition and resume normal growth rates, the cells were cultured in optimal FCS concentrations after a period of serum starvation.

A2.2 Optimal concentration of FCS

To optimize the serum concentration for culturing PCa cell lines, human PC3, LNCaP, and C4-2B4 cells were seeded at $1x10^4$ cells per well of 12-well plates and treated with five different concentrations of FCS (2%, 5%, 10%, 15%, and 20%). They were then counted every 24 hours for 4 days using a hemocytometer under a microscope. Three biological repeats were performed for each cell line, and each biological repeat had three technical repeats. Doubling time was calculated to measure growth rate under different FCS conditions, and the elapsed time in 48 hours (from 48 hours to 96 hours in this study) was divided by the number of cells that proliferated (Table A2.1). A growth curve was also created for each cell line, showing cell density and culturing time (Figure A2.1-A2.3).

Cell counting assay suggested that the optimal FCS concentration is 10% for PC3, 5% for LNCaP, and 10% for C4-2B4 (doubling time is 26.1h, 17.4h, and 26.3h, respectively). A shorter doubling time indicates faster PCa cells proliferation. The results showed that all three cell lines can proliferate in 5%, 10%, and 15% FCS, and the doubling time ranges from 30-45 hours. However, none of the PCa cell lines could proliferate in 2% FCS. For the C4-2B4 cell line, culturing the cells with 20% FCS inhibited their proliferation, while the other two cell lines showed growth. This suggests that the C4-2B4 might not be able to successfully survive in a high serum environment.

Table A2.1: Doubling time for PC3, LN-CaP and C4-2B4 in different FCS concentration

Cell line	Optimal concentration	Doubling time
PC3	5%	41.8h
	10%	26.1h
	15%	35.3h
LN-Cap	5%	17.4h
	10%	36.4h
	15%	32.8h
C4-2B4	5%	32.2h
	10%	26.3h
	15%	37.6h

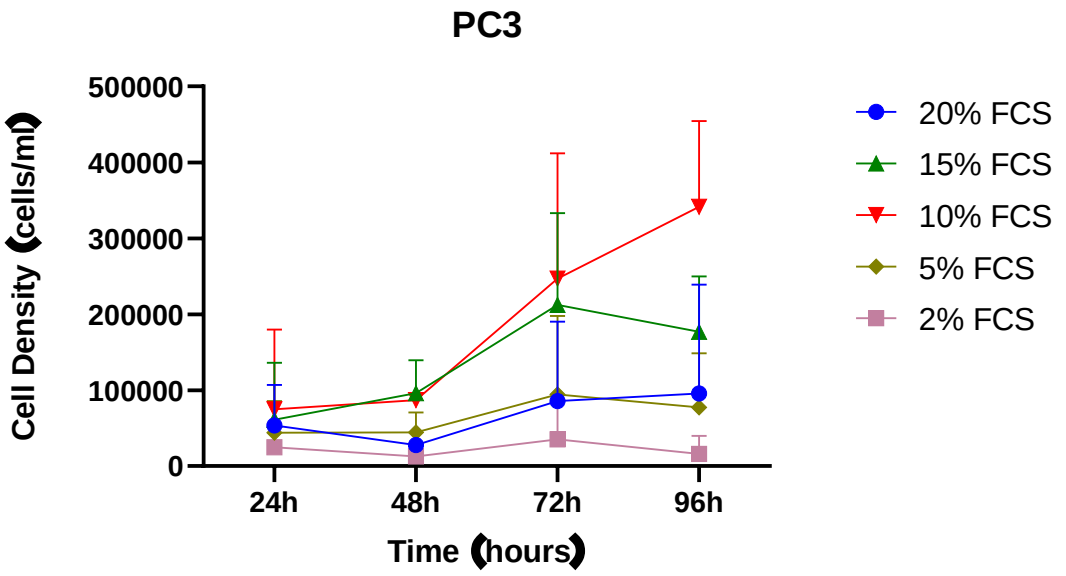

Figure A2.1: Growth curve of PC3 cell, cells grew fastest in 10% FCS. The optimal concentration of FCS for culturing PC3 cells is 10%, followed by 15%, 5% and 20%. The quantity of cells in 2% of FCS remains the same during 96 hours. Data are the mean ± SD. N=3.

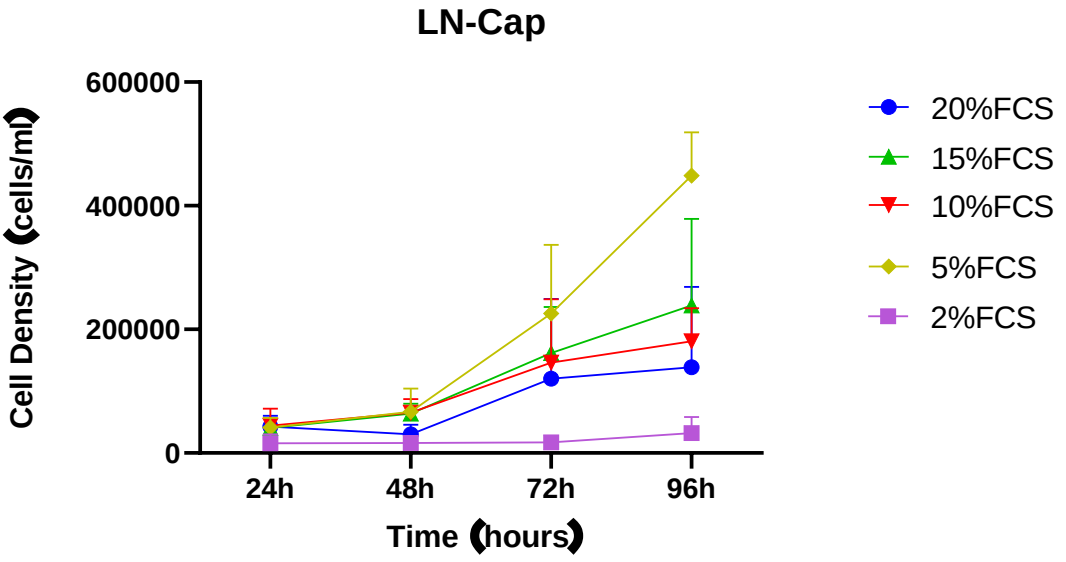

Figure A2.2: Growth curve of LNCaP cells, cells grew fastest in 5% FCS. The optimal concentration of FCS for culturing LNCaP cells is 5%, followed by 15%, 10% and 20%. The quantities of cells in 2% remain the same during 96 hours. Data are the mean ± SD. N=3.

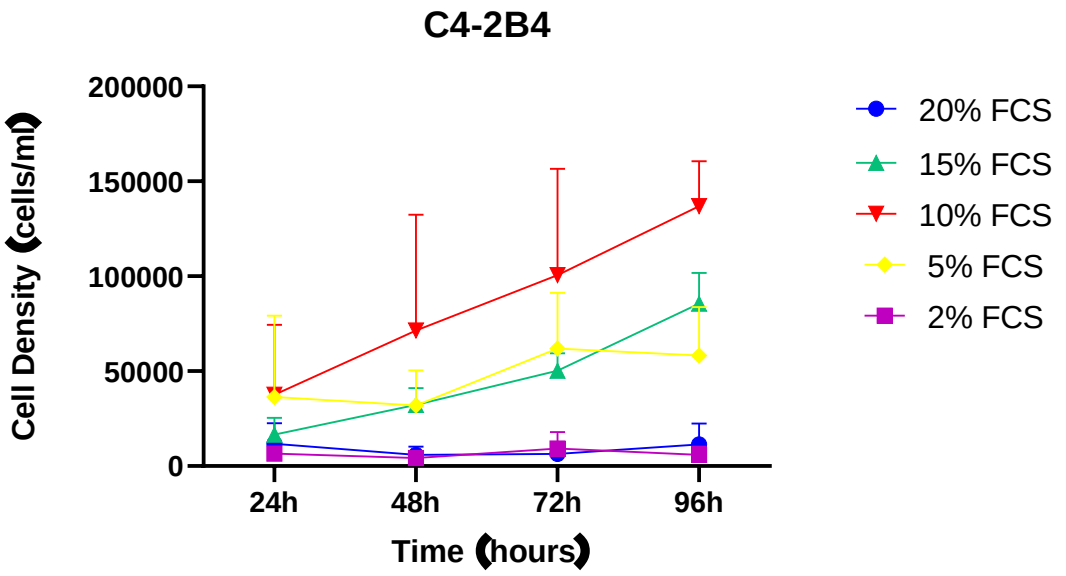

Figure A2.3: Growth curve of C4-2B4 cells, cells grew fastest in 10% FCS. The optimal concentration of FCS for culturing C4-2B4 cells is 10%, followed by 15%, 5%. The quantities of cells in 2% and 20% remain the same for 96 hours. Data are the mean ± SD. N=3.

A2.3 FCS concentration change

Based on the theory that PCa cells have the characteristics to become dormant under severe conditions, I tested whether the cells revive and grow at normal rates when the FCS concentration was changed from 2% to their optimal FCS concentration (10% for PC3 and C4-2B4; 5% for LNCaP). Cells were cultured in 2% FCS for 72 hours, and then the FCS concentration was changed to the optimal level. The cell number was counted using a hemocytometer at 72 and 168 hours.

From Figure A2.4 to Figure A2.6 below, when the FCS concentration was changed, all cell lines kept growing after changing the FCS concentration from 2% to their optimal FCS concentration. Comparing the doubling time with previous data, the doubling time was shorter in PC3, which was 17.5 hours (2% to 10% FCS) and 26.1 hours (10% FCS) respectively. It might be more aggressive in PC3 cells to recover from a dormancy situation; however, there was no significant difference between nutrition deficiency treatment and non-treatment. The growth rate of LNCaP cells was

similar to previous data, which was 18.7 hours (2% to 5% FCS) and 17.4 hours (10% FCS) in normal tissue culture. However, C4-2B4 cells took more time to proliferate after starvation treatment, 32.6 hours (2% to 10% FCS) and 26.3 hours (10% FCS) respectively (Table A2.2).

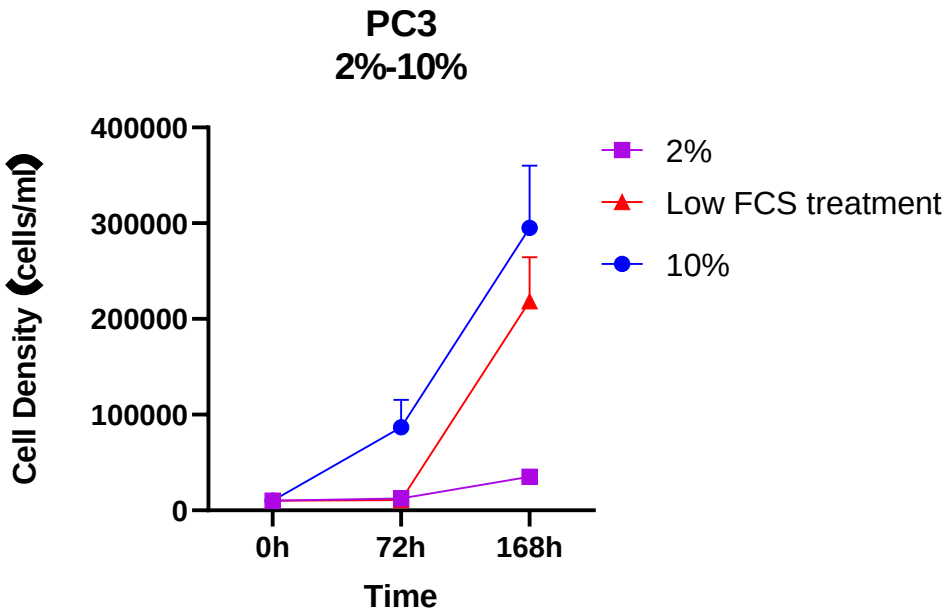

Figure A2.4: Growth curve of PC3 cells, cells remain their proliferation ability after low FCS treatment. PC3 cells in 10% of FCS medium grew well, while its in 2% almost remain the same quantities. The treatment group which changing the FCS concentration from 2% to 10% at 72h, showed a dramatically growth after changing the medium. Data are the mean ± SD. N=3.

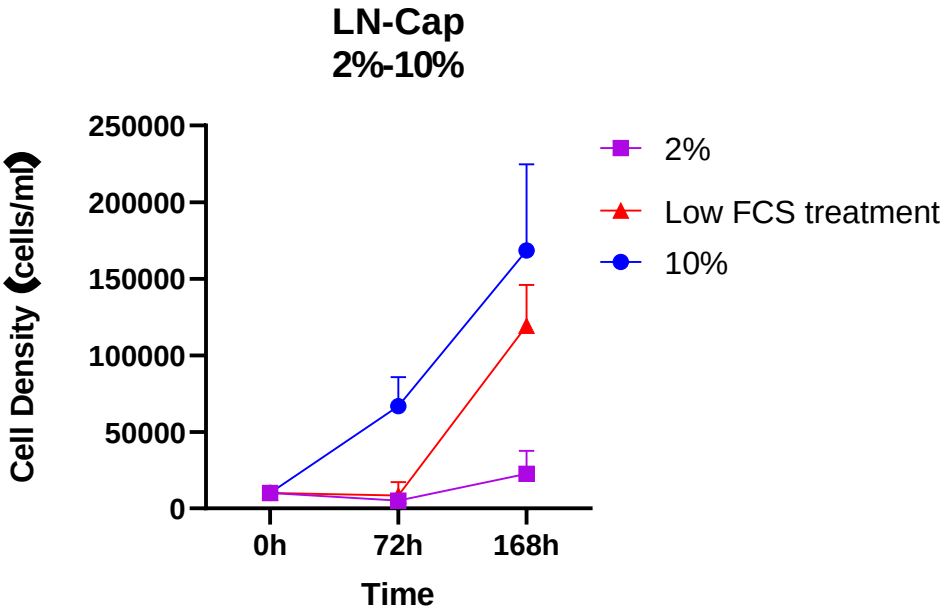

Figure A2.5: Growth curve of LNCaP cells, cells remain their proliferation ability after low FCS treatment. LNCaP cells in 5% of FCS medium grew well, while the cell numbers in the 2% treatment reduced at 72h and increased slightly at 168h, finally ended up to the similar number at first seeding numbers. The treatment group which the FCS concentration was changed from 2% to 5% at 72h, showed a dramatically growth after changing FCS concentration. Data are the mean ± SD. N=3.

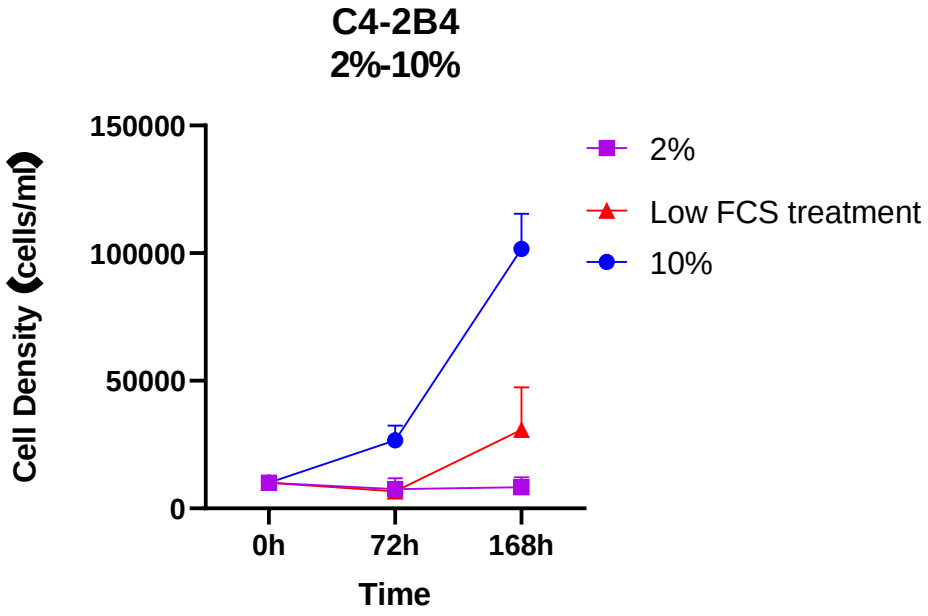

Figure A2.6: Growth curve of C4-2B4 cells, cells remain their proliferation ability after low FCS treatment. C4-2B4 cells in 10% of FCS medium grew well, while its in 2% almost remain the same quantities. The treatment group which the FCS concentration was changed from 2% to 10% at 72h, showed a slower growth rate compared to the 10% FCS group. Data are the mean ± SD. N=3.

Table A2.2: Doubling time for PC3, LNCaP and C4-2B4 by changing FCS concentration from 2% to 10%

Cell line	Doubling time （optimal FCS concentration）	Doubling time 2% to 10% (72h-168h)
PC3	26.1h	17.5h
LNCaP	17.40h	18.7h
C4-2B4	26.3h	32.6h

A2.4 Discussion

To determine the optimal concentration of FCS for the three PCa cell lines (PC3, LNCaP, and C4-2B4), I cultured the cells in different FCS concentrations (2%, 5%, 10%, 15%, and 20%) for four days and counted the cell numbers every 24 hours. I found that all cell lines could proliferate in 5%, 10%, and 15% FCS, but did not bear in 2% FCS. This suggests that 2% FCS is insufficient to support normal cell growth. My results showed that 10% FCS was optimal for both PC3 and C4-2B4 cells, while LNCaP cells grew best in 5% FCS. The different FCS requirements of the cell lines may be due to their origins; LNCaP cells are derived from lymph node metastasis, while PC3 and C4-2B4 cells are bone metastasis-derived and may have adapted to the highly nutritious bone microenvironment (Thalmann et al., 1994). Moreover, PC3 and C4-2B4 cells are androgen-insensitive, while LNCaP cells are androgen-sensitive, which may also influence their FCS requirements (Horoszewicz et al., 1983, Thalmann et al., 1994).

Previous publications have suggested that PC3 cells should be cultured in 10% FCS, while 5% and 10% FCS are suitable for LNCaP and C4-2B4 cells (Ruffion et al., 2003; Ulrix et al., 1999; Cooper et al., 2008; Babcook et al., 2014) which are consistence with my study. However, I found that 20% FCS was not optimal, as it may affect the microenvironment's osmotic pressure and ionic concentration, potentially altering hormone release and cell proliferation (Vicentini et al., 2003). The results showed no increase in cell quantities in high serum conditions.

When I changed the FCS concentration from 2% to the optimal level for each cell line, I found that all three PCa cell lines resumed proliferation at their normal growth rate after a short period of serum starvation. The PC3 cells were slightly more aggressive after low-nutrition treatment, consistent with clinical data that second-time invasive PCa is more aggressive (Van der Toom et al., 2016). The results are consistent with previous studies showing that dormant cancer cells induced by serum starvation could recover and proliferate when serum levels were replenished in the culture media

(Barney et al., 2020). However, it is unclear whether three days of serum starvation in my study was enough to induce true dormancy status, and further investigation, such as examining cell cycling status after three days of serum starvation, is necessary (Fukushima et al., 2019).

A2.5 Conclusion

The basic tissue culture optimized cell culture conditions to make sure the cells can grow normally in the process of this project. Changing the concentration of low FCS and put the cells back in optimized FCS concentration, they can grow normally. This finding speculated the cells have the characteristic of PCa cancer cells that it can be stay in dormancy status and survival from low nutritional condition. The cells keep the characteristics that have the potential to become dormancy cells which might simulate the clinical and pathologic features of PCa in patients.

A2.6 LNCaP cell line used in this chapter

The characteristics of LNCaP cell line are summarized as Table A2.3.

Table A2.3: LNCaP cell line

Cell lines	Description	Androgen-sensitive	Bone metastasis type	Source	References
LNCaP	LNCaP cells are androgen-sensitive human prostate adenocarcinoma cells. They were derived from a 50-year-old Caucasian male's left supraclavicular lymph node metastasis in 1977. It is a compensation of only using PC3 and C4-2B4 for lower metastasis bone effects.	Androgen-sensitive	/	ATCC Corporation (Manassas, Virginia, USA)	(Horoszewicz et al., 1983)

APPENDIX

A3: REAGENTS & MATERIALS

Table A3.1 Reagents and material applied in cell culture

Reagent	Source
Dulbecco's modified Eagle's medium (DMEM)	Thermo Fisher/Gibco ® (Waltham, Massachusetts, USA)
Tissue culture flasks (T25 and T75)	Thermo Fisher (Waltham, Massachusetts, USA)
Penicillin-Streptomycin (Pen-Strep)	Thermo Fisher (Waltham, Massachusetts, USA)
Foetal Calf Serum (FCS)	Sigma-Aldrich (St. Louis, Missouri, USA)
Eppendorf Tubes (0.5 mL and 1.5mL)	Eppendorf (Hamburg, Germany)
Phosphate buffered saline (PBS)	Thermo Fisher/Gibco ® (Waltham, Massachusetts, USA)
Disposable pipettes (5 mL and 10mL)	Thermo Fisher (Waltham, Massachusetts, USA)
Disposable Tips (10 µL, 20 µL, 200 µL and 1000µL)	STARLAB
Olympus inverted CK2 microscope	Olympus Corporation in Japan
Haemocytometer	Sigma-Aldrich (St. Louis, Missouri, USA)
Clear Dulbecco's modified Eagle's medium (Clear DMEM)	Thermo Fisher/Gibco ® (Waltham, Massachusetts, USA)
EDTA	Thermo Fisher (Waltham, Massachusetts, USA)
Well plates (12 wells, 24wells and 96 wells)	Sigma-Aldrich (St. Louis, Missouri, USA)
DMSO	Thermo Fisher (Waltham, Massachusetts, USA)
100 µm Cell strainers	Thermo Fisher (Waltham, Massachusetts, USA)

Table A3.2 Agonist/antagonist reagents source

Reagent	**Source**
ATP	Sigma-Aldrich (St. Louis, Missouri, USA)
PSB-12062	Sigma-Aldrich (St. Louis, Missouri, USA)
5-BDBD	Sigma-Aldrich (St. Louis, Missouri, USA)

Table A3.3 Reagents and material used in molecular biology

Reagent	**Source**
ReliaPrep™ RNA Cell Miniprep System	Promega
GoScript™ Reverse Transcriptase kit	Promega
DNA extraction kit	Promega
Taq-man qPCR kit	Thermo Fisher
PCR Mix	Thermo Fisher
QIAquick PCR Purification Kit	Promega

Table A3.4 Reagents and material used in *in vitro*

Reagent	**Source**
Ionomycin	Sigma-Aldrich
Fluo-4 Direct™ Calcium Assay Kit	Thermo Fisher (Waltham, Massachusetts, USA)
Matrigel	In-house
Eosin	In-house
Haematoxylin	In-house
Eosin	In-house
CyQUANT™ Cell Proliferation Assay Kit	Promega
AlamarBlue Cell Viability Reagent	Thermo Fisher
Caspase 3/7 Assay Kit	Promega
Matrigel	In-house
Doxorubicin	In-house

Table A3.5 Reagents and material used in *in vivo*

Reagent	Source
Ki67 cell proliferation kit	Promega
Cytokine array reagents	R & D systems

References

ABBRACCHIO, M. P., BURNSTOCK, G., BOEYNAEMS, J.-M., BARNARD, E. A., BOYER, J. L., KENNEDY, C., KNIGHT, G. E., FUMAGALLI, M., GACHET, C. & JACOBSON, K. A. 2006. International Union of Pharmacology LVIII: update on the P2Y G protein-coupled nucleotide receptors: from molecular mechanisms and pathophysiology to therapy. *Pharmacological reviews,* 58**,** 281-341.

ABRAHAO, A. C., CASTILHO, R. M., SQUARIZE, C. H., MOLINOLO, A. A., DOS SANTOS-PINTO JR, D. & GUTKIND, J. S. 2010. A role for COX2-derived PGE2 and PGE2-receptor subtypes in head and neck squamous carcinoma cell proliferation. *Oral oncology,* 46**,** 880-887.

ACOSTA, A. M., AL RASHEED, M. R., RAUSCHER, G. H., VORMITTAG, E., MON, K. S., SHARIF, A., KAJDACSY-BALLA, A. & MOHAPATRA, G. 2018. Tumor necrosis in radical prostatectomies with high-grade prostate cancer is associated with multiple poor prognostic features and a high prevalence of residual disease. *Human Pathology,* 75**,** 1-9.

ADINOLFI, E., CAPECE, M., AMOROSO, F., DE MARCHI, E. & FRANCESCHINI, A. 2015. Emerging roles of P2X receptors in cancer. *Current Medicinal Chemistry,* 22**,** 878-890.

ASE, A. R., HONSON, N. S., ZAGHDANE, H., PFEIFER, T. A. & SéGUéLA, P. 2015. Identification and characterization of a selective allosteric antagonist of human P2X4 receptor channels. *Molecular pharmacology,* 87**,** 606-616.

ASIF, A., KHALID, M., MANZOOR, S., AHMAD, H. & REHMAN, A. U. 2019. Role of purinergic receptors in hepatobiliary carcinoma in Pakistani population: An approach towards proinflammatory role of P2X4 and P2X7 receptors. *Purinergic signalling,* 15**,** 367-374.

BAKIR, B., CHIARELLA, A. M., PITARRESI, J. R. & RUSTGI, A. K. 2020. EMT, MET, plasticity, and tumor metastasis. *Trends in cell biology,* 30**,** 764-776.

BALáZS, B., DANKó, T., KOVáCS, G., KöLES, L., HEDIGER, M. A. & ZSEMBERY, Á. 2013. Investigation of the inhibitory effects of the benzodiazepine derivative, 5-BDBD on P2X4 purinergic receptors by two complementary methods. *Cellular physiology and biochemistry,* 32**,** 11-24.

BALDOCK, P. A., THOMAS, G. P., HODGE, J. M., BAKER, S. U., DRESSEL, U., O'LOUGHLIN, P. D., NICHOLSON, G. C., BRIFFA, K. H., EISMAN, J. A. & GARDINER, E. M. 2006. Vitamin D action and regulation of bone remodeling: suppression of osteoclastogenesis by the mature osteoblast. *Journal of Bone and Mineral Research,* 21**,** 1618-1626.

BANDINI, M., GANDAGLIA, G. & BRIGANTI, A. 2017. Obesity and prostate cancer. *Current Opinion in Urology,* 27**,** 415-421.

BAO, Y., WANG, L., SHI, L., YUN, F., LIU, X., CHEN, Y., CHEN, C., REN, Y. & JIA, Y. 2019. Transcriptome profiling revealed multiple genes and ECM-receptor interaction pathways that may be associated with breast cancer. *Cellular & molecular biology letters,* 24**,** 1-20.

BARNEY, L. E., HALL, C. L., SCHWARTZ, A. D., PARKS, A. N., SPARAGES, C., GALARZA, S., PLATT, M. O., MERCURIO, A. M. & PEYTON, S. R. 2020. Tumor cell–organized fibronectin maintenance of a dormant breast cancer population. *Science Advances,* 6**,** eaaz4157.

BASBAUM, A. I., BAUTISTA, D. M., SCHERRER, G. & JULIUS, D. 2009. Cellular and molecular mechanisms of pain. *Cell,* 139**,** 267-284.

BEGGS, S., TRANG, T. & SALTER, M. W. 2012. P2X4R+ microglia drive neuropathic pain. *Nature neuroscience,* 15**,** 1068-1073.

BELLO-DEOCAMPO, D. & TINDALL, D. J. 2003. TGF-ß/Smad signaling in prostate cancer. *Current drug targets,* 4**,** 197-207.

BERISH, R. B., ALI, A. N., TELMER, P. G., RONALD, J. A. & LEONG, H. S. 2018. Translational models of prostate cancer bone metastasis. *Nature Reviews Urology,* 15**,** 403-421.

BERISTAIN, A. G., ZHU, H. & LEUNG, P. C. 2011. Regulated expression of ADAMTS-12 in human trophoblastic cells: a role for ADAMTS-12 in epithelial cell invasion? *PloS one,* 6,p. e18473.

BERRIER, A. L. & YAMADA, K. M. 2007. Cell–matrix adhesion. *Journal of cellular physiology,* 213**,** 565-573.

BHANOAT, G. & LEVINE, H. 2012. What is Metastasis? *Kavli Institute for Theoretical Physics Program: Physics and Mathematics of Cancer May 21-July 13***,** 48.

BIDULA, S., NADZIRIN, I. B., COMINETTI, M., HICKEY, H., CULLUM, S. A., SEARCEY, M., SCHMID, R. & FOUNTAIN, S. J. 2022. Structural basis of the negative allosteric modulation of 5-BDBD at human P2X4 receptors. *Molecular pharmacology,* 101**,** 33-44.

BONDRE, N., ZHANG, Y. & GEDDES, C. D. 2011. Metal-enhanced fluorescence based calcium detection: Greater than 100-fold increase in signal/noise using Fluo-3 or Fluo-4 and silver nanostructures. *Sensors and Actuators B: Chemical,* 152**,** 82-87.

BOOTH, H. A. F. & HOLLAND, P. W. 2007. Annotation, nomenclature and evolution of four novel homeobox genes expressed in the human germ line. *Gene,* 387**,** 7-14.

BOSMA, G. C., CUSTER, R. P. & BOSMA, M. J. 1983. A severe combined immunodeficiency mutation in the mouse. *Nature,* 301**,** 527-530.

BOUMECHACHE, M., MASIN, M., EDWARDSON, J. M., GORECKI, D. C. & MURRELL-LAGNADO, R. 2009. Analysis of assembly and trafficking of native P2X4 and P2X7 receptor complexes in rodent immune cells. *Journal of biological chemistry,* 284**,** 13446-13454.

BOYCE, B. F. & XING, L. 2008. Functions of RANKL/RANK/OPG in bone modeling and remodeling. *Archives of biochemistry and biophysics,* 473**,** 139-146.

BOYLE, W. J., SIMONET, W. S. & LACEY, D. L. 2003. Osteoclast differentiation and activation. *Nature,* 423**,** 337-342.

BROWN, M. H. & LACEY, E. 2010. A ligand for CD5 is CD5. *The Journal of Immunology,* 185**,** 6068-6074.

BUBENDORF, L., SCHOPFER, A., WAGNER, U., SAUTER, G., MOCH, H., WILLI, N., GASSER, T. C. & MIHATSCH, M. J. 2000a. Metastatic patterns of prostate cancer: an autopsy study of 1,589 patients. *Hum Pathol,* 31**,** 578-83.

BUBENDORF, L., SCHöPFER, A., WAGNER, U., SAUTER, G., MOCH, H., WILLI, N., GASSER, T. C. & MIHATSCH, M. J. 2000b. Metastatic patterns of prostate cancer: an autopsy study of 1,589 patients. *Human pathology,* 31**,** 578-583.

BUIJS, J., VAN DER HORST, G., VAN DEN HOOGEN, C., CHEUNG, H., DE ROOIJ, B., KROON, J., PETERSEN, M., VAN OVERVELD, P., PELGER, R. & VAN DER PLUIJM, G. 2012. The BMP2/7 heterodimer inhibits the human breast cancer stem cell subpopulation and bone metastases formation. *Oncogene,* 31**,** 2164-2174.

BURNSTOCK, G. 2016. P2X ion channel receptors and inflammation. *Purinergic signalling,* 12**,** 59-67.

BURNSTOCK, G. & DI VIRGILIO, F. 2013. Purinergic signalling and cancer. *Purinergic signalling,* 9**,** 491-540.

CACKOWSKI, F. C. & HEATH, E. I. 2022. Prostate cancer dormancy and recurrence. *Cancer Letters,* 524**,** 103-108.

CAO, W., XING, H., LI, Y., TIAN, W., SONG, Y., JIANG, Z. & YU, J. 2022. Claudin18. 2 is a novel molecular biomarker for tumor-targeted immunotherapy. *Biomarker Research,* 10**,** 1-21.

CAO, Z. & KYPRIANOU, N. 2015. Mechanisms navigating the TGF-β pathway in prostate cancer. *Asian journal of urology,* 2**,** 11-18.

CAPIETTO, A.-H. & FACCIO, R. 2014. Immune regulation of bone metastasis. *BoneKEy Reports,* 3.

CARPENTER, D., MEADOWS, H. J., BROUGH, S., CHAPMAN, G., CLARKE, C., COLDWELL, M., DAVIS, R., HARRISON, D., MEAKIN, J. & MCHALE, M. 1999. Site-specific splice variation of the human P2X4 receptor. *Neuroscience letters,* 273**,** 183-186.

CARTER, P. H. & SCHIPANI, E. 2006. The roles of parathyroid hormone and calcitonin in bone remodeling: prospects for novel therapeutics. *Endocrine, Metabolic & Immune Disorders-Drug Targets (Formerly Current Drug Targets-Immune, Endocrine & Metabolic Disorders),* 6**,** 59-76.

CHADET, S., ALLARD, J., BRISSON, L., LOPEZ-CHARCAS, O., LEMOINE, R., HERAUD, A., LERONDEL, S., GUIBON, R., FROMONT, G. & LE PAPE, A. 2022. P2x4 receptor promotes mammary cancer

progression by sustaining autophagy and associated mesenchymal transition. *Oncogene,* 41**,** 2920-2931.
CHEN, J. 2016. The cell-cycle arrest and apoptotic functions of p53 in tumor initiation and progression. *Cold Spring Harbor perspectives in medicine,* 6,p. a026104.
CHEN, K., ZHANG, J., ZHANG, W., ZHANG, J., YANG, J., LI, K. & HE, Y. 2013. ATP-P2X4 signaling mediates NLRP3 inflammasome activation: a novel pathway of diabetic nephropathy. *The international journal of biochemistry & cell biology,* 45**,** 932-943.
CHEN, S. 2013. Retooling the creatinine clearance equation to estimate kinetic GFR when the plasma creatinine is changing acutely. *Journal of the American Society of Nephrology,* 24**,** 877-888.
CHEN, S., ZHANG, J., SUN, L., LI, X., BAI, J., ZHANG, H. & LI, T. 2019. miR-611 promotes the proliferation, migration and invasion of tongue squamous cell carcinoma cells by targeting FOXN3. *Oral Diseases,* 25**,** 1906-1918.
CHEN, Y., LIN, X., ZHENG, J., CHEN, J., XUE, H. & ZHENG, X. 2021. APLN: A potential novel biomarker for cervical cancer. *Science Progress,* 104**,** p. 00368504211011341.
CHONG, J.-H., ZHENG, G.-G., ZHU, X.-F., GUO, Y., WANG, L., MA, C.-H., LIU, S.-Y., XU, L.-L., LIN, Y.-M. & WU, K.-F. 2010. Abnormal expression of P2X family receptors in Chinese pediatric acute leukemias. *Biochemical and biophysical research communications,* 391**,** 498-504.
CODDOU, C., SANDOVAL, R., HEVIA, M. J. & STOJILKOVIC, S. S. 2019. Characterization of the antagonist actions of 5-BDBD at the rat P2X4 receptor. *Neuroscience letters,* 690**,** 219-224.
COLEMAN, R. E., BROWN, J. & HOLEN, I. 2020. Bone metastases. *Abeloff's Clinical Oncology***,** 809-830. pp.809-830.
COLLINS, C., ROMMENS, J. M., KOWBEL, D., GODFREY, T., TANNER, M., HWANG, S.-I., POLIKOFF, D., NONET, G., COCHRAN, J. & MYAMBO, K. 1998. Positional cloning of ZNF 217 and NABC 1: genes amplified at 20q13. 2 and overexpressed in breast carcinoma. *Proceedings of the National Academy of Sciences,* 95**,** 8703-8708.
COOPER, C. R., GRAVES, B., PRUITT, F., CHAIB, H., LYNCH, J. E., COX, A. K., SEQUERIA, L., VAN GOLEN, K. L., EVANS, A. & CZYMMEK, K. 2008. Novel surface expression of reticulocalbin 1 on bone endothelial cells and human prostate cancer cells is regulated by TNF-α. *Journal of cellular biochemistry,* 104**,** 2298-2309.
COREY, E., BROWN, L. G., QUINN, J. E., POOT, M., ROUDIER, M. P., HIGANO, C. S. & VESSELLA, R. L. 2003. Zoledronic acid exhibits inhibitory effects on osteoblastic and osteolytic metastases of prostate cancer. *Clinical Cancer Research,* 9**,** 295-306.
CORREA, R., DE CARVALHO, A., PINHEIRO, N., SIMPSON, A. & DE SOUZA, S. 2000. NABC1 (BCAS1): alternative splicing and downregulation in colorectal tumors. *Genomics,* 65**,** 299-302.
CROOKE, S. T. & BRADNER, W. T. 1976. Mitomycin C: a review. *Cancer treatment reviews,* 3**,** 121-139.
CSóKA, B., NéMETH, Z. H., SZABó, I., DAVIES, D. L., VARGA, Z. V., PáLóCZI, J., FALZONI, S., DI VIRGILIO, F., MURAMATSU, R. & YAMASHITA, T. 2018. Macrophage P2X4 receptors augment bacterial killing and protect against sepsis. *JCI insight,* 3.
CUNNINGHAM, D. & YOU, Z. 2015. In vitro and in vivo model systems used in prostate cancer research. *Journal of biological methods,* 2(1).
DAI, H., HU, W., ZHANG, L., JIANG, F., MAO, X., YANG, G. & LI, L. 2021. FGF21 facilitates autophagy in prostate cancer cells by inhibiting the PI3K–Akt–mTOR signaling pathway. *Cell Death & Disease,* 12**,** 303.
DAI, J., KELLER, J., ZHANG, J., LU, Y., YAO, Z. & KELLER, E. T. 2005. Bone morphogenetic protein-6 promotes osteoblastic prostate cancer bone metastases through a dual mechanism. *Cancer research,* 65**,** 8274-8285.
DANG, T. P. 2012. Notch, apoptosis and cancer. *Notch signaling in embryology and Cancer***,** 199-209.
DE FALCO, G. & GIORDANO, A. 2006. pRb2/p130: a new candidate for retinoblastoma tumor formation. *Oncogene,* 25**,** 5333-5340.
DEL FATTORE, A., TETI, A. & RUCCI, N. 2012. Bone cells and the mechanisms of bone remodelling. *Frontiers in Bioscience-Elite,* 4**,** 2302-2321.

DEY, P., JONSSON, P., HARTMAN, J., WILLIAMS, C., STRöM, A. & GUSTAFSSON, J.-Å. 2012. Estrogen receptors β1 and β2 have opposing roles in regulating proliferation and bone metastasis genes in the prostate cancer cell line PC3. *Molecular endocrinology,* 26**,** 1991-2003.

DHULIPALA, P. D., WANG, Y.-X. & KOTLIKOFF, M. I. 1998. The human P2X4 receptor gene is alternatively spliced. *Gene,* 207**,** 259-266.

DI GREGORIO, E., ROMITI, C., DI LORENZO, A., CAVALLO, F., FERRAUTO, G. & CONTI, L. 2023. RGD_PLGA Nanoparticles with Docetaxel: A Route for Improving Drug Efficiency and Reducing Toxicity in Breast Cancer Treatment. *Cancers,* 15(1)**,** p8.

DIEL, I. J., SOLOMAYER, E.-F., COSTA, S. D., GOLLAN, C., GOERNER, R., WALLWIENER, D., KAUFMANN, M. & BASTERT, G. 1998. Reduction in new metastases in breast cancer with adjuvant clodronate treatment. *New England Journal of Medicine,* 339**,** 357-363.

DOCHERTY, F. 2015. *Identifying and characterising dormancy in prostate cancer cells.* (Doctoral dissertation, University of Sheffield).

DOMERCQ, M., VáZQUEZ-VILLOLDO, N. & MATUTE, C. 2013. Neurotransmitter signaling in the pathophysiology of microglia. *Frontiers in cellular neuroscience,* 7**,** 49.

DRAGANOV, D., GOPALAKRISHNA-PILLAI, S., CHEN, Y.-R., ZUCKERMAN, N., MOELLER, S., WANG, C., ANN, D. & LEE, P. P. 2015. Modulation of P2X4/P2X7/Pannexin-1 sensitivity to extracellular ATP via Ivermectin induces a non-apoptotic and inflammatory form of cancer cell death. *Scientific reports,* 5**,** 1-17.

EICHELBERGER, L. E. & CHENG, L. 2004. Does pT2b prostate carcinoma exist? Critical appraisal of the 2002 TNM classification of prostate carcinoma. *Cancer,* 100**,** 2573-2576.

EKE, I., BYLICKY, M. A., SANDFORT, V., CHOPRA, S., MARTELLO, S., GRAVES, E. E., COLEMAN, C. N. & ARYANKALAYIL, M. J. 2021. The lncRNAs LINC00261 and LINC00665 are upregulated in long-term prostate cancer adaptation after radiotherapy. *Molecular Therapy-Nucleic Acids,* 24**,** 175-187.

ELTZSCHIG, H. K., SITKOVSKY, M. V. & ROBSON, S. C. 2012. Purinergic signaling during inflammation. *New England Journal of Medicine,* 367**,** 2322-2333.

FANG, W.-G., PIRNIA, F., BANG, Y.-J., MYERS, C. E. & TREPEL, J. B. 1992. P2-purinergic receptor agonists inhibit the growth of androgen-independent prostate carcinoma cells. *The Journal of clinical investigation,* 89**,** 191-196.

FANG, Y., HUANG, S., HAN, L., WANG, S. & XIONG, B. 2021. Comprehensive analysis of peritoneal metastasis sequencing data to identify LINC00924 as a prognostic biomarker in gastric cancer. *Cancer management and research***,** 5599-5611.

FARRELL, K. B., KARPEISKY, A., THAMM, D. H. & ZINNEN, S. 2018. Bisphosphonate conjugation for bone specific drug targeting. *Bone reports,* 9**,** 47-60.

FERRER, F. A., MILLER, L. J., ANDRAWIS, R. I., KURTZMAN, S. H., ALBERTSEN, P. C., LAUDONE, V. P. & KREUTZER, D. L. 1997. Vascular endothelial growth factor (VEGF) expression in human prostate cancer: in situ and in vitro expression of VEGF by human prostate cancer cells. *The Journal of urology,* 157**,** 2329-2333.

FIANDALO, M. & KYPRIANOU, N. 2012. Caspase control: protagonists of cancer cell apoptosis. *Experimental oncology,* 34**,** 165.

FIZAZI, K., CARDUCCI, M., SMITH, M., DAMIãO, R., BROWN, J., KARSH, L., MILECKI, P., SHORE, N., RADER, M. & WANG, H. 2011. Denosumab versus zoledronic acid for treatment of bone metastases in men with castration-resistant prostate cancer: a randomised, double-blind study. *The Lancet,* 377**,** 813-822.

FLANAGAN, S. 1966. 'Nude', a new hairless gene with pleiotropic effects in the mouse. *Genetics Research,* 8**,** 295-309.

FLOMBAUM, C.D., 2000, June. Metabolic emergencies in the cancer patient. In Seminars in oncology (Vol. 27, No. 3, pp. 322-334).

FLORENCIO-SILVA, R., SASSO, G. R. D. S., SASSO-CERRI, E., SIMõES, M. J. & CERRI, P. S. 2015. Biology of bone tissue: structure, function, and factors that influence bone cells. *BioMed research international,* 2015.

FREDHOLM, B. B., IJZERMAN, A. P., JACOBSON, K. A., KLOTZ, K.-N. & LINDEN, J. 2001. International Union of Pharmacology. XXV. Nomenclature and classification of adenosine receptors. *Pharmacological reviews,* 53**,** 527-552.

FUKUSHIMA, T., TANAKA, Y., HAMEY, F. K., CHANG, C.-H., OKI, T., ASADA, S., HAYASHI, Y., FUJINO, T., YONEZAWA, T. & TAKEDA, R. 2019. Discrimination of dormant and active hematopoietic stem cells by G0 marker reveals dormancy regulation by cytoplasmic calcium. *Cell Reports,* 29(12), pp.4144-4158.

GALLAGHER, J. 2004. ATP P2 receptors and regulation of bone effector cells. *JOURNAL OF MUSCULOSKELETAL AND NEURONAL INTERACTIONS,* 4**,** 125.

GATO, M. I. R., DOS REIS, A. N., DOS SANTOS SILVéRIO, F., ITO, F. T. & LOPES, K. F. 2022. Oncological Diseases. *The Golden Guide to Oncologic Pharmacy.* Springer.

Office of the Surgeon General (US). Bone Health and Osteoporosis: A Report of the Surgeon General. Rockville (MD): Office of the Surgeon General (US); 2004. PMID: 20945569

GENNIGENS, C., MENETRIER-CAUX, C. & DROZ, J. 2006. Insulin-Like Growth Factor (IGF) family and prostate cancer. *Critical reviews in oncology/hematology,* 58**,** 124-145.

GHALALI, A., WIKLUND, F., ZHENG, H., STENIUS, U. & HöGBERG, J. 2014. Atorvastatin prevents ATP-driven invasiveness via P2X7 and EHBP1 signaling in PTEN-expressing prostate cancer cells. *Carcinogenesis,* 35**,** 1547-1555.

GHALALI, A., YE, Z.-W., HöGBERG, J. & STENIUS, U. 2020. PTEN and PHLPP crosstalk in cancer cells and in TGFβ-activated stem cells. *Biomedicine & Pharmacotherapy,* 127**,** 110112.

GIORDANO, A., ROSSI, A., ROMANO, G. & BAGELLA, L. 2007. Tumor suppressor pRb2/p130 gene and its derived product Spa310 spacer domain as perspective candidates for cancer therapy. *Journal of cellular physiology,* 213**,** 403-406.

GITTENS, S. A., BANSAL, G., ZERNICKE, R. F. & ULUDAĞ, H. 2005. Designing proteins for bone targeting. *Advanced drug delivery reviews,* 57**,** 1011-1036.

GOFMAN, L., CENNA, J. M. & POTULA, R. 2014. P2X4 receptor regulates alcohol-induced responses in microglia. *Journal of Neuroimmune Pharmacology,* 9**,** 668-678.

GREENHOUGH, A., SMARTT, H. J., MOORE, A. E., ROBERTS, H. R., WILLIAMS, A. C., PARASKEVA, C. & KAIDI, A. 2009. The COX-2/PGE 2 pathway: key roles in the hallmarks of cancer and adaptation to the tumour microenvironment. *Carcinogenesis,* 30**,** 377-386.

GRIDINA, M. 2019. Improvement of the knock-in effciency in the genome of human induced pluripotent stem cells using the CRISPR/Cas9 system. *Vavilov Journal of Genetics and Breeding,* 22**,** 1026-1032.

GRöNBERG, H. 2003. Prostate cancer epidemiology. *The Lancet,* 361**,** 859-864.

GUEHRING, T., WILDE, G., SUMNER, M., GRüNHAGEN, T., KARNEY, G. B., TIRLAPUR, U. K. & URBAN, J. P. 2009. Notochordal intervertebral disc cells: sensitivity to nutrient deprivation. *Arthritis & Rheumatism: Official Journal of the American College of Rheumatology,* 60**,** 1026-1034.

GUO, L.-H., TRAUTMANN, K. & SCHLUESENER, H. J. 2004. Expression of P2X4 receptor in rat C6 glioma by tumor-associated macrophages and activated microglia. *Journal of neuroimmunology,* 152**,** 67-72.

HADJIDAKIS, D. J. & ANDROULAKIS, I. I. 2006. Bone remodeling. *Annals of the New York academy of sciences,* 1092**,** 385-396.

HAN, S. J., LOVASZI, M., KIM, M., D'AGATI, V., HASKó, G. & LEE, H. T. 2020. P2X4 receptor exacerbates ischemic AKI and induces renal proximal tubular NLRP3 inflammasome signaling. *FASEB journal: Official publication of the Federation of American Societies for Experimental Biology,* 34**,** 5465.

HATTORI, M. & GOUAUX, E. 2012. Molecular mechanism of ATP binding and ion channel activation in P2X receptors. *Nature,* 485**,** 207-212.

HE, J., ZHOU, Y., ARREDONDO CARRERA, H. M., SPRULES, A., NEAGU, R., ZARKESH, S. A., EATON, C., LUO, J., GARTLAND, A. & WANG, N. 2020. Inhibiting the P2X4 receptor suppresses prostate cancer growth in vitro and in vivo, suggesting a potential clinical target. *Cells,* 9**,** 2511.

HE, Y., XU, W., XIAO, Y.-T., HUANG, H., GU, D. & REN, S. 2022. Targeting signaling pathways in prostate cancer: Mechanisms and clinical trials. *Signal transduction and targeted therapy,* 7**,** 198.

HEERBOTH, S., HOUSMAN, G., LEARY, M., LONGACRE, M., BYLER, S., LAPINSKA, K., WILLBANKS, A. & SARKAR, S. 2015. EMT and tumor metastasis. *Clinical and translational medicine,* 4**,** 1-13.

HERCZEGH, P., BUXTON, T. B., MCPHERSON, J. C., KOVáCS-KULYASSA, Á., BREWER, P. D., SZTARICSKAI, F., STROEBEL, G. G., PLOWMAN, K. M., FARCASIU, D. & HARTMANN, J. F. 2002. Osteoadsorptive bisphosphonate derivatives of fluoroquinolone antibacterials. *Journal of medicinal chemistry,* 45**,** 2338-2341.

HLA, T. & NEILSON, K. 1992. Human cyclooxygenase-2 cDNA. *Proceedings of the national academy of sciences,* 89**,** 7384-7388.

HOFBAUER, L. C., BOZEC, A., RAUNER, M., JAKOB, F., PERNER, S. & PANTEL, K. 2021. Novel approaches to target the microenvironment of bone metastasis. *Nature reviews Clinical oncology,* 18**,** 488-505.

HONORE, P., LUGER, N. M., SABINO, M. A. C., SCHWEI, M. J., ROGERS, S. D., MACH, D. B., O'KEEFE, P. F., RAMNARAINE, M. L., CLOHISY, D. R. & MANTYH, P. W. 2000. Osteoprotegerin blocks bone cancer-induced skeletal destruction, skeletal pain and pain-related neurochemical reorganization of the spinal cord. *Nature medicine,* 6**,** 521-528.

HORNING, A. M., WANG, Y., LIN, C.-K., LOUIE, A. D., JADHAV, R. R., HUNG, C.-N., WANG, C.-M., LIN, C.-L., KIRMA, N. B. & LISS, M. A. 2018. Single-Cell RNA-seq Reveals a Subpopulation of Prostate Cancer Cells with Enhanced Cell-Cycle–Related Transcription and Attenuated Androgen ResponseHeterogeneous Androgen Responses of Prostate Cancer Cells. *Cancer research,* 78**,** 853-864.

HOROSZEWICZ, J. S., LEONG, S. S., KAWINSKI, E., KARR, J. P., ROSENTHAL, H., CHU, T. M., MIRAND, E. A. & MURPHY, G. P. 1983. LNCaP model of human prostatic carcinoma. *Cancer research,* 43**,** 1809-1818.

HSU, P. D., LANDER, E. S. & ZHANG, F. 2014. Development and applications of CRISPR-Cas9 for genome engineering. *Cell,* 157**,** 1262-1278.

HUANG, H., FENG, J., WISMEIJER, D., WU, G. & HUNZIKER, E. B. 2017. Hyaluronic acid promotes the osteogenesis of BMP-2 in an absorbable collagen sponge. *Polymers,* 9**,** 339.

HUANG, X., JIA, Z., LI, X., HU, Z., YU, X. & XIA, J. 2023. Asiaticoside hampers epithelial–mesenchymal transition by promoting PPARG expression and suppressing P2RX7-mediated TGF-β/Smad signaling in triple-negative breast cancer. *Phytotherapy Research*, *37*(5), pp.1771-1786.

HUMPHREY, P. A. 2017. Histopathology of prostate cancer. *Cold Spring Harbor Perspectives in Medicine,* 7**,** p. a030411.

HUO, J. F. & CHEN, X. B. 2019. P2X4R silence suppresses glioma cell growth through BDNF/TrkB/ATF4 signaling pathway. *Journal of cellular biochemistry,* 120**,** 6322-6329.

HWANG, C. 2012. Overcoming docetaxel resistance in prostate cancer: a perspective review. *Therapeutic advances in medical oncology,* 4**,** 329-340.

INNAMAA, A., JACKSON, L., ASHER, V., VAN SCHALKWYK, G., WARREN, A., KEIGHTLEY, A., HAY, D., BALI, A., SOWTER, H. & KHAN, R. 2013. Expression and effects of modulation of the K2P potassium channels TREK-1 (KCNK2) and TREK-2 (KCNK10) in the normal human ovary and epithelial ovarian cancer. *Clinical and Translational Oncology,* 15**,** 910-918.

JALILI, V., AFGAN, E., GU, Q., CLEMENTS, D., BLANKENBERG, D., GOECKS, J., TAYLOR, J. & NEKRUTENKO, A. 2020. The Galaxy platform for accessible, reproducible and collaborative biomedical analyses: 2020 update. *Nucleic acids research,* 48**,** pp. W395-W402.

JANCKILA, A. J., TAKAHASHI, K., SUN, S. Z. & YAM, L. T. 2001. Naphthol-ASBI phosphate as a preferred substrate for tartrate-resistant acid phosphatase isoform 5b. *Journal of Bone and Mineral Research,* 16**,** 788-793.

JENJOB, R., NGUYEN, H.-P., KIM, M.-K., JIANG, Y., KIM, J. J. & YANG, S.-G. 2021. Bisphosphonate-conjugated photo-crosslinking polyanionic hyaluronic acid microbeads for controlled BMP2 delivery and enhanced bone formation efficacy. *Biomacromolecules,* 22**,** 4138-4145.

JIN, J., XU, Y., HUO, L., MA, L., SCOTT, A. W., PIZZI, M. P., LI, Y., WANG, Y., YAO, X. & SONG, S. 2020. An improved strategy for CRISPR/Cas9 gene knockout and subsequent wildtype and mutant gene rescue. *PloS one,* 15**,** p. e0228910.

JIN, J. K., DAYYANI, F. & GALLICK, G. E. 2011. Steps in prostate cancer progression that lead to bone metastasis. *International journal of cancer,* 128**,** 2545-2561.

JONES, K., BALLESTEROS, A., MENTINK-KANE, M., WARREN, J., RATTILA, S., MALECH, H., KANG, E. & DVEKSLER, G. 2016. PSG9 stimulates increase in FoxP3+ regulatory T-cells through the TGF-β1 pathway. *PLoS One,* 11**,** p. e0158050.

JüPPNER, H., ABOU-SAMRA, A.-B., FREEMAN, M., KONG, X. F., SCHIPANI, E., RICHARDS, J., KOLAKOWSKI JR, L. F., HOCK, J., POTTS JR, J. T. & KRONENBERG, H. M. 1991. AG protein-linked receptor for parathyroid hormone and parathyroid hormone-related peptide. *Science,* 254**,** 1024-1026.

KAIGHN, M., NARAYAN, K. S., OHNUKI, Y., LECHNER, J. & JONES, L. 1979. Establishment and characterization of a human prostatic carcinoma cell line (PC-3). *Investigative urology,* 17**,** 16-23.

KANEHISA, M., SATO, Y., KAWASHIMA, M., FURUMICHI, M. & TANABE, M. 2016. KEGG as a reference resource for gene and protein annotation. *Nucleic acids research,* 44**,** pp. D457-D462.

KAWAGOE, K., WADA, M., IDICHI, T., OKADA, R., YAMADA, Y., MORIYA, S., OKUBO, K., MATSUSHITA, D., ARIGAMI, T. & KURAHARA, H. 2020. Regulation of aberrantly expressed SERPINH1 by antitumor miR-148a-5p inhibits cancer cell aggressiveness in gastric cancer. *Journal of Human Genetics,* 65**,** 647-656.

KAWAMURA, N., NIMURA, K., NAGANO, H., YAMAGUCHI, S., NONOMURA, N. & KANEDA, Y. 2015. CRISPR/Cas9-mediated gene knockout of NANOG and NANOGP8 decreases the malignant potential of prostate cancer cells. *Oncotarget,* 6**,** 22361.

KAWATE, T., MICHEL, J. C., BIRDSONG, W. T. & GOUAUX, E. 2009a. Crystal structure of the ATP-gated P2X4 ion channel in the closed state. *Nature,* 460**,** 592-598.

KAWATE, T., MICHEL, J. C., BIRDSONG, W. T. & GOUAUX, E. 2009b. Crystal structure of the ATP-gated P2X 4 ion channel in the closed state. *Nature,* 460**,** 592-598.

KELLER, E. T., ZHANG, J., COOPER, C. R., SMITH, P. C., MCCAULEY, L. K., PIENTA, K. J. & TAICHMAN, R. S. 2001. Prostate carcinoma skeletal metastases: cross-talk between tumor and bone. *Cancer and Metastasis Reviews,* 20**,** 333-349.

KHATOON, Z., FIGLER, B., ZHANG, H. & CHENG, F. 2014. Introduction to RNA‐Seq and its applications to drug discovery and development. *Drug development research,* 75**,** 324-330.

KHOSLA, S., OURSLER, M. J. & MONROE, D. G. 2012. Estrogen and the skeleton. *Trends in Endocrinology & Metabolism,* 23**,** 576-581.

KIM, W., LEE, S., KIM, H. S., SONG, M., CHA, Y. H., KIM, Y.-H., SHIN, J., LEE, E.-S., JOO, Y. & SONG, J. J. 2018. Targeting mutant KRAS with CRISPR-Cas9 controls tumor growth. *Genome research,* 28**,** 374-382.

KIRKPATRICK, F. 1990. Overview of agarose gel properties. *Current communications in cell & molecular biology*.

KRAMER, N., WALZL, A., UNGER, C., ROSNER, M., KRUPITZA, G., HENGSTSCHLäGER, M. & DOLZNIG, H. 2013. In vitro cell migration and invasion assays. *Mutation Research/Reviews in Mutation Research,* 752**,** 10-24.

KUCHIMARU, T., KATAOKA, N., NAKAGAWA, K., ISOZAKI, T., MIYABARA, H., MINEGISHI, M., KADONOSONO, T. & KIZAKA-KONDOH, S. 2018. A reliable murine model of bone metastasis by injecting cancer cells through caudal arteries. *Nature communications,* 9**,** 2981.

KUCHUK, I., HUTTON, B., MORETTO, P., NG, T., ADDISON, C. & CLEMONS, M. 2013. Incidence, consequences and treatment of bone metastases in breast cancer patients—experience from a single cancer centre. *Journal of bone oncology,* 2**,** 137-144.

KUKURBA, K. R. & MONTGOMERY, S. B. 2015. RNA sequencing and analysis. *Cold Spring Harbor Protocols,* 2015**,** pdb. top084970.

LANGLEY, R. R. & FIDLER, I. J. 2011. The seed and soil hypothesis revisited—The role of tumor‐stroma interactions in metastasis to different organs. *International journal of cancer,* 128**,** 2527-2535.

LAYHADI, J. A., TURNER, J., CROSSMAN, D. & FOUNTAIN, S. J. 2018. ATP evokes Ca2+ responses and CXCL5 secretion via P2X4 receptor activation in human monocyte-derived macrophages. *The Journal of Immunology,* 200**,** 1159-1168.

LEE, C., JIA, Z., RAHMATPANAH, F., ZHANG, Q., ZI, X., MCCLELLAND, M. & MERCOLA, D. 2014. Role of the adjacent stroma cells in prostate cancer development and progression: synergy between TGF-β and IGF signaling. *BioMed research international,* 2014.

LEE, P. Y., COSTUMBRADO, J., HSU, C.-Y. & KIM, Y. H. 2012. Agarose gel electrophoresis for the separation of DNA fragments. *JoVE (Journal of Visualized Experiments)***,** p. e3923.

LEFEBVRE, C., BACHELOT, T., FILLERON, T., PEDRERO, M., CAMPONE, M., SORIA, J.-C., MASSARD, C., LEVY, C., ARNEDOS, M. & LACROIX-TRIKI, M. 2016. Mutational profile of metastatic breast cancers: a retrospective analysis. *PLoS medicine,* 13**,** p. e1002201.

LI, D.-M. & FENG, Y.-M. 2011. Signaling mechanism of cell adhesion molecules in breast cancer metastasis: potential therapeutic targets. *Breast cancer research and treatment,* 128**,** 7-21.

LI, F., GUO, N., MA, Y., NING, B., WANG, Y. & KOU, L. 2014. Inhibition of P2X4 suppresses joint inflammation and damage in collagen-induced arthritis. *Inflammation,* 37**,** 146-153.

LI, Y. & COZZI, P. 2007. Targeting uPA/uPAR in prostate cancer. *Cancer treatment reviews,* 33**,** 521-527.

LIN, X., CHEN, Z., GAO, P., GAO, Z., CHEN, H., QI, J., LIU, F., YE, D., JIANG, H. & NA, R. 2017. TEX15: A DNA repair gene associated with prostate cancer risk in Han Chinese. *The Prostate,* 77**,** 1271-1278.

LITWIN, M. S. & TAN, H.-J. 2017. The diagnosis and treatment of prostate cancer: a review. *Jama,* 317**,** 2532-2542.

LIU, Q., ZHANG, H., JIANG, X., QIAN, C., LIU, Z. & LUO, D. 2017. Factors involved in cancer metastasis: a better understanding to “seed and soil” hypothesis. *Molecular cancer,* 16**,** 176.

LIU, Y., OUYANG, L., MAO, C., CHEN, Y., LIU, N., CHEN, L., SHI, Y., XIAO, D., LIU, S. & TAO, Y. 2022. Inhibition of RNF182 mediated by Bap promotes non-small cell lung cancer progression. *Frontiers in Oncology,* 12.

LIU, Z.-G. & JIAO, D. 2020. Necroptosis, tumor necrosis and tumorigenesis. *Cell stress,* 4**,** 1.

LOGOTHETIS, C. J. & LIN, S.-H. 2005. Osteoblasts in prostate cancer metastasis to bone. *Nature Reviews Cancer,* 5**,** 21-28.

MAKOTO 1994. The new American joint committee on cancer and international union against cancer TNM classification of prostate cancer. *Cancer*, *74*(1), pp.104-114.

MAO, Y., SHEN, J., LU, Y., LIN, K., WANG, H., LI, Y., CHANG, P., WALKER, M. G. & LI, D. 2017. RNA sequencing analyses reveal novel differentially expressed genes and pathways in pancreatic cancer. *Oncotarget,* 8**,** 42537.

MARTIN, T. A., YE, L., SANDERS, A. J., LANE, J. & JIANG, W. G. 2013. Cancer invasion and metastasis: molecular and cellular perspective. *Madame Curie Bioscience Database [Internet].* Landes Bioscience.

MARTíNEZ-NIETO, G., HELJASVAARA, R., HEIKKINEN, A., KASKI, H.-K., DEVARAJAN, R., RINNE, O., HENRIKSSON, C., THOMSON, E., VON HERTZEN, C. & MIINALAINEN, I. 2021. Deletion of col15a1 modulates the tumour extracellular matrix and leads to increased tumour growth in the mmtv-pymt mouse mammary carcinoma model. *International Journal of Molecular Sciences,* 22**,** 9978.

MATSUMURA, Y., YAMASHITA, T., SASAKI, A., NAKATA, E., KOHNO, K., MASUDA, T., TOZAKI-SAITOH, H., IMAI, T., KURAISHI, Y. & TSUDA, M. 2016. A novel P2X4 receptor-selective antagonist produces anti-allodynic effect in a mouse model of herpetic pain. *Scientific reports,* 6**,** 32461.

MAYNARD, J. P., LU, J., VIDAL, I., HICKS, J., MUMMERT, L., ALI, T., KEMPSKI, R., CARTER, A. M., SOSA, R. Y. & PEIFFER, L. B. 2022. P2X4 purinergic receptors offer a therapeutic target for aggressive prostate cancer. *The Journal of Pathology,* 256**,** 149-163.

MELANI, C., SANGALETTI, S., BARAZZETTA, F. M., WERB, Z. & COLOMBO, M. P. 2007. Amino-biphosphonate–mediated MMP-9 inhibition breaks the tumor-bone marrow axis responsible for myeloid-derived suppressor cell expansion and macrophage infiltration in tumor stroma. *Cancer research,* 67**,** 11438-11446.

MENG, X., VANDER ARK, A., DAFT, P., WOODFORD, E., WANG, J., MADAJ, Z. & LI, X. 2018. Loss of TGF-β signaling in osteoblasts increases basic-FGF and promotes prostate cancer bone metastasis. *Cancer letters,* 418**,** 109-118.

MIKOLAJEWICZ, N. & KOMAROVA, S. V. 2020. Role of UDP-sugar receptor P2Y14 in murine osteoblasts. *International journal of molecular sciences,* 21**,** 2747.

MINELLI, A., BELLEZZA, I., CONTE, C. & CULIG, Z. 2009. Oxidative stress-related aging: a role for prostate cancer? *Biochimica et Biophysica Acta (BBA)-Reviews on Cancer,* 1795**,** 83-91.

MISHRA, A., ZENNAMI, K., VELARDE, E., THOREK, D. L., YEGNASUBRAMANIAN, S., DEWEESE, T. L. & LUPOLD, S. E. 2021. Longitudinal measurement of subcutaneous and intratibial human prostate cancer xenograft growth and response to ionizing radiation by plasma Alu and LINE-1 ctDNA: A comparison to standard methods. *The Prostate,* 81**,** 745-753.

MOHAMEDI, Y., FONTANIL, T., CAL, S., COBO, T. & OBAYA, Á. J. 2021. ADAMTS-12: functions and challenges for a complex metalloprotease. *Frontiers in Molecular Biosciences,* 8**,** 686763.

MONTILLA, A., MATA, G. P., MATUTE, C. & DOMERCQ, M. 2020. Contribution of P2X4 receptors to CNS function and pathophysiology. *International journal of molecular sciences,* 21**,** 5562.

MUNDY, G. R. 2002. Metastasis to bone: causes, consequences and therapeutic opportunities. *Nature Reviews Cancer,* 2**,** 584-593.

MUNIR, A., AZAM, S., ALI, S., MEHMOOD, A. & SHAH, A. 2017. Repurposing of Modified Alpidem and Propoxyphene to Cure AURKA, BCAS1, GNAS and MLH1 Gene Mutations in Colorectal Cancer. *Drug Des,* 6**,** 2169-0138.

MURAYAMA, T. & GOTOH, N. 2019. Patient-derived xenograft models of breast cancer and their application. *Cells,* 8**,** 621.

NAMEKAWA, T., IKEDA, K., HORIE-INOUE, K. & INOUE, S. 2019. Application of prostate cancer models for preclinical study: advantages and limitations of cell lines, patient-derived xenografts, and three-dimensional culture of patient-derived cells. *Cells,* 8**,** 74.

NANDIGAMA, R., PADMASEKAR, M., WARTENBERG, M. & SAUER, H. 2006. Feed forward cycle of hypotonic stress-induced ATP release, purinergic receptor activation, and growth stimulation of prostate cancer cells. *Journal of Biological Chemistry,* 281**,** 5686-5693.

NGUYEN, K., YAN, Y., YUAN, B., DASGUPTA, A., SUN, J., MU, H., DO, K.-A., UENO, N. T., ANDREEFF, M. & BATTULA, V. L. 2018. St8SIA1 regulates tumor growth and metastasis in TNBC by activating the FAK–AkT–mTOR signaling pathway. *Molecular cancer therapeutics,* 17**,** 2689-2701.

NOVAK, I. 2011. Purinergic signalling in epithelial ion transport: regulation of secretion and absorption. *Acta Physiologica,* 202**,** 501-522.

OADES, G., COXON, J. & COLSTON, K. 2002. The potential role of bisphosphonates in prostate cancer. *Prostate cancer and prostatic diseases,* 5**,** 264-272.

OKAMOTO, T., IMAIZUMI, K. & KANEKO, M. 2020. The role of tissue-specific ubiquitin ligases, RNF183, RNF186, RNF182 and RNF152, in disease and biological function. *International Journal of Molecular Sciences,* 21**,** 3921.

ONO, T., HAYASHI, M., SASAKI, F. & NAKASHIMA, T. 2020. RANKL biology: bone metabolism, the immune system, and beyond. *Inflammation and regeneration,* 40**,** 1-16.

OSTROVSKAYA, O., ASATRYAN, L., WYATT, L., POPOVA, M., LI, K., PEOPLES, R. W., ALKANA, R. L. & DAVIES, D. L. 2011. Ethanol is a fast channel inhibitor of P2X4 receptors. *Journal of Pharmacology and Experimental Therapeutics,* 337**,** 171-179.

PAALME, V., RUMP, A., MäDO, K., TERAS, M., TRUUMEES, B., AITAI, H., RATAS, K., BOURGE, M., CHIANG, C.-S. & GHALALI, A. 2019. Human peripheral blood eosinophils express high levels of the purinergic receptor P2X4. *Frontiers in immunology,* 10**,** 2074.

PAGET, S. 1889. The distribution of secondary growths in cancer of the breast. *Lancet***,** 571-573.

PAN, C. C., KUO, D. H., SHIEH, P., CHEN, F. A., KUO, C. C. & JAN, C. R. 2010. Effect of the antidepressant paroxetine on Ca2+ movement in PC3 human prostate cancer cells. *Drug Development Research,* 71**,** 120-126.

PARKER, C. A., NILSSON, S., HEINRICH, D., HELLE, S. I., O'SULLIVAN, J., FOSSå, S. D., CHODACKI, A., WIECHNO, P., LOGUE, J. & SEKE, M. 2013. Alpha emitter radium-223 and survival in metastatic prostate cancer. *New England Journal of Medicine,* 369**,** 213-223.

PELEGRIN, P., BARROSO-GUTIERREZ, C. & SURPRENANT, A. 2008. P2X7 receptor differentially couples to distinct release pathways for IL-1β in mouse macrophage. *The Journal of Immunology,* 180**,** 7147-7157.

PERTEA, M., PERTEA, G. M., ANTONESCU, C. M., CHANG, T.-C., MENDELL, J. T. & SALZBERG, S. L. 2015. StringTie enables improved reconstruction of a transcriptome from RNA-seq reads. *Nature biotechnology,* 33**,** 290-295.

PIENTA, K. J. Preclinical mechanisms of action of docetaxel and docetaxel combinations in prostate cancer. Seminars in oncology, 2001. Elsevier, 3-7.

POLISENO, L., SALMENA, L., ZHANG, J., CARVER, B., HAVEMAN, W. J. & PANDOLFI, P. P. 2010. A coding-independent function of gene and pseudogene mRNAs regulates tumour biology. *Nature,* 465**,** 1033-1038.

PORRAS, A. & GUERRERO ARROYO, M. D. C. 2011. Role of p38α in apoptosis: implication in cancer development and therapy.

PRAETORIUS, H. A. & LEIPZIGER, J. 2010. Intrarenal purinergic signaling in the control of renal tubular transport. *Annual review of physiology,* 72**,** 377-393.

PULUKURI, S. M., GONDI, C. S., LAKKA, S. S., JUTLA, A., ESTES, N., GUJRATI, M. & RAO, J. S. 2005. RNA interference-directed knockdown of urokinase plasminogen activator and urokinase plasminogen activator receptor inhibits prostate cancer cell invasion, survival, and tumorigenicity in vivo. *Journal of biological chemistry,* 280**,** 36529-36540.

RAGGATT, L. J. & PARTRIDGE, N. C. 2010. Cellular and molecular mechanisms of bone remodeling. *Journal of biological chemistry,* 285**,** 25103-25108.

RAN, F., HSU, P. D., WRIGHT, J., AGARWALA, V., SCOTT, D. A. & ZHANG, F. 2013a. Genome engineering using the CRISPR-Cas9 system. *Nature protocols,* 8**,** 2281-2308.

RAN, F. A., HSU, P. D., LIN, C.-Y., GOOTENBERG, J. S., KONERMANN, S., TREVINO, A. E., SCOTT, D. A., INOUE, A., MATOBA, S. & ZHANG, Y. 2013b. Double nicking by RNA-guided CRISPR Cas9 for enhanced genome editing specificity. *Cell,* 154**,** 1380-1389.

RAWLA, P. 2019. Epidemiology of prostate cancer. *World journal of oncology,* 10**,** 63.

REINHOLZ, M. M., ZINNEN, S. P., DUECK, A. C., DINGLI, D., REINHOLZ, G. G., JONART, L. A., KITZMANN, K. A., BRUZEK, A. K., NEGRON, V. & ABDALLA, A. K. 2010. A promising approach for treatment of tumor-induced bone diseases: utilizing bisphosphonate derivatives of nucleoside antimetabolites. *Bone,* 47**,** 12-22.

RICE, M. A., MALHOTRA, S. V. & STOYANOVA, T. 2019. Second-generation antiandrogens: from discovery to standard of care in castration resistant prostate cancer. *Frontiers in oncology,* 9**,** 801.

ROSEN, R. D. & SAPRA, A. 2022. TNM classification. *StatPearls [Internet].* StatPearls Publishing.

RUSSELL, H. V., GROSHEN, S. G., ARA, T., DECLERCK, Y. A., HAWKINS, R., JACKSON, H. A., DALDRUP-LINK, H. E., MARACHELIAN, A., SKERJANEC, A. & PARK, J. R. 2011. A phase I study of zoledronic

acid and low‐dose cyclophosphamide in recurrent/refractory neuroblastoma: A new approaches to neuroblastoma therapy (NANT) study. *Pediatric blood & cancer,* 57**,** 275-282.

SACHS, U. J., ANDREI-SELMER, C. L., MANIAR, A., WEISS, T., PADDOCK, C., ORLOVA, V. V., CHOI, E. Y., NEWMAN, P. J., PREISSNER, K. T. & CHAVAKIS, T. 2007. The neutrophil-specific antigen CD177 is a counter-receptor for platelet endothelial cell adhesion molecule-1 (CD31). *Journal of Biological Chemistry,* 282**,** 23603-23612.

SCARDINO, P. T. 1989. Early detection of prostate cancer. *Urologic Clinics of North America,* 16**,** 635-655.

SCHENK, U., FRASCOLI, M., PROIETTI, M., GEFFERS, R., TRAGGIAI, E., BUER, J., RICORDI, C., WESTENDORF, A. M. & GRASSI, F. 2011. ATP inhibits the generation and function of regulatory T cells through the activation of purinergic P2X receptors. *Science signaling,* 4**,** p. ra12-ra12.

SCHMITT, M., CETECI, F., GUPTA, J., PESIC, M., BöTTGER, T. W., NICOLAS, A. M., KENNEL, K. B., ENGEL, E., SCHEWE, M. & CALLAK KIRISöZü, A. 2022. Colon tumour cell death causes mTOR dependence by paracrine P2X4 stimulation. *Nature***,** 1-7.

SCHNEIDER, S., MERFORT, I., IDZKO, M. & ZECH, A. 2022. Blocking P2X purinoceptor 4 signalling alleviates cigarette smoke induced pulmonary inflammation. *Respiratory Research,* 23**,** 1-9.

SCHRLSDER, F., HERMANEK, P., DENIS, L., FAIR, W. & GOSPODAROWICZ, M. 1992. The TNM classification of prostate cancer. *The Prostate,* 4**,** 129-138.

SCHULTZ, G. S. & WYSOCKI, A. 2009. Interactions between extracellular matrix and growth factors in wound healing. *Wound repair and regeneration,* 17**,** 153-162.

SEVGUL, K. & KARAKOK, M. 2016. Investigation of Gremlin 1, COL15A1 immunoreactivity and the relationship between microvessel density and Gremlin 1 in papillary renal cell carcinoma and chromophobe renal cell carcinoma. *Medical Science and Discovery,* 3**,** 184-91.

SHI, C., CHEN, X. & TAN, D. 2019. Development of patient-derived xenograft models of prostate cancer for maintaining tumor heterogeneity. *Translational andrology and urology,* 8**,** 519.

SHIOZAKI, A., KATSURAHARA, K., KUDOU, M., SHIMIZU, H., KOSUGA, T., ITO, H., ARITA, T., KONISHI, H., KOMATSU, S. & KUBOTA, T. 2021. Amlodipine and verapamil, voltage-gated Ca 2+ channel inhibitors, suppressed the growth of gastric cancer stem cells. *Annals of Surgical Oncology,* 28**,** 5400-5411.

SHORNING, B. Y., DASS, M. S., SMALLEY, M. J. & PEARSON, H. B. 2020. The PI3K-AKT-mTOR pathway and prostate cancer: At the crossroads of AR, MAPK, and WNT signaling. *International journal of molecular sciences,* 21**,** 4507.

SIMS, N. A. & GOOI, J. H. Bone remodeling: Multiple cellular interactions required for coupling of bone formation and resorption. Seminars in cell & developmental biology, 2008. Elsevier, 444-451.

SINGH, P., TOOM, S. & HUANG, Y. 2017. Anti-claudin 18.2 antibody as new targeted therapy for advanced gastric cancer. *Journal of hematology & oncology,* 10**,** 1-5.

SIVCEV, S., SLAVIKOVA, B., RUPERT, M., IVETIC, M., NEKARDOVA, M., KUDOVA, E. & ZEMKOVA, H. 2019. Synthetic testosterone derivatives modulate rat P2X2 and P2X4 receptor channel gating. *Journal of Neurochemistry,* 150**,** 28-43.

SLATER, M., DANIELETTO, S., GIDLEY‐BAIRD, A., TEH, L. & BARDEN, J. 2004. Early prostate cancer detected using expression of non‐functional cytolytic P2X7 receptors. *Histopathology,* 44**,** 206-215.

SP'NUDE, F. 1966. ', a new hairless gene with pleiotropic effects in the mouse. *Genet Res,* 8**,** 295-309.

SRIVASTAVA, P., CRONIN, C. G., SCRANTON, V. L., JACOBSON, K. A., LIANG, B. T. & VERMA, R. 2020. Neuroprotective and neuro-rehabilitative effects of acute purinergic receptor P2X4 (P2X4R) blockade after ischemic stroke. *Experimental neurology,* 329**,** 113308.

STAURENGO-FERRARI, L., ZARPELON, A. C., LONGHI-BALBINOT, D. T., MARCHESI, M., CUNHA, T. M., ALVES-FILHO, J. C., CUNHA, F. Q., FERREIRA, S. H., CASAGRANDE, R. & MIRANDA, K. M. 2014. Nitroxyl inhibits overt pain-like behavior in mice: role of cGMP/PKG/ATP-sensitive potassium channel signaling pathway. *Pharmacological Reports,* 66**,** 691-698.

STOKES, L., LAYHADI, J. A., BIBIC, L., DHUNA, K. & FOUNTAIN, S. J. 2017. P2X4 receptor function in the nervous system and current breakthroughs in pharmacology. *Frontiers in pharmacology,* 8**,** 291.

STOPECK, A. T., LIPTON, A., BODY, J.-J., STEGER, G. G., TONKIN, K., DE BOER, R. H., LICHINITSER, M., FUJIWARA, Y., YARDLEY, D. A. & VINIEGRA, M. 2010. Denosumab compared with zoledronic acid for the treatment of bone metastases in patients with advanced breast cancer: a randomized, double-blind study. *Journal of clinical oncology,* 28**,** 5132-5139.

STRONCEK, D. F., CARUCCIO, L. & BETTINOTTI, M. 2004. CD177: A member of the Ly-6 gene superfamily involved with neutrophil proliferation and polycythemia vera. *Journal of translational medicine,* 2**,** 1-9.

STURGE, J., CALEY, M. P. & WAXMAN, J. 2011. Bone metastasis in prostate cancer: emerging therapeutic strategies. *Nature reviews Clinical oncology,* 8**,** 357.

SURPRENANT, A. & NORTH, R. A. 2009. Signaling at purinergic P2X receptors. *Annual review of physiology,* 71**,** 333-359.

SUURVäLI, J., BOUDINOT, P., KANELLOPOULOS, J. & BOUDINOT, S. R. 2017. P2X4: A fast and sensitive purinergic receptor. *Biomedical journal,* 40**,** 245-256.

SUVA, L. J., WASHAM, C., NICHOLAS, R. W. & GRIFFIN, R. J. 2011a. Bone metastasis: mechanisms and therapeutic opportunities, *Nature Reviews Endocrinology,* 7**,** 208-218.

SUVA, L. J., WASHAM, C., NICHOLAS, R. W. & GRIFFIN, R. J. 2011b. Bone metastasis: mechanisms and therapeutic opportunities. *Nature Reviews Endocrinology,* 7**,** 208-218.

TABBEKH, M., FRANCISZKIEWICZ, K., HAOUAS, H., LéCLUSE, Y., BENIHOUD, K., RAMAN, C. & MAMI-CHOUAIB, F. 2011. Rescue of tumor-infiltrating lymphocytes from activation-induced cell death enhances the antitumor CTL response in CD5-deficient mice. *The Journal of Immunology,* 187**,** 102-109.

TAITT, H. E. 2018. Global trends and prostate cancer: a review of incidence, detection, and mortality as influenced by race, ethnicity, and geographic location. *American journal of men's health,* 12**,** 1807-1823.

TESTA, U., CASTELLI, G. & PELOSI, E. 2019. Cellular and molecular mechanisms underlying prostate cancer development: therapeutic implications. *Medicines,* 6**,** 82.

THALMANN, G. N., ANEZINIS, P. E., CHANG, S.-M., ZHAU, H. E., KIM, E. E., HOPWOOD, V. L., PATHAK, S., VON ESCHENBACH, A. C. & CHUNG, L. W. 1994. Androgen-independent cancer progression and bone metastasis in the LNCaP model of human prostate cancer. *Cancer research,* 54**,** 2577-2581.

TITFORD, M. 2005. The long history of hematoxylin. *Biotechnic & histochemistry,* 80**,** 73-78.

TRANG, M., SCHMALZING, G., MüLLER, C. E. & MARKWARDT, F. 2020. Dissection of P2X4 and P2X7 receptor current components in BV-2 microglia. *International journal of molecular sciences,* 21**,** 8489.

UCCELLI, L., MARTINI, P., URSO, L., GHIRARDI, T., MARVELLI, L., CITTANTI, C., CARNEVALE, A., GIGANTI, M., BARTOLOMEI, M. & BOSCHI, A. 2022. Rhenium Radioisotopes for Medicine, a Focus on Production and Applications. *Molecules,* 27**,** 5283.

ULMANN, L., HATCHER, J. P., HUGHES, J. P., CHAUMONT, S., GREEN, P. J., CONQUET, F., BUELL, G. N., REEVE, A. J., CHESSELL, I. P. & RASSENDREN, F. 2008. Up-regulation of P2X4 receptors in spinal microglia after peripheral nerve injury mediates BDNF release and neuropathic pain. *Journal of Neuroscience,* 28**,** 11263-11268.

ULMANN, L., HIRBEC, H. & RASSENDREN, F. 2010. P2X4 receptors mediate PGE2 release by tissue-resident macrophages and initiate inflammatory pain. *The EMBO journal,* 29**,** 2290-2300.

USTACH, C. V., HUANG, W., CONLEY-LACOMB, M. K., LIN, C.-Y., CHE, M., ABRAMS, J. & KIM, H.-R. C. 2010. A novel signaling axis of matriptase/PDGF-D/β-PDGFR in human prostate cancer. *Cancer research,* 70**,** 9631-9640.

VAKAR-LOPEZ, F., CHENG, C. J., KIM, J., SHI, G. G., TRONCOSO, P., TU, S. M., YU-LEE, L. Y. & LIN, S. H. 2004. Up-regulation of MDA-BF-1, a secreted isoform of ErbB3, in metastatic prostate cancer

cells and activated osteoblasts in bone marrow. *The Journal of Pathology: A Journal of the Pathological Society of Great Britain and Ireland,* 203**,** 688-695.

VALTA, M. P., TUOMELA, J., BJARTELL, A., VALVE, E., VääNäNEN, H. K. & HäRKöNEN, P. 2008. FGF‐8 is involved in bone metastasis of prostate cancer. *International journal of cancer,* 123**,** 22-31.

VAN ACKER, H. H., ANGUILLE, S., WILLEMEN, Y., SMITS, E. L. & VAN TENDELOO, V. F. 2016. Bisphosphonates for cancer treatment: mechanisms of action and lessons from clinical trials. *Pharmacology & therapeutics,* 158**,** 24-40.

VAN DER DEEN, M., AKECH, J., WANG, T., FITZGERALD, T. J., ALTIERI, D. C., LANGUINO, L. R., LIAN, J. B., VAN WIJNEN, A. J., STEIN, J. L. & STEIN, G. S. 2010. The cancer‐related Runx2 protein enhances cell growth and responses to androgen and TGFβ in prostate cancer cells. *Journal of cellular biochemistry,* 109**,** 828-837.

VAN DER TOOM, E. E., VERDONE, J. E. & PIENTA, K. J. 2016. Disseminated tumor cells and dormancy in prostate cancer metastasis. *Current opinion in biotechnology,* 40**,** 9-15.

VAN WEERDEN, W. M. & ROMIJN, J. C. 2000. Use of nude mouse xenograft models in prostate cancer research. *The Prostate,* 43**,** 263-271.

VELA, I., GREGORY, L., GARDINER, E. M., CLEMENTS, J. A. & NICOL, D. L. 2007. Bone and prostate cancer cell interactions in metastatic prostate cancer. *BJU international,* 99**,** 735-742.

VERMA, S. P. & DAS, P. 2018. Novel splicing in IGFN1 intron 15 and role of stable G-quadruplex in the regulation of splicing in renal cell carcinoma. *PLoS One,* 13**,** p. e0205660.

VICENTINI, C., FESTUCCIA, C., GRAVINA, G. L., ANGELUCCI, A., MARRONARO, A. & BOLOGNA, M. 2003. Prostate cancer cell proliferation is strongly reduced by the epidermal growth factor receptor tyrosine kinase inhibitor ZD1839 in vitro on human cell lines and primary cultures. *Journal of cancer research and clinical oncology,* 129**,** 165-174.

VICKERS, N. J. 2017. Animal communication: when i'm calling you, will you answer too? *Current biology,* 27**,** R713-R715.

WAI WONG, C., DYE, D. E. & COOMBE, D. R. 2012. The role of immunoglobulin superfamily cell adhesion molecules in cancer metastasis. *International journal of cell biology,* 2012.

WANG, M., AUDI, G., KONDEV, F., HUANG, W., NAIMI, S. & XU, X. 2017. The AME2016 atomic mass evaluation (II). Tables, graphs and references. *Chinese Physics C,* 41**,** 030003.

WANG, N., DOCHERTY, F. E., BROWN, H. K., REEVES, K. J., FOWLES, A. C., OTTEWELL, P. D., DEAR, T. N., HOLEN, I., CROUCHER, P. I. & EATON, C. L. 2014. Prostate cancer cells preferentially home to osteoblast‐rich areas in the early stages of bone metastasis: evidence from in vivo models. *Journal of Bone and Mineral Research,* 29**,** 2688-2696.

WANG, Y., YAN, Q., MO, Y., LIU, Y., WANG, Y., ZHANG, S., GUO, C., WANG, F., LI, G. & ZENG, Z. 2022a. Splicing factor derived circular RNA circCAMSAP1 accelerates nasopharyngeal carcinoma tumorigenesis via a SERPINH1/c-Myc positive feedback loop. *Molecular Cancer,* 21**,** 62.

WANG, Z., ZHU, S., TAN, S., ZENG, Y. & ZENG, H. 2022b. The P2 purinoceptors in prostate cancer. *Purinergic Signalling***,** 1-9.

WHITE, W. M., BROST, B., SUN, Z., ROSE, C., CRAICI, I., WAGNER, S. J., TURNER, S. T. & GAROVIC, V. D. 2013. Genome-wide methylation profiling demonstrates hypermethylation in maternal leukocyte DNA in preeclamptic compared to normotensive pregnancies. *Hypertension in pregnancy,* 32**,** 257-269.

WONG, S. K., MOHAMAD, N.-V., GIAZE, T. R., CHIN, K.-Y., MOHAMED, N. & IMA-NIRWANA, S. 2019. Prostate cancer and bone metastases: the underlying mechanisms. *International journal of molecular sciences,* 20**,** 2587.

WOODS, L. T., JASMER, K. J., FORTI, K. M., SHANBHAG, V. C., CAMDEN, J. M., ERB, L., PETRIS, M. J. & WEISMAN, G. A. 2020. P2Y2 receptors mediate nucleotide-induced EGFR phosphorylation and stimulate proliferation and tumorigenesis of head and neck squamous cell carcinoma cell lines. *Oral oncology,* 109**,** 104808.

WU, T., WANG, W., SHI, G., HAO, M., WANG, Y., YAO, M., HUANG, Y., DU, L., ZHANG, X. & YE, D. 2022. Targeting HIC1/TGF-β axis-shaped prostate cancer microenvironment restrains its progression. *Cell Death & Disease,* 13**,** 624.

WU, T. T., SIKES, R. A., CUI, Q., THALMANN, G. N., KAO, C., MURPHY, C. F., YANG, H., ZHAU, H. E., BALIAN, G. & CHUNG, L. W. 1998. Establishing human prostate cancer cell xenografts in bone: Induction of osteoblastic reaction by prostate‐specific antigen‐producing tumors in athymic and SCID/bg mice using LNCaP and lineage‐derived metastatic sublines. *International journal of cancer,* 77**,** 887-894.

WU, X., GONG, S., ROY-BURMAN, P., LEE, P. & CULIG, Z. 2013. Current mouse and cell models in prostate cancer research. *Endocrine-related cancer,* 20**,** R155-R170.

WYATT, L. R., GODAR, S. C., KHOJA, S., JAKOWEC, M. W., ALKANA, R. L., BORTOLATO, M. & DAVIES, D. L. 2013. Sociocommunicative and sensorimotor impairments in male P2X4-deficient mice. *Neuropsychopharmacology,* 38**,** 1993-2002.

XIANG, Z. & BURNSTOCK, G. 2005. Expression of P2X receptors on rat microglial cells during early development. *Glia,* 52**,** 119-126.

XING, S., GROL, M. W., GRUTTER, P. H., DIXON, S. J. & KOMAROVA, S. V. 2016. Modeling interactions among individual P2 receptors to explain complex response patterns over a wide range of ATP concentrations. *Frontiers in physiology,* 7**,** 294.

XIONG, Y., FENG, Y., ZHAO, J., LEI, J., QIAO, T., ZHOU, Y., LU, Q., JIANG, T., JIA, L. & HAN, Y. 2021. TFAP2A potentiates lung adenocarcinoma metastasis by a novel miR-16 family/TFAP2A/PSG9/TGF-β signaling pathway. *Cell Death & Disease,* 12**,** 352.

XU, J., LAMOUILLE, S. & DERYNCK, R. 2009. TGF-β-induced epithelial to mesenchymal transition. *Cell research,* 19**,** 156-172.

XU, X., LIU, R.-F., WAN, B.-B., XING, W.-M., HUANG, J. & HAN, Z.-G. 2011. Expression of a novel gene FAM43B repressing cell proliferation is regulated by DNA methylation in hepatocellular carcinoma cell lines. *Molecular and cellular biochemistry,* 354**,** 11-20.

YAMAMOTO, K., KORENAGA, R., KAMIYA, A., QI, Z., SOKABE, M. & ANDO, J. 2000. P2X4 receptors mediate ATP-induced calcium influx in human vascular endothelial cells. *American Journal of Physiology-Heart and Circulatory Physiology,* 279**,** H285-H292.

YAN, G., FUKABORI, Y., MCBRIDE, G., NIKOLAROPOLOUS, S. & MCKEEHAN, W. 1993. Exon switching and activation of stromal and embryonic fibroblast growth factor (FGF)-FGF receptor genes in prostate epithelial cells accompany stromal independence and malignancy. *Molecular and cellular biology,* 13**,** 4513-4522.

YAO, F., KAUSALYA, J. P., SIA, Y. Y., TEO, A. S., LEE, W. H., ONG, A. G., ZHANG, Z., TAN, J. H., LI, G. & BERTRAND, D. 2015. Recurrent fusion genes in gastric cancer: CLDN18-ARHGAP26 induces loss of epithelial integrity. *Cell reports,* 12**,** 272-285.

YAO, Z., LIN, A., YI, Y., SHEN, W., ZHANG, J. & LUO, P. 2022. THSD7B Mutation Induces Platinum Resistance in Small Cell Lung Cancer Patients. *Drug Design, Development and Therapy***,** 1679-1695.

YAZDANI, B., JAZINI, M., JABBARI, N., KARAMI, M., RAHIMIRAD, S., AZADEH, M., MAHDEVAR, M. & GHAEDI, K. 2021. Altered expression level of ACSM5 in breast cancer: an integrative analysis of tissue biomarkers with diagnostic potential. *Gene Reports,* 22**,** 100992.

YE, R., PI, M., COX, J. V., NISHIMOTO, S. K. & QUARLES, L. D. 2017. CRISPR/Cas9 targeting of GPRC6A suppresses prostate cancer tumorigenesis in a human xenograft model. *Journal of Experimental & Clinical Cancer Research,* 36**,** 1-13.

YONEDA, T. & HIRAGA, T. 2005. Crosstalk between cancer cells and bone microenvironment in bone metastasis. *Biochemical and biophysical research communications,* 328**,** 679-687.

YU, J., LIU, S., HONG, Y., MARKOWIAK, S., SANCHEZ, R., SCHROEDER, J., HEIDT, D. & BRUNICARDI, F. 2017. Cancer microarray data weighted gene co-expression network analysis identifies a gene module and hub genes shared across nine types of solid cancer. *CellR4,* 5**,** p. e2439.

ZHAN, T., RINDTORFF, N. & BOUTROS, M. 2017. Wnt signaling in cancer. *Oncogene,* 36**,** 1461-1473.

ZHANG, C., XIN, H., ZHANG, W., YAZAKI, P. J., ZHANG, Z., LE, K., LI, W., LEE, H., KWAK, L. & FORMAN, S. 2016. CD5 binds to interleukin-6 and induces a feed-forward loop with the transcription factor STAT3 in B cells to promote cancer. *Immunity,* 44**,** 913-923.

ZHANG, M., XUAN, S., BOUXSEIN, M. L., VON STECHOW, D., AKENO, N., FAUGERE, M. C., MALLUCHE, H., ZHAO, G., ROSEN, C. J. & EFSTRATIADIS, A. 2002. Osteoblast-specific knockout of the insulin-like growth factor (IGF) receptor gene reveals an essential role of IGF signaling in bone matrix mineralization. *Journal of Biological Chemistry,* 277**,** 44005-44012.

ZHANG, W., LIU, Y., YANG, B., LIU, Z. & YU, Q. 2019. Microencapsulated olfactory ensheathing-cell transplantation reduces pain in rats by inhibiting P2X4 receptor overexpression in the dorsal root ganglion. *Neuroreport,* 30**,** 120-126.

ZHENG, Y., LIN, S. X., WU, S., DAHL, D. M., BLUTE, M. L., ZHONG, W. D., ZHOU, X. & WU, C. L. 2020. Clinicopathological characteristics of localized prostate cancer in younger men aged⩽ 50 years treated with radical prostatectomy in the PSA era: A systematic review and meta‐analysis. *Cancer medicine,* 9**,** 6473-6484.